Structural studies on hydrogen-bonded and metal-organic complexes

Doherty, Cheryl Louise

Award date:
2005

Awarding institution:
University of Bath

Structural Studies on Hydrogen-Bonded and Metal-Organic Complexes

Cheryl Louise Doherty

A thesis submitted for the degree of
Doctor of Philosophy

University of Bath
Department of Chemistry
December 2005

ProQuest LLC
789 East Eisenhower Parkway
P.O. Box 1346
Ann Arbor, MI 48106-1346

For mum and dad

With love

Acknowledgements

This research was carried out under the supervision of Professor Matt Davidson and I would like to thank him for his guidance and support with all aspects of the research during the course of my time here at Bath. I am also especially grateful to my co-supervisor, Professor Paul Raithby, for his kindness and encouragement over the years, and for his help in all matters crystallographic.

I am indebted to the other Davidson group past and present members, particularly Luke, Gillian, Carly, Matt, Chris Amanda and Marie, who have made the research enjoyable and helped out in many ways. Special thanks must also go to Andy Johnson who, despite moving on to his own lab, never abandoned me and who has always been an excellent source of advice and encouragement. I am also grateful for the assistance given by the staff at the ILL, particularly Sax Mason and Garry McIntyre during neutron experiments and to Mary Mahon here at Bath for her guidance in crystallography. I have been particularly fortunate to share my time in Bath with fellow students Stephen, David and Nicola whose sympathetic ears, excellent company and willingness to lend chemicals have always proved invaluable to me. I would like to thank these and my other friends, both at Bath and away, for their support over the years. I am particularly grateful to Simon for proofreading and also for many, many cups of tea.

I gratefully acknowledge the financial support provided by the University of Bath, the EPSRC and Johnson-Matthey in the form of a case award.

Finally, special thanks go to my family, especially my mum and dad, for their support during the entirety of my education and to Dustin for his love and encouragement and most of all for being there for me.

Abstract

This thesis is divided in two parts and contains a description of work carried out on hydrogen bonded supramolecular networks using crystallographic and knowledge mining techniques, Part I 'Antioxidation', and also the application of the same structural methods to the study of some industrially relevant metal alkoxide catalysts, Part II 'Group 4 Metal Alkoxides'. Single crystal X-ray and neutron diffraction studies were used to obtain crystal structures of novel organic compounds and for the collection of data for charge density analysis of a metal alkoxide species. The work also involved a systematic analysis of data gathered from the Cambridge Structural Database.

In Part I the investigation of hydrogen bonding interactions between free radicals and hydrogen-donating species as a model for antioxidant action is described. In Chapter **1** the background and main research objectives of the research are outlined, this includes an introduction to the chemical action of antioxidants. This is followed by a brief description of hydrogen bonding and a discussion of basic crystallographic structure determination theory, which are both important topics in relation to the structural work presented in this thesis.

In Chapters **2** and **3** the supramolecular synthesis and characterisation of a number of monophenol and other donor adducts, respectively, with the radical TEMPO are presented. Chapter **2** discussed the synthesis and characterization of the hydrogen bonding interactions that occur between the stable aminoxyl radical TEMPO with a series of phenolic hydrogen donors. The chapter begins with an introduction to the reactivity and exploitation of the TEMPO radical, and an explanation of the hydrogen-bonded model for antioxidant activity. This is followed by a discussion of the solid-state structures of 4 monophenol adducts, which have been synthesised and characterised and the solution-state structure of one adduct for which it was not possible to obtain a crystal

structure. Chapter **3** is concerned with selected examples of other hydrogen bond donors, in an extension to the original model. The more reactive radical galvinoxyl is used in Chapter **4** in the synthesis of a series of galvinoxyl derivatives formed by an unexpected radical recombination. The synthesis and characterisation of 4 derivatives of galvinoxyl are described and discussed.

Part **2** of this thesis is concerned with the structural characteristics and reactivity of group 4 metal alkoxides. An introduction to the use of these complexes, and of titanium in particular, in catalysis and the structural features that are of interest is presented in Chapter **5**, as is a brief discussion of neutron diffraction techniques and their use in charge density analysis. A combined theoretical and experimental charge density study on a titanium alkoxide species typical of the catalysts we are interested in is presented in Chapter **6**. The 30 K X-ray and neutron structures have been combined and subjected to multipolar analysis; this is then compared with two theoretical models. Natural Bond Orbital (NBO) analysis and topological analysis of the charge density using the Atoms in Molecules (AIM) method have been performed and this chapter is concerned with the interpretation of these results. In Chapter **7** knowledge mining experiments using single crystal structural data obtained from the Cambridge Structural Database (CSD) are described. In these analyses structural trends in geometrical parameters in group 4 metal alkoxide complexes are probed with a view to the elucidation of structure/property relationships.

Table of Contents

Lists of Figures, Schemes and Tables

Table of Abbreviations, Acronyms and Symbols

a, b, c, α, β, γ	lattice constants and angles
Å	Ångstrom, 100 pm, 10^{-10} m
A	Hydrogen bond acceptor
AIM	Atoms in Molecules
ArO·	Aryloxyl radical
ArOH	Phenolic hydrogen donor
AsA	Ascorbic acid
BCP	Bond Critical Point
BDE	Bond Dissociation Energy
BHA	butylated hydroxyanisole
BHT	butylated hydroxytoluene
C	C-face centred unit cell
calcd	calculated
CCDC	Cambridge Crystallographic Data Centre
CP	Critical Point
Chromanol	2,2,5,7,8-pentamethyl-6-hydroxychroman
CSD	Cambridge Structural Database
cp	cyclopentadienyl (C_5H_5)
D	Hydrogen bond donor
D	distance from hydrogen bond donor to acceptor (D···A)
d	distance from hydrogen bond acceptor to hydrogen (A···H)
DFT	Density Functional Theory
DNA	Deoxyribose Nucleic Acid
DPA	diphenylamine
DPPH·	2,2-Diphenyl-1-picrylhydrazyl free radical
EPR	Electron Paramagnetic Resonance
F	Face-centred unit cell
G·	galvinoxyl free radical
GooF	goodness of fit defined as *GooF* = S = $(\Sigma_i w_i \Delta_i^2) / (n-m)^{1/}$
galvinoxyl	2,6-di-*tert*-butyl-α-(3,5-di-*tert*-butyl-4-oxo-2,5-cyclohexadien-1-ylidene)-*p*-tolyloxy
H	Hydrogen atom
HAT	Hydrogen atom transfer mechanism

H_2O_2	Hydrogen Peroxide
HSAB	Hard-soft acid-base system
HF	Hartree-Fock
I	Body-centred unit cell
ICSD	Inorganic Crystal Structure Database
IMPT	intermolecular perturbation theory
IP	Ionisation Potential
IR	Infrared
K	degrees in Kelvin
LDL	Low Density Lipoprotein
LICC	Ligand Induced Charge Concentration
Lp	lone pair
M	molecular formula
M	any metal
MDF	Metals Data File
Me	Methyl (CH_3)
$[M(OR)_x]_n$	Metal alkoxide where M is a metal with a valency of x, R is an aryl or alkyl group and n is the degree of molecular association
MP	Moller-Plesset theory
ML_x	Any specified metal M with x ligands L surrounding it
NMR	Nuclear Magnetic Resonance
NBO	Natural Bond Orbital
N_{obs}	number of crystallographically independent observations
O_2	molecular oxygen
$O_2^{-}\cdot$	Superoxide radical
OH·	hydroxyl radial
OH	hydroxyl group
OR	alkoxyl or aryloxyl group
O*i*Pr	isopropoxide
P	Primitive unit cell
PCET	Proton Concerted Electron Transfer mechanism
PDB	Brookhaven Protein Data Bank
ppm	parts per million
PUFA	Polyunsaturated fatty acids
Py	pyridyl (C_5NH_5)
pyCH2OH	hydroxymethylpyridine

r	distance from hydrogen bond donor to hydrogen (D-H)
R_1	Residual factor defined as $R_1 = \Sigma\|\|F_o\| - \|F_c\|\| / \Sigma\|F_o\|$
R·	Alkyl radical
RH	Alkyl group
RMS	Root Mean Square
ROO·	Peroxyl radical
ROS	Reactive Oxygen Species
ROOH	Hydroperoxides
t-Bu	*tert*-butyl [$-C(CH_3)_3$]
TEMPO	2,2,6,6-tetramethylpiperidine-*N*-oxyl
[$Ti(OiPr)_4$]	titanium tetraisopropoxide
Toc·	tocopherol radical
TocH	tocopherol
UQH2	Ubiquinol
VSCC	Valence Shell Charge Concentration
$wR2$	Residual factor defined as $wR2 = \Sigma_i w_i\Delta_i^2/\Sigma w_i F_o$,
X	any element
Z	number of formula units in the cell
$-\nabla^2\rho$	Laplacian ($L(\rho)$)
$\rho(r)$	Electron density
°	degrees
°C	degrees in Celsius
δ_{oct}	deviation defined as $\delta_{oct} = [\ \Sigma\ \{(a_i - a_{ideal})^2\}/15]^{1/2}$
λ	Wavelength
μ	Absorption coefficient
$\epsilon(r)$	Bond ellipticity
π	defined as $\sqrt{\sum_{i=1}^{N}\frac{\delta_i^2}{N-3}}$, where$\delta$ is deviation of the atom *i*, with respect to the Least-square plane defined by the N atoms of the ring
σ	sample standard deviation

Part I

Antioxidation

Chapter 1

Introduction

1.1 Overview

As a result of their wide-ranging importance, the role of antioxidants has been extensively studied and, in particular, the action of biological antioxidants has been the subject of special interest, as these include the most active antioxidant species known. The improvement in understanding of the reactivity and action of these species, in addition to the development of more successful analogues, is an on-going aim in the field.[1]

Part 1 of this thesis describes work carried out investigating the hydrogen bonding interactions between free radicals and hydrogen-donating species as a model for the proton transfer mechanism important in antioxidant action. This introductory chapter outlines the background and research previously carried out in this field. An overview of the background and chemical action of antioxidants is provided and, in addition, relevant concepts such as hydrogen bonding and crystallography are introduced. Further, detailed background information relating to the study is given in the relevant discussion chapters.

1.2 Antioxidation

1.2.1 Oxygen in Biological and Polymeric Systems

Exposure to molecular oxygen causes oxidative degradation in organic materials, often resulting in severe damage to important components in many different systems. For this reason, there is a long-standing interest in the action of antioxidants as they are species capable of protecting organic materials from this damage in both biological[2] and industrial[3] systems.

Oxidation causes damage in several ways. It induces the oxidative degradation of rubbers and plastics and the deterioration of foods and oils. The oxidation of unsaturated fats in critical cellular components such as cell membranes and lipoproteins, the particles carrying cholesterol and fat in the blood stream, interferes with the structure and function of the biological membranes. Proteins may also be damaged, leading to structural changes and loss of enzyme activity, while oxidative damage to DNA also occurs.

Since oxygen is an essential requirement in aerobic systems for energy production and the synthesis of biologically active compounds, living aerobic organisms are constantly exposed to this damage, commonly termed oxidative 'stress'. While in living organisms there exists natural mechanisms to protect and repair oxidative damage, exposure to radicals can overwhelm these defences, and this is thought to be responsible for many degenerative diseases and life-threatening illnesses. In recent years oxidation in biological cells has been implicated in many diseases such as Alzheimer's disease, atherosclerosis, diabetes, cancer, emphysema, iron overload, malaria, muscular dystrophy, Parkinson's disease, rheumatoid arthritis and retinal degradation.[4,5,6] Oxidative stress is also considered an important factor in the process of ageing.[7,8]

Consequently there is a great deal of interest in the role and mechanisms of antioxidant species that inhibits free radical induced oxidative stress. Our interest in the field stems from the lack of agreement on the subject of the precise mechanism by which antioxidants work.

1.2.2 Free Radicals

In the human body free radicals are formed either by environmental factors, such as radiation or pollution, or as by-products of the body's normal aerobic metabolism. A free radical can be defined as any chemical species that possesses one or more unpaired electrons and can be anionic, cationic or neutral. Ground state molecular oxygen (dioxygen) itself is a bi-radical and has two unpaired electrons in its highest energy orbital.

During metabolism molecular oxygen is taken up and converted into a useful form proceeding through several oxygen-based radical species. As a result the major radical species of interest in biological fields have been those involving oxygen. On entering the human body molecular oxygen is partially reduced in the mitochondria as part of the respiratory chain to form superoxide ($O_2^{\cdot-}$). The superoxide anion radical is also produced in copious quantities by the immune system. Once formed superoxide is further converted into other reactive oxygen species, the main ones being the hydroxyl radical (OH·), hydrogen peroxide (H_2O_2) and the peroxyl radical (ROO·). These species are collectively known as reactive oxygen species (ROS) and of these, peroxyl radicals, ROO·, and the superoxide anion radical, $O_2^{\cdot-}$, are considered to be among the most commonly occurring radical species in living cells.

1.2.3 Mechanism of Autoxidation

The process of the oxidation of organic molecules by atmospheric oxygen is called autoxidation. Autoxidation takes place under ambient conditions and proceeds *via* a free radical mechanism;[9] it is the propagation of these free radicals which causes oxidative damage. The initiation step to form the lipid radical occurs by hydrogen atom abstraction from polyunsaturated lipids (RH) by one of the ROS species described earlier (Section 1.1.2) to form alkyl radicals (R·) (Scheme 1.1).

$$RH \rightarrow R\cdot$$

Scheme 1.1: Initiation.

These alkyl radicals react very rapidly with molecular oxygen to form harmful peroxyl radicals (ROO·) (Scheme 1.2).[9]

$$R\cdot + O_2 \rightarrow ROO\cdot$$

Scheme 1.2: Formation of Peroxyl Radicals.

The free-radical chain reaction involving these peroxyl radicals proceeds rapidly as the reaction is autocatalytic, so once started it spreads rapidly and affects a great number of molecules. In biological systems, where lipid molecules are involved the process is commonly known as lipid peroxidation. The polyunsaturated fatty acids (PUFA) present in membranes are particularly susceptible to this process since they are primarily made of hydrocarbon chains (phosphoglycerides) which contain the divinyl methane unit (Figure1.1). Oxidation of this by hydrogen abstraction results in the formation of a fairly stable free radical.[10]

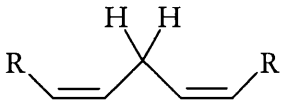

Figure 1.1: Site of hydrogen abstraction in unsaturated lipids.

This rate limiting hydrogen abstraction from the lipid polymer to produce hydroperoxides (ROOH) is represented below (Scheme 1.3).

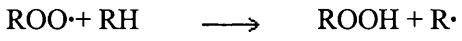

Scheme 1.3: Propagation of Autoxidation.

The peroxidation reaction is further propagated by this peroxyl radical as it reacts with fatty acids and lipids in the membranes. The chain reaction is terminated only when two of the radical species meet and react to yield non-radical products (Scheme 1.4).

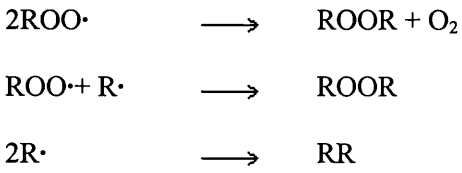

Scheme 1.4: Termination of Autoxidation.

1.2.4 Inhibition

Molecules that can safely interact with free radicals to either terminate or inhibit the oxidative chain reaction are known as antioxidants. Low concentrations of antioxidants are present naturally in aerobic organisms and are added to synthetic materials to protect them from premature decay by oxidation. To combat oxidative stress the human body is equipped with a multi-layer antioxidant protection system[11] which not only neutralizes stray radicals in living organisms but, since the defences are not completely effective,

also destroys free radical damaged proteins, removes oxidised fatty acids from membranes and repairs damaged DNA.

Antioxidants inhibit radical chain oxidation in one of two ways. Some antioxidants are preventative and work by reducing the rate of chain initiation while others are chain-breaking and prevent oxidative damage from spreading by interrupting the radical chain propagation of lipid peroxidation.[12] The antioxidant enzymes, such as superoxide dismutase, catalase or glutathione peroxidase, are an important part of the antioxidant defence system inside cells and are generally preventative in nature. For example, superoxide dismutase scavenges superoxide and converts it to less reactive species. In addition to the antioxidant enzymes there are several small molecule antioxidants, such as vitamin E and vitamin C and ubiquinol, all of which play an important role in antioxidant defence systems and act *via* a chain-breaking mechanism. Typical examples of chain breaking antioxidants include hindered phenols, e.g. 2,6-di-*tert*-butyl-4-methylphenol (butylated hydroxytoluene, BHT) and aromatic amines, e.g. diphenylamine (DPA) (Figure 1.2).

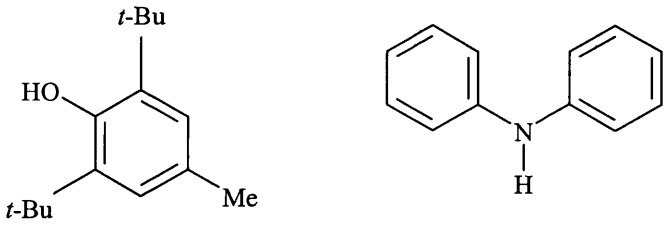

BHT DPA

Figure 1.2: Structure of BHT and DPA.

The most widely studied group of antioxidants is phenol based. These are ubiquitous in biological systems and are also commonly used as antioxidants in synthetic polymers and as food additives.[2] As a result of these factors phenols have attracted much interest in the

field[13] and both natural and synthetic antioxidants have been extensively explored in the literature.[12]

The antioxidant properties of phenols, and other chain-breaking antioxidants, are due to their ability to quench the chain carrying peroxyl radicals of the substrate by transfer of the hydroxylic hydrogen to form hydroperoxides. The chain-breaking mechanism by which phenols inhibit autoxidation is shown below (Scheme 1.5).

$$ROO\cdot + ArOH \rightarrow ROOH + ArO\cdot$$

$$ROO\cdot + ArO\cdot \rightarrow \text{non-radical products}$$

Scheme 1.5: Chain-Breaking Mechanism of Inhibition.

Firstly the phenolic antioxidant ArOH donates a hydrogen atom to a peroxyl radical ROO·. This is followed by the reaction of the aryloxyl radical with another peroxyl radical to terminate the chain by forming non-radical products. In order to work effectively, this reaction must proceed at a rate faster than that of the peroxyl radical with the lipid chain. As a result, the effectiveness of any chain-breaking antioxidants is related to the rate-limiting step of the hydrogen abstraction. Successful inhibition of the autoxidation reaction thus depends on the ability of an antioxidant to fulfil both of the requirements stated above and so is determined by several key characteristics, in particular bond dissociation energy (BDE) and ionization potential (IP) are two major factors that determine the mechanism and the efficacy of antioxidants.[14] Firstly, a relatively low O-H BDE facilitates the H-atom abstraction reaction between the antioxidant and the chain carrying peroxyl radical, so that it occurs at a rate much faster than that at which the chain-propagating step of the lipid peroxidation proceeds.[15,16] As a result, this parameter has been thoroughly studied and there have been numerous reports in the recent literature on the determinations of the BDEs of phenolic derivatives, with the

aim of understanding how the strength of the phenolic bond is affected by nature, position, and number of substituents.[17]

In addition, since the antioxidant activity of phenols inevitably results in formation of phenoxyl radicals, it is therefore of importance to consider the reactivity of the antioxidant-derived radical. Hydrogen transfer from a phenol produces a phenoxyl radical which is more stable due to delocalisation around the aromatic ring (Figure 1.3).

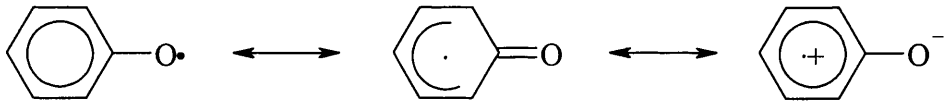

Figure 1.3: Delocalisation in phenoxyl radicals (adapted from reference 17).

For successful antioxidant action the radicals produced must not propagate the autoxidation chain. This ability to stabilise the resulting aryloxyl radical prevents the propagation of the autoxidation chain. Instead, the phenoxyl radicals are generally neutralised by reaction with a second peroxyl radical. It is also important to maintain a relatively high IP, which decreases the electron-transfer rate between antioxidant and oxygen and thus reduces the pro-oxidative potency of the antioxidant.[18,19,20] Finally, the antioxidant must possess an appropriate solubility to allow mobility between membranes and lipoprotein.[21] The widespread abundance of phenolic antioxidants reflects their excellent hydrogen donating ability and the fact that the phenoxyl radicals are both stable and unreactive toward oxygen.[22,23]

Vitamin E is an extremely well studied example of a chain breaking antioxidant, and one important to the work reported here. Vitamin E is the major lipid-soluble antioxidant in human blood plasma, low-density lipoprotein (LDL) and cellular membranes. Due to its high activity and importance in the body, vitamin E is of particular interest to researchers

in the field and has been the focus of extensive original studies and has been reported in numerous reviews.[24,25,26] Vitamin E is composed of the α-, β-, γ- and δ-tocopherols, which are all structurally related and differ only in the number and position of methyl substituents on the phenolic ring. The structure of these components is given in Figure 1.4.

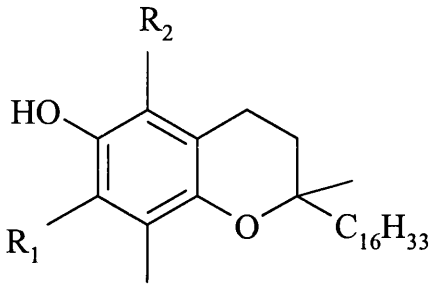

α-tocopherol R_1 = Me, R_2 = Me

β-tocopherol R_1 = H, R_2 = Me

γ-tocopherol R_1 = Me, R_2 = H

δ-tocopherol R_1 = H, R_2 = H

Figure 1.4: The structure of vitamin E.

α-tocopherol is biologically and chemically the most active component of vitamin E, acting as a chain-breaking antioxidant in biological membranes and lipoproteins by reducing chain-propagating peroxyl species (ROO·) to the corresponding hydroperoxide (ROOH) (Figure 1.5).

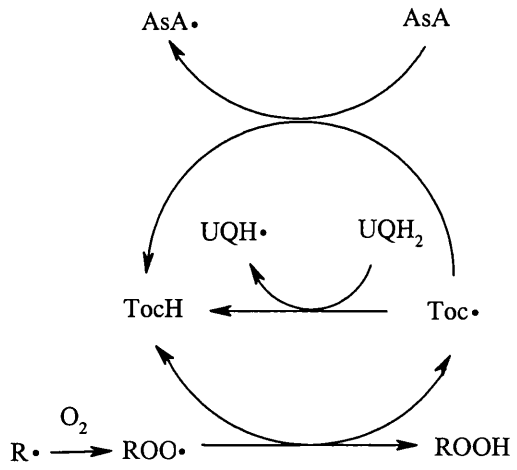

Figure 1.5: Scheme of antioxidant inhibition and regeneration in the cell membrane.

As described earlier for the general reaction of ArOH with a radical, the mechanism of reaction of α-tocopherol with peroxyl radicals (ROO·) involves the loss of an H atom during reduction of ROO· to ROOH, yielding the α-tocopherol radical (Toc·). *In vitro* studies have revealed that in low density lipids α -tocopherol can act, not only as a powerful antioxidant, but also as a pro-oxidant under mild oxidising conditions which consume α-tocopherol (TocH) very slowly.[27,28] This step is prevented in some systems by regenerating the starting phenol. In human cell membrane this is accomplished by vitamin C (ascorbic acid, AsA) in the aqueous phase and ubiquinol (UQH_2) in the lipid layer.[29,30]

The aspects of α-tocopherol's chemical structure that are responsible for its exceptional antioxidant efficiency have been thoroughly investigated.[22,31,32,33,34,35,36] Since the bond strength of the O-H bond is important in determining the antioxidant activity of phenols and species with lower O-H BDEs are generally better antioxidants,[23,36,37,38,39] the BDEs of the O-H bond in the tocopherols, in particular, have been thoroughly studied. Existing studies have shown that the O-H bond strength in the tocopherols depends on the substituent pattern of the phenol, and many research teams have studied this effect.[17,40] Substituents that are able to stabilise the forming phenoxyl radical by delocalising the developing electron spin, lower the barrier for a hydrogen transfer reaction. So, it has been found that substitution with electron-donating groups at positions *ortho* and *para* to the phenolic O-H group also leads to compounds having lower BDEs. However, good electron donating substituents also lead to a decrease in the IP of the phenol, thereby rendering the compound directly reactive with oxygen.[22,,41]

Ingold and co-workers further proposed that the excellent antioxidant activity of vitamin E is in part due to the stabilization of the phenoxy radical by the conjugative electron delocalisation contributed mainly from the lone pair of the *para* OR group (Figure 1.6).[22, 32, 34, 35]

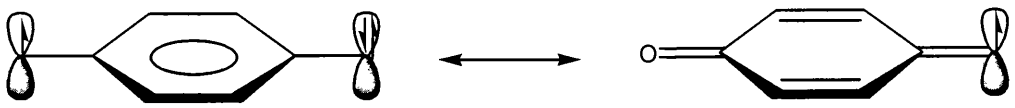

Figure 1.6: Stabilisation of radical centre by electron delocalisation.

The *para* oxygen allows the resonance stabilisation of the forming radical, which weakens the OH bond by making the reaction more exothermic. However, the atom can stabilise the phenoxy radical in this way only provided that the *p*-type lone pair orbital overlaps with the semi-occupied molecular orbital of the radical. The extent of this overlap is dependant on the dihedral angle between the *p*-type orbital and the aromatic plane (Figure 1.7).

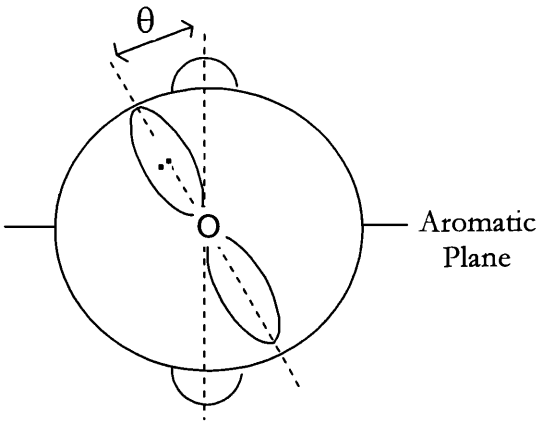

Figure 1.7: Dihedral angle, θ, between the methoxy oxygen 2*p* orbital and the radical orbital (adapted from reference 35).

Overlap between these orbitals, and hence the stabilisation, is maximised at 0° and minimised at 90°. Hence, the greater the overlap between this lone pair orbital and the phenoxyl radical orbital, the more efficient the phenol is as an antioxidant. As a result, the heterocyclic ring is a chief cause of the high antioxidant activity of α-tocopherol and related compounds. It ensures that the 2*p*-type lone pair of electrons on the ring oxygen

adopts the correct orientation, approximately perpendicular to the plane of the aromatic ring, to allow stabilisation of the developing phenoxyl radical. In most biological conditions the α-tocopherol radical is adequately resonance stabilised. It will not continue the propagation step of the chain reaction, but will eventually combine with another oxyl radical to yield non-radical products.

Further stabilisation occurs as chain transfer is retarded when the phenoxyl oxygen is sterically protected by the presence of two *ortho* alkyl groups, as has been shown by measurement of the rate constants which decrease as the bulk of the *ortho* substituents increases along the series H< Me < CMe_3.[32] In α-tocopherol, the presence of the two alkyl groups (-R) in appropriate positions on the aromatic ring these structural factors that govern the rate of the hydrogen abstraction are optimised. Consideration of these factors show on structural grounds the tocopherols can all be expected to be good chain-breaking antioxidants as the O-H bond energy is significantly reduced by the presence of the *para* oxygen atom.

The high activity of vitamin E and thorough understanding of the structural factors leading to this efficacy has consequently lead to the study of related phenols in the quest for novel highly active antioxidants. Burton *et al.* showed that a tocopherol model compound 2,2,5,7,8-pentamethyl-6-hydroxychroman (Figure 1.8), based on the parent structure, and α-tocopherol itself were the best phenolic antioxidants known at the time, and were even better than the major commercial antioxidants such as 2,6-di-tert-butyl-4-alkylphenols for which BHT is an example.[35]

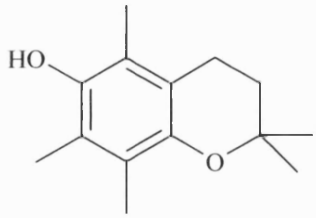

Figure 1.8: Structure of 2,2,5,7,8-pentamethyl-6-hydroxychroman.

As described for the case of vitamin E, the heterocylic ring in this compound maintains the orientation of the *para* oxygen, enabling it to take part in delocalisation with the ring (Figure 1.9).

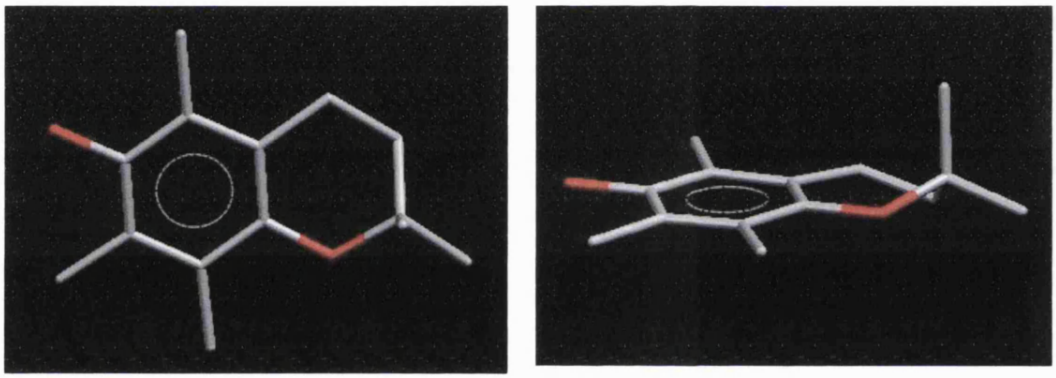

Figure 1.9: Mercury image of 2,2,5,7,8-pentamethyl-6-hydroxychroman demonstrating the orientation of the oxygen atoms.[42]

This is in contrast to the case of *para*-methoxyphenol, in which the methoxy group can undergo free rotation and as a result has a significantly reduced rate of hydrogen donation than the fused ring structure.[22] The model chromanol compound, Figure 1.8, is very similar to α-tocopherol and lacks only the alkyl chain, which is important in making the compound lipid soluble but does not contribute significantly to the antioxidant activity. Furthermore, it has been found that an even more active antioxidant, 2,3-dihydro-5-hydroxy-2,2,4,6,7-pentamethylbenzofuran (Figure 1.10) which consists of a fused five-membered heterocyclic ring.

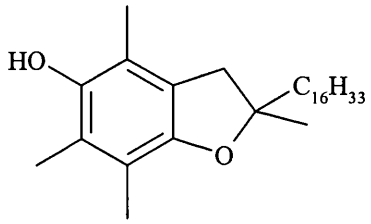

Figure 1.10: Structure of 2,3-dihydro-5-hydroxy-2,2,4,6,7-pentamethylbenzofuran.

The reason for the higher activity in this case is that the dihedral angle, as defined in Figure 1.7, in the benzofuran is even closer to the optimum 0° than in hydroxychromans.

2,3-dihydro-5-hydroxy-2,2-dipentyl-4,6-di-tert-butyl-benzofuran, (Figure 1.11), is a novel antioxidant that has been designed, synthesised and found to exert a potent antioxidant activity against lipid peroxidation.[43]

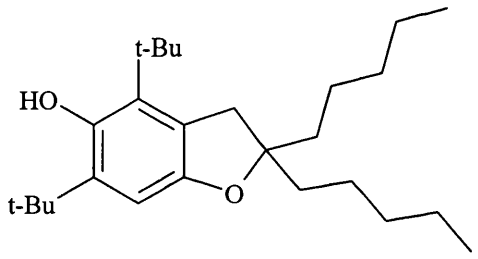

Figure 1.11: Structure of 2,3-dihydro-5-hydroxy-2,2-dipentyl-4,6-di-tert-butyl-benzofuran.

The appropriate substituents and side chains, which determine the localisation, retainment, and mobility within lipid particle, are in place. This is the first systematically designed man-made compound that has outperformed the natural vitamin. This species was reported to have 1.5-1.9 times higher biological activity than α-tocopherol.

Another important class of antioxidants are the polyphenolics. Flavanoids are one common type of polyphenol and have been reported to be chain-breaking inhibitors of the pereoxidation process by several different mechanisms, including hydrogen transfer.[44,45]

A number of studies in particular have been reported on the structure-activity relationship in the flavanoid antioxidants.[46,47]

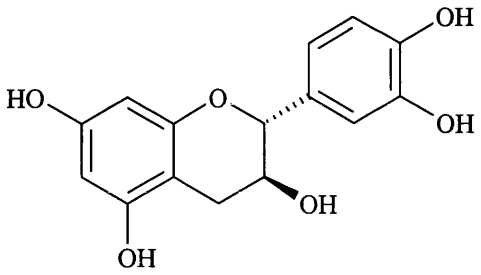

Figure 1.12: Structure of catechin, a ubiquitous monomeric flavanol.

There are also a large number of antioxidants developed for use in commercial materials, and many of these are based on the most highly active phenolic antioxidants found in nature. The hindered phenol BHT and aromatic amine DPA (Figure 1.2) are examples of antioxidants which find widespread application in synthetic materials, the related phenol 2-*tert*-butyl-4-methoxyphenol (butylated hydroxyanisole, BHA) is a synthetic analogue of the natural antioxidant vitamin E, and is also widely used in industry as an antioxidant and preservative in foods and rubbers (Figure 1.13).[3]

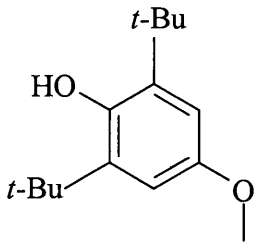

Figure 1.13: Structure of BHA.

1.2.5 Mechanism of Chain-Breaking Inhibition

As discussed above (Section 1.2.4), the antioxidant activity of tocopherols is attributed to their ability to scavenge free radicals. It is generally accepted that chain-breaking

antioxidants such as phenols provide protection by scavenging the peroxyl radicals which otherwise propagate autoxidation in lipids and synthetic hydrocarbons *via* hydrogen atom abstraction from the phenol to the radical. However, the precise mechanistic details of this reaction are yet to be fully elucidated.

It has been established that there are two possible pathways for ArOH to scavenge free radicals; the direct hydrogen atom transfer (HAT) mechanism[22,35,48] and the proton-concerted single electron transfer (PCET)[49] mechanism, or a combination thereof.[50] A thorough understanding of the extent to which each of these possible mechanisms is important in the reaction of antioxidants with peroxyl radicals would ultimately lead to the development of more effective antioxidant species. This has lead to both experimental and theoretical investigations into the mechanism to bring some clarification.

The first mechanism involves the direct transfer of a proton and electron together, as a hydrogen atom. In the HAT mechanism phenolic antioxidants are able to inhibit autoxidation by providing a hydrogen atom that is more easily abstracted to give the oxygen-centred phenoxy radical (ArO˙). This produces resonance stabilised phenoxy radicals, which react with a second peroxyl radical to give non-radical products in preference to reacting further with the lipid polymer (Scheme 1.6).[51,52,53]

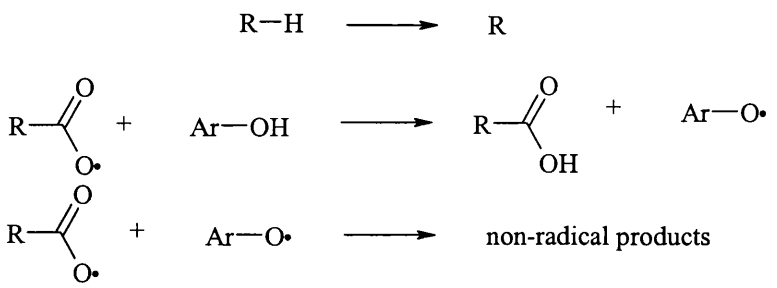

Scheme 1.6: Mechanism for HAT.

In this case the reaction rate is determined to a certain extent by the O-H BDE of ArOH, and hence this parameter has been thoroughly studied. The efficiency of the antioxidant ArOH also depends on the stability of the phenoxyl radical ArO· produced, which in turn is determined by factors such as the number of hydrogen bonds, conjugation and resonance effects.

The PCET mechanism has generally received less attention, but has been investigated by some groups.[54] While there is as yet no widely accepted definition of PCET, this term is often applied to mechanisms in which the proton and electron are transferred between different sets of orbitals. This mechanism involves the separate transfer of a proton and an electron, so that first the radical cation is formed and then this is followed by rapid and reversible deprotonation (Scheme 1.7).

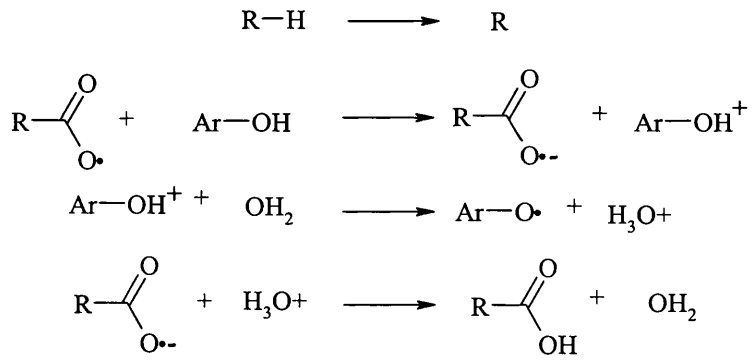

Scheme 1.7: Mechanism for PCET.

The radical cation arising form the electron transfer must be stable, so it does not react with substrate molecule, so the IP is the most significant energetic factor in determining the scavenging activity of the antioxidant. The net result of the two mechanisms is the same, however if the radical cation $ArOH^+$ in the PCET mechanism has sufficient lifetime it can attack substrates and thereby exert mutagenic effects.

Both the HAT and PCET mechanisms have previously been used to describe the chain breaking action of phenolic antioxidants *in vivo* by several different groups of researchers. Svanholm *et al.* have proposed that a first step in the antioxidant activity of tocopherol produces a cation radical by one electron abstraction.[55] However, Burton *et al.* have reported the observation of a substantial deuterium kinetic effect in the reaction of α-tocopherol with peroxyl radicals. From this result they suggested that the rate controlling direct hydrogen atom transfer occurs in the antioxidant activity of tocopherols.[22] Mukai *et al.* have also demonstrated through second-order rate constant measurements that the antioxidant activity of tocopherol compounds relates to the total electron-donating character of the alkyl group substituents on the aromatic ring, indicating the PCET mechanism.[23]

In addition, theoretical studies have indicated that these antioxidants may act *via* a dual mechanism wherein under some conditions one mechanism can predominate over the other, depending on the reactive species and on the medium.[56,57] Fukuzumi *et al.* have demonstrated experimental evidence for this in tocopherol analogues, showing each mechanism to exist for the hydrogen transfer to the DPPH· (1,1-diphenyl-2-piceylhydrazyl) or G· (galvinoxyl) radicals under different solvent conditions.[58,59]

Consideration of all of these prior results suggest that vitamin E analogues might act as antioxidants by a dual mechanism of PCET and HAT. The two mechanisms may occur in parallel and, under some conditions, one mechanism can predominate over the other to some extent depending on the reactive species and on the medium. Thus, further elucidation on this matter is highly desirable.

1.2.6 Proton Transfer *via* a Hydrogen Bond

It is well known that hydrogen bonding facilitates many cases of proton transfer, but the exact relationship is still not clearly understood. Bűrgi and Dunitz first pointed out the similarity between these two distinct events in their study of the OH bond distances in the O-H...O hydrogen bond system.[60] A structure correlation between the lengthening of one O-H bond as the other shortened was found, and considered as a reaction path for a proton transfer reaction. Hence, the hydrogen bond can be generally regarded as an incipient stage of a proton transfer process.[50,,61] This is true for strong hydrogen bonds as well as for weak ones; however, only for strong hydrogen bonds is the stage of proton transfer quite advanced and so do such proton transfer processes occur with significant rates. In considering the hydrogen bond in this way a stable hydrogen bond can be thought of as a "frozen" stage of the proton transfer reaction between the atoms D and A. This means that a partial bond is already established as the D-H is weakened. Hence, it is possible to consider that such hydrogen bonded species represent a form of trapped intermediate in the proton transfer process, and their study may provide information regarding the transition state geometry for a particular proton transfer reaction.

The consideration of hydrogen bonds as the beginning of a proton transfer reaction has proved to be important in the study of antioxidant action. It has become feasible in recent years to carry out high-level electronic structure calculations to obtain accurate geometries and energies of transition states and compute the activation energies, thus allowing the detailed study of reaction profiles. This has been exploited in the study of hydrogen atom transfer reactions for phenolic antioxidants. Liu *et al.* performed density functional calculations on the transition states of monophenols and catechol during H-atom abstraction by a methyl radical.[62]

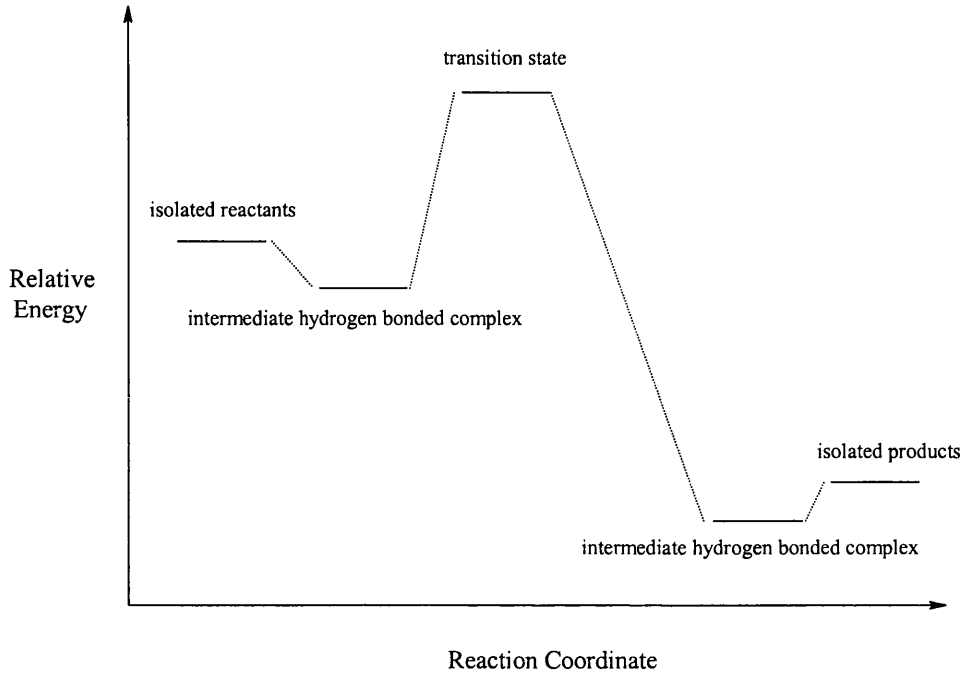

Scheme 1.8: Reaction profiles of $CH_3\cdot$ with monosubstituted phenols and catechols (adapted from reference 62)

The calculation of reaction pathway energy profiles demonstrated that a hydrogen-bonded intermediate is commonly formed from the isolated molecules and methyl radical before the formation of the transition state. Then, in the process of product formation, the hydrogen bonded phenoxyl-methane complex is initially formed before the isolated products are produced (Scheme 1.8).

O'Malley et al. obtained similar reaction pathways through DFT calculations on the hydrogen abstraction from a series of substituted phenols by hydroperoxyl radicals (Scheme 1.9).[63]

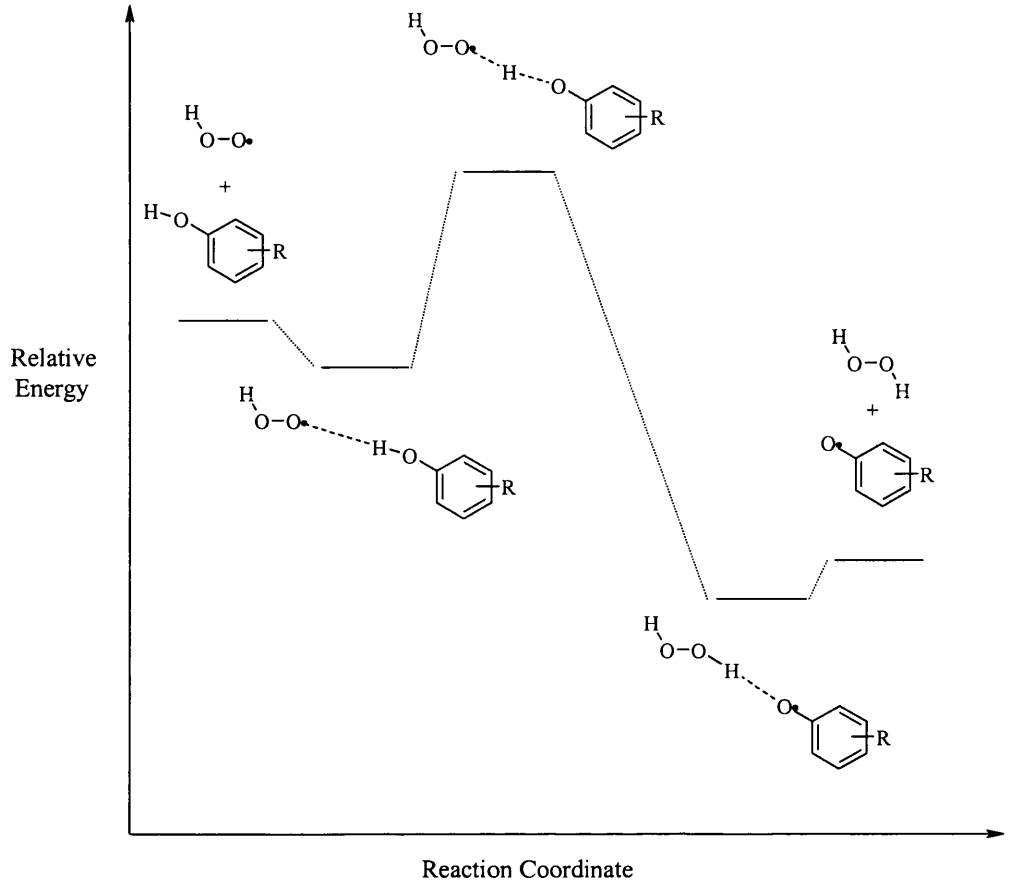

Scheme 1.9: Reaction profiles of the hydrogen transfer reaction to HOO· from monosubstituted phenols (adapted from reference 63)

The geometry of the hydrogen bonded system and the transition state in these computational studies was used to provide insight into the reaction mechanism. From this it may be suggested that the study of experimentally obtained intermediate or transition state geometries will also provide information useful in this regard.

1.3 Hydrogen Bonding

1.3.1 Introduction to Hydrogen Bonding

As the importance of hydrogen bonding in relation to hydrogen transfer has been stated, it is therefore helpful to discuss the nature and context of this important interaction in relation to the work reported herein. Discovered almost 100 years ago, the hydrogen bond is a fundamentally important phenomenon in structural chemistry and biology. It is crucial in determining the structure and function of an extensive range of chemical systems and so has been proved to be amongst the most important non-covalent interactions. The topic consequently still attracts a great deal of interest in diverse fields of the literature.

In biological systems the hydrogen bond is tremendously important as it is responsible for building tertiary and quaternary structures in macromolecules. The bond is weak relative to covalent interactions, allowing rapid association and dissociation of species at ambient temperature, this is a vital prerequisite for biological reactions to take place. Hydrogen bonding also plays a particularly dominant role in the field of supramolecular chemistry, as it is an important interaction for the ordering of molecules in a crystal. The identification of commonly occurring hydrogen bonding motifs, often called synthons, combined with an understanding of the way in which hydrogen bonds control and direct the assembly of molecular architectures allows target crystal packing assemblies to be engineered. The design and synthesis of target architectures is an extremely important concept in crystal engineering, molecular recognition and self-organisation. The widespread importance and applicability of hydrogen bonding illustrate the necessity of developing a greater understanding of the nature and function of relatively weak interactions such as the hydrogen bond.

1.3.2 Fundamental Characteristics

Definition

Today it is recognised that the hydrogen bond is a very broad phenomenon and as yet no definitive description or uniformly applied terminology is agreed upon. Pauling gave one of the earliest definitions of a hydrogen bond:

``Under certain conditions an atom of hydrogen is attracted by rather strong forces to two atoms instead of only one, so that it may be considered to be acting as a bond between them. This is called a hydrogen bond. It is now recognised that [...] the hydrogen bond is largely ionic in character, and is formed only between the most electronegative atoms".[64]

This definition describes the classical view of the hydrogen bond; however it restricts the hydrogen atom to be bound to very electronegative atoms only. It is now known that hydrogen bonding interactions can take place under extremely variable circumstances, including where non-conventional groups such as C-H donors or π-acceptors are involved. A widely accepted definition given by Pimentel and McClellan expands Pauling's description to allow the chemical nature of the atoms involved and their geometry to remain unspecified:

"a hydrogen bond is said to exist when

(1) there is evidence of a bond and

(2) *there is evidence that this bond sterically involves a hydrogen atom already bonded to another atom".*[65]

Steiner has further modified point (2) to require that the donor atom acts as a proton (not electron) donor in order to exclude pure van der Waals bonding contacts and agostic interactions.[66]

The phenomenon arises as a result of the relative electronegativities of the atoms involved. It is a weak association between a hydrogen atom that is covalently bound to one electronegative atom while interacting electrostatically with a second. The electrons in the covalent bond are pulled away from the hydrogen towards the electronegative atom, creating a dipole. In practise the other atoms involved need not be very electronegative, it is sufficient only that the bond is slightly polar. This leaves the hydrogen atom with a partial positive charge so that it will interact with an area of electron density occurring nearby such as another electronegative atom that can donate a lone pair of electrons, or a π-bond.

Parameters and Geometry

In this thesis the two electronegative atoms involved in the hydrogen bonding are termed donor (D) and acceptor (A) atoms and the hydrogen bond is referred to as D-H···A. The usual convention for the representation of the parameters *d* (the H···A distance), D (the D···A distance), θ (the D-H···A angle), ϕ (the H···A-Y angle) and *r* (the D-H distance) is followed here.

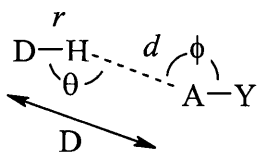

Figure 1.14: Definition of the geometrical parameters *d*, D, θ, ϕ and *r* for a hydrogen bond

Where neutron data is available to provide accurate positions for the hydrogen atoms the parameters *d*, θ and *r* are usually quoted, but where only X-ray data is available it is

common practise to use either hydrogen bond lengths normalised to the standard neutron distance, or to use the parameter D instead of *d*.

It is well established that in addition to simple donor-acceptor interactions hydrogen bonds may involve a donor bonding to more than one acceptor, or likewise an acceptor to multiple donors (Figure 1.15).

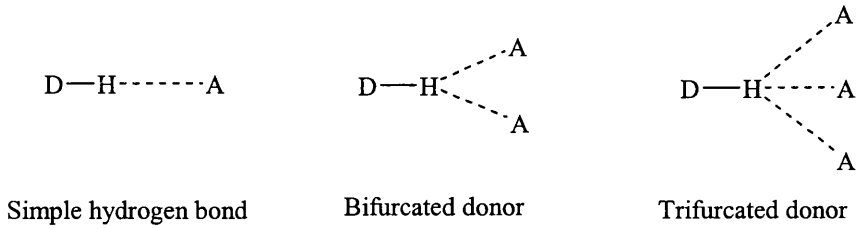

Figure 1.15: Different types of hydrogen configurations

In cases with two or three acceptors this is called a bifurcated or trifurcated hydrogen bond respectively. Likewise, acceptors may form bifurcated or trifurcated bonds by interacting with more than one donor. The combination of one or more of these classes of hydrogen bonds may form networks throughout the extended structure of a crystal in one, two or three dimensions. Hence solid-state structure is determined by the cooperative effects of the hydrogen bonding throughout the whole structure, not just at particular donor and acceptor atoms.

Properties

The nature of the hydrogen bonding interaction is not constant but includes electrostatic, covalent and dispersion contributions in varying weights. As a result individual hydrogen bond energies cover a range of values typically from 0.2 – 40 kcal mol^{-1}, placing them intermediate in strength between other dipole-dipole interactions and strong covalent and

ionic bonds. The strength of the hydrogen bond is generally greater than other similar dipole-dipole interactions due to the small size of the hydrogen atom and the absence of any core electrons. Though individually weak, the cumulative effects of many hydrogen bonds control and direct the structures of molecular assemblies as they are both strong and directional, and even allow compounds that will not crystallise under normal circumstances to crystallise on the inclusion of a hydrogen bonding solvent into the crystal lattice. Hydrogen bonding strength is found to increase with increasing electronegativity of the donor and acceptor atoms; this is due to a greater de-screening of the hydrogen nucleus by the donor and therefore a stronger attraction to the acceptor. Hydrogen bonds are also highly directional. For single component systems the shortest distances occur at relatively linear angles of θ, whereas longer bonds are observed with a larger angular range.

A system of classification of hydrogen bonds has been proposed by Jeffrey[67] which uses the labels weak, moderate and strong to categorise hydrogen bond strengths based upon the nature of the acceptor and donor. However, it should be noted that there is natural overlap in any such classifications. A brief summary of functional groups that typically form hydrogen bonds that fall into these categories is given in Table 1.1 below.

	Typical donors	Typical acceptors
Strong	O^+-H, N^+-H	F^-, O^--H, O^--C, O^-P, N^-
Moderate	O-H, N-H, N(H)-H	O, O=C, N
Weak	C-H, Si-H	C≡C/spC, or an aromatic ring

Table 1.1: Hydrogen bond classifications

Hydrogen bonds classified as "strong" occur between donors strongly deficient in electron density and acceptors with large amounts of electron density. Strong hydrogen bonds are usually linear and cover only a small angular range. In some cases, such as F-H-F$^-$ and O-H-O$^-$, where D is highly electronegative and A has a large excess of electron charge, the proton is not bonded covalently to either D or A. Instead, there is an equal sharing of the hydrogen atom, which is symmetrically placed between the two so D-H ≈ H···A or $r \approx d$.[68]

The interaction with the acceptor in normal (moderate and weak) hydrogen bonds is primarily electrostatic so the hydrogen is always clearly covalently bonded to the donor atom and asymmetrically placed between the donor and acceptor atoms, i.e. D-H < A···H. Normal hydrogen bonds are many times weaker than covalent bonds and so their statistics tend to be more dependent upon the environment in comparison with covalent and the stronger hydrogen bonds. As a result they have a wide spread of bond lengths and angles when observed in the crystalline state where there is a compromise with other packing forces. It is furthermore quite common to see bifurcated interactions in these easily distortable systems. Moderate hydrogen bonds are generally formed by neutral donor and acceptor groups in which the donor atoms are electronegative with respect to hydrogen and the acceptor atoms have unshared lone-pairs of electrons. Of the moderate hydrogen bonds those involving oxygen and nitrogen atoms are particularly important in biological molecules, hence O-H···O interactions are the most studied of all hydrogen bonds and there is a vast array of structural and spectroscopic data available.[57]

Weak hydrogen bonds are formed when the hydrogen atom is covalently bound to an atom only slightly more electronegative relative to hydrogen, or when the acceptor has no lone pairs but has π-electrons, for example C_6H_6 or C≡C. The distance D-H is much less than H···A for weak hydrogen bonds, often greater than the combined van der Waals radii

for the participating atoms. Weak hydrogen bonds with C-H groups as donors have been studied extensively, and the C-H···O hydrogen bond is now a well-established interaction in structural chemistry. [51] When the ability of carbon atoms to act as proton donors in hydrogen bonds was first proposed,[69] it was initially challenged and remained the subject of some controversy for many years. The matter was settled by a study conducted[70] on neutron diffraction results, which revealed statistical evidence that supported the existence of C-H···O hydrogen bonds in crystals.

1.3.3 Hydrogen Bonding Interactions of Radicals

In the study of hydrogen bonding, much emphasis has been given to the study of hydrogen bonds formed between neutral molecules. By comparison, the interaction between radicals and molecules has previously been little studied.[71] This is unsurprising, as a majority of chemical entities are closed-shell, however open-shell hydrogen-bonded systems do exist and play a key role in several fields. In addition to the study of hydrogen abstraction reaction,[72,73] open-shell hydrogen bonds are important in many enzymatic systems[74,75] and in the Earth's atmosphere.[76]

A number of experimental methods, including Electron Spin Resonance (ESR), infrared spectroscopy (IR) and photoelectron spectroscopy (PES) have been used to study open-shell hydrogen bonding interactions. However, because radicals are not generally stable species, experimental structural studies on open-shell hydrogen bonds are fairly difficult to conduct. So, theoretical studies on open-shelled hydrogen bonds remain prevalent in the literature.[77,78]

1.3.4 Co-crystallisation in Supramolecular Synthesis

The design of molecular solids with desired physical and chemical properties forms the basis of the field of crystal engineering and is a major endeavour in current chemistry research.[79,80] Crystal engineering is recognised today as an important form of supramolecular synthesis in which the main forces responsible for holding the molecules together in an ordered supramolecular assembly are non-covalent in nature. However, the cumulative effects of many such interactions are relatively poorly understood, for example it is now known that crystal structures cannot be rationalised and predicted on the basis of strong hydrogen bonding alone, but that weaker interactions can also have a significant effect on determining overall structure. Hence the controlled synthesis of solid-state materials to order in a predictable manner, the ultimate goal of crystal engineering, has proved difficult to achieve. The systematic study of co-crystals gives the opportunity to develop an understanding of the interplay between competing intermolecular interactions, which can later be incorporated into predictive supramolecular synthesis.

A co-crystal is defined as a crystalline material that consists of different molecular (and electrically neutral) species held together by non-covalent forces. The preparation of such multi-component molecular crystals is a supramolecular synthesis, forming non-covalent rather than covalent bonds between molecular components during co-crystallisation. Co-crystallisation is distinct from homomeric crystallisation in a number of ways. Firstly, in contrast to the single component design of motifs in the solid-state, co-crystallisation components are more able to adopt an optimal geometry, leading to a more favourable interaction. Furthermore, heteromeric molecular complexes are only formed by co-crystallisation if the crystal with mixed composition is more stable than that of each pure compound. That is, a co-crystal will be formed only if the non-covalent

forces between the different component molecules are stronger than those between the molecules in the corresponding homomeric crystals.

As a result co-crystals can be difficult to prepare, but known methods for their synthesis are *via* the evaporation of a heteromeric solution or by grinding the two components together.[81,82] In the first case, the two components must have similar solubilities to prevent the least soluble component crystallising as a neat compound, instead of forming a molecular complex. Even if formed in a liquid state, the complex must be stable enough to sustain the crystallisation process. Co-crystals have been previously used in the study of packing patterns, hydrogen-bond motifs and intermolecular forces;[83,84,85] a thorough understanding of which is essential in the controlled design of supramolecular architecture.

1.4 Crystallographic Structure Determination

1.4.1 Crystallography

The work underlying Part I of this thesis is the development of low-temperature techniques for mounting and collecting X-ray diffraction data leading to the crystallographic trapping of transient adducts. So, although single crystal X-ray diffraction studies have come to be generally considered as a routine analysis method, the nature of the study reported herein requires a more comprehensive discussion of diffraction theory and techniques than would otherwise be necessary for other structural studies.

Crystallography is a well-established technique for the determination of the solid-state structure of crystalline materials, even allowing the resolution of individual atoms with sufficiently high-resolution data. An accurate knowledge of molecular structure is a fundamental aim in chemistry as it is important both for identification purposes and for elucidating three-dimensional geometry, which may be required for investigations into reactivity, bonding or energy relationships. In particular the relationship between structure and property is an area that has received much interest, since an understanding of the nature of this relationship allows the directed development of compounds that exhibit desired properties. The most common experimental technique used is single crystal X-ray crystallography. The method involves the interpretation of a pattern obtained from X-rays diffracted through a lattice of identical molecules to give a map of the molecular electron distribution of electrons in the crystal. If single crystals are unavailable it is possible to use a powder sample where a micro-crystalline sample is used. In addition to this particles such as neutrons and electrons are also diffracted by molecular species and may be used instead of X-rays.

The theory and practice of the varied crystallographic techniques are discussed extensively in a number of texts.[86,87,88,89] While a full, detailed discussion behind crystallography and diffraction lies outside the scope of this thesis, the following section will cover a brief description of the relevant aspects as pertaining to the work described in this thesis.

1.4.2 Diffraction

Crystallography uses the property of diffraction, a wave-like interaction between radiation and matter, to probe solid-state structure. It is well known that the diffraction of visible light on passing through a grating occurs when the spacing of the slits approaches the wavelength of the light, giving rise to a pattern of dark and light areas. The openings in the grating each act as a source of radiation and the waves, with their varying relative phases, interfere with each other to create a diffraction pattern. Any regularly spaced arrangement of objects can act as a diffraction grating for radiation with a wavelength comparable to that of the spacing, so in order to use diffraction to look at atoms and bonds radiation of a wavelength on the atomic scale (10^{-10} m = 1 Å) is required. It occurs that, for crystals, the inter-molecular spacing is comparable to the wavelengths of X-rays (λ), which range from hard UVs (10^{-8} m $\approx$100 Å) to gamma rays (10^{-12} m $\approx$0.1 Å).[86] However, it is also possible to use suitably energetic electrons or neutrons as an alternative radiation source for studying crystalline structure.

A crystal was first successfully used as a diffraction grating for X-rays in 1912 by Max von Laue, demonstrating both the wave-like properties of X-rays and the suitability of the X-ray wavelength for studying inter-atomic distances. X-rays are scattered by the electron clouds associated with the atoms in the structure and, since electrons are in general localised tightly around the nuclei, the location of the electron density provides a

useful model of the atomic positions within a molecule. However, since hydrogen atoms possess only one electron they scatter X-rays very weakly, for this reason they are rarely resolved by X-ray diffraction methods.

On the irradiation of a crystal X-rays are diffracted from the electron clouds making each of the atoms a weak, secondary source of waves propagating in all directions. The diffracted beams of X-rays interfere with each other constructively in some directions to reinforce the wave, and destructively in others to reduce the wave. The result is that the diffraction pattern from a crystal is a regular three-dimensional array of spots of varying intensity, with the position and intensities of these diffracted X-ray beams holding information on the structure of the crystal from which they have been diffracted. This array of diffraction spots, the diffraction pattern, is related to the crystal system that generated it by an inverse relationship and so is called the reciprocal lattice.

In a diffraction experiment the direction and intensity of each of the scattered X-rays are measured and then processed, using a Fourier transformation, to calculate an electron density map of the crystal. From this map it is possible to deduce the type and positions of the atoms and thereby obtain a complete geometrical description of the crystal structure.

1.4.3 Crystal Symmetry

An understanding of the symmetry within crystalline materials is essential in solving a diffraction pattern, as it is the translation symmetry in crystalline materials that enables the diffraction pattern to be interpreted as a reciprocal lattice. The atoms and molecules in a single crystal are arranged in an essentially infinitely repeating pattern; the smallest division of the crystal that, on translation in three-dimensions, can generate the complete

crystal structure is called the unit cell. In many cases the unit cell contains several fragments or molecules that are all related to each other by symmetry. The unique fragment from which the complete structure is generated is known as the asymmetric unit, and performing symmetry operations on this fragment generates the unit cell.

The unit cell is defined by its three non-coplanar axes **a**, **b** and **c** and the inter-axial angles α, β and γ. Any one crystal will contain a choice of unit cells, but by convention a cell is chosen which displays all the rotational and translational symmetry of the lattice, it also usually has short axial lengths and angles close to 90° for convenience. There are seven basic shapes for unit cells that depend on whether or not the edges are equal and the angles are 90°, these correspond to the seven crystal systems (Table 1.2).

A useful construction is the concept of a crystal lattice, which is a hypothetical lattice based on the unit cell selected. It is obtained by selecting any point in a crystal and joining it to identical points in surrounding unit cells, it is usually the edges of the unit cell that are taken to form the crystal lattice. There are four lattice types possible; the basic lattice for each crystal system is primitive (P) and by the addition of face or body centering there are then 3 variants of this primitive lattice C-face centered (C), body-centered (I) and face-centered (F). Taken together the seven crystal systems and four lattice types give 14 possible combinations called the Bravais Lattices, these are shown in the following table (Table 1.2) with the minimum symmetry of each, and the conventions for unit cell choice and axis naming.

Crystal System	Bravais Lattice	Parameters	Symmetry
Triclinic	P	$a\neq b\neq c$; $\alpha\neq\beta\neq\gamma$	None
Monoclinic	P, C	$a\neq b\neq c$; $\alpha=\gamma=90^\circ$; $\beta\neq 90^\circ$	Mirror (or glide) plane or a 2-fold axis
Orthorhombic	P, I, F	$a\neq b\neq c$; $\alpha=\beta=\gamma=90^\circ$	Any three mutually perpendicular 2-fold axes or mirror (or glide) planes
Tetragonal	P, I	$a=b\neq c$; $\alpha=\beta=\gamma=90^\circ$	One 4-fold axis
Trigonal	P, R	$a=b=c$; $\alpha=\beta=\gamma\neq 90^\circ$	One 3-fold axis
Hexagonal	P	$a=b\neq c$; $\alpha=\beta=90^\circ$; $\gamma=120^\circ$	One 6-fold axis
Cubic	P, F, I	$a=b=c$; $\alpha=\beta=\gamma=90^\circ$	Four 3-fold axis

Table 1.2: The parameters of the seven crystal systems.

It should be noted that while, for example, a triclinic cell could happen to have α and γ close to 90°, this does not mean that the structure is monoclinic as the appropriate symmetry would not be present.

The combination of the 14 Bravais Lattices with all of the symmetry elements possible in three-dimensional space generates a total of 230 arrangements, known as space groups, which describe all the possible ways of arranging identical points in a repeating, three-dimensional lattice structure. The space group of a crystalline material can be deduced by observing absences in the diffraction pattern. In some positions in the diffraction pattern where there might be expected to be a peak by geometry, the intensity of the diffracted beam is zero and the reflection is absent. These are termed systematic absences and are a result of destructive interference from planes related by symmetry operations involving translations (Bravais centerings, glides and screw axes) causing extinctions in certain classes of reflections in the diffraction pattern. Centering causes absences throughout the entire data set, whereas glide planes and screw axes cause absences in specific sub-sets of

the data. Hence the symmetry in a lattice can be deduced from the diffraction pattern by examination of absences in the diffraction data.

1.4.4 Diffraction From 3-Dimensional Crystals

An extremely powerful way to describe the geometry, but not the intensity, of diffraction is using *Bragg's law.* This was derived by W.L. Bragg to provide a simple, geometrical explanation for the directional features observed in a diffraction pattern and allow the interpretation of these patterns. However, it does not represent the actual physics of diffraction, but is a model used to describe the events observed.

Bragg considered diffraction from a crystal as the reflection of an X-ray beam from atoms lying in a series of planes, the imaginary planes of the crystal lattice. On irradiation, X-ray beams diffracted from successive planes interfere with each other and a diffraction spot, also known as a reflection, is only observed when these scattered waves are in phase with each other and interfere constructively. This only occurs for those scattered waves for which the angle of reflectance is equal to the angle of incidence, since two waves scattered from particles in adjacent planes are only in phase if the difference in path length between them equals an integral number of wavelengths of the radiation employed (Figure 1.16).

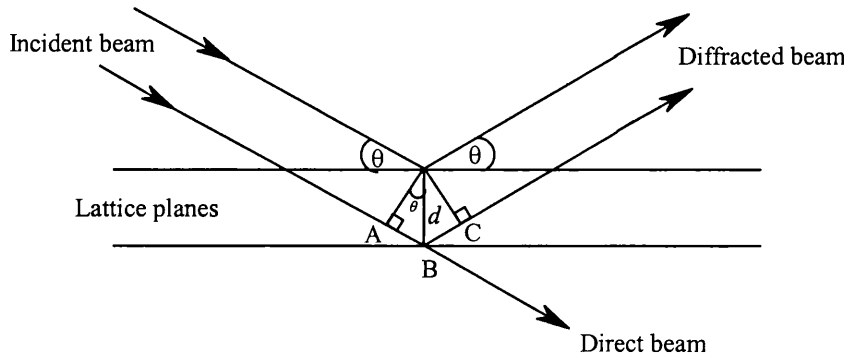

Figure 1.16: Scattering from multiple planes

This relationship for rays reflected by two adjacent planes where the path difference (AB + BC), which by geometry is equal to $2d_{hkl}\sin\theta$ is normally expressed as:

$$n\lambda = 2d\sin\theta$$

Equation 1.1

Where λ the wavelength of the incident radiation, d is the spacing between the lattice planes and θ is the angle of incidence. Rearrangement of this equation shows that the lattice spacing d is inversely related to the angle of reflectance, θ, showing the reciprocal nature of the geometrical relationship between a crystal lattice and its diffraction pattern.

The sets of reflecting planes associated with each diffracted beam are called Miller planes and can be identified by their Miller indices *hkl*. Each reflection is also labelled by the three indices *hkl*, indicating the plane in the reciprocal lattice from which it originated. The indices are obtained by taking the fractional coordinates at which the Miller plane intersects the unit cell axis, inverting and then clearing the fractions.

Bragg's Law demonstrates that the directions of the diffracted beams are determined by the crystal lattice spacings, so the shape and size of the unit cell can be deduced from the scattering angle of the diffracted beams. However, the Bragg model does not explain the observed variation in the intensities of reflections; some are strong while others are weak, or even absent. The intensities of the different scattered beams contains information about atoms within the unit cell as the relative intensities of the reflections are related to the arrangement and identities of the atoms in the unit cell by a Fourier transformation.

Each reflection *hkl* is described in amplitude ($|F_{hkl}|$) and phase ($\exp[i\phi(hkl)]$) by the structure factor F_{hkl} (equation 1.2).

$$F_{hkl} = |F_{hkl}| \cdot \exp[i\phi(hkl)]$$

Equation 1.2

The structure factor is a measure of the combined scattering of all the atoms in the unit cell that makes up a reflection. Since the radiation scattered by one atom will interfere constructively or destructively with radiation scattered by other atoms in the unit cell, each reflection *hkl* contains information about the entire unit cell. For this reason it is necessary to determine the structure factor for all reflections *hkl*, then a Fourier transform can be used to calculate the electron density in the unit cell (Equation 1.3).

$$\rho(xyz) = 1/V \sum_{hkl} |F_{hkl}| \exp[i\varphi(hkl)]\exp[-2\pi i(hx + ky + lz)]$$

Equation 1.3

As the observed intensity I_{hkl} of diffraction spots is proportional to the structure factor $|F_{hkl}|^2$, it is possible to obtain $|F_{hkl}|$ experimentally by measuring peak intensities; however the corresponding phase is not directly measurable. This gives rise to one of the most fundamental problems in crystallography: the phase problem. Both the phase and amplitudes are necessary in order to calculate an electron density map using a Fourier transformation, but it is only experimentally possible to obtain the amplitude of the reflection.

In order to solve a crystal structure a technique for obtaining the approximate phases of the X-ray reflections must be applied in order to overcome the phase problem. A number of methods have been developed for this purpose. One of the most commonly used in small molecule crystallography is using *Direct Methods*, which makes the assumption

that electron density can never be negative, and is evenly distributed throughout the unit cell and is close to zero except at the positions of atoms. Alternatively the *Patterson Method* uses the presence of large atoms, which dominate the scattering, to correctly assign the phases.

1.4.5 Structure Determination

In order to solve a crystal structure, the data is first converted from intensities to observed structure factor amplitudes (F_o). The relationship between intensity and the structure factor amplitude is affected by several factors that vary from reflection to reflection. So once the intensity of a Bragg reflection has been measured it must be corrected during this data reduction by some values that take these factors into account (Equation 1.4).

$$|F_{hkl}| = I_{hkl}(K\ L\ p\ A)$$

Equation 1.4

|F(hkl)|, the structure amplitude, is the amplitude of the diffracted wave measured relative to the amplitude of scattering of a single electron, which is taken as unity at $\sin\theta = 0$, and K is a scale factor. The Lorentz factor, L, takes into consideration how long each set of lattice planes was in the reflecting position, and it depends on the technique used for data collection. The polarisation factor p originates from the fact that the variation of the reflection efficiency of X-rays with the scattering angle depends on the state of polarization of the incident beam. Finally the transmission factor A takes into account the reduction of the intensity due to absorption of X-rays by the crystal.

The first stage in the analysis of diffraction data from a crystal is indexation of the diffraction pattern, this involves determination of the unit cell dimensions and the identification of any symmetry elements present to give the space group. The next step is

to generate a trial structure using one of the methods outlined above (Section 1.4.4), which can then be refined. Once a suitable trial structure has been found, the calculated diffraction intensities for this structure can be compared with the observed ones. The process of structure refinement adjusts and refines this starting model to obtain the best fit to the experimental data. The refinement process uses an iterative mathematical method known as least-squares analysis, during every refinement new atoms may be added to the structure or changes made to existing ones to see how this affects the agreement with the observed data. In a least squares refinement an error function M defined as the sum of the squares of discrepancies between observation and calculation is minimised by adjustment of the parameters of the trial structure (Equation 1.5).

$$M = \Sigma w(|F_o| - |F_c|)^2$$

Equation 1.5

Δ_i is usually either $|F_o|_i - |F_c|_i$ or $F_{o,i}^2 - F_{c,I}^2$ and each reflection has a weight w_i and n is the number of reflections and m is the number of parameters. Over many cycles of refinement the most accurate fit between model and the experimental data is achieved. The final model obtained has to be assessed for its correctness against the experimental data, the main indicating factors of the quality of a structure solution is the *R factor, R_1,* and the *weighted R factor, wR_2,* and these are usually quoted as percentages:

$$R_1 = \Sigma||F_o| - |F_c|| \,/\, \Sigma|F_o|$$

Equation 1.6

$$wR2 = \Sigma_i \, w_i\Delta_i^2/\Sigma w_i F_{o,i}^2$$

Equation 1.7

Where F_c is the calculated structure factor and F_o the observed structure factor. A low R factor indicates a good fit of the calculated model to the observed data. R_1 usually drops throughout refinement to 5% or lower for a good structure determination, rising to about 7% as the highest acceptable for publication. A further guide to the quality of a structure solution is the size of the estimated standard deviations (e.s.d.s) on the atomic positions and bond parameters. The goodness of fit or Goof, S, is also quoted and should be close to 1 if the weighting scheme is appropriate (Equation 1.8).

$$S = (\Sigma_i w_i \Delta_i^2) / (n-m)^{1/2}$$

Equation 1.8

In addition to adequate R parameters and Goof a completed refinement should sufficiently model all electron density, so there should be no 'significant' features, peaks or holes, in the electron density map.

1.4.5 References

[1] Wright, J.S. *Chem. Brit.* **2003**, *39* (2), 25.
[2] Scott, G., ed. *Atmospheric Oxidation and Antioxidants*, Elsevier: New York, **1965**.
[3] Ranney, M.W. *Antioxidants Recent Developments*, Chemical Technology Review No. 127, Noyes Data Corporation, **1979**.
[4] Sies, H. *Angew. Chem. Int. Ed. Engl.* **1986**, *25*, 1058.
[5] Halliwell, B. *FASEB J.* **1987**, *1*, 1358.
[6] Holvoet, P.; Collen, D. *FASEB J.* **1994**, *8*, 1279.
[7] Scott, G. *Chem. Brit.* **1995**, *31* (11), 879.
[8] Esterbauer, H.; Cheeseman, K.H. *Chem. Phys. Lipids,* **1987**, *45*: 103.
[9] Ingold, K.U. *Acc. Chem. Res.* **1969**. *2*, 1.
[10] Porter, N.A. *Acc. Chem. Res.* **1986**, *19*, 262.
[11] Mead, J.F. In *Free Radicals in Biology Volume1;* Prior, W.A., Academic Press, New York, **1976**; Chapter 2, pp 51.
[12] Ingold, K.U. *Acc. Chem. Res.* **1961**. *61*, 563.
[13] Mahoney, L.R. *Angew. Chem. Int. Ed. Engl.* **1969**, *8*, 547.
[14] Wright, J. S.; Johnson, E. R.; DiLabio, G. A. *J. Am. Chem. Soc.* **2001**, *123*, 1173-1183.
[15] Tanaka, K.; Sakai, S.; Tomiyama, S.; Nishiyama, T.; Yamada, F. *Bull. Chem. Soc. Jpn.* **1991**, *64*, 2677.
[16] Wayner, D.D. M.; Lusztyk, E.; Page, D.; Ingold, K.U.; Mulder, P.; Laarhoven, L.J.J.; Aldrich, H.S. *J. Am. Chem. Soc.* **1995**, *117*, 8737 and references therein.
[17] Mulder, P.; Korth, H.-G.; Pratt, D.A.; DiLabio, G. A.; Valgimigli, L.; Pedulli, G.F.; Ingold, K.U. *J. Phys. Chem. A.* **2005**, *109*, 2647 and the references therein.
[18] Wright, J.S.; Johnson, E.R.; DiLabio, G.A. *J. Am. Chem. Soc.* **2001**, *123*, 1173.
[19] Pratt, D.A.; DiLabio, G.A.; Brigati, G.; Pedulli, G.F.; Valgimigli, L. *J. Am. Chem. Soc.* **2001**, *123*, 4625.
[20] Zhang, H.-Y.; Sun, Y.-M.; Wang, S.-L. *Chem. Eur. J.* **2003**, *9*, 502.
[21] Gotoh, G.; Noguchi, N.; Tsuchiya, J.; Morita, K.; Sakai, H.; Shimasaki, H.; Niki, E. *Free Radical Res.* **1996**, *24*, 123.
[22] Burton, G.W.; Doba, T.; Gabe, E.J.; Hughes, L.; Lee, F.L.; Prasad, L.; Ingold, K.U. *J. Am. Chem. Soc.* **1985**, *107*, 7053.
[23] Mukai, K,; Fukuda, K.; Tajima, K.; Ishizu, K. *J. Org. Chem.* **1988**, *53*, 430.
[24] Burton, G.W.; Ingold, K.U. *Acc. Chem. Res.* **1986**, *19*, 194.
[25] Brigelius-Floḥé, R.; Traber, M.G. *FASEB J.* **1999**, *13*, 1145
[26] .Niki, E.; Noguchi, N. *Acc. Chem. Res.* **2004**, 37(1) 45.
[27] Nagaoka, S.; Sawada, K.; Fukumoto, Y.; Nagashima, U.; Katsumata, S.; Mukai, K. *J. Phys. Chem.* **1992**, *96*, 6663.
[28] Nagaoka, S.; Inoue, M.; Nishioka, C.; Nishioku, Y.; Tsunoda, S.; Ohguchi, C.; Ohara, K.; Mukai, K.; Nagashima, U. *J. Phys. Chem. B* **2000**, *104*, 856.
[29] Scott, G. *Chem. Brit.* **1995**, 879.
[30] Bisby, R.H.; Parker, A.W. *Arch. Biochem. Biophys.*, **1995**, *317*, 170.
[31] Mukai, K.; Ohbayashi, S.; Nagaoka, S.; Ozawa, T.; Azuma, N. *Bull. Chem. Soc. Jpn.* **1993**, *66*, 3808.
[32] Burton, G.W.; Le Page, Y.; Gabe, E.J.; Ingold, K.U. *J. Am. Chem. Soc.* **1980**, *102*, 7792.
[33] Burton, G.W.; Ingold, K.U. *J. Am. Chem. Soc.* **1981**, *103*, 6472.
[34] Burton, G.W.; Hughes, L.; Ingold, K.U. *J. Am. Chem. Soc.* **1983**, *105*, 5950.
[35] Doba, T.; Burton, G.W.; Ingold, K.U. *J. Am. Chem. Soc.* **1983**, *105*, 6505.
[36] Migliavacca, E.; Carrupt, P-A.; *Testa, B. Helv. Chim. Acta,* **1997**, *80*, 1613.
[37] MacFaul, P.A.; Ingold, K.U.; Lusztyk, J. *J. Org. Chem.* **1996**, *61*(4), 1316.
[38] Lucarini, M.; Pedrielli, P.; Pedulli, G.F.; Cabiddu, S.; Fattuoni, C. *J. Org. Chem.* **1996**, *61*(26), 9259.
[39] Brigati, G.; Lucarini, M.; Mugnaini, V.; Pedulli, G.F. *J. Org. Chem.* **2002**, *67*(14), 4828.
[40] Blanksby, S.J.; Ellison, G.B. *Acc. Chem. Res.* **2003**, *36*, 255.
[41] Vojdani, A.; Bazargan, M.; Vojdani, E.; Wright, J. *Cancer Detect. Prev.* **2000**, *24*(6), 508.
[42] Mercury image for compound refcode MOPHLB from November 2004 CSD.
[43] Watanabe, a.; Noguchi, N.; Fujisawa, A.; Kodama, T.; Tamura, K.; Cynshi, O.; Niki, E. *J. Am. Chem. Soc.* **2000**, *122*, 5438.
[44] Torel, J.; Cillard, J.; Cillard, P. *Phytochemistry* **1986**, *25*(2), 383.

[45] Sichel, G.; Corsaro, C.; Scalia, M.; Dibilio, A.J.; Bonomo, R.P. *Free Radical Bio. Med.* **1991**, *11*(1), 1.
[46] Jovanovic, S.V.; Steenken, S.; Tosic, M.; Marjanovic, B.; Simic, M.G. *J. Am. Chem. Soc.* **1994**, *116*, 4846.
[47] Jovanovic, S.V.; Steenken, S.; Hara, Y.; Simic, M.G. *J. Chem. Soc., Perkin Trans. 2* **1996**, 2497.
[48] de Heer, M.I.; Mulder, P.; Korth, H.G.; Ingold, K.U.; Lusztyk, J. *J. Am. Chem. Soc.* **2000**, *122*, 2355.
[49] Nagaoka, S.; Kuranaka, A.; Tsuboi, H.; Hagashima, U.; Mukai, K. *J. Phys. Chem.* **1992**, *96*, 2754.
[50] Evans, C.; Scaiano, J.C.; Ingold, K.U. *J. Am. Chem. Soc.* **1992**, *114*, 4589.
[51] Wright, J.S.; Johnson, E.R.; Di Labio, G.A. *J. Am. Chem. Soc.*, **2001**, *123*, 1173.
[52] Leopoldini, M.; Marino, T.; Russo, N.; Toscano, M. *J. Phys. Chem. A*, **2004**, *108*, 4916.
[53] Leopoldini, M.; Pitarch, I.P.; Russo, N.; Toscano, M. *J. Phys. Chem. A*, **2004**, *108*, 92.
[54] Zhang, H.; Sun, Y.; Wang, X. *J. Org. Chem.* **2002**, *67*, 2709.
[55] Svanhokm, U.; Bachgaard, K.; Parker, V. *J. Am. Chem. Soc.*, **1974**, *96*, 2409.
[56] Migliavacca, E.; Carrupt, P.-A.; Testa, B. *Helv. Chim. Acta.* **1997**, *80*, 1613.
[57] Wright, J.S.; Johnson, E.R.; DiLabio, G.A. *J. Am. Chem. Soc.* **2001**, *123*, 1173.
[58] Nakanishi, I.; Fukuhara, K.; Shimada, T.; Ohkubo, K.; Iizuka, Y.; Inami, K.; Mochizuki, M.; Urano, S.; Itoh, S.; Miyata, N.; Fukuzumi, S. *J. Chem. Soc., Perkin Trans.* **2002**, *2*, 1520.
[59] Nakanishi, I.; Kawashima, T.; Ohkubo, K.; Kanazawa, H.; Inami, K.; Mochizuki, M.; Fukuhara, K.; Okuda, H.; Ozawa, T.; Itoh, S.; Fukuzumi, S.; Ikota, N. *Org. Biomol. Chem.*, **2005**, *3*, 626.
[60] Bűrgi, H.-B.; Dunitz, J.D. *Acc. Chem. Res.* **1983**, *16*, 153.
[61] Desiraju, G.R.; Steiner, T. *The Weak Hydrogen Bond In Structural Chemistry and Biology*, IUCr Monographs on Crystallography; Oxford Science Publications, Oxford University Press, New York, **1999**; pp21.
[62] Sun, Y.-M.; Liu, C.-B. *Eur. J. Org. Chem.* **2004**, 120.
[63] Singh, N.; O'Malley, P.J.; Popelier, P.L.A. *Phys. Chem. Chem. Phys.* **2005**, *7*, 614.
[64] Pauling, L. *The Nature of the Chemical Bond*, 3rd Edition, Cornell University Press, New York, **1960**.
[65] Pimentel, G.C.; McClellan, A.L. *The Hydrogen Bond*, Freeman, San Francisco, **1960**.
[66] Steiner, T. *Angew. Chem. Int. Ed. Engl.* **2002**, *41*(1), 49.
[67] Jeffrey, J.A. *Introduction to Hydrogen Bonding,* University Press, Oxford, **1997**.
[68] Emsley, J. *J. Chem. Soc. Rev.* **1980**, *9*, 91.
[69] Sutor, J.D. *Nature*, **1962**, *195*, 68.
[70] Taylor, R.; Kennard, O. *J. Am. Chem. Soc.* **1982**, *104*, 5063.
[71] Francisco, J.S. *Angew. Chem., Int. Ed.* **2000**, *39*, 4570.
[72] Espinosa-Garcia, J. *J. Am. Chem. Soc.* 2004, 126, 920.
[73] Ramirez-Arizmendi, L.E.; Heidbrink, J.L.; Guler, L.P.; Kenttaemaa, H.I. *J. Am. Chem. Soc.* **2003**, *125*, 2272.
[74] De Visser, S.P.; Shaik, S.J. *J. Am. Chem. Soc.* **2003**, *125*, 7413.
[75] Grimaldi, S.; Ostremann, T.; Weiden, N.; Mogi, T.; Miyoshi, H.; Ludwig, B.; Michel, H.; Prisner, T.F.; MacMillan, F. *Biochemistry*, **2003**, *42*, 5632.
[76] Leopold, K.R.; Canagaratna, M.; Phillips, J.A. *Acc. Chem. Res.* **1997**, *30*, 57.
[77] Qi, X.-J.; Liu, L.; Fu, Y.; Guo, Q.-X. *Structural Chemistry.* **2005**, *16*(3), 347.
[78] Parreira, R.L.T.; Galembeck, S.E. *J. Am. Chem. Soc.* **2003**, *125*, 15614..
[79] Lehn, J.-M. *Supramolecular Chemistry: Concepts and Perspectives*, VCH, Weinheim, **1995**.
[80] Desiraju, G.R. *Crystal Engineering. The Design of Organic Solids*, Materials Science Monographs 54, Elsevier, Amsterdam, **1987**.
[81] Etter, M.C. Adsmond, D.A. *J. Chem. Soc. Chem. Commun.* **1990**, *8*, 589.
[82] Pedireddi, V.R.; Jones, W.; Chorlton, A.P.; Docherty, R. *J. Chem. Soc. Chem. Commun.* **1996**, *8*, 987.
[83] Aakeröy, C.B.; *Acta Crystallogr.* **1997**, *B53*, 569.
[84] Desiraju, G.R. *J. Chem. Soc. Chem. Commun.* **1997**, 1475.
[85] Etter M.C.; Baures, P.W. *J. Am. Chem. Soc.* **1988**; *110*, 639.
[86] Stout, G.H.; Jensen, L.H. *X-ray Structure Determination – A Practical Guide.* , 2nd edition, Wiley, New York, **1989**.
[87] Hukins, D..L. *X-ray Diffraction By Disordered and Ordered Systems.* Pergamon Press; Oxford, **1981**.
[88] Wormald, J. *Diffraction Methods.* OUP, Oxford, **1973**.

[89] Clegg, W. *Crystal Structure Determination.* OUP, Oxford, **1998**.

Chapter 2

Monophenolic Hydrogen-Bonded Radical Adducts

2.1 Background

Antioxidants are the subject of a great deal of interest in the literature due to their involvement in important biological and industrial processes. Attention has recently been focused on the elucidation of the details of the hydrogen atom abstraction mechanism by which chain-breaking antioxidants operate. Phenols, including vitamin E derivatives, represent the major class of natural and synthetic chain-breaking antioxidants known and are the most widely studied. Indeed, they have been extensively examined by both experimental and theoretical means. The improvement in understanding of the reactivity and action of these species is part of an ongoing objective within the field to develop more active analogues of these antioxidants.

This chapter is concerned with a study of the hydrogen bonding interactions that occur between the stable aminoxyl radical 2,2,6,6,-tetramethylpiperidine-*N*-oxyl (TEMPO) and a range of monophenolic hydrogen bond donors, in order to probe the hydrogen abstraction process. The synthesis and subsequent characterisation by X-ray diffraction techniques of a series of such hydrogen bonded adducts are reported herein. Before this a brief review of the literature on the utilisation of the TEMPO radical and on known hydrogen-bonded adducts, particularly those containing open-shell interactions will be discussed.

In order to model the interaction of antioxidant species with radicals the radical TEMPO is used as it is isoelectronic with the peroxyl radical, a radical commonly encountered that causes oxidative damage in nature (Chapter 1.2.3). TEMPO is an archetype of the

dialkylnitroxyl class of radicals that are stable (persistent) and non-conjugating. The high stability of this class of radicals is accounted for by the delocalisation of the unpaired electron over the nitrogen-oxygen bond (Figure 2.1).

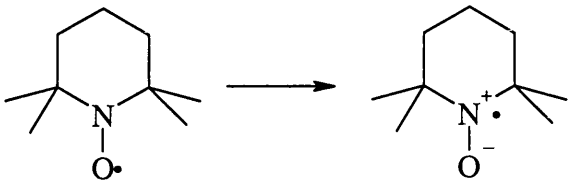

Figure 2.1: Delocalisation of unpaired electron over nitrogen-oxygen bond.

As a result, stable nitroxyl radicals have found important applications in diverse fields. These include its use in oxidation processes,[1,2,3,4,5] as a spin-label in the study of complex chemical environments,[6,7,8] as a mediator in living free radical polymerisation,[9,10] and as a ligand in a number of transition metal complexes in the search for new molecular magnets.[11] In addition, TEMPO has previously been used in the mechanistic study of other radical reactions.[12,13]

The intrinsic reactivity of TEMPO with phenols is illustrated by a consideration of the relative O-H BDEs. As the O-H BDE values in the great majority of phenolic compounds are in the range 80-90 kcal mol^{-1} [14] and the experimentally determined O-H BDE value of TEMPO is 69.6 kcal mol^{-1} [15] therefore the actual abstraction of H-atoms from phenolic compounds by TEMPO is not favoured. Based on this it can be expected that the hydrogen bonded structure obtained is representative of an intermediate stage in the hydrogen abstraction process. This can be illustrated by the reaction profile proposed previously by other authors[16,17] for the hydrogen atom abstraction from phenols by radicals (Figure 2.2).

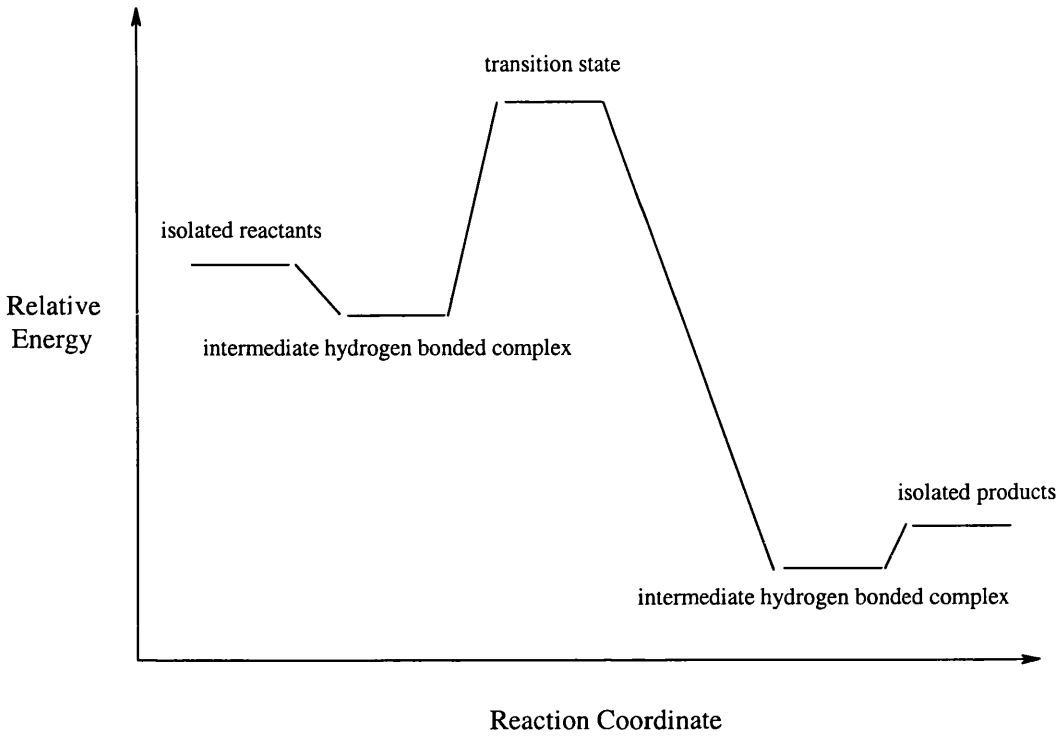

Figure 2.2: Proposed reaction scheme for hydrogen abstraction.

This hydrogen-bonded intermediate provides an experimentally obtained model for hydrogen abstraction in antioxidant action.

It is well known that intermolecular interactions such as hydrogen bonding also largely determine supramolecular organisation. Due to the current interest in the field of crystal engineering on the purposeful design of such interactions into solid-state structures, the impact of specific intermolecular interactions on solid-state structures is widely studied. There has been considerable interest in developing an understanding of the interplay between different competing hydrogen bonding schemes in a variety of systems. A detailed understanding of this relationship and of the stabilisation energy provided by the intermolecular interactions in such molecular crystals provides knowledge which can be extrapolated to create synthetic strategies that include the deliberate design of specific interactions into a given structure. The preparation of multi-component molecular

complexes (co-crystals) offers a method for investigating the way in which forces such as these influence solid-state structure.

There are many previous X-ray crystallographic studies on multi-component crystals in the literature. While this includes diverse examples of co-crystals involving phenols with various hydrogen bonding acceptors,[18,19,20] the co-crystallisation of phenols with TEMPO, or indeed any radical species, has not been previously reported. There are a number of structures published for mono-component crystal systems of TEMPO and other nitroxyl radicals.[21,22] Considering the extensive physical and theoretical studies it is surprising how little structural work there is in the literature on open-shell hydrogen bonds. Recent interest in the solid-state structures of nitroxide radicals has instead focused on their potential as organic-based molecular magnets. In this context, a number of hydrogen-bonded nitroxides have been characterised by X-ray crystallography.[23,24,25,26] In addition, there have been numerous examples of spectrochemical investigation of hydrogen bonds involving nitroxide radicals. IR,[27] EPR[28] and ^{13}C NMR[29] have all previously been used to investigate the nature and strength of open-shell hydrogen bonds formed in solution by TEMPO and its derivatives.

Our group previously performed the synthesis and characterisation of the first ever reported binary co-crystal involving TEMPO, with a tris-phenol system based on BHT.[30] It was formed by co-crystallisation from a toluene solution at minus 30° C under inert conditions and was characterised by neutron diffraction in order to accurately find the hydrogen atoms. The salient features of this structure are the presence of three geometrically different, but similarly short, O-H···O hydrogen bonds. A secondary interaction between an *ortho*-aryl hydrogen atom and the TEMPO oxygen was also observed. EPR on the product also showed that the spin density of the hydrogen-bonded species in solution remains primarily on the TEMPO moiety.

This chapter deals with an extension of this original concept to build up a series of hydrogen-bonded adducts of TEMPO with a range of simple monphenols, in which the steric bulk of the *ortho*-aryl substituents is systematically varied. The series of phenols studied in this chapter are shown below (Figure 2.3).

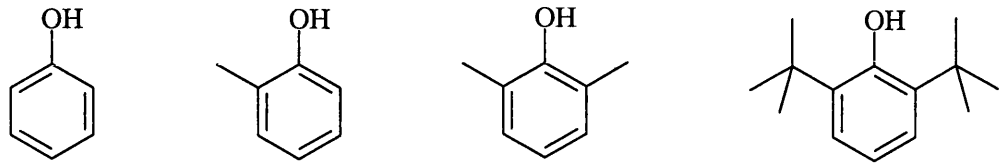

Figure 2.3: Phenols for multi-component adducts.

This study found that in order to crystallise and structurally characterise simple adducts of TEMPO with phenols special techniques are required since many melt below room temperature. The X-ray diffraction analysis of materials that melt below room temperature is quite rare due to the practical difficulties in obtaining diffraction data from such materials. Improvements in equipment, techniques for mounting and *in situ* crystal growth have allowed the single crystal X-ray diffraction analysis of low-melting single component materials to become more common. However, there are few such analyses on low-melting multi-component materials. The low temperature requirements complicate the synthesis and solid state characterisation of multi-component crystals, even for many of the simplest molecules. As a consequence, studies of co-crystalline molecular materials have, to date, generally been restricted to those that are solid under ambient conditions. One exception is the *in-situ* growth of co-crystals of pyrazine with *n*-alkyl carboxylic acids on the diffractometer.[31] The melting points for these co-crystals range from 240-282 K.

In order to overcome the problems of handling low-melting co-crystals, the crystals used for X-ray analysis reported herein were selected and mounted using the low-temperature setup shown below (Figure 2.4).

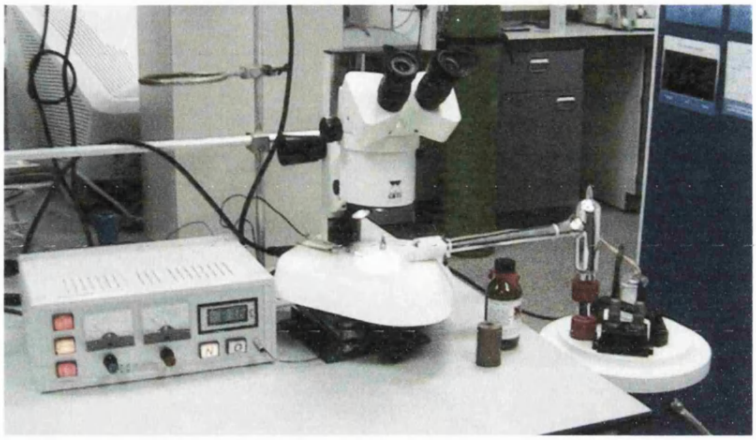

Figure 2.4: Low-melting mounting apparatus.

This equipment uses a liquid nitrogen reserve (right) and an electronic controller (left) to pump a cool stream over the microscope apparatus (centre), keeping the crystals intact while an appropriate sample is chosen for analysis.

The results in this chapter consist of a systematic study of the structural features of a range of adducts of simple phenols with TEMPO. The phenols involved were chosen to vary the steric environment around the expected hydrogen bond interaction. This was carried out in the hope that it would be possible to give insight into the hydrogen atom abstraction mechanism from phenols by radicals, as observed in antioxidant action. The remainder of this chapter discusses the results obtained.

2.2 Syntheses and Isolation of Monophenol Adducts

The structures of four hydrogen-bonded adducts of the free radical TEMPO with phenols have been determined by single crystal X-ray diffraction (Scheme 2.1).

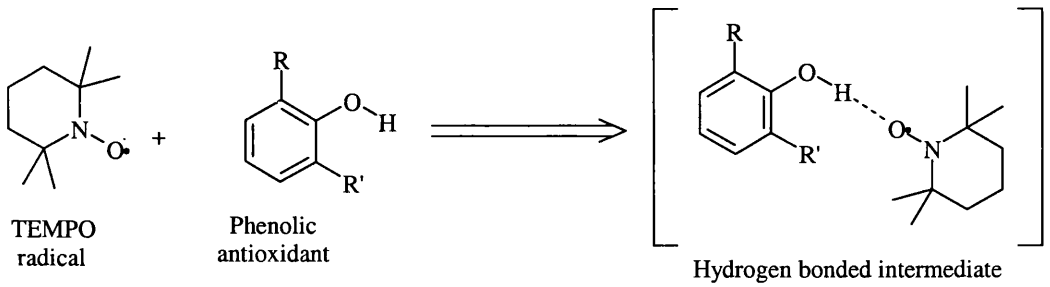

Where R and R' = H, Me or ^{t}Bu

Scheme 2.1: Synthesis of complexes **1-4.**

These were synthesised from a wide range of commercially available phenol derivatives of the general formula 2,4,6-R-C_6H_2OH, where the R groups were a combination of H, Me or ^{t}Bu. Phenol was sublimed twice before use, while other starting materials were used as received. The resulting compounds **1** - **4** will be discussed in the following section. These co-crystals were prepared from 1:1 stoichiometric mixtures of TEMPO and the appropriate phenol, the stoichiometry being selected by consideration of the monomeric supramolecular motif predicted on the basis of the expected O-H···O motif between the two components. As it is now well-established that intermolecularly hydrogen-bonded phenolic molecules are essentially unreactive to all radicals and that only "free" non-hydrogen-bonded phenols react,[32,33,34] these supramolecular syntheses were carried out in non-protic solvents. Furthermore, techniques for handling air-sensitive materials were employed.

The general procedure that appears to give the best results was a combination of stoichiometric amounts of the radical and phenol species, added in dry toluene solvent

under inert conditions. The mixture was gently warmed to give a clear red solution in all cases. The adduct products were obtained by crystallisation at low temperatures (193 K), resulting in red crystalline products suitable for analysis by X-ray diffraction. The crystalline product in all cases has a melting point that is significantly different from that of either component as all product species melt at temperatures under room temperature.

The crystalline products are not stable enough to be isolated *in vacuo*, but were analysed by X-ray diffraction and elemental analysis. In most cases the product obtained was of the expected 1:1 ratio of TEMPO and phenol. Interestingly, the supramolecular synthesis of **2** from an equal ratio of starting materials did not result in the formation of the 1:1 adduct as in the **1**, **3** and **4** cases. Instead, the crystal structure obtained indicated the exclusive formation of the 2:1 species of TEMPO and phenol. Elemental analysis on a pure liquid product obtained by vacuum sublimation of a neat stoichiometric mixture, or "melt", of the two components generally confirmed this complexation stoichiometry, although due to the volatile nature of the separate components some deviations in observed values were found.

The method appears to be quite tolerant with respect to the alkyl substituents present on the aromatic ring. However, variation to more polar substituents caused solubility problems and did not lead to the formation of a co-crystallisation product, but instead lead to the preferential crystallization of a mono-component product (usually the phenolic component).

2.3 X-ray Crystal Structures of Monophenol Adducts

The molecular structures of the four hydrogen-bonded adducts presented here were determined by single crystal X-ray diffraction. Crystals suitable for crystallographic analysis were successfully grown for multi-component complexes of phenol, *o*-methylphenol, dimethylphenol and di-*tert*-butylphenol with TEMPO (**1-4** respectively).

The method used to obtain single crystals of these multi-component complexes, suitable for X-ray analysis, was the slow cooling of a dry toluene solution containing the two components to 193 K. The crystalline product in all cases has a melting point that is significantly different from that of either component, as all product species melt at temperatures under room temperature. The crystallographic data collections in this chapter were carried out at 100 K, except in the case of **2**. This data collection was taken at 30 K due to slightly poorer quality of the crystals and as the preliminary investigation had indicated some structural features of significant interest.

The crystal structures and their hydrogen bonding are described and compared in the following sections; each of the crystal structures obtained will be discussed separately. Numbering of these complexes is consistent throughout. Selected crystallographic data is given for each structure in the appropriate section and full crystallographic tables containing the atomic coordinates and the equivalent isotropic displacement parameters are listed in Appendix A. In analysis of the diffraction data hydrogen atoms were all fixed by a riding model, except the hydrogen atoms involved in the O-H···O interaction which were in each case found by an analysis of the difference map and allowed to refine freely. All non-hydrogen atoms were refined anisotropically and all hydrogen atoms isotropically, including the freely refined O-H···O atoms. A summary of the X-ray crystallographic data obtained for these complexes is given below (Table 2.1).

	1	2	3	4
Empirical formula	$C_{15}H_{24}NO_2$	$C_{25}H_{44}N_2O_3$	$C_{17}H_{28}NO_2$	$C_{23}H_{40}NO_2$
M	250.35	420.62	278.40	290.10
Crystal system	Monoclinic	Orthorhombic	Monoclinic	Triclinic
Space group	$P2_1/n$	$P\,b\,c\,a$	$P2_1/n$	P-1
a / Å	5.802(1)	10.958(1)	8.130(1)	12.124(2)
b / Å	22.420(5)	32.428(1)	18.191(3)	13.770(2)
c / Å	11.097(3)	13.962(1)	11.203(2)	14.601(2)
α / °	90	90	90	72.122(1)
β / °	90.106(1)	90	94.218(1)	74.801(1)
γ / °	90	90	90	77.596(1)
U / Å^3	1443.50(6)	4961.34(10)	1652.36(5)	2214.68(6)
Z	4	8	4	2
μ (Mo-Kα) / mm^{-1}	1.152	1.126	1.119	0.068
Reflections collected	21029	14739	37864	52189
Independent reflections	3290	5210	5987	21128
R(int)	0.1517	0.0341	0.1566	0.0495
R1, wR2	0.0548, 0.1193 for 2187 data	0.0702, 0.1692 for 4055 data	0.0541, 0.1362 for 4726 data	0.0554, 0.1460 for 15953 data
R indices (all data)	0.0999, 0.1382	0.0917, 0.1820	0.0715, 0.1499	0.0807, 0.1639

Table 2.1: Crystal and refinement data for complexes **1-4.**

2.3.1 (Phenol):(TEMPO) Adduct

The co-crystal formed of phenol (C_6H_6O) with TEMPO ($C_9H_{18}NO$), **1**, was shown by crystallography to contain one equivalent of each component. The X-ray analysis shows that the asymmetric unit consists of two independent molecules, one molecule of TEMPO and one of phenol, leading overall to the observed 1:1 mixture. The basic molecular structure of **1** and the atomic numbering scheme are shown in Figure 2.5. Relevant bond intramolecular bond lengths and angles are collected in Table 2.2.

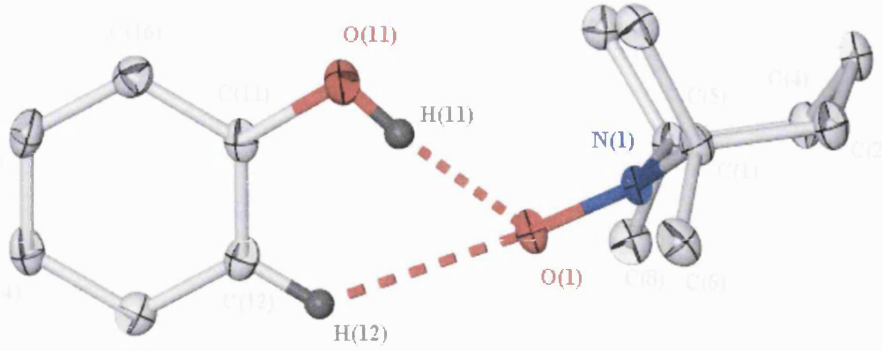

Figure 2.5: Structure of **1**, hydrogen atoms not involved in primary hydrogen bonds omitted for clarity and ellipsoids shown at 50% probability.

Bond lengths		Bond angles	
O(1)-N(1)	1.290 (2)	O(1)-N(1)-C(1)	116.30(11)
N(1)-C(1)	1.500(2)	O(1)-N(1)-C(5)	115.90(11)
N(1)-C(5)	1.502(2)		
O(11)-C(11)	1.367(2)	O(11)-C(11)-C(12)	122.50(15)
C(11)-C(12)	1.378(2)	O(11)-C(11)-C(16)	117.50(16)
C(11)-C(16)	1.398(2)	C(12)-C(11)-C(16)	120.01(16)

Table 2.2: Selected bond lengths (Å) and angles (°) of **1**.

At the molecular level, the crystal structure determination of the individual components is unremarkable. As this is the case, the most interesting aspects of the structure are the presence of supramolecular interactions.

The co-crystal consists of discrete (phenol):(TEMPO) dimers, which are chiefly aggregated *via* two different types of hydrogen bonds: an O-H···O and a C-H···O interaction. It was found that the nitroxide oxygen atom acts as a bifurcated acceptor, interacting with two different hydrogen bond donor groups. The hydrogen bond data is shown in Table 2.3.

D-H...A	d(D-H)	d(H···A)	D(D···A)	<(DHA)
O(11)-H(11)···O(1)#1	0.86(3)	1.86(3)	2.724(2)	174(2)
C(12)-H(12)···O(1)#1	0.95(12)	2.60	3.300(2)	130.5
C(6)-H(6A)···π	0.977	2.794[i]	3.780	168.80[ii]
C(8)-H(8B)···π #2	1.000	2.935[i]	3.903	170.75[ii]

Table 2.3: Hydrogen bond parameters in **1** [Å and °]. Symmetry transformations used to generate equivalent atoms: #1 x+1/2,-y+1/2,z-1/2 #2 ½-x,1/2+y,1/2-z. (i) Perpendicular distance from the H atom to the centroid C(11) C(16), (ii) angle between the C-H bond and the centroid C(11)-C(16).

The primary contact interconnecting the two different molecules in this co-crystal is a short [2.724(2)Å] and near linear [174(2)°] O-H···O· hydrogen bond between the phenol and the TEMPO oxygen atom (O(11)···O(1)). Although there are few examples of O· acceptor in the literature it is instead reasonable to compare these bonds to those involving carbonyl acceptors, which are extremely common. A search of the CSD for carbonyl hydrogen bond acceptors and phenolic donors gave the following distribution of bond parameters (Figure 2.7):[35]

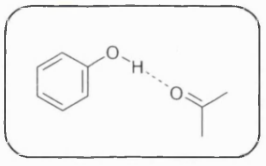

Figure 2.6: Search fragment for CSD search for ArOH···O (carbonyl) interactions (Figure 2.7).

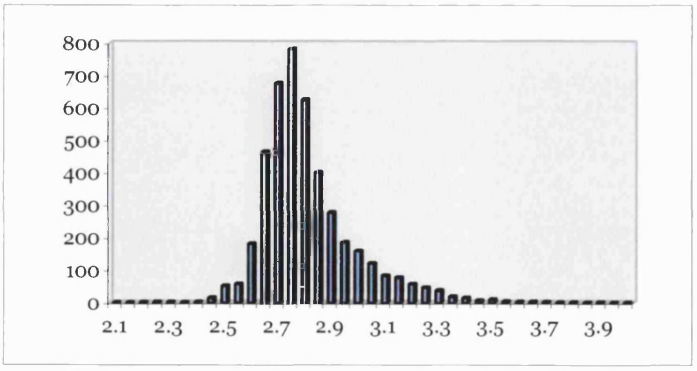

Figure 2.7: Distribution of O···O bond lengths for ArOH···O=C hydrogen bonds (Å).

The O-H···O· interaction present in **1** is comparable with the carbonyl-phenol hydrogen bonds found in the database. This interaction is therefore consistent with the criteria suggested by Taylor and Kennard[36] for a moderate hydrogen bonding interaction. It is also interesting to note the angle formed at the nitroxyl oxygen atom between N-O and the donor (D), as both π and σ models have been proposed for the hydrogen bonding in the literature.[37,38,39]

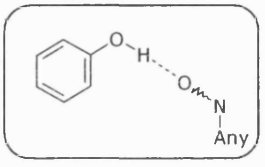

Figure 2.8: Fragment for search of the CSD for N-O···H-OAr angle.

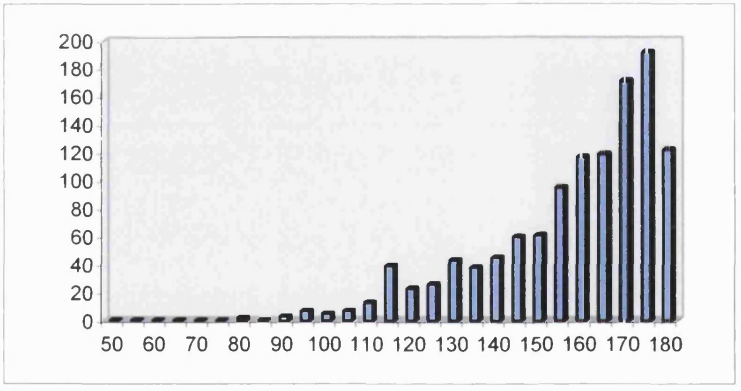

Figure 2.9: CSD search for the NOD angle in N-O···H-OAr contacts (°).

The angle for this feature observed in **1** is 119.27°, which is quite acute relative to the vast majority, though the hydrogen bond is of moderate length. This is indicative of a great degree of flexibility in the orientation of which the TEMPO moiety may interact

Bearing in mind the calculated transition state structures discussed in the introduction (Section 2.1), it is useful to consider the position of this (freely refined) phenolic hydrogen, with respect to the plane of the aromatic ring. The calculated deviation from a

least squares plane (defined by all six aryl carbons C(11)-C(16) and O(11)) for H(11) is -0.005(0.021)Å. Given that the RMS deviation of the fitted atoms is 0.004Å, it is clear that the phenolic hydrogen atom in this case remains, within experimental error, in line with the aryl plane. It may also be noted that the angle between the two ring planes, calculated from the angle between the least squares planes of each ring, is 84.89(0.05)°. There is additionally a twist allowing the TEMPO methyl substituents to be positioned on either side of the ring which can be described by the torsion angle C(16)–C(12)–C(5)–C(1) 65.7°. This twist between the rings is illustrated in Figure 2.5 and may be attributable to the steric requirements of the TEMPO methyl groups.

The TEMPO moiety in **1** is also engaged in a secondary heteromeric C-H···O· hydrogen bonding interaction *via* one of the *ortho*-C-H groups on the phenol [3.297(2)Å, 130.0(2)°; C(16)-H(16)···O(1)]. The resulting central motif in this co-crystal is a 6-membered (O···HOCCH) ring involving the free radical oxygen atom (Figure 2.8); this forms a dimer unit that packs as discrete, bimolecular entities in the extended structure.

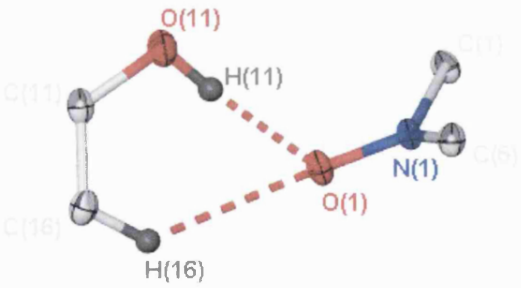

Figure 2.10: Core structure of **1** showing 6-membered ring motif, thermal ellipsoid of non-hydrogen atoms shown at 50% probability.

On a supramolecular scale, these neighbouring hydrogen-bonded dimers are oriented laterally in a top-to-tail fashion and on closer examination there seems to be relatively

close contacts between the phenol aryl ring and methyl C-H from the TEMPO (Figure 2.11).

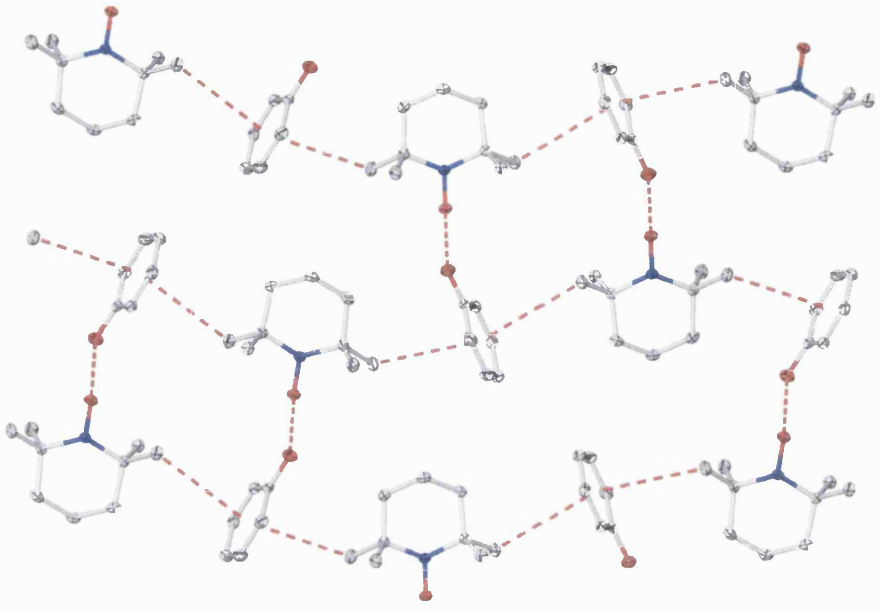

Figure 2.11: View down the *a*-axis of **1** showing the intermolecular O-H···O and C-H···π interactions. Hydrogen atoms are omitted for clarity and thermal ellipsoids are shown at 50%.

The closest distance between the centroid of the phenol aromatic ring (Cg(1)) and the TEMPO methyl carbons either side [3.780Å Cg(1)···C(6) and 3.903 Å Cg(1)···C(8)] and the considerable linearity of the D-H···A angle in each case [168.80° C(6)-H(6A)···π, 170.72° C(8)-H(8B)···π] may be indicative of attractive CH-π interactions. However, this bond length is on the borderline of those considered as an actual interaction, even for the CH-π class, which are generally quite long. Hence, it can be assumed that these CH-π interactions make only a minor contribution to the stabilisation of the structure. These weak CH-π interactions form 1-dimensional chains of alternating phenol and TEMPO running down the *b*-axis of the crystal. These chains are interlinked by much shorter and presumably stronger O-H···O· interactions to form layers within the structure. There are no intermolecular interactions between these layers. These interactions and the layer structure of **1** are illustrated in Figures 2.12 and 2.13 respectively.

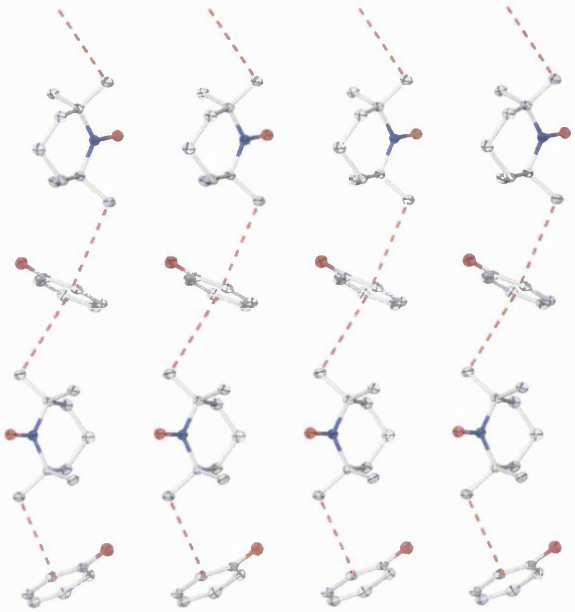

Figure 2.12: Tape structure of **1** viewed down the *c*-axis. All hydrogen atoms are omitted for clarity and other atoms are shown as 50% probability thermal ellipsoids.

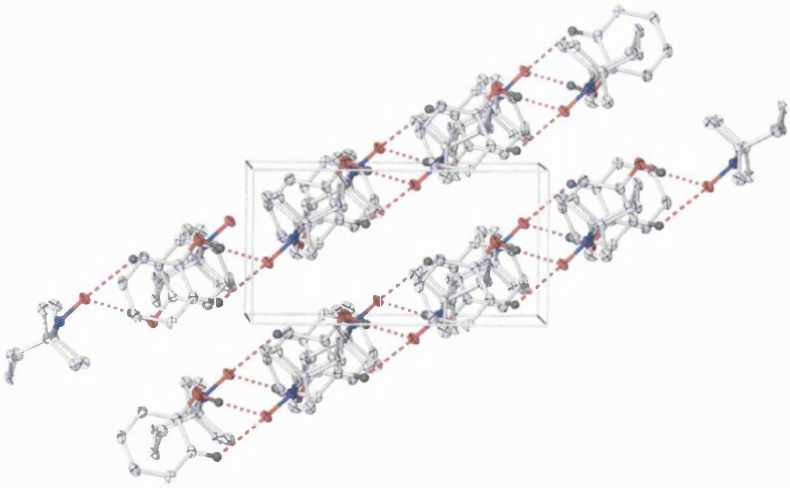

Figure 2.13: Layer structure of **1** viewed down the *b*-axis. All fixed hydrogen atoms omitted for clarity and other atoms are shown as 50% probability thermal ellipsoids.

There are no remarkable π -π distances observed in this co-crystal, or any other significant intermolecular interactions.

2.3.2 (*Ortho*-Methylphenol):(TEMPO)$_2$

The co-crystallisation of *ortho*-methylphenol (C_7H_9O) with TEMPO formed crystals of **2,** the 1:2 adduct (*ortho*-methylphenol):(TEMPO)$_2$. This structure was obtained at 30K as the 150K structure showed relatively poorer quality. The molecular structure and numbering scheme of **2** is represented in Figure 2.14. Relevant bond lengths and angles are collected in Table 2.4.

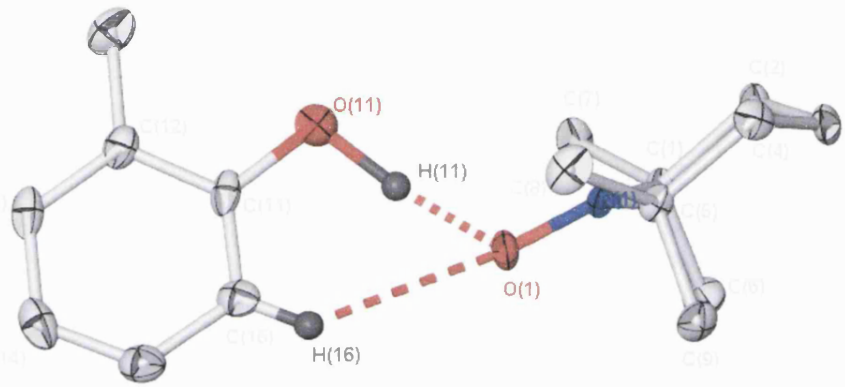

Figure 2.14: Structure of hydrogen-bonded moiety in **2**, thermal ellipsoids at 50% probability and most hydrogen atoms omitted for clarity.

Bond lengths		Bond angles	
O(1)-N(1)	1.287(2)	O(1)-N(1)-C(1)	116.02(18)
N(1)-C(1)	1.494(3)	O(1)-N(1)-C(5)	115.86(18)
N(1)-C(5)	1.497(3)		
O(2)-N(2)	1.290(2)	O(2)-N(2)-C(21)	115.60(17)
N(2)-C(21)	1.500(3)	O(2)-N(2)-C(25)	115.93(17)
N(2)-C(25)	1.494(3)		
O(11)-C(11)	1.374(3)	O(11)-C(11)-C(12)	121.1(2)
C(11)-C(12)	1.371(4)	O(11)-C(11)-C(16)	115.3(3)
C(11)-C(16)	1.411(3)	C(12)-C(11)-C(16)	123.5(3)

Table 2.4: Selected bond lengths (Å) and angles (°) of **2.**

Although the crystal structure of **2** was found to contain the bifurcated hydrogen bond motif found in **1** (Figure 2.13), the asymmetric unit also contains another molecule of TEMPO, which is not involved in any hydrogen bonding (Figure 2.15).

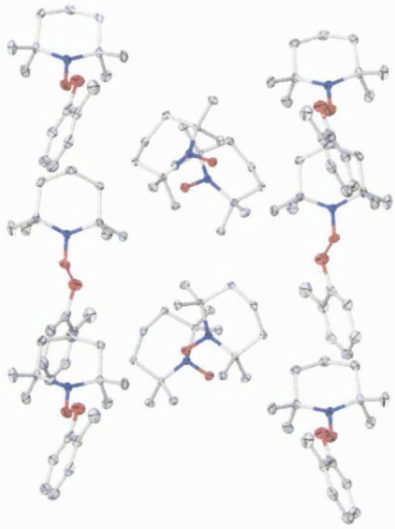

Figure 2.15: View of **2** down the *a*-axis.

The absence of any hydrogen bonding from the second TEMPO molecule suggests that such interactions are not necessary to stabilise the species in the solid-state, hence that the observed hydrogen bonding represents a real stabilisation of the product. The intramolecular distances and angles remain consistent with the expected values.

The hydrogen bonding assembly for **2** consists of one short O–H···O· bond [O(1)···O(11) 2.747(3)Å], which is also quite linear [172(5)°], and one longer hydrogen bond [3.241(3)Å, 129.9°, C(12)···O·(1)]. All hydrogen bond parameters for **2** are shown in Table 2.5.

D-H...A	d(D-H)	d(H···A)	d(D···A)	<(DHA)
O(11)-H(11)...O(1)#1	1.29(6)	1.46(6)	2.747(3)	172(5)
C(12)-H(12)...O(1)#1	0.95	2.55	3.241(3)	129.9
C(2)-H(2B)···π #2	0.97	3.061[i]	3.946	152.36[ii]

Table 2.5: Hydrogen bond parameters in **2** [Å and °]. Symmetry transformations used to generate equivalent atoms: #1 -x,y-1/2,-z+3/2 #2 ½-x,-y,z-1/2. (i) Perpendicular distance from the H atom to the centroid C(11) C(16), (ii) angle between the C-H bond and the centroid C(11)-C(16).

It is important to note the position of H(11) between the donor and acceptor atoms. Compared to **1**, in which the hydrogen atom was much closer to the closed-shell oxygen atom [0.86(3)Å, D-H and 1.86(3)Å, H···A], this hydrogen atom in **2** resides at a much more equal distance between the donor and acceptor atoms [1.29(6) Å, D-H and 1.46(6)Å, H···A]. The planarity of the freely refined hydrogen, H(11), with respect to the aromatic ring C(11)-C(16) may also be considered (Figure 2.16). The deviation of H(11) in **2** from the least squares plane defined by the aryl ring is -0.147(0.057)Å. The RMS deviation of the fitted atoms in this case is 0.014Å. This result is evidence that the phenoxyl hydrogen atom does not remain within the aryl plane, as was found for **1**.

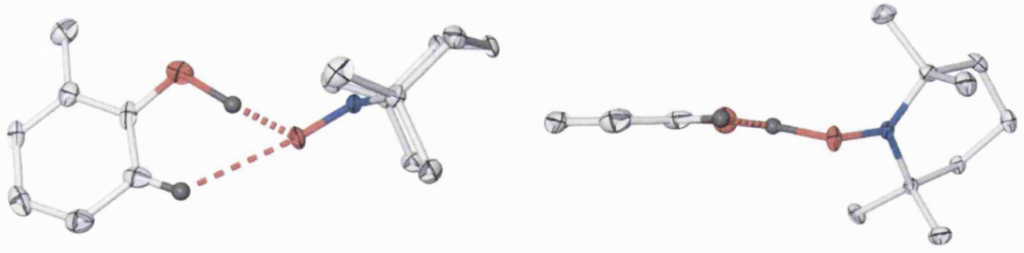

Figure 2.16: (a) 6-membered ring motif in **2** viewed down onto aryl plane, (b) orthogonal view of the ring motif. Uninvolved hydrogen atoms removed for clarity and thermal ellipsoid of non-hydrogen atoms shown at 50% probability.

As mentioned earlier, several computational calculations on the transition state of hydrogen atom transfer have suggested that the transition state geometry involves twisting the hydrogen out of this position (Chapter 1.2.6).[40,41] On this basis, together with the more central position of the H(11) atom between the donor and acceptor moieties, the hydrogen-bonded structure of **2** as a model for hydrogen atom abstraction represents a relatively more advanced stage of hydrogen transfer.

2 also exhibits a twist between the two ring planes, described by the torsion angle (C(16)–C(12)–C(5)–C(1), of 119.9°. Again, it is proposed that this orientation is adopted to avoid steric crowding of the methyl substituents between the two moieties. The angle between the least-squares planes fitted to the two rings for **2** is found to be 65.97(0.06)°. In addition, the N-O···D in **2** is found to be 118.78°, which is comparable for the value determined for **1**.

In addition to the primary 6-membered ring motif there are some additional close contacts in **2**. Each aryl ring exhibits a close contact with the CH_2 on a neighbouring TEMPO molecule, one not involved in an O-H···O hydrogen bond interaction (Figure 2.17).

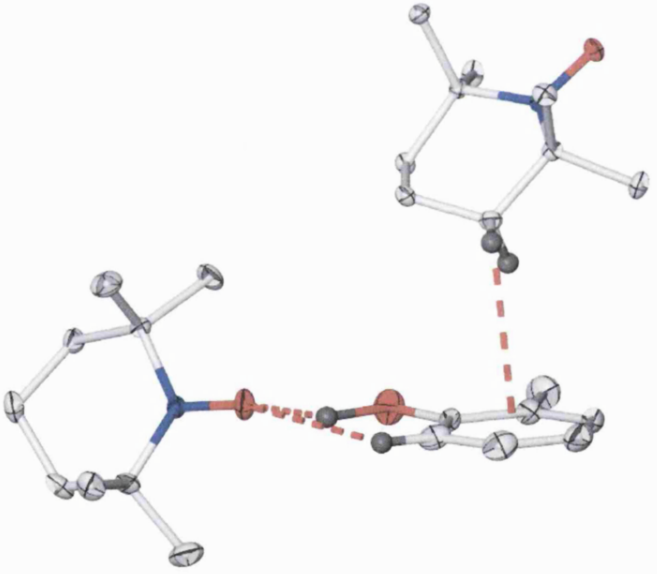

Figure 2.17: Long C-H···π interaction in **2**, ellipsoids at 50% probability and uninvolved hydrogen atoms omitted for clarity.

As observed in **1**, which exhibited similar short contacts, this C-H···π interaction is quite long [3.931Å, C(2)-H(2B)···π] but exhibit a high degree of linearity [152.30°, C(2)-H(2B)···π] . There are no further intermolecular interactions present in **2**.

2.3.3 (Dimethylphenol):(TEMPO) Adduct

The crystallisation of TEMPO with dimethylphenol in a 1:1 ratio afforded adduct **3** (TEMPO).(dimethylphenol). The structure determination of **3** shows that the compound contains one equivalent of each component. The molecular structure of **3** is shown in Figure 2.18. Relevant bond parameters are collected in Table 2.6.

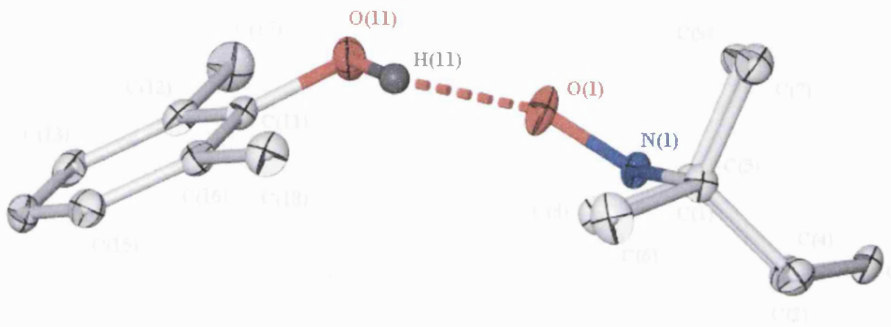

Figure 2.18: Structure of **3.** Fixed hydrogen atoms are removed for clarity, thermal ellipsoids shown at 50%.

Bond lengths		Bond angles	
O(1)-N(1)	1.291(2)	O(1)-N(1)-C(1)	115.18(8)
N(1)-C(1)	1.499(2)	O(1)-N(1)-C(5)	116.35(8)
N(1)-C(5)	1.499(2)		
O(11)-C(11)	1.376(2)	O(11)-C(11)-C(12)	115.63(9)
C(11)-C(12)	1.404(2)	O(11)-C(11)-C(16)	122.44(9)
C(11)-C(16)	1.399(2)	C(12)-C(11)-C(16)	121.91(9)

Table 2.6: Selected bond lengths (Å) and angles (°) of **3.**

As found for the other adducts in this chapter, the intramolecular bond parameters are unsurprising. On the supramolecular level **3** adopts the by now familiar O-H···O hydrogen bonded dimeric structural motif. However, this heteromeric O-H···O interaction between the two components is not supported by the C-H···O interaction found in the other members of the series, as this phenol does not have a suitable aryl-CH donor available. Hydrogen bond parameters for **3** are shown in Table 2.7.

D-H···A	d(D-H)	d(H···A)	D(D···A)	<(DHA)
O(11)-H(11)···O(1)#1	0.83(2)	2.00(2)	2.799(2)	160.6(19)
C(3)-H(3A)···π	0.990	2.609[i]	3.488	147.96[ii]
C(7)-H(7B)···π #2	0.980	3.174[i]	3.705	115.68[ii]

Table 2.7: Hydrogen bond parameters for **3** [Å and °]. Symmetry transformations used to generate equivalent atoms: #1 -x+1,-y,-z #2 ½+x,-y-1/2,1/2+z. (i) Perpendicular distance from the H atom to the centroid C(11) C(16), (ii) angle between the C-H bond and the centroid C(11)-C(16).

The O-H···O hydrogen bond is somewhat longer [2.799(2)Å] than the corresponding interaction in **1** and **2** [2.724(2)Å and 2.748(2)Å respectively]. In addition, the torsion angle between the two ring planes in **3** is -10.8° (C(16)–C(12)–C(5)–C(1)), which is significantly smaller than the corresponding values found in **1** and **2**. There is also an even further reduced angle between the two planes [$55.82(0.02)^{\circ}$] compared to that was found for **1** and **2** [$84.89(0.05)^{\circ}$ and $65.97(0.06)^{\circ}$ respectively]. This is illustrated in the space-filling diagram below (Figure 2.19). It seems reasonable to suggest that this conformation of the rings relative to each other leads to a slightly longer hydrogen bonding interaction due to the steric requirements of the opposing sets of methyl substituents, that in this structure are oriented in closer proximity.

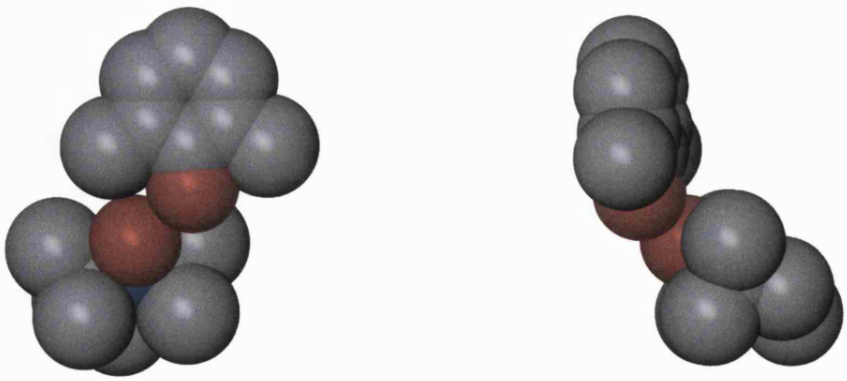

(a) **(b)**

Figure 2.19: Space-filling views of **3** showing the relative orientation of the rings. (a) View on the aryl plane, (b) View perpendicular to the aryl plane.

Figure 2.19 also clearly depicts the angle of approach between the N-O acceptor and the phenolic donor. The N-O···D angle in **3** is found to be 138.73°, which is notably larger than the value determined for **1** and **2** [65.7° and 119.9° respectively].

It is also interesting to note that in **3** the hydrogen involved in the O-H···O interaction (H11) exhibits a significant twist out of the plane of the aryl ring (Figure 2.20 and 2.21).

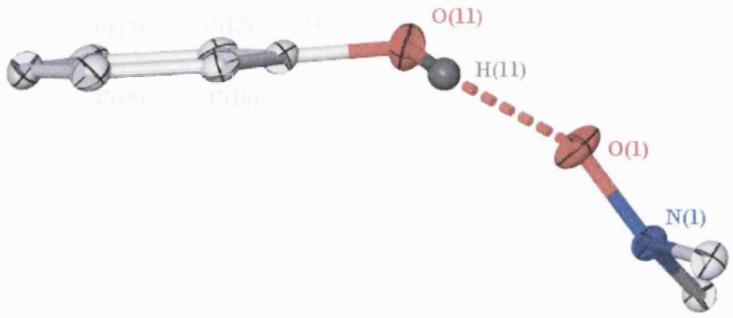

Figure 2.20: Geometry around the O-H···O hydrogen bond, viewed orthogonally to the plane of the aryl ring. Fixed hydrogen atoms are removed for clarity, thermal ellipsoids shown at 50%.

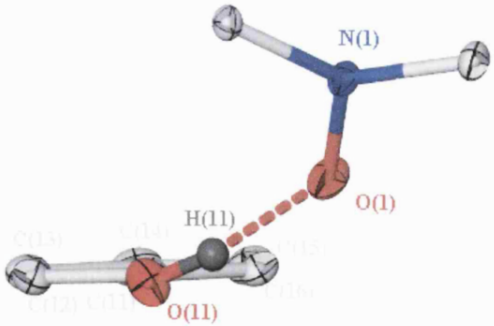

Figure 2.21: Geometry around the O-H···O hydrogen bond, view down O(11)-C(11). Fixed hydrogen atoms are removed for clarity, thermal ellipsoids shown at 50%.

In the structure of **1** the equivalent hydrogen atom was hydrogen bonded to the TEMPO oxygen but remained in the plane of the aryl ring, **2** showed some deviation from the aryl plane [-0.143(0.057)Å]. The deviation of H(11) from the aryl plane in **3** is even greater at -0.276 (0.020)Å, where the RMS deviation of the fitted atoms is 0.008Å. However, in this case the hydrogen atom remains significantly closer to the donor oxygen species [0.83(2)Å, O(11)-H(11) and 2.00(2)Å, O(1)···H(11) respectively]. As found in **2**, on the basis of the twisted geometry in the transition state,[42,43] these features indicate that H(11) in this case can be considered to represent a relatively advanced stage of hydrogen transfer transient species partway between the hydrogen-bonded intermediate and the transition state.

In addition to the primary O-H···O interaction this structure exhibits several other close contacts. There are two further short contacts, which occur between the aryl ring and carbon donors on the TEMPO moiety. These interactions are illustrated in Figure 2.22.

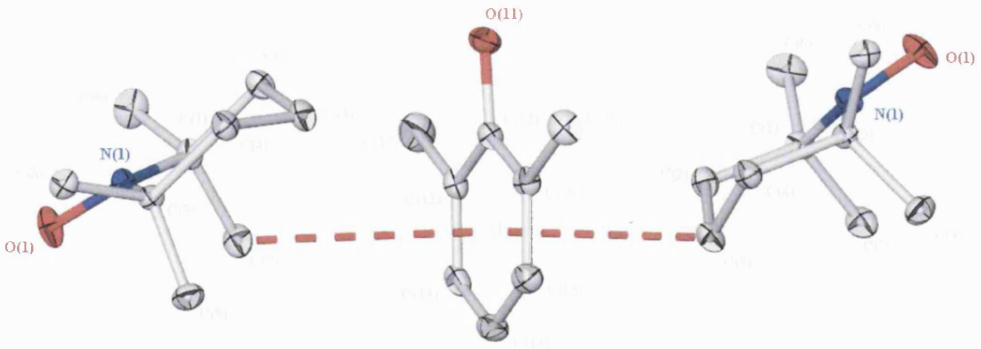

Figure 2.22: Long C-H···π interactions in **3**. The centroid (Cg) on the aryl ring is labelled (1). Hydrogen atoms are omitted for clarity and thermal ellipsoids are shown at 50%.

In one such contact between a TEMPO CH_2 and the aryl ring of the phenol moiety [3.488Å, C(3) – Cg(1)]. A second interaction occurs between the phenol methyl carbon, which sits at a slightly longer distance from the ring centroid [3.705Å, C(7) – Cg(1)].

Since the methyl hydrogen atoms are fixed *via* a riding model the angle is essentially meaningless in this instance, yet the orientation of the two components and in addition to the close contact distance suggests the presence of a hydrogen bonding interaction between one the methyl carbons and the TEMPO oxygen atom. In **3,** these three different hydrogen-bonding schemes combine to give a 2-dimensional layer structure, in which there are no further interactions between the layers. The overall packing in **3** is illustrated in Figures 2.23 and 2.24.

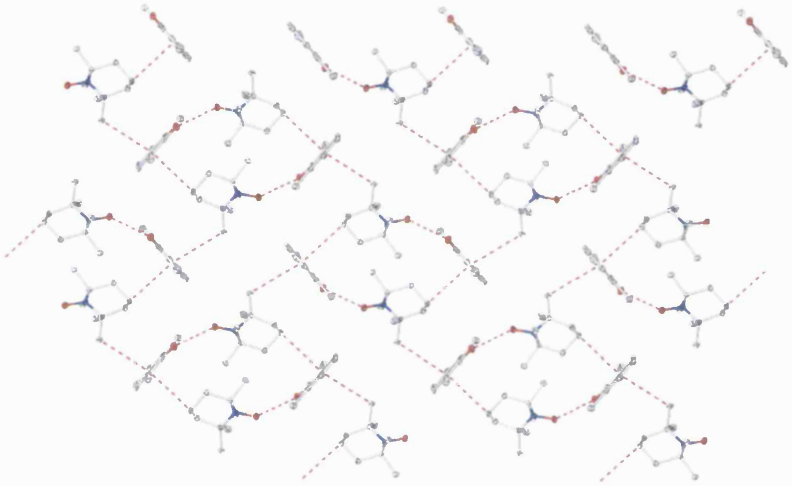

Figure 2.23: Layer structure of **3** viewed down the *a*-axis, all fixed hydrogen atoms omitted for clarity and other atoms are shown as 50% probability thermal ellipsoids.

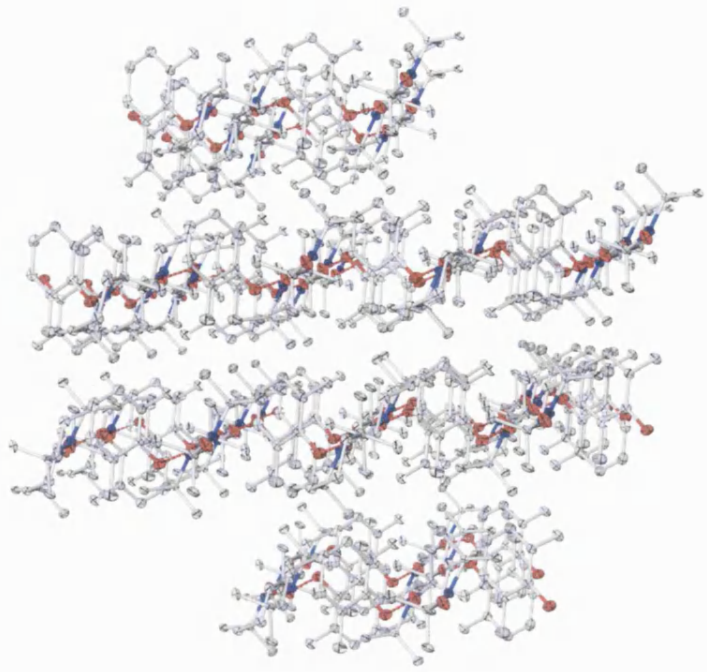

Figure 2.24: Layer structure of **3** viewed in perspective on the *ac*-plane, all hydrogen atoms omitted for clarity and other atoms are shown as 50% probability thermal ellipsoids.

2.3.4 (Di-*tert*-butylphenol):(TEMPO) Adduct

The co-crystallisation of di-*tert*-butylphenol with TEMPO led to the formation of the 1:1 complex. The crystal structure of **4** revealed that the asymmetric unit contains two independent molecules of both the phenol and TEMPO components. These interact to form two crystallographically independent O-H···O bonded dimers. The molecular structure of both hydrogen-bonded pairs, viewed separately for clarity, are illustrated along with the numbering scheme in Figure 2.25. Relevant bond parameters are collected in Table 2.8.

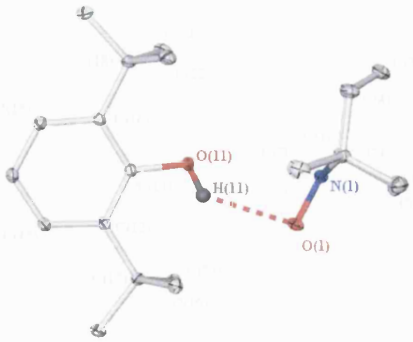

(a)

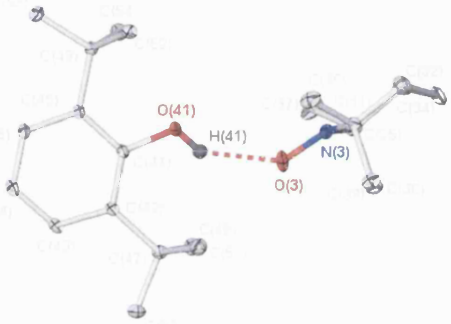

(b)

Figure 2.25: Molecular structure of **4**. (a) O(1)···O(11) fragment, (b) O(3)···O(41) fragment. All fixed hydrogen atoms are omitted for clarity, thermal ellipsoids are shown at 50%.

Bond lengths		Bond angles	
O(1)-N(1)	1.287(1)	O(1)-N(1)-C(1)	116.96(6)
N(1)-C(1)	1.499(1)	O(1)-N(1)-C(5)	116.90(6)
N(1)-C(5)	1.493(1)		
N(3)-O(3)	1.283(1)	O(3)-N(3)-C(31)	114.87(6)
N(3)-C(31)	1.494(1)	O(3)-N(3)-C(35)	114.88(7)
N(3)-C(35)	1.497(1)		
O(11)-C(11)	1.373(1)	O(11)-C(11)-C(12)	122.29(7)
C(11)-C(12)	1.410(2)	O(11)-C(11)-C(16)	115.25(7)
C(11)-C(16)	1.415(2)	C(12)-C(11)-C(16)	122.46(6)
O(41)-C(41)	1.367(1)	O(41)-C(41)-C(46)	114.52(7)
C(42)-C(41)	1.416(2)	O(41)-C(41)-C(42)	123.00(8)
C(46)-C(41)	1.415(2)	C(46)-C(41)-C(42)	122.47(6)

Table 2.8: Selected bond lengths (Å) and angles (°) of **4.**

The intramolecular bond parameters in **4** are do not differ from values typically expected for the individual components. As expected, the crystal is built with the characteristic hydrogen bonded dimers through the mediating hydrogen bonding of the hydroxy groups (O-H···O interactions). The hydrogen bond parameters are given in Table 2.9.

D-H...A	d(D-H)	d(H···A)	d(D···A)	<(DHA)
O(11)-H(11)···O(1)	0.828(18)	2.327(17)	2.953(1)	132.8(15)
O(41)-H(41)···O(3)	0.805(18)	2.031(18)	2.720(1)	143.4(16)
C(7)-H(7A)···π #1	0.965	2.756[i]	3.576	145.21[ii]
C(34)-H(34B)···π #2	0.962	2.824[iii]	3.741	159.67[iv]

Table 2.9: Hydrogen bond parameters in **4** [Å and °]. Symmetry transformations used to generate equivalent atoms: #1 x,y-1,z #2 x,y,1+z. (i) Perpendicular distance from the H atom to the centroid C(41) C(46), (ii) angle between the C-H bond and the centroid C(41)-C(46), (iii) Perpendicular distance from the H atom to the centroid C(11) C(16), (iv) angle between the C-H bond and the centroid C(11)-C(16)

As in the case of **3**, there are no available *ortho*-aryl hydrogen atoms on the phenolic species so the supporting C-H···O heteromeric motif is not seen in this structure. The two pairs of hydrogen-bonded components each exhibit a distinctly different bonding environment. The O-H···O bonds are consistent in length with the others observed in this series. The O(11)-H(11)···O(1) interaction, at 2.953(1)Å, is around 8% longer than the corresponding O(41)-H(41)...O(3) hydrogen bond. The DHA angles are also rather more acute than found previously [132.8(15)°, O(11)-H(11)-O(1) and 143.4(16)° O(41)-H(41)-O(3)]. This may be attributable to the repulsive effect of the bulky *ortho* substituents present on both moieties involved in the hydrogen bond.

It is also interesting to note that, in contrast to the dimethyl substituted species, **3**, the structure of both dimers in the asymmetric unit of **4** exhibit a distinct twist between the planes of the two rings. This twist, described by the torsion angle C(16)-C(12)-C(5)C(1)

and C(46)-C(42)-C(35)C(31), is found to be 90.1° and 94.2° for the ring involving O(11) and O(41) respectively. These values are more similar to the structures of **1** [65.7°] and **2** [119.9°], which both contain secondary C-H···O interactions and hence are less sterically hindered, than to the dimethyl substituted case **3**, [10.8°]. The space-filling diagram (Figure 2.26) illustrates the relative orientation of the two rings.

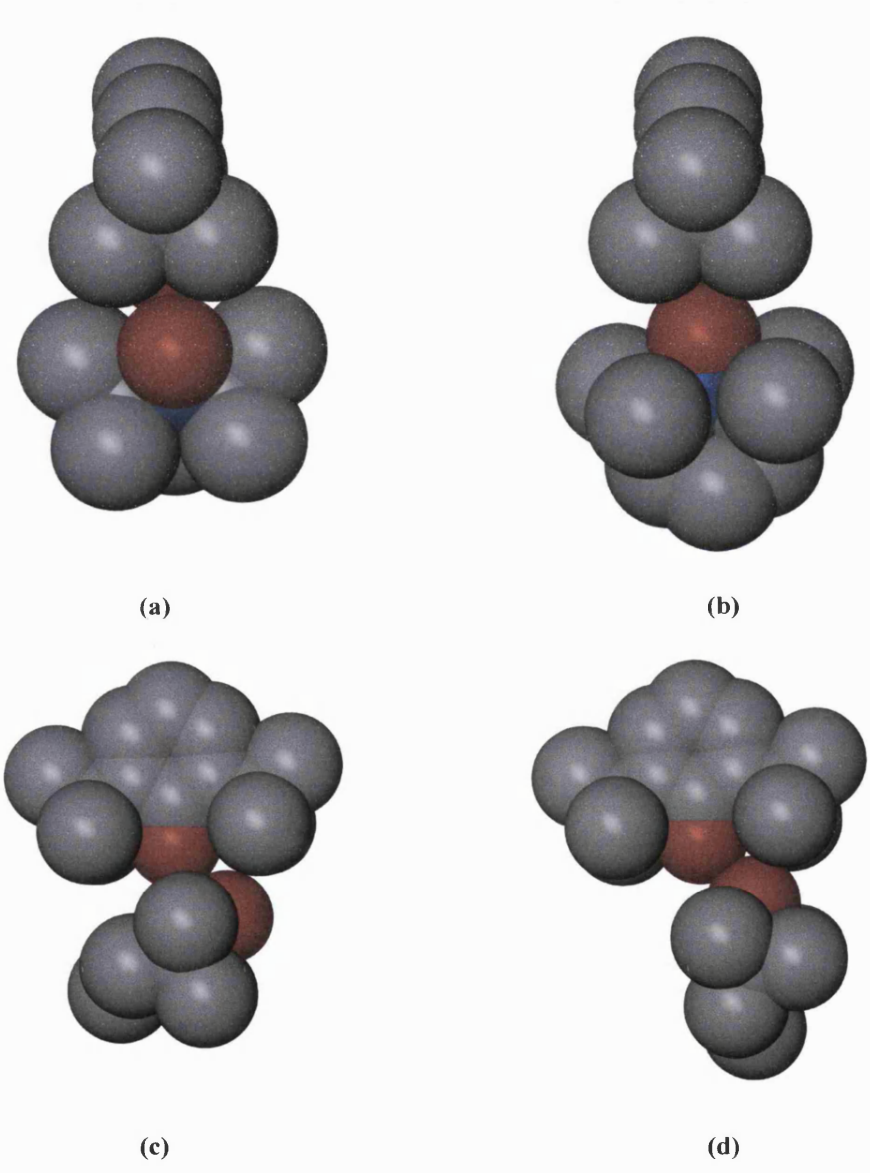

Figure 2.26: Space-filling views of **4** showing the relative orientation of the rings. (a) View through the aryl plane for O(11)-H(11)···O(1), (b) Equivalent view for O(41)-H(41)···O(3). (c) Orthogonal view of the aryl plane for O(11)-H(11)···O(1) (d) Orthogonal view of the aryl plane for O(41)-H(41)···O(1).

The calculation of the angle between each of the hydrogen bonded pairs is 87.32(0.02)° and 85.38(0.03)° for O(11)···O(1) and O(41)···O(3) respectively. It is also evident from Figure 2.26 that the approach of the TEMPO oxygen atoms towards the O-H donor groups is at two considerably different orientations. The angle formed by N-O···D is of interest for this purpose. These are 89.40° O(11)-O(1) and 129.9° O(41)-O(3) respectively. The angle between O(11)-O(1) in particular is very acute and is the most acute found in this study, such an angle is also quite rare in published structures (Figure 2.27). Those hits found with angles of less than around 100° are generally longer contacts.

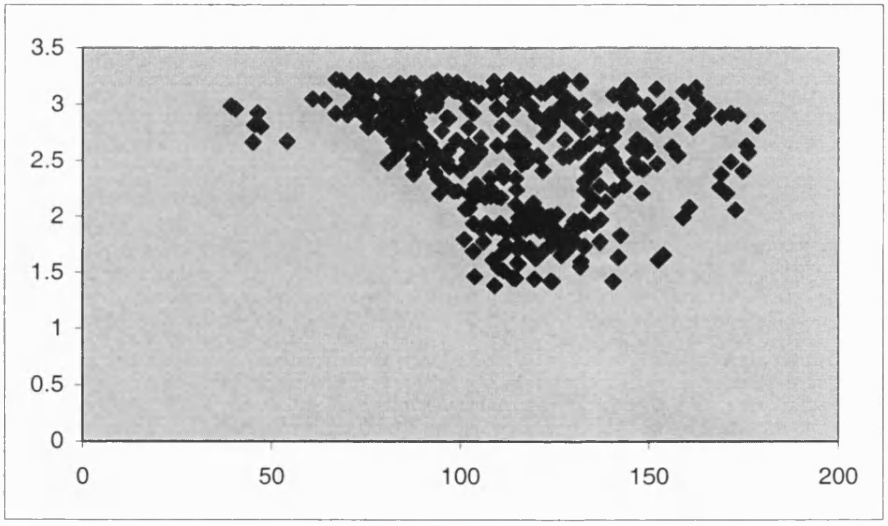

Figure 2.27: Plot of ArOH···O-N-X contacts (angle (N-O···O) vs distance (D···A)).[44]

The resulting geometry indicates that in this instance the TEMPO oxygen π-orbitals appear to be involved rather than σ orbitals (Figure 2.28).[37,38,39]

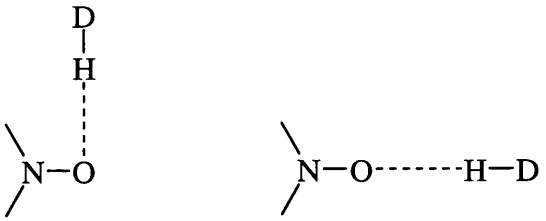

Figure 2.28: Possible alternative forms of hydrogen bond donation to the N-O group.

The position of the hydrogen atom involved in the O-H···O hydrogen bond is also interesting to note in **4**. The deviations of H(11) and H(41) from the respective aryl planes are 0.060(0.016)Å and 0.029(0.016)Å respectively (RMS 0.001Å and 0.003Å respectively for atoms fitted to the planes). While this is indicative of some small rotation, it is not as pronounced as was found for **3**. The geometries around this hydrogen bond in each of the two fragments in the asymmetric unit are illustrated below (Figures 2.29).

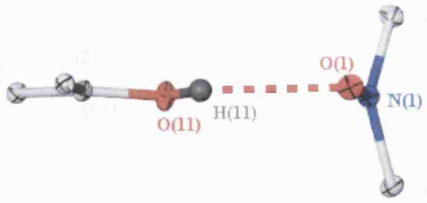

(a)

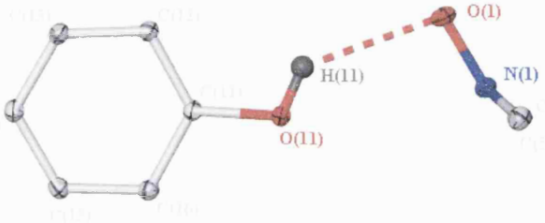

(b)

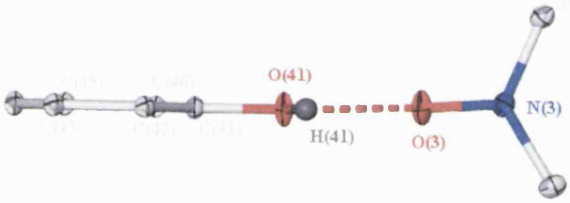

(c)

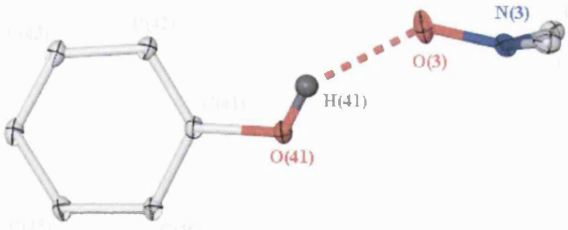

(d)

Figure 2.29: Geometry around the O-H···O hydrogen bond in both independent fragments in **4**. All fixed hydrogen atoms are omitted for clarity, thermal ellipsoids are shown at 50%. (a) View on the aryl plane for O(11)-H(11)···O(1), (b) view through the aryl plane for O(11)-H(11)···O(1), (c) view on the aryl plane for O(41)-H(41)···O(1),.(d) view through the aryl plane for O(41)-H(41)···O(3).

There is, as observed previously for similar adducts, evidence for some long C-H-π contacts within the structure of **4**. There are two such contacts in **4**; a TEMPO CH_2 lying close to the centroid (Cg1) [[3.488Å, C(34)···Cg(1)], and a TEMPO CH_3 lying close to the centroid (Cg2) [[3.705Å, C(7)···Cg(2)] (Figure 2.30).

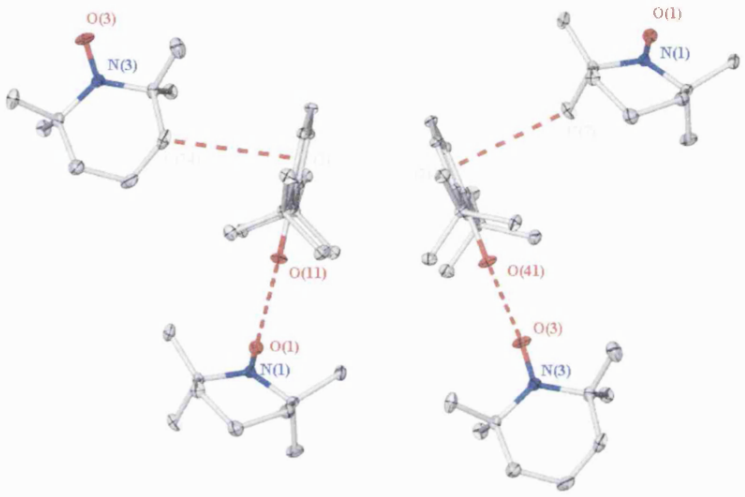

Figure 2.30: Long C-H···π interactions in **4**. The centroids (Cg) on the aryl rings are labelled (1) and (2). Selected atoms are labelled, hydrogen atoms are omitted for clarity and thermal ellipsoids are shown at 50%.

In the supramolecular structure of **4** the combination of O-H···O and C-H···π interactions forms zigzag chains (Figure 2.31). These chains are not linked further by additional hydrogen bonds and there are no further close contacts in this structure to be considered as intermolecular interactions.

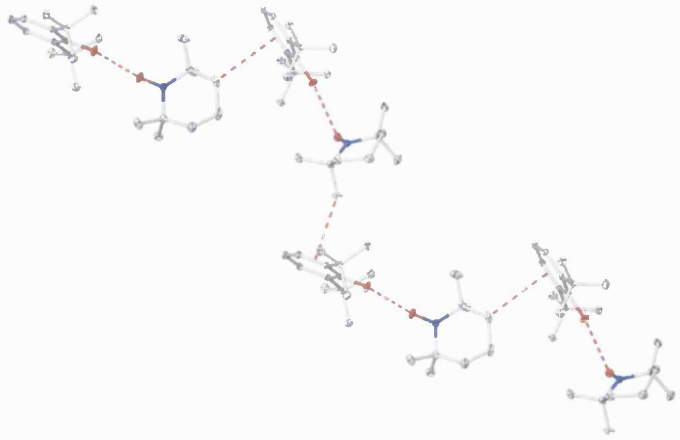

Figure 2.31: Chain structure of **4** viewed down the *a*-axis, all hydrogen atoms omitted for clarity and other atoms are shown as 50% probability thermal ellipsoids.

2.4 Solution-State Characterisation of a Model for Vitamin E

The phenol 2,2,5,7,8-pentamethyl-6-hydroxychroman (Figure 2.32), hereafter referred to as chromanol, is often used as a model compound for studies of structural and physiochemical aspects of α-tocopherol biological activity. It is structurally very similar to α-tocopherol, lacking only the alkyl side chain, which is important in making the compound lipid soluble but is not believed to contribute significantly to the overall antioxidant activity. The structure and numbering scheme used in the NMR assignments reported here are presented in Figure 2.32.

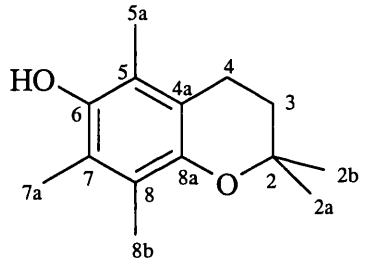

Figure 2.32: Structure and numbering scheme of 2,2,5,7,8-pentamethyl-6-hydroxychroman.

While the co-crystallisation of this chromanol species with TEMPO was attempted, crystals for the hydrogen bonded molecular complexes were not obtained. As a result it instead seemed worthwhile to examine the solution-state behaviour of this hydrogen-bonded system. To this purpose the effect an increasing concentration of radical has on the ^{13}C NMR signals for the carbon atoms on a hydrogen-bonded protic species, such as chromanol, is of interest. The following section describes the measurement of ^{13}C contact shifts for this chromanol model induced by the TEMPO free radical for a series of relative concentrations.

The study of ^{13}C NMR contact shifts provides a useful tool for the investigation of molecular interaction between free radicals and various closed shell molecules. Aminoxyl radicals, such as TEMPO, have previously been used as probes in similar

studies of molecular interactions. The interactions of nitroxide radicals with various types of protic molecules have been monitored by means of NMR and EPR methods.[37,38,39] TEMPO itself has been previously used as a spin probe to study the nature of the hydrogen bonding with simple phenolic O-H groups[29] and in the elucidation of the properties of α-tocopherol derivatives.[45,46] To date, however, there has been no such study published on the interaction of chromanol (Figure 2.33) with TEMPO.

In solution the TEMPO radical interacts with proton donors to form transient hydrogen-bonded complexes. This interaction between the nitroxide radical and various proton donor molecules generally induces downfield ^{13}C NMR contact shifts in the signals of aliphatic carbon signals for the non-radical component. The magnitude of the shift depends to some extent on the number of protons on the carbon atom, which increases in the order $C>CH>CH_2>CH_3$. It has been found that the formation of intermolecular hydrogen bonds between a phenol and TEMPO causes the appearance of an upfield shift, that is a negative spin density, on the carbon nuclei in the C-O-H fragment in the phenol.[47]

The measurements of ^{13}C contact shift were carried out for constant concentration of chromanol solution in acetone-d_6 (0.25 mol dm^{-3}). The radical TEMPO was added in concentrations ranging between 0 to 0.35 mol dm^{-3} in 0.05 mol dm^{-3} intervals. The results of these analyses are collected in Table 2.10 and are reported in ppm. The chemical shifts induced by the radical, $\Delta\delta_r$, for each carbon nuclei in chromanol are also presented together in Figure 2.33. This induced shift is also reported in ppm and is calculated using $\Delta\delta_r = \delta_r - \delta_o$, where δ_r is the shift in the presence of the radical and δ_o is the shift in acetone-d_6 only, without the radical.

	C(6)	C(8a)	C(8)	C(7)	C(5)	C(4a)	C(2)
Chromanol only	145.44	145.27	122.06	121.55	119.62	116.67	71.95
TEMPO 0.05	145.4	145.26	122.09	121.55	119.66	116.67	71.94
TEMPO 0.1	145.41	145.31	122.18	121.59	119.73	116.71	71.97
TEMPO 0.15	145.31	145.31	122.2	121.59	119.76	116.76	71.96
TEMPO 0.20	145.37	145.31	122.23	121.6	119.79	116.71	71.96
TEMPO 0.25	145.29	145.29	122.26	121.58	119.81	116.7	71.94
TEMPO 0.30	145.33	145.33	122.31	121.62	119.86	116.73	71.97
TEMPO 0.35	145.33	145.33	122.36	121.63	119.91	116.74	71.97

Conc.(moldm^{-3})	C(3)	C(2a), C(2b)	C(4)	C(5a), C(7a), C(8a)		
Chromanol only	32.91	26.06	20.78	11.84	11.11	10.9
TEMPO 0.05	33	26.18	20.88	12.05	11.23	11.12
TEMPO 0.1	33.16	26.37	21.03	12.31	11.4	11.4
TEMPO 0.15	33.23	26.45	21.11	12.45	11.48	11.48
TEMPO 0.20	33.3	26.54	21.17	12.59	11.7	11.55
TEMPO 0.25	33.38	26.66	21.26	12.8	11.94	11.67
TEMPO 0.30	33.48	26.75	21.35	12.93	12.08	11.75
TEMPO 0.35	33.59	26.89	21.46	13.15	12.31	11.88

Table 2.10: ^{13}C NMR data for chromanol (ppm) on addition of the free radical TEMPO.

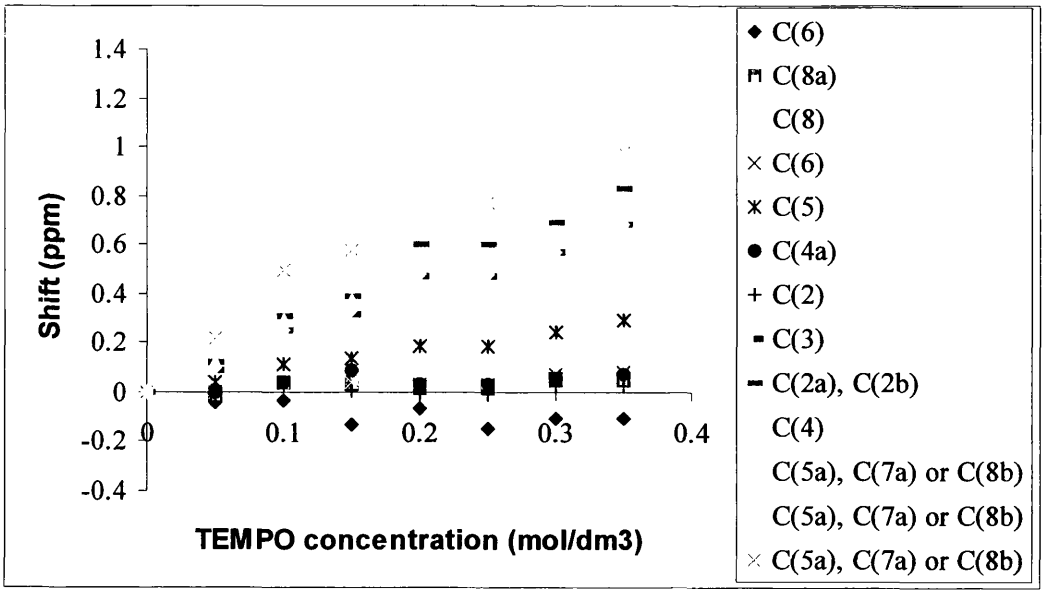

Figure 2.33: The dependence of ^{13}C contact shift for chromanol on concentration of TEMPO.

The ^{13}C shifts show an approximately linear dependence on the concentration of the radical. As expected, most of the carbon signals show a downfield shift on increasing

radical concentration. The smallest shift was observed for the quaternary carbons, and the largest for those on the methyl groups, which is also consistent with the order reported in the literature, observed in structurally related ester compounds.[43,44] The shift for the *ipso*-carbon, C(6), adjacent to the oxygen atom hydrogen bonding to the radical, is upfield. As an upfield shift indicates the formation of hydrogen bonds of noticeable strength, this result confirms the expectation that chromanol can form such hydrogen bonds, despite being unable to trap this complex crystallographically. Calculation of the gradient, using a linear regression trendline, gives a result of –0.42 ppm·dm^3 mol^{-1} for C(6). Compared with published results for phenol (-0.20ppm·dm^3 mol^{-1}) and di-*tert*-butylphenol (0.28ppm·dm^3 mol^{-1}) these results indicate that the hydrogen bonding interaction with chromanol is notably stronger.

2.5 Concluding Remarks

In the solid state, it has been found that the essential motif in the packing of **1-4** is a dimeric unit aggregated *via* O-H···O hydrogen bonds that are supported, where possible, by C-H···O interactions. These primary interactions are summarised below for convenience (Table 2.11).

Complex	D-H...A	d(D-H)	d(H···A)	D(D···A)	<(DHA)
1	O(11)-H(11)···O(1)	0.86(3)	1.86(3)	2.724(2)	174(2)
1	C(12)-H(12)···O(1)	0.95(12)	2.60	3.300(2)	130.5
2	O(11)-H(11)···O(1)	1.29(7)	1.46(6)	2.747(3)	172(5)
2	C(12)-H(12)···O(1)	0.95	2.55	3.241(3)	129.9
3	O(11)-H(11)···O(1)	0.83(2)	2.00(2)	2.799(2)	160.6(19)
4	O(11)-H(11)···O(1)	0.828(18)	2.327(17)	2.953(1)	132.8(15)
4	O(41)-H(41)···O(3)	0.805(18)	2.031(18)	2.720(1)	143.4(16)

Table 2.11: Summary of Hydrogen bond parameters (Å) and angles (°).

The O-H···O bond parameters for these open-shell adducts are comparable with similar closed-shell species in the existing literature, ranging from 2.720(1) – 2.953(1)Å and with appreciable linearity [132.8(15) – 174(2)°]. Several hydrogen bonding interactions involving C-H donors were also revealed. It is well established that hydrogen bonds involving CH groups are weaker than those with OH or NH groups, due to the difference in electronegativity of the donor atom involved. Hence, it is generally considered that they tend to occur when other packing forces and stereochemical constraints bring CH bonds and electronegative acceptor atoms within the range of electrostatic interaction, about 3.0Å, but that they do not have a major influence on molecular aggregation when in the presence of stronger types of hydrogen bond.[48] This study agrees with this premise as the O-H···O is present in every case and a secondary C-H···O interaction occurs only if the bonding environment allows it. The donor-acceptor distance in the C-H···O interactions are longer than the O-H···O interactions, as expected for this class of interaction, [3.300(2)Å, 130.5° in **1** and 3.241(2)Å, 129.9° in **2**].

Furthermore, a study of the N-O···D angles in the primary hydrogen bonding interaction shows a wide angular range [89.40° – 138.73°]. This exemplifies both π- and σ- type interaction bonding interaction from the NO radical in this series. The TEMPO oxygen is thus shown to exhibit a great degree of flexibility in the orientation in which it may interact.

The present study also highlights the position of the phenolic hydrogen atom relative to the aryl plane. In particular the dimethylphenol adduct, **3** shows structural evidence of this hydrogen atom being twisted out of plane. This is expected for the transition state structure from calculated geometries in hydrogen atom abstraction reactions, suggesting that the structure of **3**, and to a lesser extent **2** and **4**, represents a more advanced stage of hydrogen atom transfer. The ^{13}C contact shifts further showed that the α-tocopherol model compound chromanol is also able to form hydrogen bonds of appreciable strength with TEMPO radical in solution, though no co-crystals were able to be isolated to provide solid-state evidence for this interaction. In addition to these structural features, these X-ray crystal structures are useful in themselves as examples of solid-state open-shell hydrogen bonds, binary co-crystals and low-melting samples that are challenging to analyse experimentally.

2.6 Experimental

General Considerations

All manipulations were performed under a dry argon atmosphere using standard Schlenk-line and glovebox techniques. Glassware was dried for several hours prior to use in an oven maintained at 130 °C. All solvents were distilled from the appropriate drying-agents under a nitrogen atmosphere, degassed and then stored under argon. Phenol was purchased from Aldrich and sublimed prior to use. All other chemicals were used as supplied by Acros, Aldrich, Avocado, Fluka or Lancaster. Deuterated NMR solvents were purchased from Goss Scientific Ltd. and, where appropriate, dried before use.[

Characterisation Details

Elemental analyses were performed by the University of Bath Microanalysis Service on an Exeter Analytical Inc. CE-440 Elemental Analyser. Elemental analyses obtained for these complexes are generally within acceptable tolerances of the expected values, although in a few cases discrepancies between the calculated and observed values are observed which may be a result of the low melting point and volatility of the co-crystalline samples. Due to the difficulty in removing solvent as the components are quite volatile neat solutions of the co-crystalline components were sublimed to obtain a sample for examination.

All NMR spectra were recorded at 293K. All ^{1}H- and ^{13}C NMR spectra were recorded on a Bruker Avance 300 MHz or a Bruker Avance 400 MHz spectrometer. Chemical shifts are reported in units of ppm referenced to the chemical shifts of residual protio solvent resonances ($CHCl_3$ δ 7.27). For the solution chemical shift studies in Section 2.4 chemical shifts were referenced to the position of CO signal of acetone, as it has been shown that this signal is not influenced by the changes of radical concentration.[29]

Mass spectra for samples were submitted for analysis at EPSRC National Mass Spectroscopy Service Centre by GC-EI-MS at a very low cone voltage, but the molecular ions were not detected and will not be reported here.

Solid-State Structure Determination

Single crystal x-ray diffraction data were collected on an Enraf Nonius Kappa CCD instrument equipped with an Oxford Cryosystems Cryostream cooling device. For the 30 K study (complex **2**) a HeliX, also from Oxford Cryostysems was used. Crystalline samples were coated in an inert perfluorinated ether oil, mounted on glass fibres and transferred to the cold nitrogen gas stream of the diffractometer. Diffraction of the graphite-monochromated Mo-Kα radiation (λ=0.71073 Å) was detected by means of a CCD area detector. Data acquisition was controlled by the Nonius COLLECT software package.[49] Generally, an entire hemisphere of reciprocal space was collected regardless of Laué symmetry. Scan speed and width were chosen based on scattering power and peak rocking curves. Unit cell determination and refinement were subsequently performed using DENZO and SCALEPACK.[50] The structure was solved by direct methods using Sir-92,[51] Sir-97[52] or SHELXS-86,[53] and the lighter atoms were located from subsequent Fourier difference syntheses. The structures were refined by full matrix least-squares analysis on F^2 using SHELXL-97.[54,55] The hydrogen atom positions were calculated geometrically and refined with a riding model. The positions of OH hydrogen atoms were located in difference Fourier maps and allowed to refine freely. All non-hydrogen atoms were refined anisotropically and the hydrogens were refined isotropically. The program X-Seed[56] was used for drawing the molecules and WINGX[57] was used to prepare material for publication.

Synthesis and characterisation of adducts 1 – 4

Formation of (1)

Scheme:

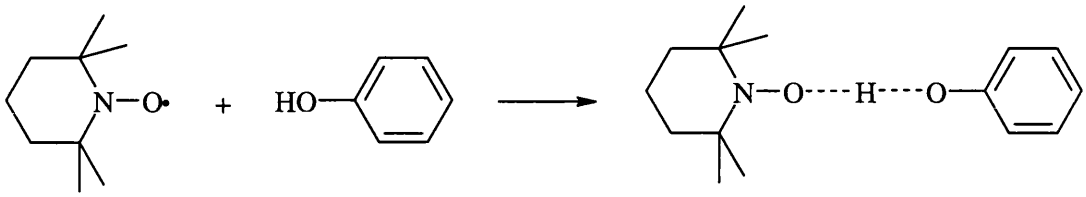

Dry toluene (10 ml) was added, under argon, to a schlenk containing solid phenol (0.47 g, 5 mmol) and 2,2,6,6-tetramethylpiperidine-1-oxyl (TEMPO) (0.78 g, 5 mmol). The two solids initially formed a melt, with some bubbling, which was stirred at room temperature for 30 minutes resulting in a clear red solution. On leaving the solution at –80°C a crop of red crystals suitable for X-ray diffraction were obtained. The product was isolated by removing solvent with a filter cannula, yield obtained 1.02 g, 82%. M.p. -33°C. Elemental analysis: Calcd for $C_{15}H_{24}O_2N$: C, 71.95 %, H, 9.67 %, N, 5.60 %. Found: C, 65.3 %; H, 8.65 %; N, 5.17 %.

Formation of (2)

Scheme

:

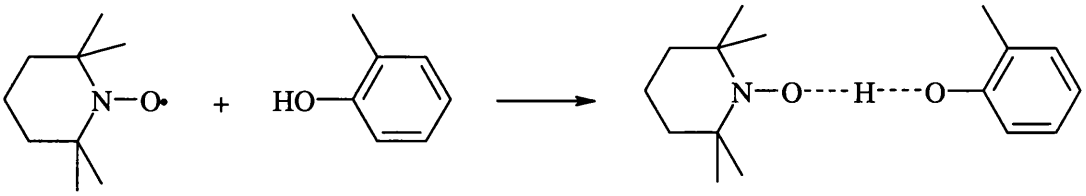

Dry toluene (10 ml) was added, under argon to a schlenk containing solid *ortho*-methylphenol (1.54 g, 5 mmol) and 2,2,6,6-tetramethylpiperidine-1-oxyl (TEMPO) (1.56

g, 10 mmol). This was heated until dissolved and stirred at room temperature for 30 minutes to give a clear red solution. On leaving the solution at –80°C a crop of red crystals suitable for X-ray diffraction were obtained. The product was isolated by removing solvent with a filter cannula, yield obtained 1.54 g, 73%. M.p. –21°C. Elemental analysis: Calcd for $C_{25}H_{44}O_3N_2$: C, 71.37 %; H, 10.55%; N, 6.66 %. Found: C, 72.1 %; H, 9.77 %; N, 5.36 %,

Formation of (3)

Scheme:

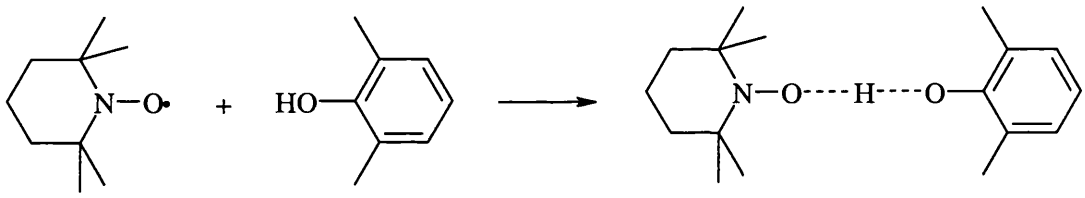

Dry toluene (10 ml) was added, under argon to a schlenk containing the liquid phenol (0.61 g, 5 mmol) and 2,2,6,6-tetramethylpiperidine-1-oxyl (TEMPO) (0.78 g, 5 mmol). This was stirred at room temperature for 30 minutes to give a clear red solution. On leaving the solution at –80°C a crop of red crystals suitable for X-ray diffraction were obtained. The product was isolated by removing solvent with a filter cannula, yield obtained 0.95 g, 68%. M.p. –17°C. Elemental analysis: Calcd for $C_{17}H_{28}O_2N$: C, 73.32 %; H, 10.14%; N, 5.03 %. Found: C, 73.4%; H, 10.2%; N, 5.43%,

Formation of (4)

Scheme:

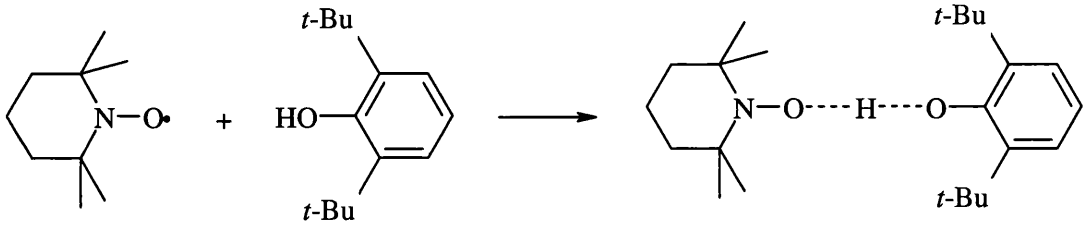

Dry toluene (10 ml) was added, under argon to a schlenk containing solid phenol (1.81 g, 5 mmol) and 2,2,6,6-tetramethylpiperidine-1-oxyl (TEMPO) (0.78 g, 5 mmol). This was stirred at room temperature for 30 minutes to give a clear red solution. On leaving the solution at –80°C a crop of red crystals suitable for X-ray diffraction were obtained. The product was isolated by removing solvent with a filter cannula, yield obtained 1.31 g, 90%. M.p. 9°C. Elemental analysis: Calcd for $C_{23}H_{40}O_2N$: C, 76.18 %; H, 11.13 %; N, 3.86 %. Found: C, 77.15 %; H, 9.98 %; N, 1.60 %,

2.7 References

[1] deNooy, A.E.J.; Besemer, A.C.; van Bekkum, H. *Synthesis (Stuttgart)*, **1996**, 1153.
[2] De Luca, L.; Giacomelli, G.; Porceddu, A. *Org. Lett.*, **2001**, *3*, 3041.
[3] Sheldon, R.A.; Arends, I.W.C.E., *Adv. Synth. Catal.*, **2004**, *346*, 1051.
[4] Bobitt, J.M.; Flores, C.L., *Heterocycles,* **1988**, *27*, 509.
[5] deNooy, A.E.J.; Besemer, A.C.; van Bekkum, H., *Synthesis*, **1996**, 1153.
[6] Borbat, P.P; Costa-Filho, A.J.; Earle, K.A.; Moscicki, J.K.; Freed, J.H. *Science,* **2001**, *291*, 266.
[7] Keana, J.F.W. *Chem. Rev.*, **1978**, *78*, 37.
[8] Wang, Q.; Zhao, Y.; Song, L.X.; Fan, Z.Q.; Feng, L.X. *Macromol. Chem. Phys.*, **2001**, *202*, 448.
[9] Benoit, D.; Chaplinski, V.; Braslau, R.; Hawker, C.J. *J. Am. Chem. Soc.*, **1999**, *121*, 3904.
[10] Hawker, C.J., *Acc. Chem. Res,* **1997**, *30*, 373.
[11] Gatteschi, D., *Adv. Mater.* **1994**, *6*, 635.
[12] Albeniz, A.C.; Espinet, P.; Lopez-Fernandez, R.; Sen, A., *J. Am. Chem. Soc.*, **2002**, *124*, 11278.
[13] Maryjaszewski, K., *Macromolecules*, **1998**, *31*, 4710.
[14] Lucarini, M.; Mugnaini, V.; Pedulli, G.F., *J. Org Chem.* **2002**, *67*, 928.
[15] Mordwell, F.G.; Liu, W.-Z. *J. Am. Chem. Soc.* **1996**, *118*, 10819.
[16] Sun, Y.-M.; Liu, C.-B. *Eur. J. Org. Chem.* **2004**, 120.
[17] Singh, N.; O'Malley, P.J.; Popelier, P.L.A. *Phys. Chem. Chem. Phys.* **2005**, *7*, 614.
[18] Vishwexhar, P.; Nangia, A.; Lynch, V.M. *CrystEngComm,* **2003**, *5*(31), 164.
[19] MacGillivray, L.R.; Reid, J.L.; Ripmeester, J.A. *J. Am. Chem. Soc.* **2000**, *122*, 7817.
[20] Oswald, I.D.H.; Motherwell, W.D.S.; Parsons, S. *Acta Cryst.* **2004**, *E60*, 1967.
[21] Martin, R.E.; Pannier, M.; Diederich, F.; Gramlich, V.; Hubrich, M.; Speiss, H.W. *Angew. Chem. Int. Ed. Engl.* **1998**, *37*, 2834.
[22] Berliner, L.J. *Acta Crystallogr., Sect. B. Struct. Crystallogr. Cryst. Chem.* **1970**, *26*, 1198.
[23] Cirujeda, J.; Ochando, L.E.; Amigo, J.M.; Rovira, C.; Rius, J.; Veciana, J. *Angew. Chem., Int. Ed. Engl.* **1995**, *34*, 55.
[24] Park, J.G.; Paulsen, C.; Rey, P.; Rovira, C.; Veciana, J. *J. Chem. Soc. Chem. Commun.* **1995**, 709.
[25] Cirujeda, J.; Mas, M.; Molins, E.; Depanthou, F.L.; Laugier, J.; Matsushita, M.M.; Izuoka, A.; Sugawara, T.; Kobayashi, T.; Wada, N.; Takeda, N.; Ishikawa, M. *J. Am. Chem. Soc.* **1997**, *119*, 4369.
[26] Pontillon, Y.; Akita, T.; Grand, A.; Kobaryashi, K.; Lelievre-Berna, E.; Pecaut, J.; Ressouche, E.; Schweizer, J. *J. Am. Chem. Soc.* 1999, 121, 10126.
[27] Franchi, P.; Luciarini, M.; Pedrielli, P.; Pedulli, G.F. *CHEMPHYSCHEM*, **2002**, *3*, 789.
[28] Morishima, I.; Endo, K.; Yonezawa, T. *J. Am. Chem. Soc.* **1971**, *93*, 2048.
[29] Shenderovich, I.G.; Kecki, Z.; Wawer, I.; Denisov, G.S. *Spectroscopy Letters,* **1997**, *30*(8), 1515.
[30] Ahrens, B.; Davidson, M.G.; Forsyth, V.T.; Mahon, M.F.; Johnson, A.L.; Mason, S.A.; Price, R.D.; Raithby, P.R. *J. Am. Chem. Soc.* **2001**, *123*, 9164.
[31] Bond, A.D. *Cryst. Eng. Commun.* **2003**, 250.
[32] Amorati, R.; Luciarini, M.; Mugnaini, V.; Pedulli, G.F. *J. Org. Chem.* **2003**, *68*, 5719.
[33] Foti, M.; Barclay, L.R.C.; Ingold, K.U. *J. Am. Chem. Soc.* **2002**, *124*, 12881.
[34] De Heer, M.I.; Mulder, P.; Korth, H.-G.; Ingold, K.U.; Lusztyk, J. *J. Am. Chem. Soc.* **2000**, *122*, 2355.
[35] CSD search using Version 1.7, Nov 2004 update. Filters used were 3-D coordinates determined, no errors and R<0.1.
[36] Taylor R.; Kennard, O. *J. Am. Chem. Soc.*, 1982, **104**, 5063.
[37] Morishima, I.; Endo, K.; Yonezawa, T. *Chemical Physics Letters*, **1971**, *9*(2), 143.
[38] Morishima, I.; Endo, K.; Yonezawa, T. *J. Chem. Phys.*, **1973**, *58*(8), 3146.
[39] Morishima, I.; Endo, K.; Yonezawa, T. *J. Am. Chem. Soc.* **1973**, *95*(26), 8627.
[40] Sun, Y.-M.; Liu, C.-B. *Eur. J. Org. Chem.* **2004**, 120.
[41] Singh, N.; O'Malley, P.J.; Popelier, P.L.A. *Phys. Chem. Chem. Phys.* **2005**, *7*, 614.
[42] Sun, Y.-M.; Liu, C.-B. *Eur. J. Org. Chem.* **2004**, 120.
[43] Singh, N.; O'Malley, P.J.; Popelier, P.L.A. *Phys. Chem. Chem. Phys.* **2005**, *7*, 614.
[44] Database search defined contacts as less than the sum of van der Waals radii +0.5Å in CSD, Nov 1994 edition, filters used were: R<0.1, no errors, 3-D coordinates determined.
[45] Witkowski, S.; Wawer, I. *J. Chem. Soc., Perkin Trans. 2,* **2002**, 433.
[46] Witkowski, S.; Maciejewska, D.; Wawer, I. *J. Chem. Soc., Perkin Trans. 2,* **2000**, 1471.

[47] Kolodziejski, W.; Kecki, Z. *Chem. Phys. Letts.* **1978**, *54*, 286.
[48] Desiraju, G.R.; Steiner, T. *The Weak Hydrogen Bond In Structural Chemistry and Biology*, IUCr Monographs on Crystallography; Oxford Science Publications, Oxford University Press, New York, **1999**.
[49] Nonius, COLLECT; Nonius BV, Delft, The Netherlands, **1998**.
[50] Otwinowski, A.; Minor, W. *Macromolecular Crystallography*, Part A, Carter, C.W.; Sweet, R.M. Eds.; *Methods in Enzymology,* Volume 276; Academic Press; New York; **1997**; pp 307-326.
[51] Altomare, A.; Gascarano, G.; Giacovazzo, C.; Guagliardi, A. *J. Appl. Cryst.* **1993**, *26*, 343.
[52] Altomare, A.; Burla, M.C.; Carnalli, M.; Cascarano, G.; Giavazzo, C.; Guagliardi, A.; Moliterni, A.G.G.; Polidor, G.; Spagan, R. *J. Appl. Cryst.* **1999**, *32*, 115.
[53] Sheldrick, G.M. *Crystallographic Computing 3*, Sheldrick, G.M.; Kruger, C.; Goddard, R. Eds.; Oxford University Press; **1985**, pp 175-189.
[54] Sheldrick, G.M. *Acta Crystallogr.* **1990**, *A46*, 467.
[55] Sheldrick, G.M. SHELXL-97, Institüt für Anorganisxhe Chemie der Universität, Tammanstrasse 4, D-3400 Göttingen, Germany, **1997**.
[56] Barbour, L.J. *J. Supramol. Chem.* **2001**, *1*, 189.
[57] Farrugia, L.J. *J. Appl. Cryst.* **1999**, *32*, 837.

Chapter 3

Other Hydrogen Donor Radical Adducts

3.1 Background

In Chapter 2 the preparation of a series of multi-component adducts of phenol derivatives with the stable radical TEMPO was described. A strategy was developed for the generation and crystallographic analysis of these low-melting supramolecular materials. In this chapter these preliminary studies are built upon and the use of alternative hydrogen bond donor sources is explored in pursuit of a more varied steric and electronic environment. There are a considerable number of potential hydrogen bond donors available for this purpose. The examples presented in this chapter represent groups with known antioxidant activity: polyphenols, hindered amines, and oximes. This chapter begins with a brief review of the structure and antioxidant activity of these donor species as is pertinent to this work.

While monophenols, such as α-tocopherol and its structurally related derivatives, are well-established as chain-breaking antioxidants and, as a result, have been widely studied, there are other classes of antioxidants which may act by a similar mechanism that have not been investigated to the same extent. Polyphenols are one such important class of compounds that have proven antioxidant activity and, consequently, considerable interest has been focused on their study.[1,2,3] Many polyphenols contain a benzene ring with *meta*-substituted hydroxyl groups. It has been postulated that these species can act *via* several mechanisms, but the *meta* dihydroxy groups have been indicated as hydrogen donors in some instances and so are responsible for the antioxidant activity of the species.[1,4,5]

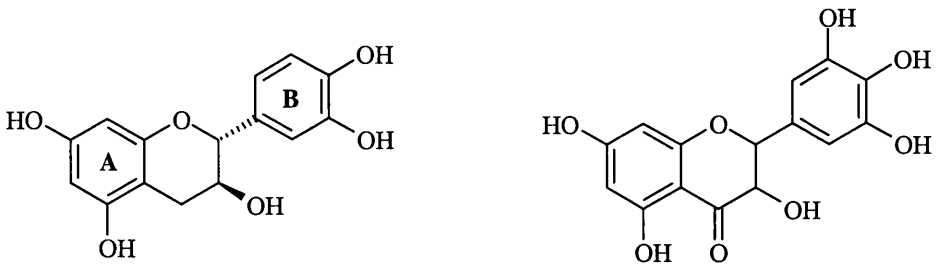

(a) (b)

Figure 3.1: Molecular of polyphenolic flavanols with known antioxidant activity (a) catechin, (b) myricetin. The established labels A and B denote the different rings.

The same dihydroxy substitution pattern is found in alkylresorcinols, species which have also been reported to act as antioxidants and protect polyunsaturated fatty acids against peroxidation.[6,7]

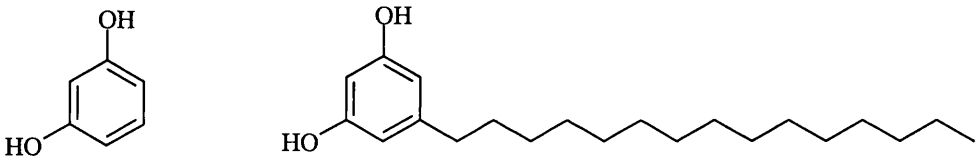

(a) (b)

Figure 3.2: Molecular structures of (a) resorcinol and (b) pentadecylresorcinol, a common alkylresorcinol.

It is known that the *meta*-hydroxy group orientation does not stabilise radical formation by resonance effects and so is not expected to support antioxidant activity by hydrogen donation. However, experiments have shown that oxidation of flavanoids with a catechol structure will take place exclusively in the B ring[4] with the loss of a hydrogen atom from one of the two *meta*-hydroxy groups. Furthermore, quantum chemical calculations on alkylresorcinols have demonstrated that the hydroxyl group attached to the ring is the first target for the hydrogen abstraction.[8] For this reason resorcinol (*m*-dihydroxybenzene), a *meta*-dihydroxy substituted species, is a worthwhile candidate for study.

The hydrogen bonding within resorcinol itself has been well studied in the literature.[9,10,11] Resorcinol has also been reported in a successful co-crystallisation with hexamethylenetriamine.[12] In this co-crystallisation the resorcinol and hexamethylenetriamine molecules are connected by O-H···N hydrogen bonds of (2.67(3) Å, 124(1)°, O···N and 2.73(2) Å, 124(1)°, O···N) in length.

Another hydrogen donor group of interest is the oxime functionality. Some polyphenol systems, structurally related to those shown above, such as catacholoximes[13] and flavanone oximes[14] have also been shown to show antioxidant activity towards lipid systems. In industry, the simple oximes ethyl methyl ketone oxime and cyclohexanone oxime are both commonly used as antioxidants in the protection of paints and lacquers.[15]

From a supramolecular perspective, the oxime functionality has several interesting features.[16] The oxime moiety contains one hydrogen-bond donor and two acceptor atoms, in a similar manner to carboxylic acids. However while carboxylic acids have been extensively explored as a building block in crystal engineering, the supramolecular chemistry of oximes have been investigated to a comparatively far lesser extent. Oxime groups also possess stronger hydrogen bonding capabilities than alcohols, phenols and carboxylic acids.[17,18] In the solid state oximes are usually associated with aggregation *via* O-H···N of *ca.* 2.8Å in a dimer motif.[19,20,21] This oxime-oxime dimer leads to the formation of a hydrogen bonded 6-membered ring; a synthon has been found to be particularly persistent in the crystal structures of oximes. One simple system useful for the analysis of supramolecular contacts is benzaldehyde oxime (Figure 3.3) shown below.

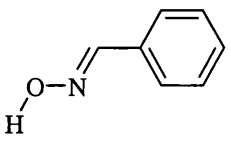

Figure 3.3: Structure of Benzaldehyde oxime.

In addition, hydrogen bond donors based on elements other than oxygen, such as N-H and systems containing acidic C-H groups, have also been shown to participate in structurally significant interactions.[22,23] However, none have yet been reported with radical hydrogen bond acceptors in binary systems. Amines such as diphenyl amine (DPA) and its derivatives are frequently added to commercial and industrial materials to act as antioxidants.[15] However, the mechanism is less well studied than the natural phenolic and polyphenolic antioxidants.

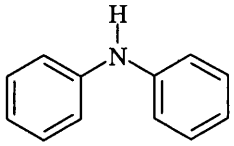

Figure 3.4: Molecular structure of diphenylamine.

It was found during the course of this study that the binary adducts of these hydrogen donor species with TEMPO, as found for the phenol derivatives in Chapter 2, melted below room temperature. The strategy for obtaining X-ray diffraction data on low-melting samples described in Chapter 2 was thus further utilised in the analysis of these multi-component complexes. The results in this chapter consist of a systematic variation of the hydrogen bond donor groups, and the effect of this on the structural features exhibited, in multi-component adducts with TEMPO. The presence of more than one type of potential hydrogen bond donor allows the opportunity to study the interaction between competing patterns. Three adducts are presented herein comprising differing combinations of O-H, N-H and C-H donors, the remainder of this chapter discusses the results obtained.

3.2 Syntheses and Isolation of Radical Adducts 5-7

The structures of a further three hydrogen-bonded adducts of the free radical TEMPO, this time with different hydrogen bond donors have been determined by single crystal X-ray diffraction techniques. These were synthesised from commercially available starting materials.

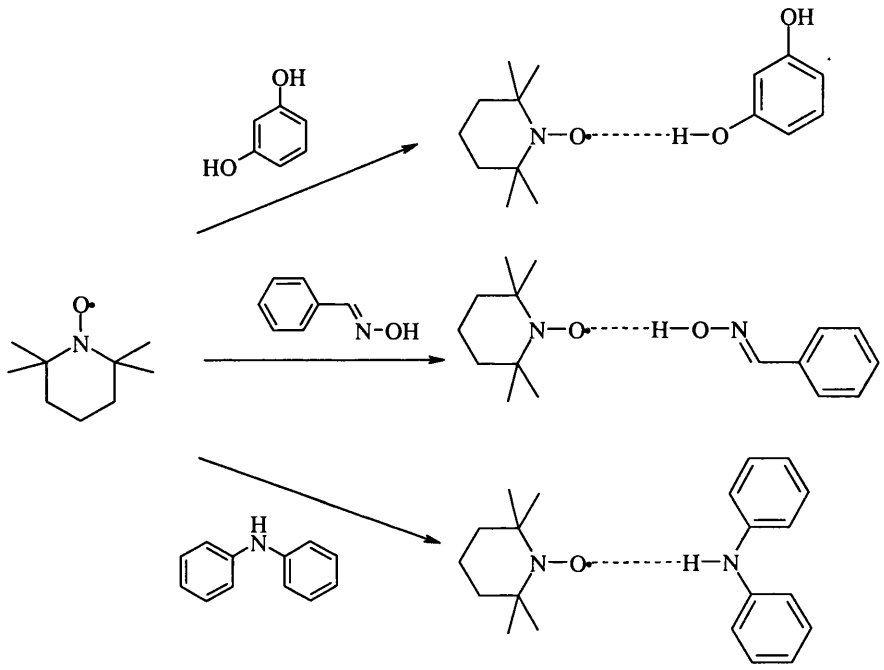

Scheme 3.1: Synthesis of complexes **5-7**.

These co-crystals were prepared by the same general method as described in Chapter 2. These supramolecular syntheses were carried out in non-protic solvents and handled employing techniques used for handling air-sensitive materials. The crystalline product obtained in all cases has a melting point that is below room temperature.

3.3 X-ray Crystal Structures of Radical Adducts

X-ray structures were obtained for all three TEMPO adducts. The structures of these complexes **5-7** will be discussed in this section and a summary of the X-ray crystallographic data obtained is below (Table 3.1). Full crystallographic tables can be found in Appendix A. Numbering of these complexes is consistent where possible with that used previously in Chapter 2.

	5	**6**	**7**
Empirical formula	$C_{15}H_{24}NO_3$	$C_{16}H_{25}N_2O_2$	$C_{30}H_{47}N_3O_2$
M	266.35	277.38	481.71
Crystal system	Monoclinic	Monoclinic	Orthorhombic
Space group	$P2_1/c$	$P2_1/c$	*P b c a*
a / Å	7.892(1)	8.690(1)	12.432(1)
b / Å	12.458(2)	10.283(1)	20.413(1)
c / Å	15.388(3)	16.299(1)	22.302(1)
α / °	90	90	90
β / °	91.952(1)	95.991(1)	90
γ / °	90	90	90
U / Å^3	1512.05(4)	1589.38(4)	5659.68(12)
Z	4	4	8
μ (Mo-Kα) / mm^{-1}	1.170	1.159	1.131
Reflections collected	27786	30976	71544
Independent reflections	3441	6867	6832
R(int)	0.0362	0.0771	0.1009
R1, wR2	0.0486, 0.1300 for 2903 data	0.0458, 0.1221 for 5573 data	0.0445, 0.036 for 4805 data
R indices (all data)	0.0577, 0.1375	0.0609, 0.1351	0.0767, 0.1188

Table 3.1: Crystal and refinement data for complexes **5-7.**

3.3.1 (resorcinol):(TEMPO) Adduct

The co-crystallisation of resorcinol with TEMPO formed **5**, which was shown by crystallography to be the 1:1 adduct $(C_6H_6O_2)$:$(C_9H_{18}NO)$. The asymmetric unit consists of one resorcinol and one TEMPO molecule. The basic structure of **5** and the atomic numbering scheme are shown in Figure 3.5. Relevant bond lengths and angles are collected in Table 3.2.

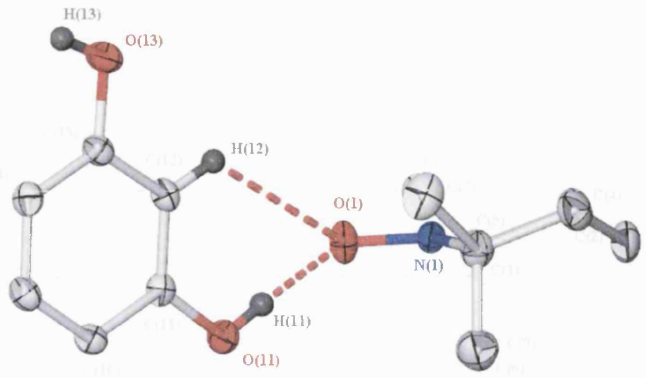

Figure 3.5: Molecular structure of **5,** hydrogen atoms not involved in primary hydrogen bonds omitted for clarity and ellipsoids shown at 50% probability.

Bond lengths		Bond angles	
O(1)-N(1)	1.290(2)	O(1)-N(1)-C(1))	115.60(10)
N(1)-C(1)	1.503(2)	O(1)-N(1)-C(5)	117.38(10)
N(1)-C(5)	1.494(2)		
O(11)-C(11)	1.371(2)	O(11)-C(11)-C(12)	122.10(11)
C(11)-C(12)	1.388(2)	O(11)-C(11)-C(16)	116.99(12)
C(11)-C(16)	1.391(2)	C(12)-C(11)-C(16)	120.90(12)
O(13)-C(13)	1.363(2)	O(13)-C(13)-C(12)	116.69(11)
C(13)-C(12)	1.394(2)	O(13)-C(13)-C(14)	122.57(12)
C(13)-C(14)	1.390(2)	C(14)-C(13)-C(12)	120.72(12)

Table 3.2: Selected bond lengths (Å) and angles (°) of **5.**

As found for co-crystalline complexes in Chapter 2, the intramolecular bond parameters in **5** are unremarkable. However, the availability in this system of two phenolic hydroxy groups provides scope for a range of intermolecular interactions. Although the basic O-H···O· structural motif observed in structures **1-4** is present, the assembly of these dimers in the extended structure is disrupted from the discrete pairs observed in **1** by the presence of the additional hydroxy group on the aryl ring.

The supramolecular structure in **5** comprises two different O-H···O interactions, one involving an O· acceptor and the other an O (non-radical). In **5** one oxygen atom on

resorcinol forms a bifurcated hydrogen bond. This oxygen atom acts as a hydrogen acceptor with the phenolic oxygen atom of an adjacent resorcinol molecule and as a hydrogen donor with an adjacent TEMPO O·. There are also close contacts between *ortho*-aryl hydrogen atoms and the hydrogen bond acceptor oxygen atoms. The hydrogen bond parameters are shown in Table 3.3.

D-H...A	d(D-H)	d(H···A)	D(D···A)	<(DHA)
O(11)-H(11)...O(1)#1	0.81(2)	1.84(2)	2.634(2)	168(2)
O(13)-H(13)...O(1)#2	0.84(2)	1.95(3)	2.774(2)	167(2)
C(12)-H(12)...O(1)#1	0.95	2.91	3.527(2)	123.3
C(14)-H(14)...O(11)#3	0.95	2.94	3.583(2)	125.8

Table 3.3: Hydrogen bond parameters in **5** [Å and °]. Symmetry transformations used to generate equivalent atoms: #1 -x+2,y+1/2,-z+1/2 #2 -x+3,y-1/2,-z+1/2, #3 3-x,y-1/2,1/2-z.

The O-H···O hydrogen bonds in **5** have similar length and angles to that found in the previous chapter. It is important to note that the two interactions are also of similar length to each other [2.634(1)Å, O(11)···O(1), 2.774(2)Å, O(13)···O(1)], even though one involves a radical oxygen acceptor. This feature supports the postulation that O-H···O· hydrogen bonds are of comparable strength to those O-H···O bonds that do not involve a radical acceptor.

The *ortho*-aryl C-H interactions are *ca.* 7% longer than the equivalent interactions noted in Chapter 2. It seems reasonable to suggest that the dominant interactions in this structure are the competing O-H···O motifs and that in the crystal packing these are optimised at the expense of the weaker C-H···O interactions.

The open shell O-H···O· interaction occurs between O(11) and O(1). It is interesting to consider the position of the freely refined hydrogen atom in this interaction relative to the plane of the aryl ring. The core atoms involved in this interaction are depicted in Figure 3.6.

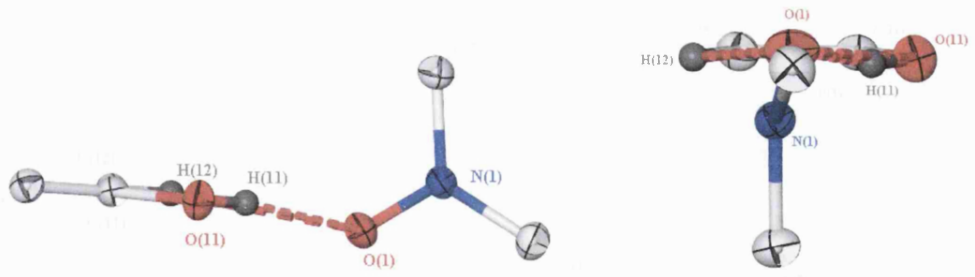

(a) **(b)**

Figure 3.6: 6-membered ring formed by chelating hydrogen bonds in **5,** (a) View down C(11)-C(12), (b) view down O(11)-C(11). Thermal ellipsoids are shown at 50% probability.

It is possible to judge the position of this hydrogen, relative to the aryl plane, by a calculation of its deviation to a least squares plane defined by the atoms in the ring. For H(11) this value is 0.005(0.020)Å, where the RMS deviation for the fitted atoms is 0.008Å. It is evident in this case that H(11) remains planar with the ring system.

Some notable observations also can be made concerning the relative orientation of the TEMPO molecule to the aryl ring. A space-filling diagram illustrates this orientation below (Figure 3.7). The TEMPO molecule is twisted relative to the aryl ring by 75.2°, (calculated using torsion angle between C(12)-C(16)-C(1)-C(5)). This conformation is probably adopted to minimise steric hindrance caused by the TEMPO methyl groups. **5** also exhibits an N-O···D angle of 134.43°, which is in-line with the values obtained for this parameter in Chapter 2.

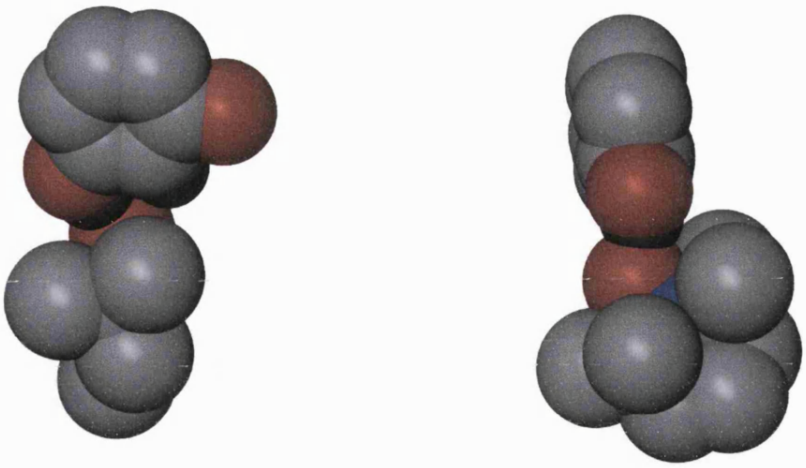

(a) **(b)**

Figure 3.7: Space-filling views of **5** showing the relative orientation of the rings. (a) Face-on view of the aryl plane for O(11)-H(11)···O(1), (b) View perpendicular to the aryl plane for O(11)-H(11)···O(1).

The second O-H···O interaction occurs between O(11) and O(13). There are three possible ways for the resorcinol moiety to hydrogen bond to itself (Figure 3.8). Of these three possible conformations resorcinol OH groups, the bonding scheme exhibited in **5** is that of the divergent form (b) (Figure 3.9).

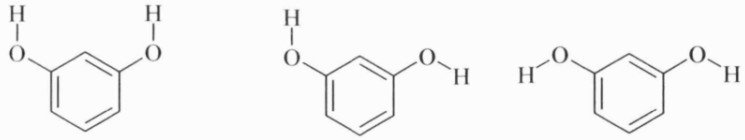

(a) **(b)** **(c)**

Figure 3.8: Structure of the three possible configurations leading to different synthons which can be formed by hydrogen bonding within resorcinol. (a) discrete dimer (b) zigzag chain (c) linear chain.

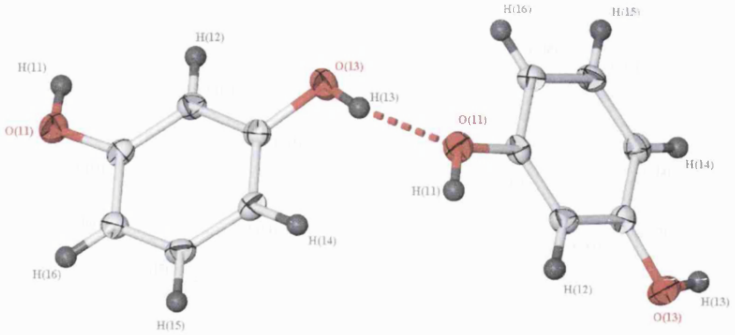

Figure 3.9: Structure of **5** showing the O(11)-O(13) hydrogen bond, thermal ellipsoids shown at 50% probability.

This hydrogen bond perpetuates into the lattice leading to the formation of O-H···O bonded chains of resorcinol. This resorcinol chain runs down the *b*-axis of the crystal structure in a zigzag and the TEMPO molecules form a bifurcated hydrogen bond to O(11) on alternate sides of this chain (Figure 3.10).

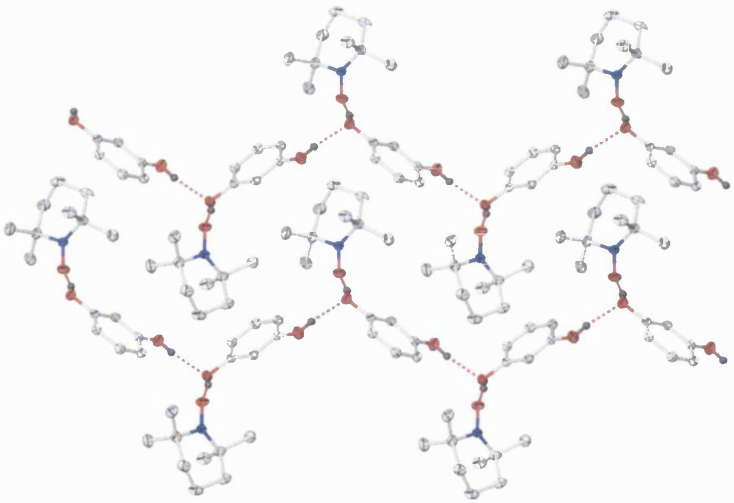

Figure 3.10: View down the *c*-axis showing the intercalating chains in **5**, all fixed hydrogen atoms are omitted for clarity and thermal ellipsoids are shown at 50% probability.

In addition to these moderately strong hydrogen-bonding motifs, there are a number of longer-range interactions to be considered. There are close contacts joining the chains

running along the *b*-axis between one O-H group on resorcinol and a CH_2 group on a TEMPO molecule from an adjacent chain [3.387Å, C(3)···O(13)]. These interconnections join together adjacent chains and thus extend the supramolecular structure from a 1-dimensional chain into a 2-dimensional network (Figure 3.11).

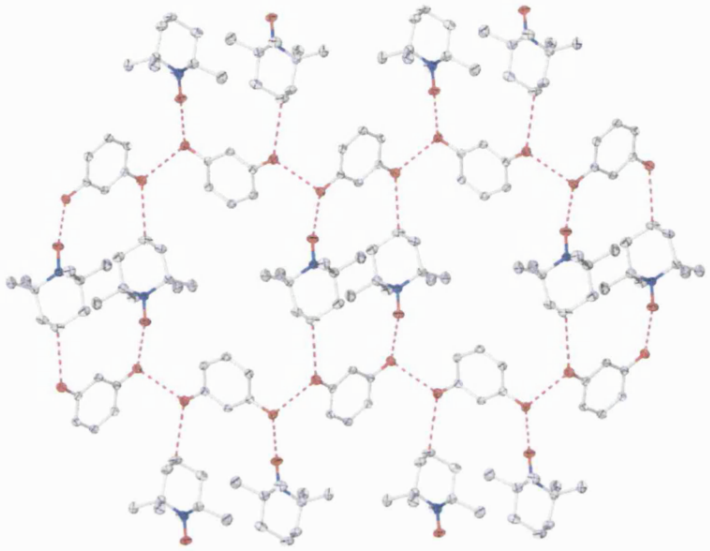

Figure 3.11: View down the *c*-axis showing the intercalating chains in **5,** all fixed hydrogen atoms are omitted for clarity and thermal ellipsoids are shown at 50% probability.

There are, additionally, C-H···π interactions between the centroid of the aryl ring [Cg(1)] and a TEMPO methyl group [3.849Å, Cg(1)···C(6)]. These weaker contacts stretch out above and below the 2-dimensional network joining together the separate layers (Figure 3.12 and 3.13).

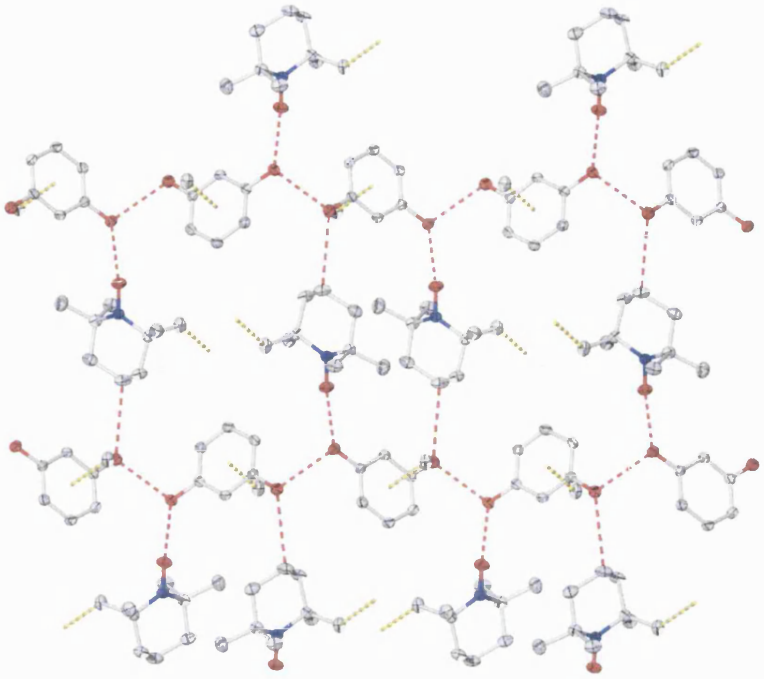

Figure 3.12: Long-range interactions in **5,** all hydrogen atoms are omitted for clarity and thermal ellipsoids are shown at 50% probability.

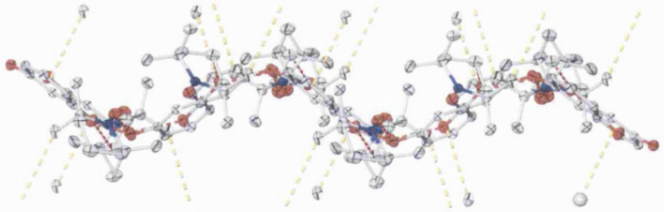

Figure 3.13: View down the *c*-axis showing the intercalating chains in **5,** all fixed hydrogen atoms are omitted for clarity and thermal ellipsoids are shown at 50% probability.

While it has been stated that finite dimers are preferred over infinite chains in adducts with resorcinol, as π-π stacking stabilises the hydrogen bond assembly,[24] **5** shows no evidence of π-π stacking interactions. Hence, the formation of infinite chains over finite dimers is preferred in this case.

3.3.2 (benzaldehyde oxime)·(TEMPO) Adduct

The co-crystallisation of benzaldehyde oxime (C_7H_7NO) and TEMPO ($C_9H_{18}NO$) yielded **6**. The structure determination of **6** shows that the compound contains one equivalent of each component, without any remarkable intramolecular bond lengths or bond angles. The molecular structure of **6** and atomic numbering scheme are shown in Figure 3.14. Relevant bonds and angles are collected in Table 3.4.

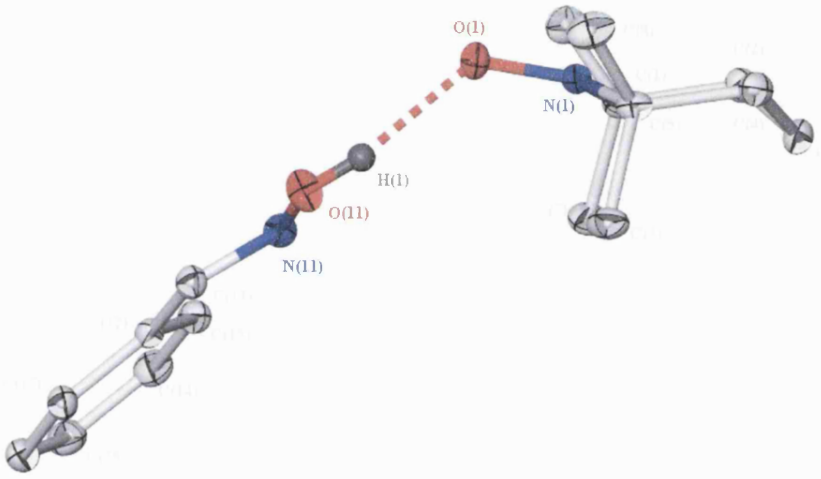

Figure 3.14: Molecular structure of **6**, fixed hydrogen atoms omitted for clarity and thermal ellipsoids shown at 50% probability.

Bond lengths		Bond angles	
O(1)-N(1)	1.290(1)	O(1)-N(1)-C(1)	116.58(6)
N(1)-C(1)	1.492(1)	O(1)-N(1)-C(5)	116.21(7)
N(1)-C(5)	1.500(1)		
O(11)-N(11)	1.404(1)	C(11)-N(11)-O(11)	110.25(7)
N(11)-C(11)	1.283(1)	N(11)-C(11)-C(12)	120.82(7)

Table 3.4: Selected bond lengths (Å) and angles (°) of **6**.

As the oxime component is able to act as both a donor and an acceptor in hydrogen bonding interactions there is potential for a range of competing hydrogen-bonding

schemes. In this case the oxime moiety is engaged in several different hydrogen bonding interactions. The hydrogen bond parameters for these interactions are given in Table 3.5.

D-H...A	D(D-H)	d(H···A)	d(D···A)	<(DHA)
O(11)-H(1)···O(1)	0.907(15)	1.786(15)	2.681(15)	168.1(15)
C(3)-H(3B)···O(11)_#1	0.97	2.89	3.349(1)	110.1
C(11)-H(11)···O(11)_#2	0.93	2.79	3.520(1)	136.6

Table 3.5: Hydrogen bonding in **6** [Å and °]. Symmetry transformations used to generate equivalent atoms: #1 1+x,y,z, #2 –x,1-y,2-z.

On the supramolecular level this structure is aggregated *via* a combination of O-H···O and two different types of C-H···O hydrogen bonds. The two independent moieties in asymmetric unit are involved in an intramolecular O-H···O hydrogen bond, as might be expected on the basis of the previously characterised structures of TEMPO adducts. The two components are held together and aggregation occurs *via* O-H···O interactions, between the O-H groups of the oxime and the oxygen centre of the TEMPO radical. The oxime moiety in **6** also forms self-complementary intermolecular hydrogen bonds with a neighbouring oxime group to make an oxime dimer, which is made possible due to the E configuration of the oxime moiety [178.8°, C(12)-C(11)-N(11)-O(11)]. This forms centrosymmetric, nearly planar 8-membered rings consisting of two C-H···O hydrogen bonds. There are additionally short C-H···O interactions between TEMPO CH_2 groups and neighbouring oxime oxygen atoms.

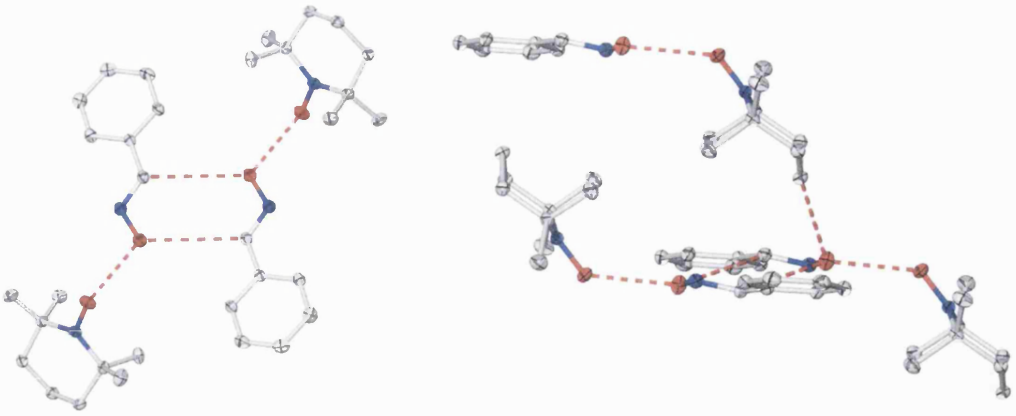

(a) **(b)**

Figure 3.15: (a) View of dimer structure in **6** including O-H···O bond, (b) perpendicular view of the dimer showing the C-H···O interaction. Hydrogen atoms are omitted for clarity and thermal ellipsoids are shown at 50%.

The open-shell O-H···O hydrogen bond is comparatively shorter than others determined in this series [2.681(15)Å, O(11)···O(1)] and is also effectively linear [168.1(15)°, O(11)-H(11)···O(1)] indicating its probable strength. As H(1) is freely refined, there are some notable observations that can be made concerning its position. Calculation of the deviation of H(1) from a least squares plane defined by the other 9 non-hydrogen atoms in the oxime moiety gives result of 0.217(0.001)Å for H(1), while the RMS deviation of the fitted atoms is 0.053Å. This is quite a large deviation and suggests an appreciable movement out of the plane of the hydroxy hydrogen atom. It is also interesting to note the orientation of the two rings relative to each other (Figure 3.16). The N-O···D angle in **6** is 133.15°, which is consistent with the other adducts obtained **1-5**.

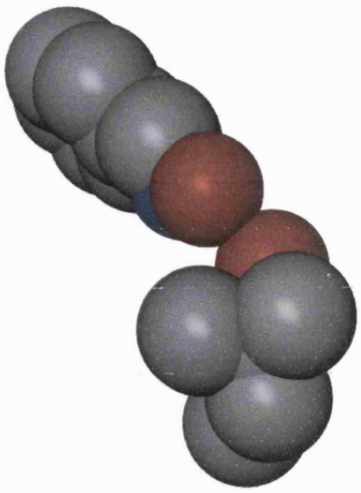

Figure 3.16: Space-filling views of **6** perpendicular to the aryl plane showing the relative orientation of the oxime and TEMPO rings.

The C-H···O hydrogen bonds from which the oxime dimer is assembled are also of reasonable length and linearity for this type of interaction [3.520(1)Å, 136.6°]. In oxime crystal structures the 6-membered ring system involving two O-H···N bonds commonly found is considered a defining feature of the supramolecular structure of oximes, so it is surprising that it does not remains a principal motif in this binary adduct. As the oxime OH group is involved in a hydrogen bonding interaction with the TEMPO moiety, it is not free to form the 6-membered ring system.

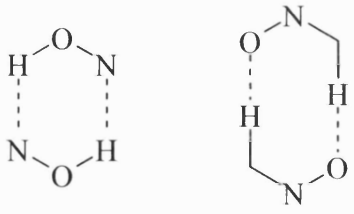

Figure 3.17: 6-membered and 8-membered ring hydrogen bond synthons found in oxime crystal structures.

A CSD search for the 8-membered synthon revealed only 14 hits, for which the mean O···C distance in these structures is 3.480Å. (Search for 8-membered ring dimer system

in oxime, filters used were R<0.1, no errors and 3-D coordinates determined. The remaining C-H···O hydrogen bond [3.349(1)Å, 110.1°] is reasonably short, and is also at quite an acute angle.

The combination of these different hydrogen bond motifs determines the packing in the supramolecular structure of **6**. The oxime moieties are arranged trans with respect to each other and form oxime-oxime dimers. Each oxime oxygen atom in these dimers is also linked to neighbouring TEMPO molecules by O-H···O hydrogen bonds, which interconnect the structure into 1-D chains via C-H···O hydrogen bonds (Figure 3.18). The oxime-oxime interaction links these chains to form channels along the *c*-axis (Figure 3.19).

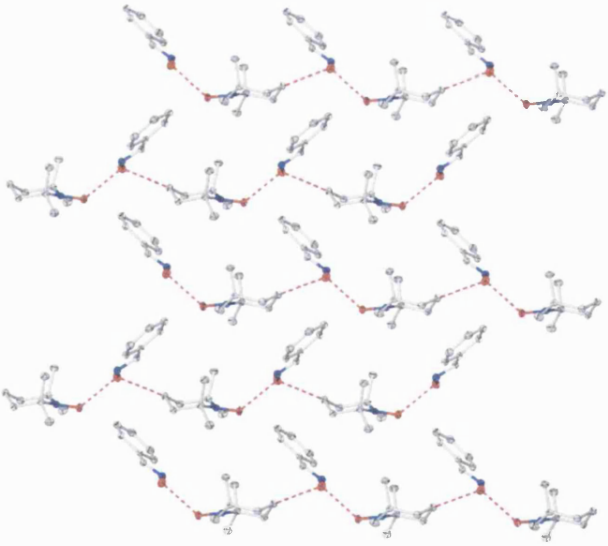

Figure 3.18: Projection along *ac* showing the chains of O-H···O, C-H···O. Hydrogen atoms are removed for clarity and thermal ellipsoids are shown at 50%.

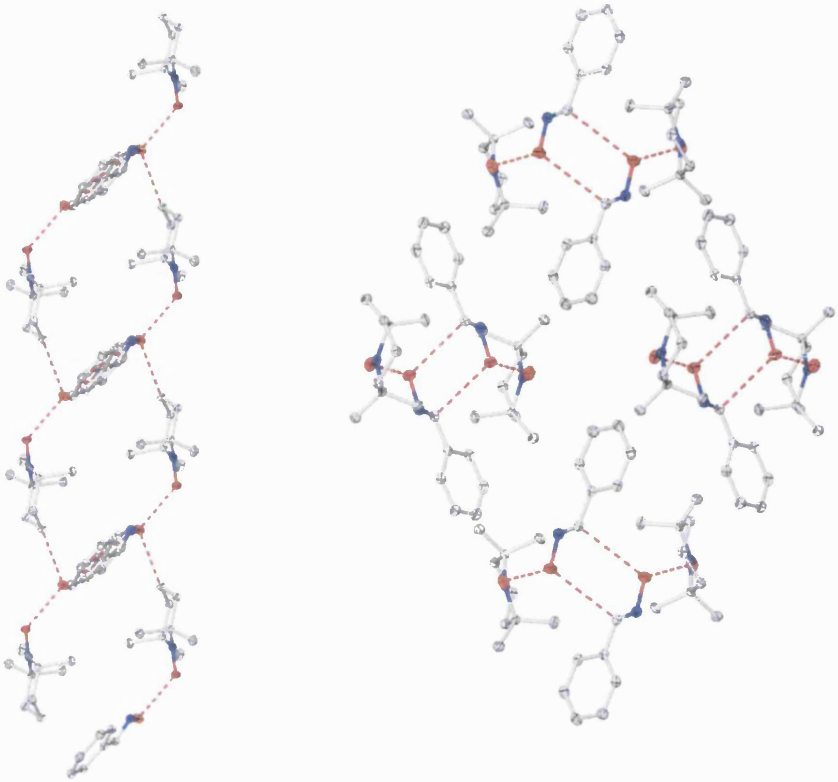

(a) **(b)**

Figure 3.19: (a) Projection in the *ab* plane showing the aggregation of the dimer units along the axis forming channels down the *c*-axis, (b) Perpendicular view down the *a*-axis showing the dimer unit chains. Hydrogen atoms are removed for clarity and thermal ellipsoids are shown at 50%.

3.3.3 (diphenylamine)·(TEMPO) Adduct

Co-crystallisation of diphenylamine with TEMPO afforded adduct **7**. The structure determination of **7** showed that the asymmetric unit contains two crystallographically independent molecules of TEMPO and one molecule of diphenylamine without any remarkable intramolecular bond lengths or bond angles. The molecular structure of **7** and atomic numbering scheme is shown in Figure 3.20. Relevant bond parameters are collected in Table 3.6.

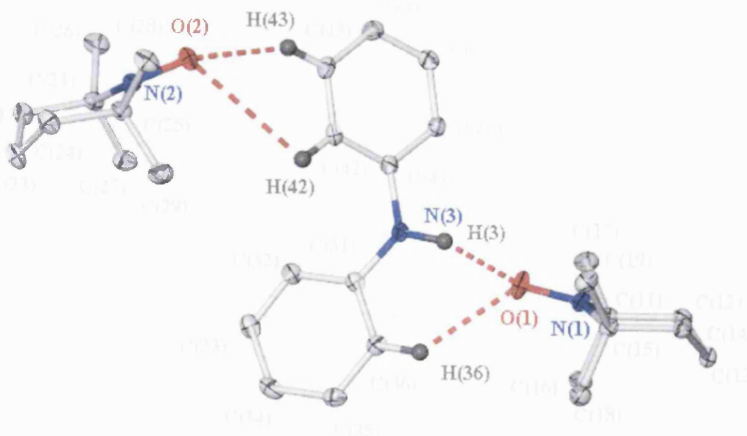

Figure 3.20: Molecular structure of **7**, non-hydrogen bonding hydrogen atoms omitted for clarity and ellipsoids shown at 50% probability.

Bond lengths		Bond angles	
O(1)-N(1)	1.283(2)	O(1)-N(1)-C(11)	116.20(10)
N(1)-C(11)	1.494(2)	O(1)-N(1)-C(15)	115.29(10)
N(1)-C(15)	1.501(2)	C(11)-N(1)-C(15)	124.71(10)
O(2)-N(2)	1.285(2)	O(2)-N(2)-C(21)	115.73(10)
N(2)-C(21)	1.498(2)	O(2)-N(2)-C(25)	115.71(10)
N(2)-C(25)	1.501(2)	C(21)-N(2)-C(25)	124.68(10)
N(3)-C(31)	1.392(2)	C(31)-N(3)-C(41)	128.27(12)
N(3)-C(41)	1.401(2)		

Table 3.6: Selected bond lengths (Å) and angles (°) of **7**.

The two aryl rings in the diphenylamine moiety exhibit a twist of 41.03 (0.03)° relative to each other (Figure 3.20). This is a common occurrence for this ring frame, as a result of steric hindrance between the aryl hydrogen atoms H(32) and H(42). On a supramolecular level the two different molecules in this co-crystal are interconnected *via* two different intramolecular hydrogen bonds. In one such interaction, the amine N-H group is engaged in an N-H···O interaction with the TEMPO oxygen atom on one of the two TEMPO molecules. The second occurs between the second molecule of TEMPO and an aryl C-H group from diphenylamine. A similar stoichiometry in the crystal structure was obtained for adduct **2**, the difference being that in this case the second molecule is not

uncoordinated as occurred in **2**, but is instead engaged in a second type of hydrogen bond (Figure 3.21). Furthermore, both of these interactions are supported by secondary *ortho*-aryl C-H hydrogen bonds. The hydrogen bond parameters for **7** are shown in Table 3.7.

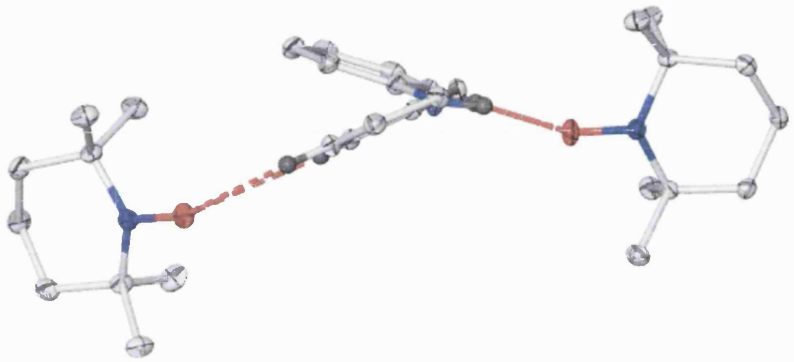

Figure 3.21: Perpendicular view of **7**, non-hydrogen bonding hydrogen atoms omitted for clarity and ellipsoids shown at 50% probability.

D-H...A	d(D-H)	d(H···A)	d(D···A)	<(DHA)
N(3)-H(3)···O(1)	0.88(2)	1.98(2)	2.825(2)	160.8(14)
C(36)-H(36)···O(1)	0.95	2.51	3.271(2)	137.0
C(43)-H(43)···O(2)	0.97(2)	2.33(2)	3.204(2)	149.1(11)
C(42)-H(42)···O(2)	0.95	3.24	3.635(2)	106.8
C(16)-H(16A)···O(2)#1	0.98	2.684	3.647	167.2
C(18)-H(18C)···O(2)#1	0.98	2.724	3.690	168.8

Table 3.7: Hydrogen bonding in **7** [Å and °]. Symmetry transformations used to generate equivalent atoms: #1 7/2-x,y-1/2,z.

The open shell N-H···O· interaction occurs between N(3) and O(1). The donor-acceptor distance for the N-H···O interaction in **7** is sufficiently short to suggest the occurrence of intermolecular hydrogen bonding [2.825(2)Å]. As the isotropic van der Waals radii for nitrogen is slightly larger than for oxygen,[25] the slight increase in D···A over the values obtained previously for open-shell O-H···O bonds is expected. It should also be noted that a search of the CSD for intermolecular contacts between N-H donor and O-N acceptors[26] gives a mean value for N···O as 2.935Å (Figure 3.22).

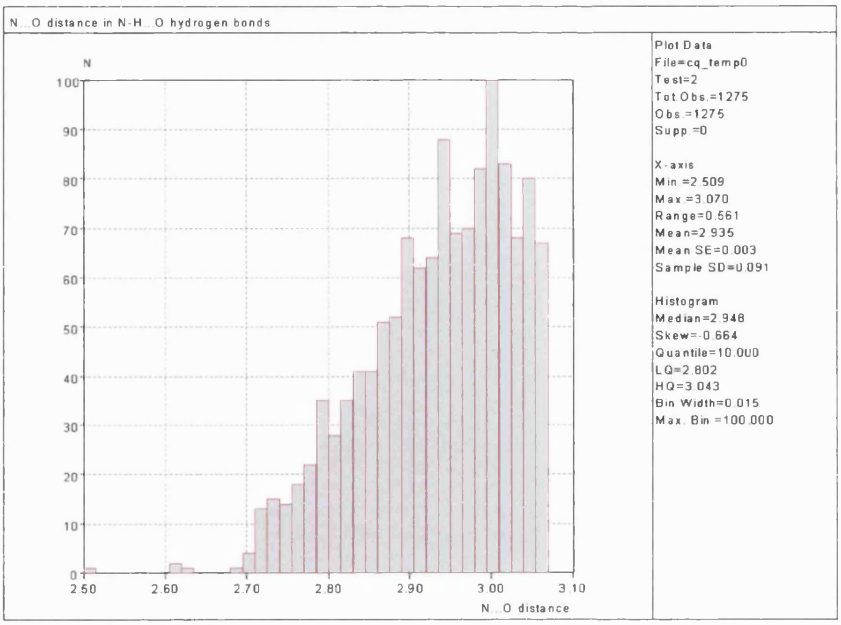

Figure 3.22: Histogram showing results of CSD search for N-H···O hydrogen bonds.

As H(3) is freely refined in **7**, it is interesting to note its position relative to the plane of the aryl ring. This may be judged by a calculation of its deviation to a least squares plane defined by the atoms in the ring. For H(3) this value is 0.196(0.003)Å, where the RMS deviation for the fitted atoms is 0.003Å. This is quite a large deviation from planarity, which suggests the hydrogen atom is approaching the transition state geometry.[27,28] The core atoms involved in this interaction are depicted in Figure 3.23.

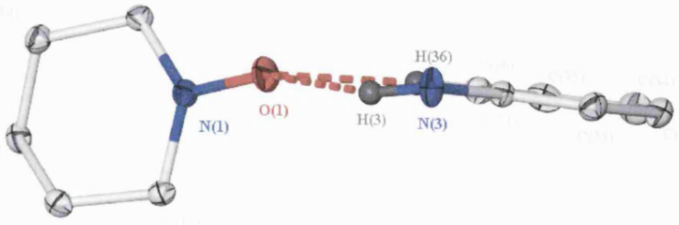

Figure 3.23: Core structure of the N(3)-H(3)···O(1) hydrogen bond in **7**, non-hydrogen bonding hydrogen atoms omitted for clarity and ellipsoids shown at 50% probability.

It is also clear that the relative orientation between the ring on the donor and on the acceptor is twisted, as found for other adducts with unhindered *ortho* ring positions. The torsion angle between these two ring planes in **7** is 97.4° [C(32)–C(36)–C(15)–C(11)]. Also the N-O···D angle is 161.35°, which is much larger than the other adducts characterised previously [range 89.40-138.73° for **1-6**]. These features are further illustrated in Figure 3.24.

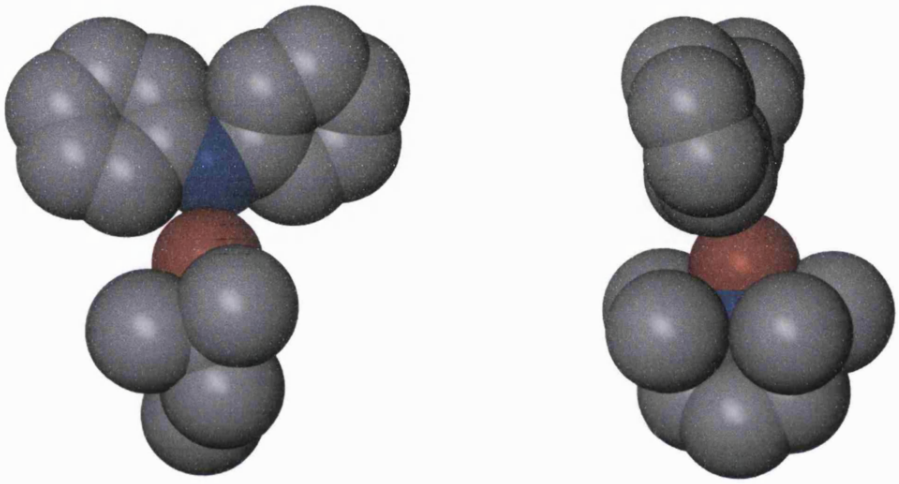

(a) **(b)**

Figure 3.24: Space-filling views of the N(3)-H(3)···O(1) interaction in **7** (a) View of the aryl plane, (b) view perpendicular to the aryl plane showing the relative orientation of the DPA and TEMPO rings.

There are three separate open-shell C-H···O hydrogen bonds in **7.** As C-H groups are weaker hydrogen donors than the more electronegative N-H and O-H bonds, C-H···O hydrogen bonds are expected to be weaker, and longer, than their N-H···O and O-H···O equivalents. The C(36)···O(1) and C(43) ···O(2) interactions are of comparable length to those obtained for previous adducts [3.271(2)Å and 3.204(2)Å]. The third between C(42) and O(2) is longer at 3.635(2)Å, which is likely to be due to the acute angle C-H-O [106.8°]. This highlights an important feature of the hydrogen bond competition within these adducts. In previous structures, C-H···O interactions were obtained only in support

of a shorter O-H···O interaction. In this situation the bond distance and angles are determined, to some degree, by this constraint. In **7** the interaction involving C(36) is only *ca.* 3% longer than the one involving C(43), while the latter may be considered the primary interaction to the O(3) TEMPO oxygen atom. Indeed, in **7** an open-shell C-H···O hydrogen bond is formed at the expense of an additional N-H···O, suggesting that the stabilisation energy of the two hydrogen-bonding schemes is comparable.

The position of the freely refined H(43) may be considered in a similar manner to H(3). The deviation is calculated as 0.007(0.002)Å, with a RMS for the fitted atoms of 0.012Å. In comparison to the other open-shell hydrogen bonds, this hydrogen atom clearly remains within the aryl plane. The core atoms involved in this interaction are depicted in Figure 3.25.

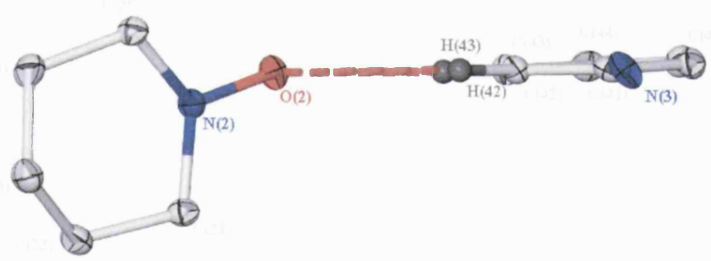

Figure 3.25: Core structure of the C(43)-H(43)···O(2) hydrogen bond in **7**, non-hydrogen bonding hydrogen atoms omitted for clarity and ellipsoids shown at 50% probability.

There are several differences in the geometry around the C(43)···O(2) interaction by comparison to the N(3)···O(1). The torsion angle between these two ring planes in **7** is 93.9° [C(42)–C(44)–C(25)–C(21)] and the N-O···D angle is 149.84°. This is illustrated in the space-filling diagram below (Figure 3.26).

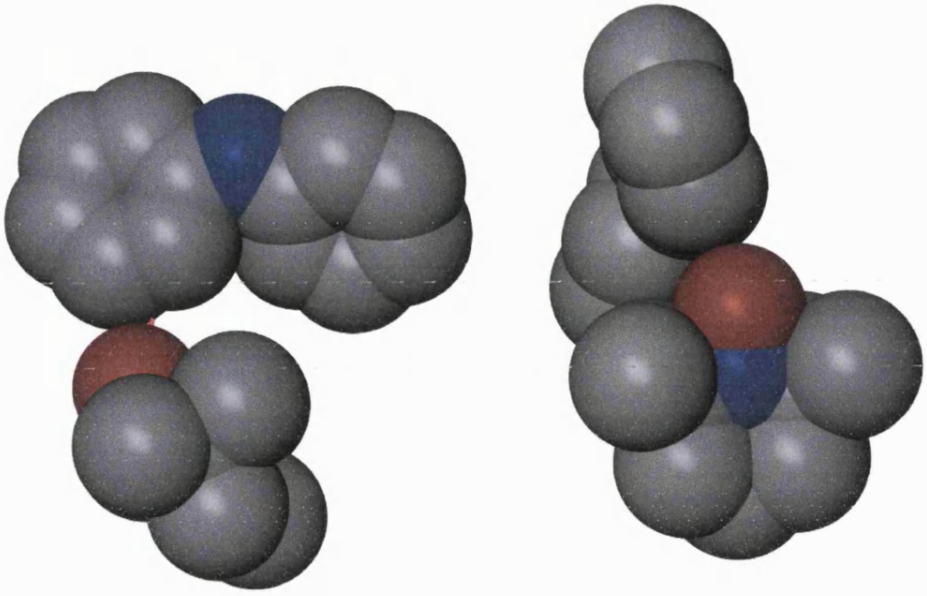

(a) **(b)**

Figure 3.26: Space-filling views of the C(43)-H(43)···O(2) interaction in **7** (a) View of the aryl plane, (b) view perpendicular to the aryl plane showing the relative orientation of the DPA and TEMPO rings.

There are some further long-range interactions to be considered. The methyl groups C(16) and C(18) are 3.647Å and 3.690Å from O(2) respectively. These interactions assemble the hydrogen bonded (diphenylamine)·$(TEMPO)_2$ units into zigzagging chains which run along the *b*-axis. In the crystal packing the aryl rings are staggered, so there are no π-π stacking interactions.

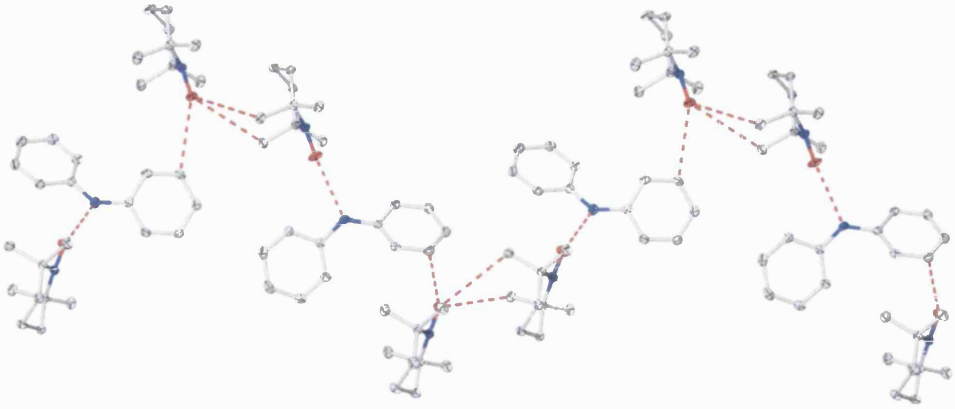

Figure 3.27: Long-range interactions in **7** viewed along the *b*-axis, all hydrogen atoms are omitted for clarity and thermal ellipsoids are shown at 50% probability.

3.4 Concluding Remarks

The dominating intermolecular interaction observed in structures **5-7** is an open-shell hydrogen bond from several different donor groups to the TEMPO oxygen atom. Although the donors studied in this chapter offered several options for assembly, this primary motif (X-H···O·) remains intact. In the case of **6** this open-shell motif displaces the persistent oxime-oxime dimer synthon, which indicates this motif provides a significant stabilisation in the solid-state. The structure of **7** contains both the expected N-H···O interaction alongside an additional, and extremely short, C-H···O open-shell hydrogen bond. As both are present, rather than the exclusive formation of either one, it can be inferred that the two offer a similar stabilisation energy for the co-crystal. These structures also contain a multitude of weaker C-H···π interactions, but they do not display the same consistency and regularity as the primary open-shell X-H...O· hydrogen bond. This demonstrates the ability of stronger hydrogen bonds to dictate the structural outcome over weaker interactions.

Several conclusions can be drawn concerning the molecular geometry around the primary hydrogen bonds. The orientation (torsion angle) of the two rings with respect to each other in these molecules fall in the range of 75.2 – 97.4°. Comparison with the same feature in the phenol adducts (Chapter 2) indicates that there is a preference for staggered orientation of the two ring systems. This is not surprising as the methyl substituents on the TEMPO moiety provide a barrier to rotation in this manner.

In each primary open-shell interaction, the hydrogen atom involved was freely refined. It is interesting to note that in **7** the N-H···O interaction, presumed to be the strongest on electronegativity grounds, the freely refined H(3) is found to lie 0.196(0.003)Å out of the plane of the aryl ring. This large deviation suggests that the hydrogen atom is approaching the transition state geometry, as seen earlier in the adducts **2**, **3** and **4**. In the

same structure, the short and primary C-H···O interaction has a relatively small deviation of 0.007(0.002)Å.

3.4 Experimental

For details on the general considerations, characterisation and solid-state determination see Chapter 2 (Section 2.4).

Synthesis and characterisation of adducts 5 - 7

Formation of (5)

Scheme:

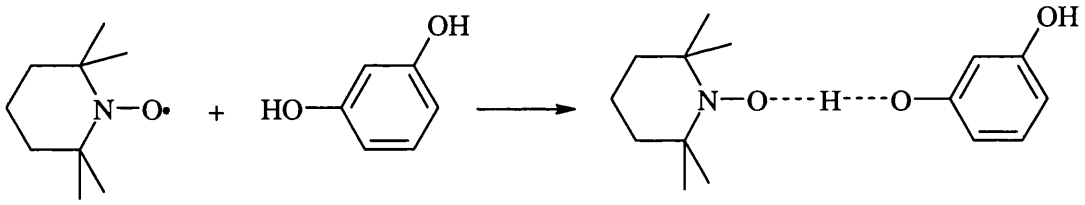

Dry toluene (10 ml) was added, under argon, to a schlenk containing solid resorcinol (0.55 g, 5 mmol) and 2,2,6,6-tetramethylpiperidine-1-oxyl (TEMPO) (0.78 g , 5 mmol). This was stirred at room temperature for 30 minutes resulting in a clear red solution. On leaving the solution at –80°C a crop of red crystals suitable for X-ray diffraction were obtained. The product was isolated by removing solvent with a filter cannula, yield obtained 0.98 g, 74 %. M.p. -11°C. Elemental analysis: Calcd for $C_{15}H_{24}O_3N$: C, 67.62 %, H, 9.08%, N, 5.26 %. Found: C, 67.5%; H, 10.1%; N, 6.62%.

Formation of (6)

Scheme:

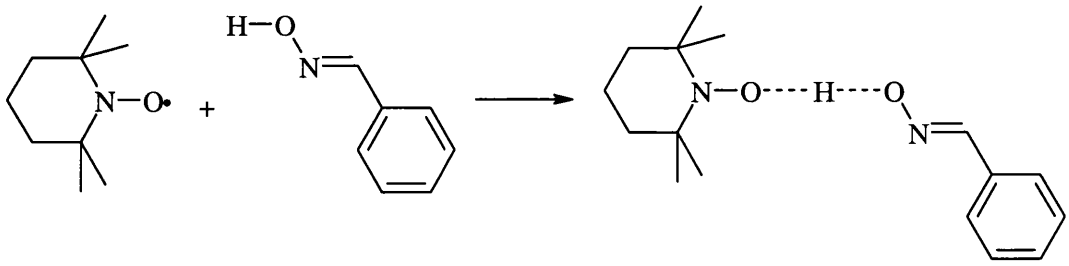

Dry toluene (10 ml) was added, under argon to a schlenk containing liquid benzaldehyde amine (0.54 g, 5 mmol) and 2,2,6,6-tetramethylpiperidine-1-oxyl (TEMPO) (0.78 g, 5 mmol). This was heated until dissolved and stirred at room temperature for 30 minutes to give a clear red solution. On leaving the solution at –80°C a crop of pale red crystals suitable for X-ray diffraction were obtained. The product was isolated by removing solvent with a filter cannula, yield obtained 1.16 g, 84 %. M.p. –18°C. Elemental analysis: Calcd for $C_{16}H_{25}O_2N_2$: C, 69.27 %, H, 9.09 %, N, 10.10 %. Found: C, 67.7%; H, 9.41%; N, 10.4%,

Formation of (7)

Scheme:

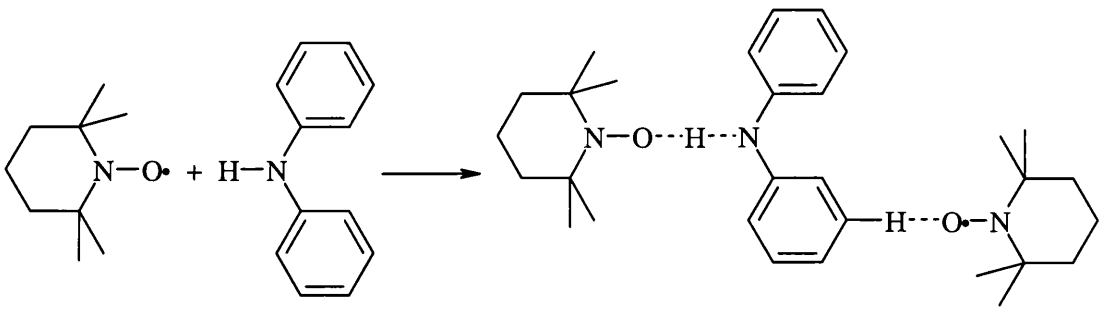

Dry toluene (10 ml) was added, under argon to a schlenk containing solid diphenylamine (0.84 g, 5 mmol) and 2,2,6,6-tetramethylpiperidine-1-oxyl (TEMPO) (1.56 g, 10 mmol). This was stirred at room temperature for 30 minutes to give a clear red solution. On leaving the solution at –80°C a crop of red crystals suitable for X-ray diffraction were

obtained. The product was isolated by removing solvent with a filter cannula, yield obtained 1.75 g, 73 %. M.p. –8°C. Elemental analysis: Calcd for $C_{30}H_{47}O_2N_3$: C, 74.79 %; H, 9.84 %; N, 8.73%. Found: C, 77.5%; H, 8.96%; N, 9.34%,

3.5 References

[1] Pietta, P.-G. *J. Nat. Prod.* **2000**, *63*, 1035.
[2] Rice-Evans, C.A.; Diplock, A.T. *Free Radic. Biolol. Med.* **1993**, *15*, 77.
[3] Rice-Evans, C.A.; Packer, L. Flavanoids in Health and Disease, New York, Marcel Dekker, Inc.; **1998**.
[4] Cren-Olivé, C.; Hapiot, P.; Pinson, J.; Rolando, C. *J. Am. Chem. Soc.* **2002**, *124*, 14027.
[5] Wright, J.S.; Johnson, E.R.; Di Labio, G.A. *J. Am. Chem. Soc.* **2001**, *123*, 1173.
[6] Kozubek, A.; Tyman, J.H.P. *Chem. Rev.* **1999**, *99*(1), 1 and the references herein.
[7] Kamal-Eldin, A.; Pouru, A.; Eliasson, C.; Åman, P. *J. Sci. Food Agric.* **2000**, *81*, 353.
[8] Hladyszowski, J.; Zubik, L.; Kozubek, A. *Free Rad. Res.* **1998**, *28* (4), 359.
[9] Robertson, J.M. *Proc. R. Soc. London, Ser. A,* **1936,** *157*, 79.
[10] Bacon, G.E.; Curry, N.A. *Proc. R. Soc. London, Ser. A,* **1956,** *235*, 552.
[11] Robertson, J.M. Ubbelohde, A.R. *Proc. R. Soc. London, Ser. A,* **19368** *167*, 122.
[12] Mahmoud, M. M.; Wallwork, S.C. *Acta Cryst.* **1979**, B35, 2370.
[13] Ley, J.P.; Bertram, H.-J. *Eur. J.Lipid Sci.Tech.* **2002**, 6, 319.
[14] Metodiewa, D.; Kochman A.; Koceva-Chyla A. *Anticancer Research.* **1999**, 19(2A), 1249.
[15] Ranney, M.W. *Antioxidants Recent Developments*, Chemical Technology Review No. 127, Noyes Data Corporation, **1979**.
[16] C. B. Aakeröy, A. M. Beatty, and D. S. Leinen, *Cryst. Growth. Des.* **2001**, *1*, 47.
[17] A. W. Marsman, E. D. Leussing, J. W. Zwikker, and L. W. Jenneskens, *Chem. Mater.* **1999**, *11*, 1484.
[18] Geiseler, G.; Fruwert, J. *Z. Phys. Chem.* **1960**, *26*, 111 and references therein.
[19] Etter, M.C.; Macdonald, J.C.; Bernstein, J. *Acta Cryst.* **1990**, *B46*, 256.
[20] Karle, I.L.; Ranganathan, D.; Haridas, V. *J. Am. Chem. Soc.* **1996**, *118*, 7128.
[21] Hokelek,, T.; Tas, M.; Bati, H. *Cryst. Res. Technol. 39*, **2004**, *4*, 363.
[22] Jeffrey, J.A. *Introduction to Hydrogen Bonding,* University Press, Oxford; **1997**, pp56-79.
[23] Steiner, T. *Angew. Chem. Int. Ed. Engl.* **2002**, *41*(1), 49.
[24] MacGillivray, L.R.; Reid, J.L.; Ripmeester, J.A. *J. Am. Chem. Soc.* **2000**, *122*, 7817.
[25] Bondi, A.J. *J. Phys. Chem.* **1964**, *68*, 441.
[26] CSD search on version 5.26 obtained 779 hits using the following filters: no errors, R<0.1, 3-D coordinates determined.
[27] Sun, Y.-M.; Liu, C.-B. *Eur. J. Org. Chem.* **2004**, 120.
[28] Singh, N.; O'Malley, P.J.; Popelier, P.L.A. *Phys. Chem. Chem. Phys.* **2005**, *7*, 614.

Chapter 4

Structural Characterisation of Galvinoxyl Radical Derivatives

4.1 Background

The previous two chapters have described the supramolecular synthesis and X-ray crystal structures of a number of hydrogen-bonded adducts involving the persistent free radical TEMPO. In an extension of our investigations into these open-shell interactions with various species possessing at least one moderately strong hydrogen bond donor group, a further persistent radical was chosen for study, namely, galvinoxyl (2,6-di-*tert*-butyl-α-(3,5-di-*tert*-butyl-4-oxo-2,5-cyclohexadien-1-ylidene)-*p*-tolyloxy). Having investigated the interactions of an aminoxyl radical, it was thought that the supramolecular synthesis of related hydrogen-bonded interactions involving a phenoxyl radical would be useful in order to investigate the postulation that such open-shell structural motifs are not restricted to aminoxyl radicals. Galvinoxyl is well known to react rapidly with phenols to give the corresponding phenoxyl radicals and hydrogalvinoxyl as products.[1] However, during the course of the investigation into the supramolecular synthesis of hydrogalvinoxyl adducts with phenoxyl radicals, unexpected results were obtained. These reactions, instead, led to the formation of the radical-radical recombination products. This chapter will report our results relating to this investigation, describing the preparation and characterisation of four galvinoxyl derived products obtained by the reaction of galvinoxyl in quantitative amounts with either phenol or amine species. The introduction first begins with a brief review of the current understanding of the structure and reactivity of the galvinoxyl free radical.

The hindered phenoxyl radical galvinoxyl, first reported in 1957,[2,3] is a persistent radical which is stabilized by the presence of bulky *tert*-butyl groups near the radical site. Since then, galvinoxyl has primarily been studied on the basis of observed magnetic behaviour. It has been found that between 300 K and 85 K galvinoxyl shows ferromagnetic behaviour, due to parallel stacking between planar galvinoxyl molecules, while below 85 K it undergoes a phase transition that results in antioferromagnetic behaviour.[4,5] Galvinoxyl has also found widespread use as a radical scavenger of shorter lived radicals[6,7,8] and as such is usually considered an inhibitor of autoxidation.

Williams first reported the X-ray single crystal structure determination of the free galvinoxyl radical in 1969.[9] This confirmed the planarity of the ring system, with an angle of only 12° between the rings. The molecular structure also exhibited C_2 symmetry with both C-O bonds of equal length (1.721Å). This indicates that the unpaired electron is delocalised throughout the conjugated bond system. The main resonance structures for this are shown in Figure 4.1.

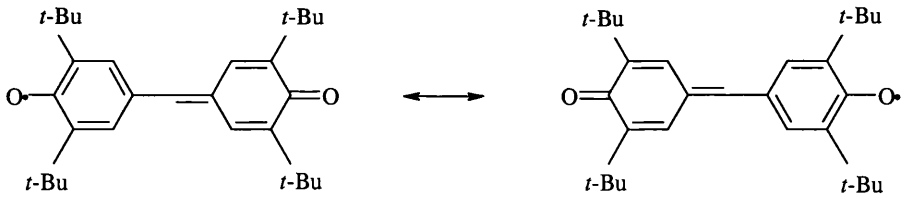

Figure 4.1: Diagram of the major resonance structures for the galvinoxyl free radical.

The electronic structure was also recently examined[10] in order to study its magnetic properties. It is noteworthy that very few crystal structures derived from galvinoxyl have been published. In a search of the CSD[11] to date only 5 structures showed the relevant related molecular structure. The solution-state chemistry of the galvinoxyl radical however, is extremely well studied. It has been previously shown that galvinoxyl appears to react quantitatively with carbon and oxygen centre radicals, which is quite unusual.[12]

The reaction of galvinoxyl with reactive radicals such as *tert*-butoxy and superoxide in particular is quite well known and this reaction forms cyclohexadienone intermediates.[13] It is also known to react rapidly with phenols *via* a hydrogen abstraction process and is often used as a hydrogen abstraction agent (Figure 4.2).

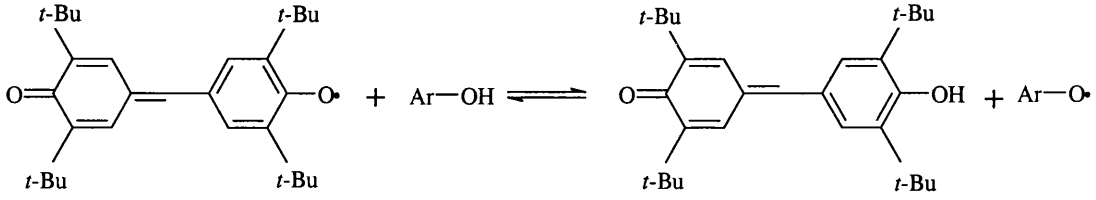

Figure 4.2: The reaction between the galvinoxyl free radical and a phenol.

Confirmation of the formation of the phenoxyl radical species (ArO·) on the reaction of phenols with galvinoxyl has been obtained by ESR methods.[14] There are a large number of kinetic studies on the hydrogen abstraction from phenols using galvinoxyl to generate the phenoxyl radicals, as shown above in Figure 4.2, which have recently been used in mechanistic studies to elucidate hydrogen atom transfer reaction mechanisms.[15,16,17]

4.2 Syntheses and Characterisation of Galvinoxyl Recombination Products

Considering the known rapid reactivity of galvinoxyl with phenols under deaerated conditions, it was envisaged that the supramolecular synthesis of the hydrogen-bonded phenoxyl adduct would be achieved in a similar manner to the equivalent aminoxyl interaction observed in Chapters 2 and 3. As it has been suggested that phenols that are substituted at all *ortho* and *para* positions are less susceptible to recombination reactions such as these, it was thought that the sterically hindered hydrogalvinoxyl species would not participate in recombination thus allowing the crystallographic trapping of hydrogen-bonded hydrogalvinoxyl:phenoxyl radical adducts. However, the observed mode of reaction is not so simple and instead in each case recombination of the two species occurs, leading the production of coupled species. The recombination of phenoxyl radicals is known,[1] and the possible products reported previously are summarised in Figure 4.3.

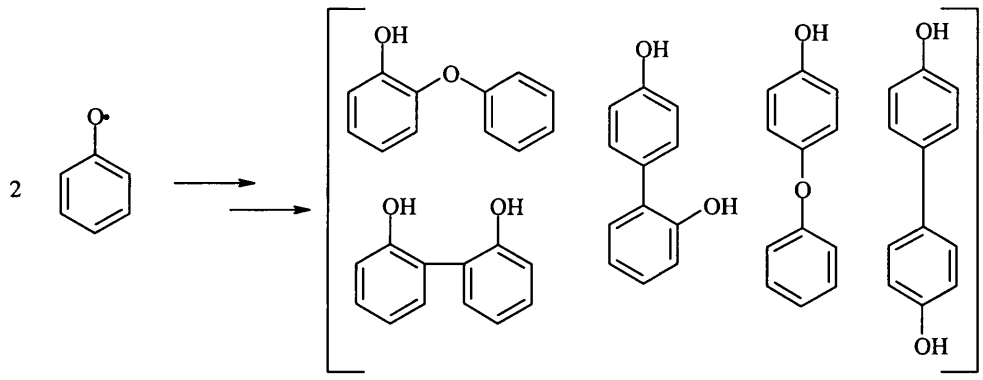

Figure 4.3: Possible products from phenoxy radical recombination reactions.

Four derivatives of galvinoxyl that have been synthesised in this manner are reported in this chapter. The reaction led to the consumption of 2 equivalents of galvinoxyl radical to each equivalent of the hydrogen atom donor species leading to the formation of the radical recombination product. The syntheses were carried out in refluxing acetonitrile

containing the appropriate protic species and 2 equivalents of galvinoxyl (Scheme 4.1). In the synthesis of **8**, one reaction afforded a small number of clear yellow crystals that were analysed by X-ray diffraction. However, subsequent reactions to synthesise sufficient material for characterisation by other methods were unsuccessful. The reactions to synthesise all the other compounds in this chapter proceeded rapidly to afford the corresponding coupled product and the yields obtained are moderate to high.

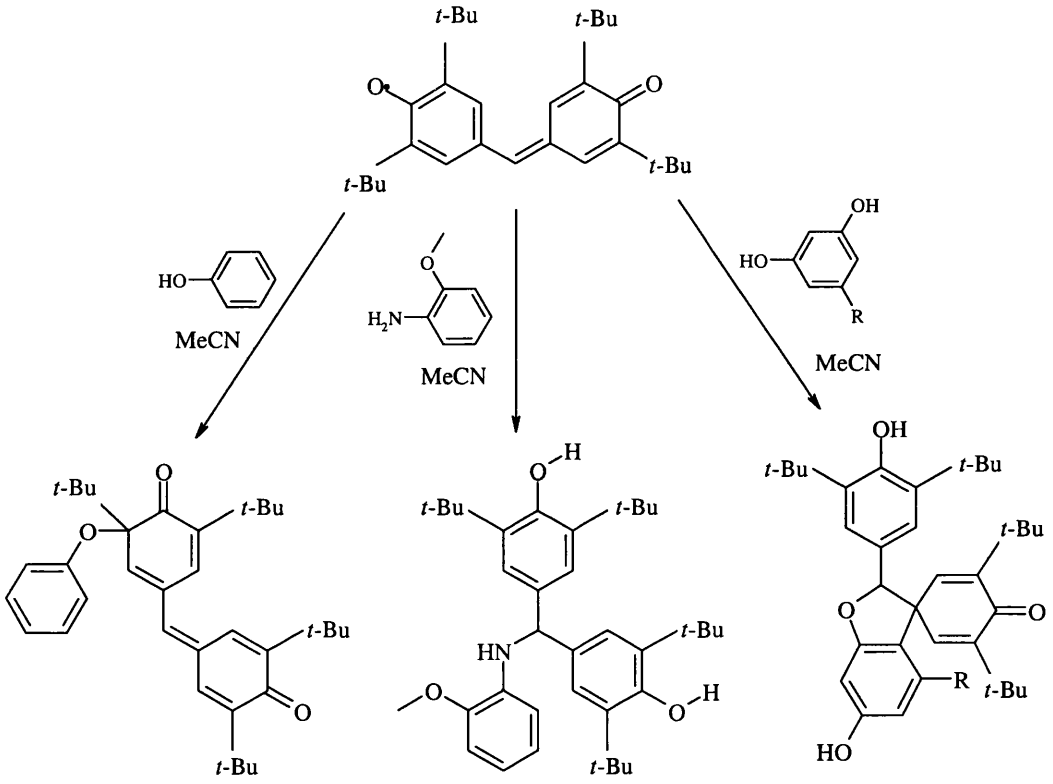

Scheme 4.1: Preparation of **8-11**.

The reaction of two equivalents of galvinoxyl with a single equivalent of phenol or the aromatic amine *o*-methoxyphenylamine results in the coupled species **8** and **9** respectively (Scheme 4.1). In the former recombination occurs at the *ortho* position as would be expected (Figure 4.3) while the amine couples at the methine carbon position on galvinoxyl. A similar coupling reaction at this position has been reported previously.[18,19] Similarly, the reaction of two equivalents of galvinoxyl with one equivalent of the closely

related bisphenols resorcinol and orcinol yields the compounds **10** and **11** respectively (Scheme 4.1). The coupling and an unexpected cyclisation in these cases led to multi-ring product species incorporating a fused ring system and a spiro union. The products **9-11** were isolated and dried *in vacuo* and were subsequently characterised by ^{1}H and ^{13}C NMR, which were performed in $CDCl_3$ solution, and by elemental analysis to confirm the identity of each.

4.3 X-ray Crystal Structures of Galvinoxyl Recombination Products

The crystal structures of each of the four galvinoxyl derivatives described above, **8-11** respectively, were determined with single crystal X-ray diffraction. Crystals suitable for crystallographic analysis were successfully grown from acetonitrile solution at 243 K. The crystal structures and their hydrogen bonding are described and compared in the following sections; each of the crystal structures obtained will be discussed separately. Where comparisons with mean literature values are discussed, these values are taken from the published tables of bond lengths in organic compounds, determined by X-ray and neutron diffraction.[20] Numbering of these complexes is consistent throughout, where possible. Selected crystallographic data is given for each structure in the appropriate section and full crystallographic tables containing the atomic coordinates and the equivalent isotropic displacement parameters are listed in Appendix A. In analysis of the diffraction data all hydrogen atoms were fixed by a riding model, other atoms were refined anisotropically and allowed to refine freely. A summary of the X-ray crystallographic data obtained for these complexes is given below (Table 4.1).

	8	**9**	**10**	**11**
Empirical formula	$C_{37}H_{49}O_3N$	$C_{36}H_{51}NO_3$	$C_{37}H_{49}NO_4$	$C_{36}H_{48}O_4$
M	555.77	545.78	571.77	544.74
Crystal system	Monoclinic	Triclinic	Monoclinic	Monoclinic
Space group	$P2_1/c$	P-1	$P2_1$	$P2_1/c$
a / Å	9.879(1)	9.870(1)	9.597(1)	11.147(1)
b / Å	27.473(1)	12.730(1)	9.646(1)	25.458(1)
c / Å	13.053(1)	13.646(2)	17.963(1)	12.177(1)
α / °	90	83.021(1)	90	90
β / °	105.013(1)	75.349(1)	93.110(0)	111.179(1)
γ / °	90	75.096(1)	90	90
U / Å^3	3421.74(12)	1600.1(1)	1660.42(6)	3222.19(8)
Z	4	2	2	4
μ (Mo-Kα) / mm^{-1}	1.079	1.133	1.144	1.123
Reflections collected	20018	8404	32838	59057
Independent reflections	4670	3284	7561	7315
R(int)	0.0640	0.0641	0.1056	0.1058
R1, wR2	0.0624, 0.1126 for 3783 data	0.0645, 0.1465 for 2315 data	0.0478, 0.0963 for 5446 data	0.0583, 0.1259 for 4514 data
R indices (all data)	0.0856, 0.1197	0.1022, 0.1753	0.0838, 0.1081	0.1131, 0.1479

Table 4.1: Crystal and refinement data for complexes **8-11**

3.4.1 Molecular Structure of 8

The reaction of the free radical galvinoxyl with phenol formed **8**, which was shown by crystallography to be the *ortho*-coupled product 2,6-Di-*tert*-butyl-4-(3,5-di-*tert*-butyl-4-oxo-cyclohexa-2,5-dienylidenemethyl)-6-phenoxy-cyclohexa-2,4-dienone ($C_{35}H_{46}O_3$). The asymmetric unit consists of two molecules, one of the galvinoxyl derivative product and one molecule of acetonitrile solvent. The basic structure of **8** and the atomic numbering scheme are shown in Figure 4.4. The intramolecular bond lengths and angles are collected in Table 4.2.

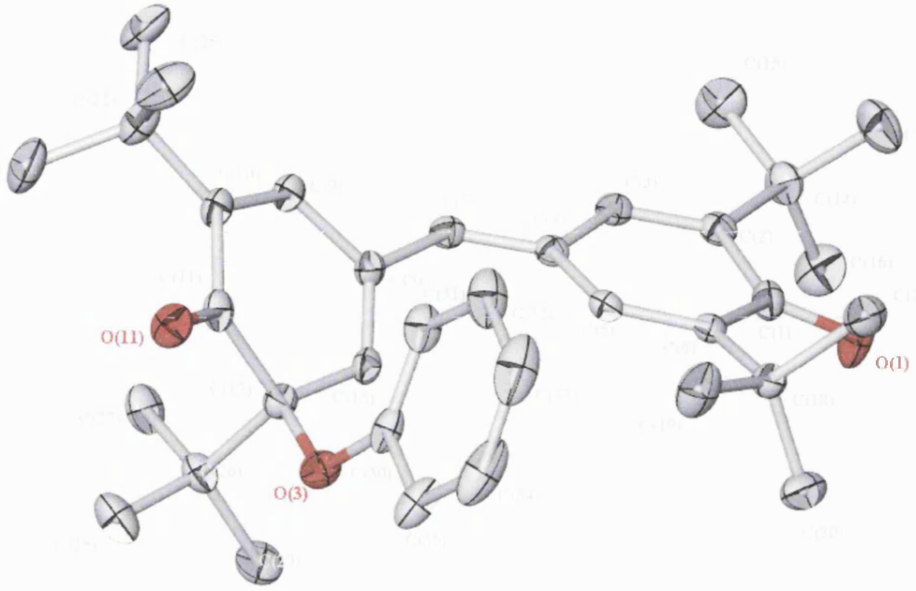

Figure 4.4: Molecular structure and numbering scheme of **8**, hydrogen atoms and acetonitrile solvate molecules omitted for clarity, thermal ellipsoids shown at 50% probability.

Bond lengths		Bond angles	
O(1)-C(1)	1.232(3)	C(4)-C(7)-C(8)	128.6(2)
C(1)-C(2)	1.488(3)		
C(2)-C(3)	1.347(3)	O(1)-C(1)-C(2)	120.6(2)
C(3)-C(4)	1.443(3)	O(1)-C(1)-C(6)	120.4(2)
C(4)-C(5)	1.449(3)	C(2)-C(1)-C(6)	119.0(2)
C(5)-C(6)	1.345(3)		
C(6)-C(1)	1.490(3)	O(11)-C(11)-C(10)	122.7(2)
C(4)-C(7)	1.359(3)	O(11)-C(11)-C(12)	119.2(2)
		C(10)-C(11)-C(12)	118.2(2)
O(11)-C(11)	1.222(3)		
C(8)-C(9)	1.468(3)	O(3)-C(12)-C(11)	109.78(17)
C(9)-C(10)	1.345(3)	C(30)-O(3)-C(12)	119.76(17)
C(10)-C(11)	1.487(3)		
C(11)-C(12)	1.543(3)	C(1)-C(2)-C(14)	119.4(2)
C(12)-C(13)	1.494(3)	C(1)-C(6)-C(18)	119.12(19)
C(13)-C(8)	1.343(3)		
C(7)-C(8)	1.462(3)	O(3)-C(12)-C(26)	103.92(18)
		C(11)-C(12)-C(26)	108.45(18)
O(3)-C(12)	1.437(3)	O(3)-C(12)-C(13)	110.61(17)
O(3)-C(30)	1.383(3)	C(13)-C(12)-C(26)	110.02(17)
		C(13)-C(12)-C(11)	113.59(19)
C(2)-C(14)	1.527(3)		
C(6)-C(18)	1.526(3)		
C(10)-C(22)	1.532(3)		
C(12)-C(26)	1.592(3)		

Table 4.2: Selected bond lengths (Å) and angles (°) of **8**.

The bond lengths and angles in **8** are within the expected values for the individual bond types.[20] The molecule consists of two cyclohexadienone and one phenoxy ring systems, one of the cyclohexadienone rings is further conjugated with a double bond to a methine carbon. The observed methine C(4)-C(7)-C(8) angle is 128.60° and the phenyl-methine distances are 1.462Å [C(7)-C(8)] and 1.359Å [C(7)-C(4)] respectively. The mean carbon-carbon bond distances in C=C-C(=O) are 1.457Å for conjugated single bonds, 1.487Å for unconjugated single and 1.329Å for double bonds in cyclohexa-2,5-dien-1-ones. The length of the carbon-oxygen distances [1.232(3)Å, O(1) and 1.222(3)Å, O(11)] are in full agreement with expected values [mean for carbon-oxygen distance in C=C-C=O 1.222Å and $(C=C)_2$-C=O 1.233Å]. The bond distances for the *t*-Bu groups are also within the expected range [mean values of 1.522Å for $(Csp^3)_3$-C-C=C, 1.588Å for $(Csp^3)_3$-C-C-$(Csp^3)_3$].

Another feature of interest is the orientation of the two conjugated ring systems with respect to each other. The overall molecular conformation of **8** can be defined in terms of the angles around the methine carbon atom C(7). The angle between the two least-squares planes fitted to the ring carbon atoms C(1)-(6) and C(8)-(13) is 43.35(0.08)°. In order to minimise repulsion between the hydrogen atoms, H(5) and H(13), the molecule adopts a twisted conformation. The twist between the two rings separated by a methine bridge can be described by the difference in the torsion angles [C(5)-C(4)-C(7)-C(8)] and [C(13)-C(8)-C(7)-C(4)]. In **8** the observed twist angle is 36.3° and the H(5)···H(13) distance, based on calculated hydrogen positions, is 2.275Å.

The conjugated cyclohexa-2,5-dienone ring is almost planar, with the notable exceptions of the C(1) and O(1) atoms. The calculation of a least-squares plane fitted through the atoms C(1)-(6) confirms this as the deviation of C(1) and O(1) is -0.092 (0.002)Å and -0.322 (0.003)Å respectively, while the RMS deviation of the fitted atoms is 0.057Å. The

methine carbon also deviates significantly from planarity with this ring [–0.167(0.003)Å]. The second cyclohexadienone ring adopts a partially puckered conformation as a result of the presence of the phenoxy substituent. This is illustrated by consideration of a least squares plane fitted to the ring atoms C(8)-C(13) (Table 4.3).

Deviation	Atom
-0.055 (0.001)	C(8)
0.071 (0.002)	C(9)
0.027 (0.002)	C(10)
-0.131 (0.002)	C(11)
0.140 (0.001)	C(12)
-0.052 (0.001)	C(13)
-0.444 (0.003)	O(11)
-0.154 (0.003)	C(7)

Table 4.3: Deviations of ring atoms from least squares plane in **8** (Å). RMS deviation of fitted atoms [C(8)-C(13)] = 0.089.

As found in the first cyclohexadienone ring, the atoms in the C=O group are also significantly removed from the least-squares plane [-0.052 (0.001)Å and –0.444(0.003)Å respectively], as is the methine carbon connecting the two ring systems [-0.154(0.003)Å]. One carbon atom in this ring C(12) is 4-coordinate, bonding to two ring atoms [C(11) and C(13)], the phenoxy group [O(30)] and a *t*-Bu group [C(26)]. The combination of the ring system and the requirements of the tetravalent C(12) distorts the ring shape, leading to the large deviations from the plane particularly for C(12). The angles around C(12) approach the ideal tetrahedral geometry, indicating that C(12) can be described as having sp^3 hybridisation, yet there is some deviation [103.92(18)°, O(3)-C(12)-C(26), 113.59(19)°, C(13)-C(12)-C(11)]. This may be ascribed to the constraint of the ring system and also to the steric requirements of the two bulky *t*-Bu and PhO groups. A least squares plane was fitted to the benzene ring atoms [C(30)-C(35)] in the PhO ring and the largest deviation of the carbons which should be co-planar is 0.006(0.002)Å, which is not experimentally significant in these data showing this ring to be planar, as expected. This aryl ring is also orientated away from the neighbouring *t*-Bu group, as might be expected to avoid steric crowding. In this configuration, the methyl atom C(19) is in close contact

with the phenoxy aryl ring [C(30)-C(35)] (Figure 4.5). The distance between the O(3) aryl ring centroid (Cg1) and the *t*-Bu group on the adjacent ring system [3.726Å, C(19) - (Cg1)] is reasonably short, indicating the presence of an C-H···π intermolecular interaction.

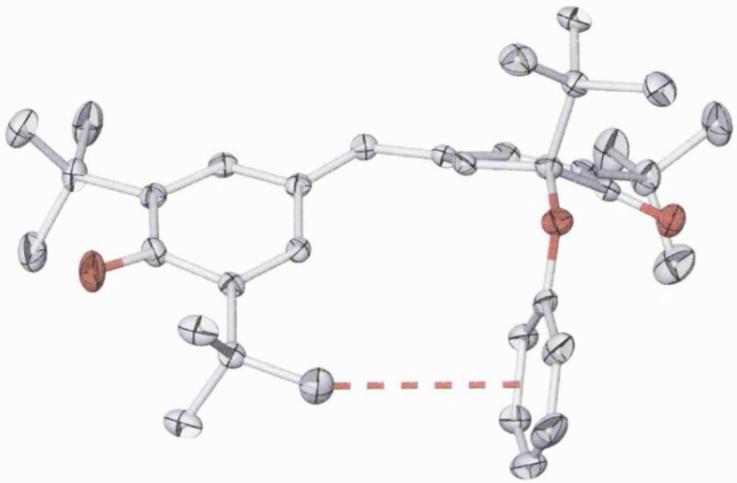

Figure 4.5: View of **8** showing the intramolecular C-H···π contact as a dashed red line, hydrogen atoms omitted for clarity and ellipsoids shown at 50% probability.

In addition to this intramolecular hydrogen bond, the supramolecular structure is comprised of discrete molecules, which aggregate *via* intermolecular C-H···O hydrogen bonds into the lattice. The hydrogen bond parameters are shown in Table 4.4 and the packing of the molecules in **8** is shown in Figure 4.6.

D-H···A	d(D-H)	d(H···A)	d(D···A)	<(DHA)
C(42)-H(42C)···O(11)#1	0.96	2.51	3.338(4)	145.0
C(29)-H(29A)···O(1)#2	0.96	3.040	3.347(3)	100.31
C(19)-H(19C)···Cg(1)	0.96	3.287[i]	3.726	109.97[ii]

Table 4.4: Hydrogen bond parameters in **8** [Å and °]. Symmetry transformations used to generate equivalent atoms: #1 x,-y+1/2,z+1/2, #2 2-x,-y,1-z. (i) Perpendicular distance from the H atom to the centroid C(30) C(35), (ii) angle between the C-H bond and the centroid C(30)-C(35),

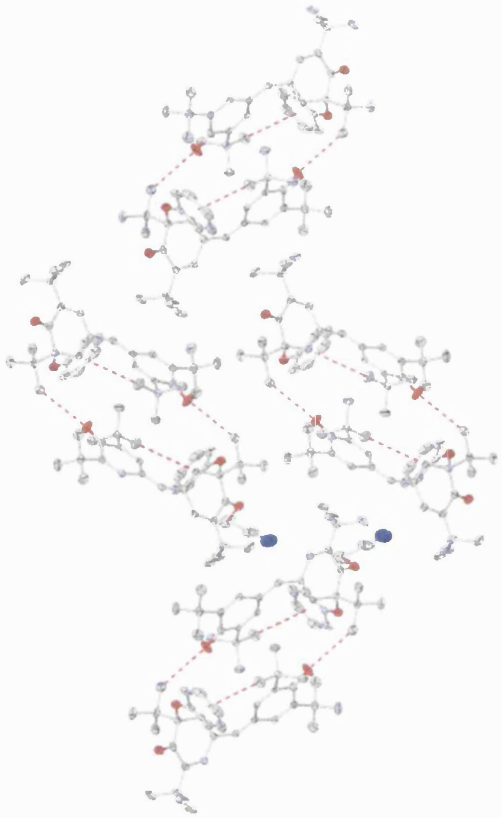

Figure 4.6: View down the *a*-axis of the unit cell in **8**. Hydrogen atoms omitted for clarity and ellipsoids shown at 50% probability, hydrogen bonds shown as dashed red lines.

The oxygen atom of the cyclohexa-2,5-dienone ring O(11) is involved in a C-H···O hydrogen bond with a methyl group on a neighbouring molecule C(19) [3.347(3)Å, C(29)···O(11)]. The head-to-tail formation of these hydrogen bonds forms dimers in the lattice. The acetonitrile (CH_3CN) solvent molecule present in the lattice is also involved in an intermolecular hydrogen bond *via* the methyl carbon C(42) [3.338(4)Å, C(42)···O(11)]. Interestingly, in this case no other specific interatomic interactions, such as π-π stacking or additional weak hydrogen bonds, take part in the creation of the supramolecular structure of **8**.

4.3.2 Molecular Structure of 9

The reaction of the free radical galvinoxyl with *o*-methoxyphenylamine formed **9**, which was shown by crystallography to be the coupled product 4-4'-{[(2-methoxyphenyl) amino]methylene}bis(2,6-di-tert-butylphenol) ($C_{36}H_{51}O_3N$). The asymmetric unit consists of one independent molecule of the product only. The basic structure of **9** and the atomic numbering scheme are shown in Figure 4.7 and relevant intermolecular bond lengths and angles are collected in Table 4.5.

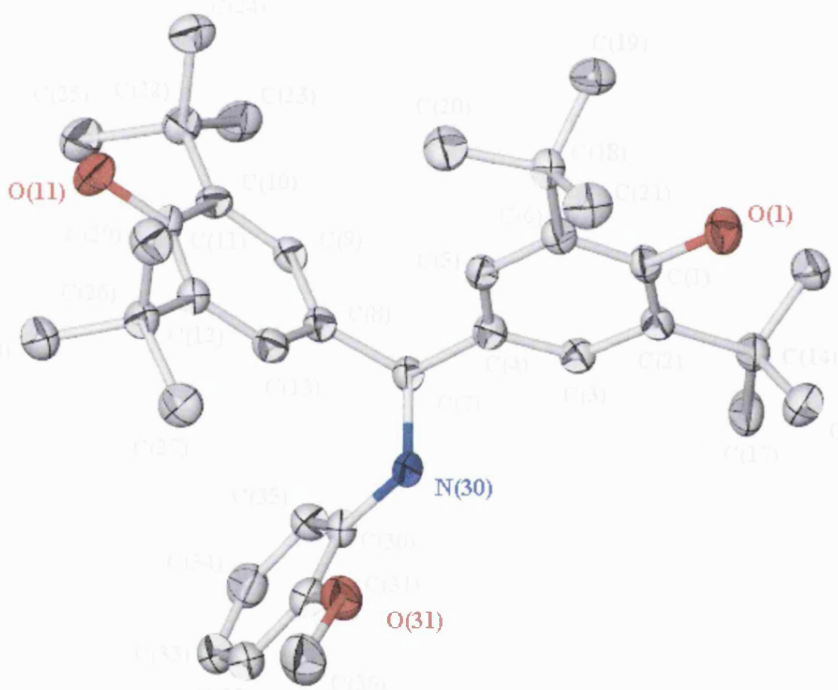

Figure 4.7: Molecular structure and numbering scheme of **9,** hydrogen atoms omitted for clarity, thermal ellipsoids shown at 50% probability.

Bond lengths		Bond angles	
O(1)-C(1)	1.388(5)	C(4)-C(7)-C(8)	112.2(3)
C(1)-C(2)	1.407(6)		
C(2)-C(3)	1.396(6)	O(1)-C(1)-C(2)	118.1(4)
C(3)-C(4)	1.385(6)	O(1)-C(1)-C(6)	118.6(4)
C(4)-C(5)	1.383(6)	C(2)-C(1)-C(6)	123.3(4)
C(5)-C(6)	1.411(6)		
C(6)-C(1)	1.403(6)	O(11)-C(11)-C(10)	121.6(4)
C(4)-C(7)	1.529(6)	O(11)-C(11)-C(12)	114.9(4)
		C(10)-C(11)-C(12)	123.6(4)
O(11)-C(11)	1.387(5)		
C(8)-C(9)	1.387(6)	C(8)-C(7)-C(4)	106.6(3)
C(9)-C(10)	1.399(6)	C(8)-C(7)-C(30)	113.7(3)
C(10)-C(11)	1.406(6)	C(30)-N(30)-C(7)	120.8(3)
C(11)-C(12)	1.403(6)	C(30)-C(31)-C(32)	121.1(5)
C(12)-C(13)	1.398(6)		
C(13)-C(8)	1.382(6)		
C(7)-C(8)	1.527(6)		
N(30)-C(7)	1.469(5)		
N(30)-C(30)	1.405(5)		
C(30)-C(31)	1.398(6)		

Table 4.5: Selected bond lengths (Å) and angles (°) of **9.**

The product **9** consists of two hydroxy-substituted phenyl rings and one other methoxy substituted ring system. The coupling reaction in this case has taken place at the C(7) position and as a result, unlike compound **8**, in **9** C(7) is tetravalent. The phenyl-carbon distances are 1.529(6)Å [C(7)-C(4)] and 1.527(6)Å [C(7)-C(8)] respectively, which are consistent with single C-C bonds. Although the bond distances around the C(7) are normal, the angles indicate some strain as for instance the observed angle C(4)-C(7)-C(8) is 112.2(3)°. The bond distances in the three aromatic rings and *t*-Bu groups are all in agreement with the expected range for these systems. The tetrahedral C(7) also draws the two *t*-Bu substituted rings into closer contact in **9**. This leads to an alteration in the orientation of the two aromatic ring systems with respect to each other. All three aromatic rings are close to being perfectly planar, within experimental error. The largest deviation from the appropriate least-squares plane for each ring is 0.077(0.0029)Å [C(1)], 0.0172(0.0029)Å [C(11)] and –0.0108(0.0029)Å [C(30)] where the RMS deviation of the fitted atoms in each case is 0.0052Å, 0.0120Å and 0.0068Å respectively. The ring

carbons with the largest deviations in **9**, C(1) and C(11), also showed the largest deviation in the equivalent carbon positions in compound **8**. The length of the C-O distances [1.388(5)Å, O(1)-C(1) and 1.387(5)Å, O(11)-C(11)] are in agreement with mean literature values for single C-O bonds [1.362Å].

The angle between the two least-squares planes fitted to the ring carbon atoms C(1)-(6) and C(8)-(13) is 80.98(0.12)°. As observed in **8**, the two rings are twisted relative to each other, however in **9** this twist is far more pronounced. The twist, calculated by taking the difference in the torsion angles [C(5)-C(4)-C(7)-C(8)] and [C(13)-C(8)-C(7)-C(4)] gives a value of 100.8°. This allows the two rings into closer contact, as required by the tetrahedral C(7), while minimising the steric strain. As a result of this conformation, C(5) and the centroid for the ring C(8)-C(13),Cg(1), are brought into close contact [3.687Å, C(5)...Cg(1)] indicating the presence of an intramolecular C-H···π interaction (Figure 4.8). The hydrogen bond parameters for **9** are collected in Table 4.6.

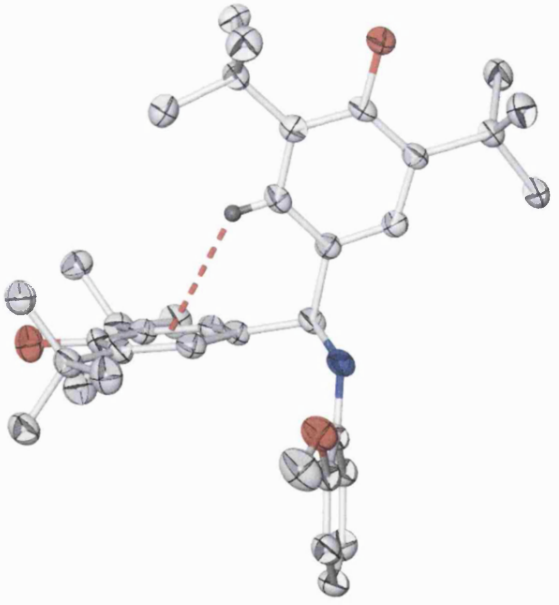

Figure 4.8: Intramolecular hydrogen bond between C(5) and the ring centroid Cg(1), uninvolved hydrogen atoms omitted for clarity, thermal ellipsoids shown at 50% probability.

D-H···A	d(D-H)	d(H···A)	d(D···A)	<(DHA)
O(11)-H(11)···Cg(1)	0.82	2.987	3.318	106.80
C(5)-H(5)···Cg(1)#1	0.93	3.001[i]	3.677	130.65[ii]

Table 4.6: Hydrogen bond parameters in **9** [Å and °]. Symmetry transformations used to generate equivalent atoms: #1 1+x,-y,z. (i) Perpendicular distance from the H atom to the centroid C(1) C(6), (ii) angle between the C-H bond and the centroid C(1)-C(6).

The supramolecular structure of **9** consists of only one set of O-H···π hydrogen bonds between the centroid on the methoxyphenylamine aromatic ring, Cg(2), and O(11) [3.318Å]. This links the molecules into chains running along the *a*-axis. The arrangements of molecules in the crystal as viewed along the *a*-axis and the unit cell viewed down the *a*-axis are illustrated below (Figures 4.9 and 4.10 respectively).

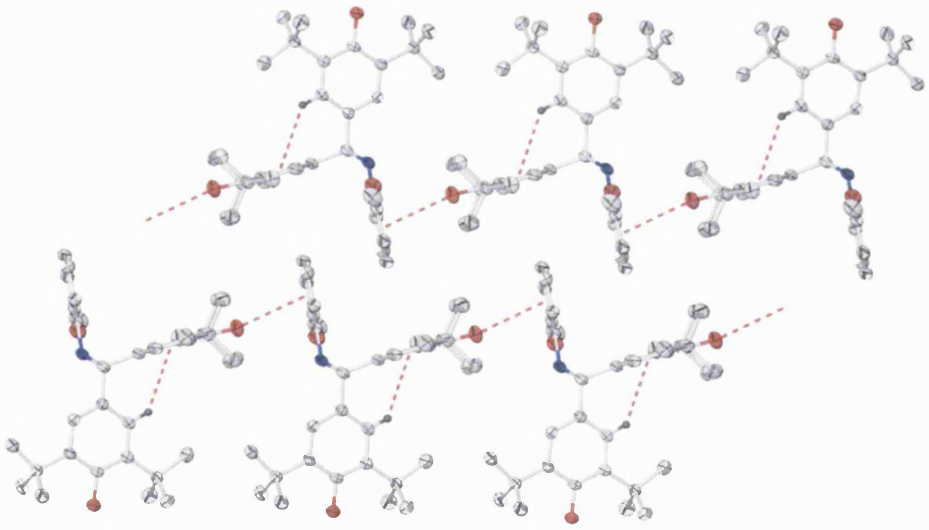

Figure 4.9: View showing the O-H···π bonded chains running along the *a*-axis of the unit cell in **9**. Hydrogen atoms not involved in hydrogen bonding omitted for clarity and ellipsoids shown at 50% probability, hydrogen bonds shown as dashed red lines.

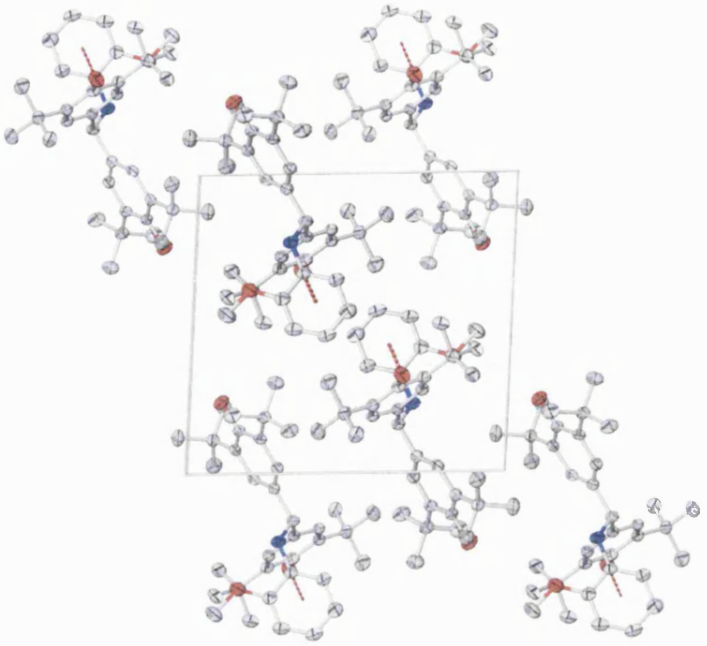

Figure 4.10: The unit cell in **9**, view down the *a*-axis showing the O-H···π bonded chains as dashed red lines into the page. Hydrogen atoms omitted for clarity and ellipsoids shown at 50% probability.

There are no examples of π- π stacking interactions in this structure. It seems reasonable to attribute this to the twisted arrangement of the three aromatic rings, which does not allow such efficient packing in the crystal as a flat molecule would and hence disrupting this type of stacking.

4.3.3 Molecular Structure of 10

The reaction of the free radical galvinoxyl with the phenol resorcinol formed **10**, which was shown by crystallography to be the coupled product 6-hydroxy-2-(4-hydroxy-3,5-di-*tert*-butylphenyl)-3',5'-di-*tert*-butyl-4'*H*-spiro[1-benzofuran-3,1'-cyclohexa-2,5-dien]-4'-one, ($C_{35}H_{46}O_4$). In this case a spiro union has been formed at C(8) and cyclisation has formed an additional 5-membered ring. The asymmetric unit consists of two molecules, one each of the product ($C_{35}H_{46}O_3$) and one molecule of acetonitrile (CH_3CN) solvent.

This compound crystallised in the monoclinic space group $P2_1$ as a racemic mixture. The basic structure of **10** and the atomic numbering scheme are shown in Figure 4.11. Relevant bond lengths and angles are collected in Table 4.7.

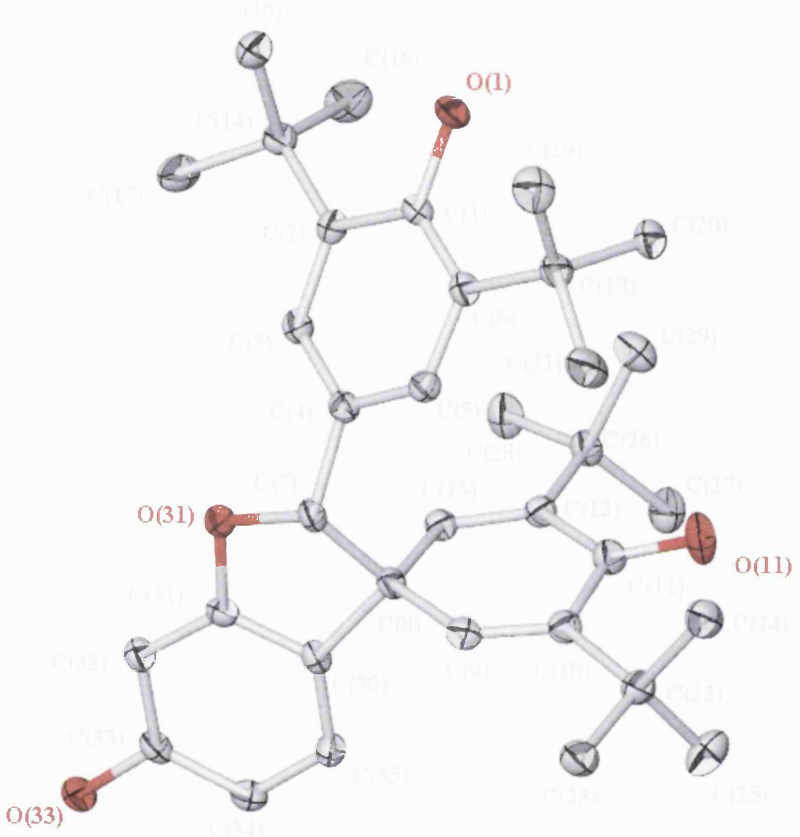

Figure 4.11: Molecular structure and numbering scheme of **10**, hydrogen atoms and acetonitrile solvate molecule omitted for clarity and ellipsoids shown at 50% probability.

Bond lengths		Bond angles	
O(1)-C(1)	1.374(2)	C(4)-C(7)-C(8)	114.93(16)
C(1)-C(2)	1.413(3)		
C(2)-C(3)	1.394(3)	O(1)-C(1)-C(2)	115.55(17)
C(3)-C(4)	1.383(3)	O(1)-C(1)-C(6)	121.95(16)
C(4)-C(5)	1.390(3)	C(2)-C(1)-C(6)	122.49(18)
C(5)-C(6)	1.389(3)		
C(6)-C(1)	1.409(3)	O(11)-C(11)-C(10)	120.08(18)
C(4)-C(7)	1.510(3)	O(11)-C(11)-C(12)	120.92(19)
		C(10)-C(11)-C(12)	119.00(17)
O(11)-C(11)	1.220(2)		
C(8)-C(9)	1.492(3)	C(7)-C(8)-C(9)	112.85(16)
C(9)-C(10)	1.339(3)	C(7)-C(8)-C(13)	110.52(16)
C(10)-C(11)	1.510(3)	C(7)-C(8)-C(30)	98.31(14)
C(11)-C(12)	1.490(3)	C(9)-C(8)-C(13)	113.17(16)
C(12)-C(13)	1.339(3)	C(9)-C(8)-C(30)	112.70(16)
C(13)-C(8)	1.490(3)	C(13)-C(8)-C(30)	108.28(15)
C(7)-C(8)	1.576(3)		
		C(31)-O(31)-C(7)	106.02(14)
O(31)-C(7)	1.458(2)	O(31)-C(7)-C(4)	110.11(16)
O(31)-C(31)	1.377(2)	O(31)-C(7)-C(8)	105.25(14)
O(33)-C(33)	1.384(2)		
		C(1)-C(2)-C(14)	121.35(17)
C(10)-C(22)	1.531(3)	C(1)-C(6)-C(18)	122.80(17)
C(12)-C(26)	1.532(3)	C(11)-C(10)-C(22)	118.58(17)
		C(11)-C(12)-C(26)	118.88(17)

Table 4.7: Selected bond lengths (Å) and angles (°) of **10.**

The molecule consists of an aromatic hydroxy substituted phenyl ring, a cyclohexadienone ring and a dihydrobenzafuran ring, the latter two of which are joined through a spiro-carbon atom. The values of carbon-carbon distances observed in **10** are consistent with literature mean values, as are the carbon-oxygen distances [1.374(2)Å, O(1)-C(1); 1.220(2)Å, O(11)-C(11); 1.458(2)Å, O(31)-C(7)]. The bond distances for the *t*-Bu groups are also within the expected range as found in earlier structures. The C(7) and C(8) atoms are both tetravalent in **10**. The phenyl-carbon distances to C(7), the tetrahedral centre linking all three rings, are 1.510(3)Å [C(7)-C(4)], 1.576(3)Å [C(7)-C(8)] and 1.458(2)Å [O(31)-C(7)]. These values are within the normal range expected for C-C single and C-O single bonds. The observed angles at this atom however, are somewhat removed from the ideal tetrahedral geometry [114.93(16)°, C(4)-C(7)-C(8); 110.11(16) °, O(31)-C(7)-C(4); 105.25(14)° O(31)-C(7)-C(8)], indicating some strain

which is most probably due to the steric bulk of the two rings being drawn into close contact. There is also much reduced twist between the planes of the two *t*-Bu substituted rings, compared to that observed in **9**. The angle between the least-squares planes fitted to these rings is 52.65(0.06)°. The two rings in **10** sit in a staggered, face-on orientation. In this case, the requirements of the spiro-carbon atom C(8) does not allow the orthogonal orientation observed in compound **9** between the two *t*-Bu substituted rings.

The planarity of the two aromatic rings present is confirmed by calculating the least-squares planes though the atoms C(8)-C(13) and C(30)-C(35), followed by an analysis of the displacements of atoms from the appropriate plane. The largest displacements observed for a ring carbon are –0.056(0.002)Å and -0.015(0.002)Å for C(11) and C(33) respectively. The RMS deviations for the fitted atoms in these cases are 0.035Å and 0.011Å respectively. As was found for structures **8** and **9**, the largest deviations occur at the carbon position of oxygen substitution. The 5-membered ring in the dihydrobenzofuran ring system is not completely co-planar with the benzene ring due to the geometric requirements of the tetrahedral carbon atoms C(7) and C(8). The cyclohexadienone ring is also almost planar, showing the greatest deviation at the position of oxygen substitution. The largest deviation in this ring is –0.021(0.002)Å for C(1), where the RMS deviation of the fitted atoms is 0.014Å.

Due to the polycyclic nature of this molecule involving the spiro-ring system, very short non-bonded intramolecular distances are observed. There are however, several significant intermolecular distances present in **10**, the hydrogen bond parameters for these are given in Table 4.8.

D-H···A	d(D-H)	d(H···A)	d(D···A)	<(DHA)
C(42)-H(42A)···N(4)#1	0.98	2.70	3.442(3)	132.8
O(33)-H(33)···N(4)#2	0.84	2.04	2.877(3)	172.6
O(1)-H(1)···O(33)#3	0.84	2.18	2.7525(19)	125.0
C(25)-H(25C)···O(11)#4	0.98	2.70	3.619(3)	156.7

Table 4.8: Hydrogen bond parameters in **10** [Å and °]. Symmetry transformations used to generate equivalent atoms: #1 -x+2,y-1/2,-z #2 x-1,y,z #3 x+1,y-1,z #4 2-x,½+y,1-z.

As might be expected, on the basis of steric concerns, the relatively unhindered hydroxy group O(33)-(H33) is involved in hydrogen bonding to form the supramolecular structure of **10**. The primary structural motif is chains formed by O-H···O interactions between the hydroxyl oxygens, O(33) and O(1), in neighbouring molecule. The oxygen atom O(33) is bifurcated, acting as a hydrogen bond acceptor towards O(1) and also forming a hydrogen bond interaction as a donor towards the N(4) atom on the acetonitrile solvent residue (Figure 4.12). Though of moderate length for this class of intermolecular interaction, the O-H···O hydrogen bond forms an acute angle [125.0°].

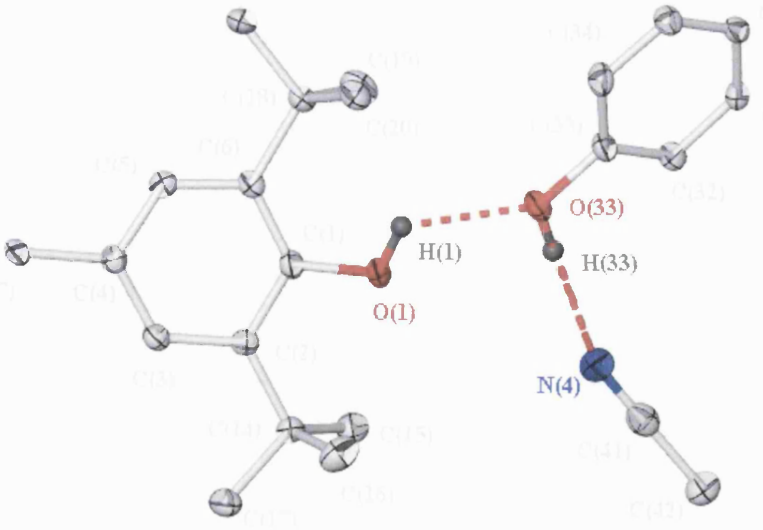

Figure 4.12: Core structure of O-H···O bonding motif in **10**, hydrogen bonds shown as dashed red lines. Hydrogen atoms not involved in hydrogen bonding omitted for clarity and ellipsoids shown at 50% probability.

These interactions link the molecules in a head-to-tail fashion, forming chains in the *ab*-plane (Figure 4.13). There are in addition short hydrogen bonding interactions between the carbonyl oxygen O(11) and the methyl group C(25) on a neighbouring molecule [3.619Å, O(11)···C(25)], forming zigzagging chains which run along the *b*-axis. This hydrogen bonding further links the O-H···O bonded chains into a 2-dimensional network. The arrangement of molecules in the crystal as viewed in projection on the *bc*-plane illustrating the zigzag chain formed by this interaction is shown in Figure 4.14.

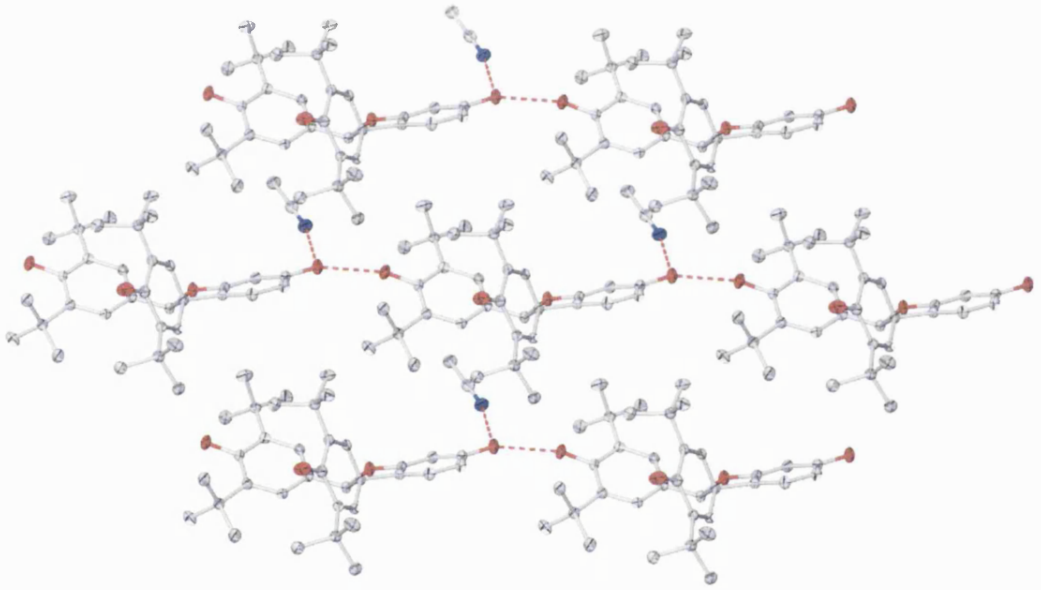

Figure 4.13: Projection view in the *ab*-plane showing the chains of O-H···O and O-H···N interactions in **10**, hydrogen bonds shown as dashed red lines. Hydrogen atoms omitted for clarity and ellipsoids shown at 50% probability.

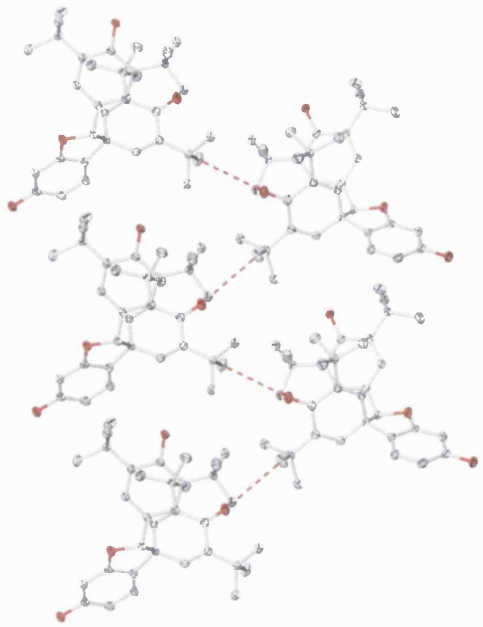

Figure 4.14: Projection view in the *bc*-plane showing the zigzag chains of C-H···O interactions in **10** running along the *b*-axis, hydrogen bonds shown as dashed red lines. Hydrogen atoms omitted for clarity and ellipsoids shown at 50% probability.

The acetonitrile solvent molecules also participate in short, head-to-tail C-H···N interactions, forming chains directly along the *b*-axis (Figures 4.15 and 4.16). This chain forms links between the chains of product molecules, extending the supramolecular structure from a 2-dimensional network into a 3-dimensional lattice.

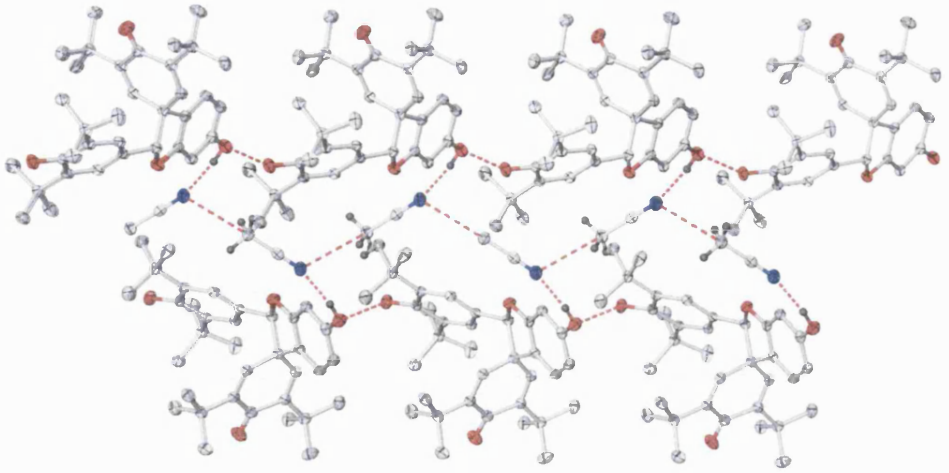

Figure 4.15: View down the *a*-axis showing the hydrogen-bonded chains of acetonitrile solvate running along the *b*-axis, hydrogen bonds shown as dashed red lines. Hydrogen atoms omitted for clarity and ellipsoids shown at 50% probability.

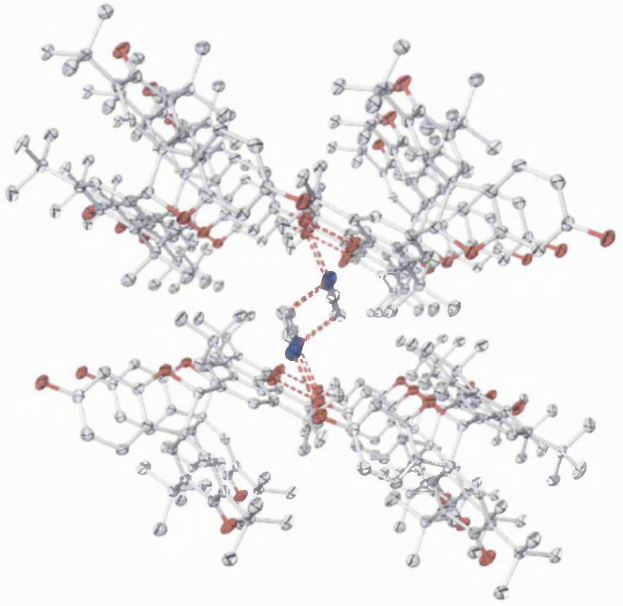

Figure 4.16: Perspective view down the *b*-axis showing the cavity containing the acetonitrile solvent molecules, hydrogen bonds shown as dashed red lines. Hydrogen atoms omitted for clarity and ellipsoids shown at 50% probability.

There are no further intermolecular interactions in this structure as the twisted conformation of the ring precludes the potential for π-π stacking interactions.

4.3.4 Molecular Structure of 11

The reaction of the free radical galvinoxyl with the phenol orcinol formed **11**, which was shown by crystallography to have formed a spiro union to give the coupled product 6-hydroxy-2-(4-hydroxy-3,5-di-*tert*-butylphenyl)-3',5'-di-*tert*-butyl-4-methyl-4'*H*-spiro[1-benzofuran-3,1'-cyclo hexa-2,5-dien]-4'-one ($C_{36}H_{48}O_4$). The asymmetric unit consists of one molecule of the product only. The basic structure of **11** and the atomic numbering scheme are shown in Figure 4.17. Relevant bond lengths and angles are collected in Table 4.9.

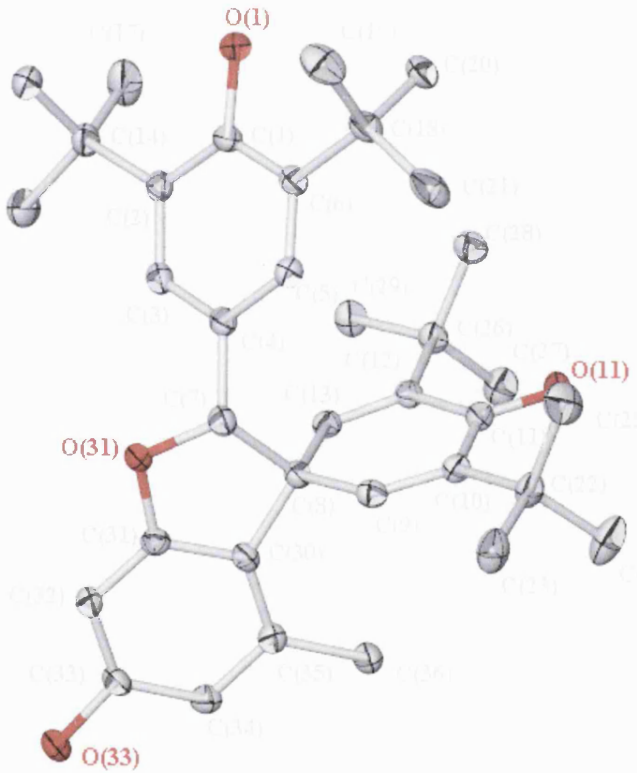

Figure 4.17: Molecular structure of **11**, hydrogen atoms omitted for clarity and ellipsoids shown at 50% probability.

Bond lengths		Bond angles	
O(1)-C(1)	1.379(2)	C(4)-C(7)-C(8)	115.86(15)
C(1)-C(2)	1.406(3)		
C(2)-C(3)	1.397(3)	O(1)-C(1)-C(2)	122.09(17)
C(3)-C(4)	1.385(3)	O(1)-C(1)-C(6)	115.20(16)
C(4)-C(5)	1.386(2)	C(2)-C(1)-C(6)	122.68(16)
C(5)-C(6)	1.391(3)		
C(6)-C(1)	1.410(3)	O(11)-C(11)-C(10)	119.99(16)
C(4)-C(7)	1.506(3)	O(11)-C(11)-C(12)	120.53(16)
		C(10)-C(11)-C(12)	119.48(15)
O(11)-C(11)	1.234(2)		
C(8)-C(9)	1.493(3)	C(7)-C(8)-C(9)	109.47(15)
C(9)-C(10)	1.332(2)	C(7)-C(8)-C(13)	110.12(14)
C(10)-C(11)	1.496(3)	C(7)-C(8)-C(30)	99.31(13)
C(11)-C(12)	1.488(3)	C(9)-C(8)-C(13)	112.72(15)
C(12)-C(13)	1.337(2)	C(9)-C(8)-C(30)	113.25(15)
C(13)-C(8)	1.491(2)	C(13)-C(8)-C(30)	111.17(15)
C(7)-C(8)	1.588(2)		
		C(31)-O(31)-C(7)	107.20(13)
O(31)-C(7)	1.446(2)	O(31)-C(7)-C(4)	110.46(14)
O(31)-C(31)	1.378(2)	O(31)-C(7)-C(8)	106.74(14)
O(33)-C(33)	1.375(2)		
		C(1)-C(2)-C(14)	122.58(16)
C(10)-C(22)	1.538(3)	C(1)-C(6)-C(18)	122.08(16)
C(12)-C(26)	1.532(2)	C(11)-C(10)-C(22)	119.14(15)
		C(11)-C(12)-C(26)	118.88(17)

Table 4.9: Selected bond lengths (Å) and angles (°) of **11.**

The basic skeleton of **11** is closely related to that of **10**, the only difference being the addition of a methyl substituent in the 4-position of the fused dihydrobenzofuran ring system. As a result **11** consists of the same combination of an aromatic hydroxy substituted phenyl ring, a cyclohexadienone ring and a dihydrobenzafuran ring as observed in **10**. Again, the latter two of these ring systems have joined to form a spiro union at the C(8) atom. The bond lengths and angles are consistent with those expected on the basis of mean literature values, and those obtained for the closely related structure **10**. The carbon-oxygen distances [1.379(2)Å, O(1)-C(1); 1.234(2)Å, O(11)-C(11)] are in agreement with the arrangement of a single bonds at C(1) and a double bond at C(11). The bond distances for the *t*-Bu groups are also within the expected range as found in earlier structures. The C-C single bonds around the tetrahedral carbon centres C(7) and C(8) are within the expected range but, as observed in **10**, the angles around these carbon

atoms deviates from the ideal tetrahedral geometry indicating strain caused by the fused ring and spiro ring structure [115.86(16)°, C(4)-C(7)-C(8); 110.46(14) °, O(31)-C(7)-C(4); 106.74(14)° O(31)-C(7)-C(8) around C(7) and 99.31(13)°, C(7)-C(8)-C(30); 112.72(15) °, C(9)-C(8)-C(13); 113.25(15)° C(9)-C(8)-C(30)]. As might be expected from similar analogues, the orientation between the two *t*-Bu substituted rings, C(1)-C(6) and C(8)-C(13) respectively, is similar to that found in **10**, the angle between the least-squares planes fitted to these ring atoms is 54.29(0.06)°. The familiar staggered, face-on orientation between the rings is observed.

The calculation of the least-squares planes through the ring atoms for each ring has confirmed the degree of planarity present. The greatest deviation from the least-squares plane in the aromatic ring C(30)-C(35) was observed for C(30) [-0.004(0.002)Å], where the RMS deviation observed for all fitted atoms was 0.003Å. The greatest deviation from planarity in the second aromatic ring, C(1)-C(6), was observed for C(3) [0.006(0.002)Å], where the RMS deviation observed for all fitted atoms was 0.004Å. Consequently both of these rings are close to being perfectly planar, within experimental error. A larger deviation is observed in the cyclohexadienone ring C(8)-C(13), where the maximum deviation observed is 0.011(0.002)Å for C(12) and the RMS observed for fitted atoms was 0.009Å. The 5-membered ring containing O(31) is almost co-planar with the fused benzene ring, except for one atom, C(7), which is constrained by its tetrahedral geometry and lies out of the plane. The 5-membered ring is hence distorted and puckered at the C(7)-atom position from a planar conformation. The deviation out of the least-squares plane for C(7) is –0.201(0.004)Å, compared with 0.079(0.003)Å and 0.073(0.003)Å for C(8) and O(31) respectively.

Unlike **10**, **11** did not crystallise with a molecule of acetonitrile solvent in the lattice even though both were grown under the same conditions in acetonitrile solvent. As the solvent was involved in two different hydrogen bonds in **10**, both of which were appreciably

short and linear considering the type of atoms involved [2.877(3)Å, 172.6° O(33)-H(33)···N(4); 3.442(3)Å, 132.8° C(42)-H(42A)···N(4)] an alteration in the supramolecular structure in the absence of these interactions would be expected.

The supramolecular structure in **11** consists of two different hydrogen-bonding motifs; the hydrogen bond parameters for these are given in Table 4.10.

D-H...A	d(D-H)	d(H...A)	d(D...A)	<(DHA)
O(33)-H(33)...O(11)#1	0.84	1.92	2.7582(18)	174.4
O(1)-H(1)...O(33)#2	0.84	2.27	2.8600(18)	127.8

Table 4.10: Hydrogen bond parameters in **11** [Å and °]. Symmetry transformations used to generate equivalent atoms: #1 x-1,y,z #2 x+1,y,z+1.

Oxygen O(33) remains involved as a hydrogen bonding donor and acceptor, but in this case it is with O(11) and O(1) respectively. Where in **10** the O-H···N interaction formed in preference to the O-H···O, the lack of solvent present has allowed the former to occur. The O-H...O interaction formed between O(33) and O(11) is also shorter, as expected from the van der Waals radii of the respective elements involved. The following projection view in the *ab*-plane illustrates that there are no additional intermolecular interactions to be noted (Figure 4.18).

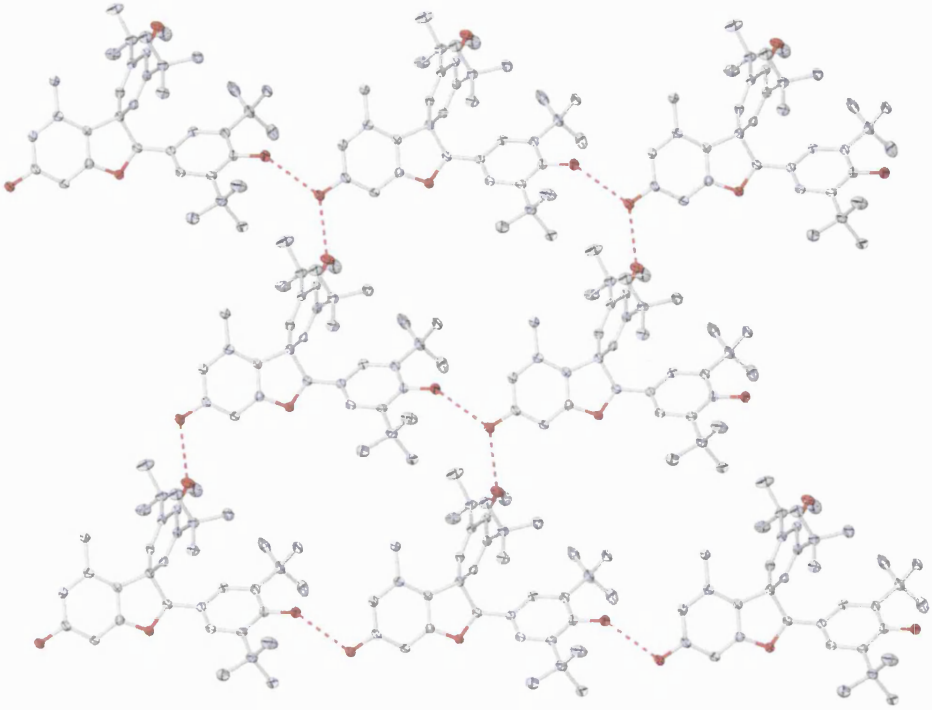

(a)

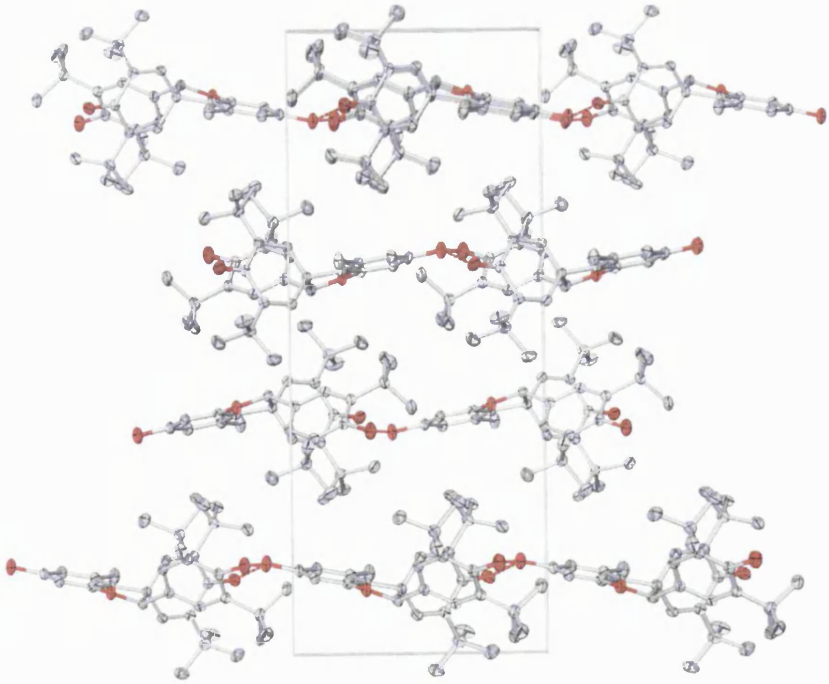

(b)

Figure 4.18: (a) View down the *b*-axis showing the 2-dimensional hydrogen-bonded network, (b) an orthogonal view down the *c*-axis showing there are no hydrogen bonding interactions between the 2-dimensional hydrogen-bonded sheets. Hydrogen bonds shown as dashed red lines, hydrogen atoms omitted for clarity and ellipsoids shown at 50% probability.

4.4 Concluding Remarks

In conclusion, it is evident that the phenoxy radicals formed during the course of these reactions were insufficiently stable to be able to crystallographically trap open-shell hydrogen bonded adducts with hydrogalvinoxyl. It has been demonstrated that these species are susceptible to recombination, leading to the formation of multi-ring species and exhibiting addition of the phenoxyl species at several positions. In the case of **10** and **11** the subsequent cyclisation at the methine carbon position led to the formation of an additional fused heterocyclic ring and a spiro-union. Intramolecular bond lengths and angles were consistent with those expected, taking into account the strain exerted by the multi-ring systems. Intramolecular hydrogen bonds have also been noted, as the tetravalent C(8) induces close proximity allowing intramolecular C-H$\cdots\pi$ interactions in the case of both.8 and 9.

4.5 Experimental

For most details on the general considerations, characterisation and solid-state determination see Chapter 2 (Section 2.4).

Formation of 8

Scheme:

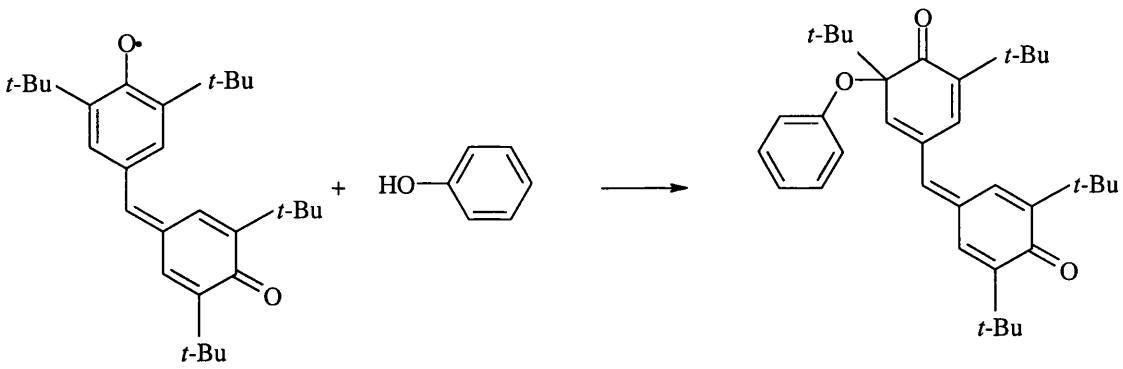

Dry acetonitrile (20 ml) was added, under argon to a schlenk containing solid galvinoxyl (0.84 g, 2 mmol) and phenol (0.10 g, 1 mmol). The solution was refluxed for 3 hours leading to the formation of a clear yellow solution. On leaving the solution at –30°C a small number of yellow crystals suitable for X-ray diffraction were obtained. For information on characterisation see section 4.2.

Formation of 9

Scheme:

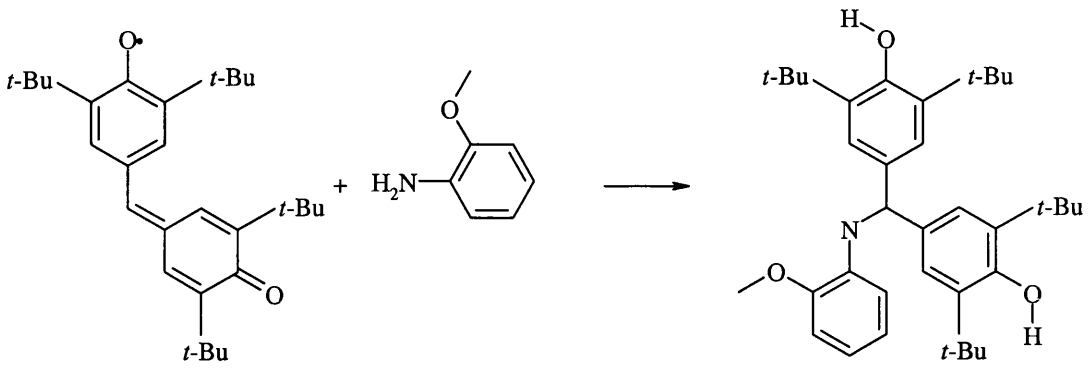

Dry acetonitrile (20 ml) was added, under argon to a schlenk containing solid galvinoxyl (0.84 g, 2 mmol) and the amine (0.13 g, 1 mmol). The solution was refluxed for 3 hours leading to the formation of a clear yellow solution. On leaving the solution at –30°C a crop of yellow crystals suitable for X-ray diffraction were obtained. The solvent was removed *in vacuo* to give a yellow solid product, yield obtained 0.23 g, 42 %. M.p. 145°C. ^{1}H NMR (400 MHz, $CDCl_3$, 25 °C, TMS): δ = 1.48 (36H, s, CC<u>H</u>$_3$); 2.17 (5H, s, <u>H</u>C=C); 5.55 (3H, s, OC<u>H</u>$_3$); 7.01 (1H, m, Ar<u>H</u>); 7.16 (1H, m, Ar<u>H</u>); 7.26 (4H, m, Ar<u>H</u>); 7.36 (1H, m, Ar<u>H</u>); 7.61 (1H, m, Ar<u>H</u>); ^{13}C{^{1}H} NMR (75 MHz, $CDCl_3$, 25 °C, TMS): δ = 23.8, 30.3, 34.4, 35.5, 77.3, 127.6, 128.1, 128.2, 129.9, 136.6, 136.4, 144.5, 126.9, 148.8. Elemental analysis: Calcd for $C_{36}H_{51}O_3N$: C, 79.21 %, H, 9.42 %, N, 2.57 %. Found: C, 81.8%; H, 9.51%; N, 0.60%,

Formation of 10

Scheme:

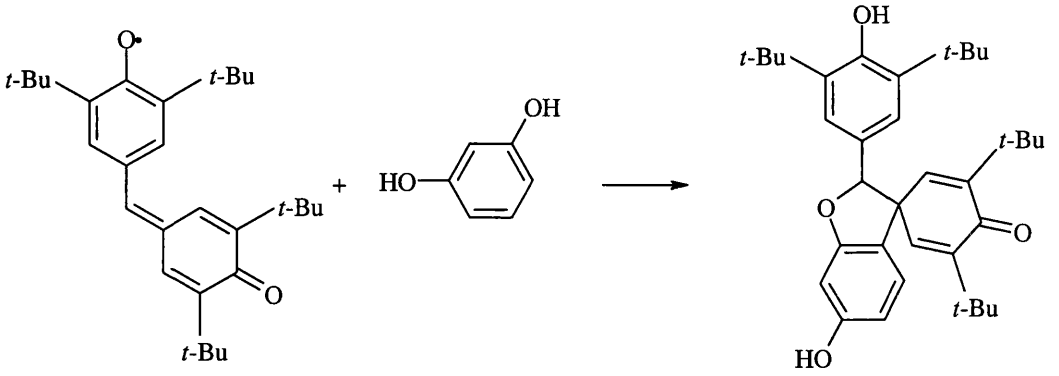

Dry acetonitrile (20 ml) was added, under argon to a schlenk containing solid galvinoxyl (0.84 g, 2 mmol) and resorcinol (0.11 g, 1 mmol). The solution was refluxed for 3 hours leading to the formation of a clear yellow solution. On leaving the solution at –30°C a crop of yellow crystals suitable for X-ray diffraction were obtained. The solvent was removed *in vacuo* to give a yellow solid product, yield obtained 0.48 g, 84 %. M.p. 139°C. ^{1}H NMR (400 MHz, $CDCl_3$, 25 °C, TMS): δ = 1.22 (18H, s, CC<u>H</u>$_3$); 1.39 (18H, s, CC<u>H</u>$_3$); 5.48 (1H, s, C<u>H</u>O); 6.92 (1H, m, Ar<u>H</u>); 7.08 (2H, m, Ar<u>H</u>); 7.18 (2H, m, Ar<u>H</u>); 7.29 (2H, m, Ar<u>H</u>); 7.61 (1H, m, Ar<u>H</u>); ^{13}C{^{1}H} NMR (100 MHz, $CDCl_3$, 25 °C, TMS): δ = 27.1, 27.9, 28.4, 29.1, 52.3, 91.3, 97.1, 106.7, 119.3, 119.8, 123.0, 134.0, 138.9, 139.0, 142.4, 147.4, 151.7, 155.6, 159.2. Elemental analysis: Calcd for $C_{37}H_{49}O_4N$: C, 77.71, H, 8.64, N, 2.45%. Found: C, 78.4; H, 8.95; N, 1.86%.

Formation of 11

Scheme:

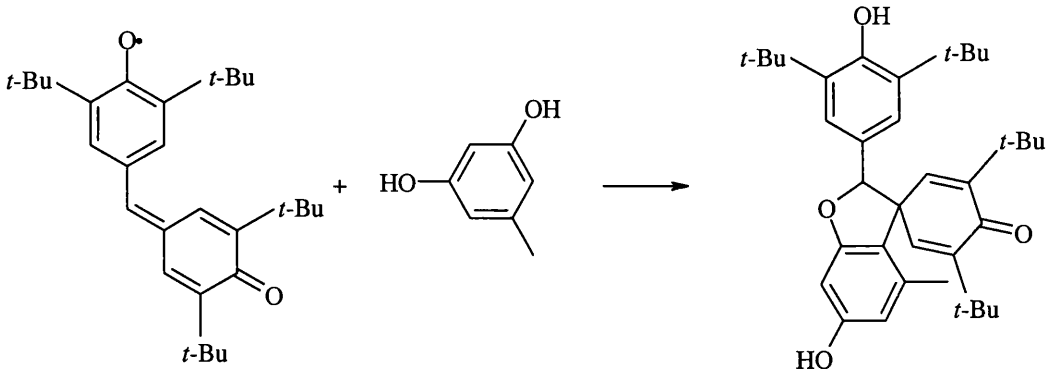

Dry acetonitrile (20 ml) was added, under argon to a schlenk containing solid galvinoxyl (0.84 g, 2 mmol) and orcinol (0.13 g, 1 mmol). The solution was refluxed for 3 hours leading to the formation of a clear yellow solution. On leaving the solution at –30°C a crop of yellow crystals suitable for X-ray diffraction were obtained. The solvent was removed *in vacuo* to give a yellow solid product, yield obtained 0.43 g, 78 %. M.p. 149°C. ^{1}H NMR (400 MHz, $CDCl_3$, 25 °C, TMS): δ = 1.24 (18H, s, CC$\underline{H}_3$); 1.31 (18H, s, CC$\underline{H}_3$); 4.42 (3H, s, C$\underline{H}_3$); 5.07 (1H, bs, O$\underline{H}$); 5.56 (1H, s, C$\underline{H}$O); 6.11 (2H, m, Ar$\underline{H}$); 6.48 (1H, s, C=C$\underline{H}$); 6.78 (1H, s, C=C$\underline{H}$); 6.89 (2H, m, Ar$\underline{H}$). Elemental analysis: Calcd for $C_{36}H_{48}O_4$: C, 79.36, H, 8.87, N, 0%. Found: C, 78.3; H, 8.93; N, 0 %,

4.6 References

[1] Denisov, E.T.; Khudyakov, I.V. *Chem. Rev.* **1987**, *87*, 1313.
[2] Coppinger, G.M. *J. Am. Chem. Soc.* **1957**, *79*, 501.
[3] Kharasch, M.S.; Yoshi, B.S. *J. Org. Chem.***1957**, *22*, 1435.
[4] Awaga, K.; Ohamoto, H.; Mitani, T.; Maruyama, Y.; Sugano, T.; Kinoshita, M.; *Solid State Commun.* **1989**, *71*(12), 1173.
[5] Awaga, K.; Sugano, T.; Kinoshita, M.; Matsuo, T.; Suga, H. *J. Chem. Phys.* **1987**, *87*, 3062.
[6] Bartlett, P.D.; Funahashi, T. *J. Am. Chem. Soc.* **1962**, *84*, 2596.
[7] Bartlett, P.D.; Gontarev, B.A.; Sakuri, H. *J. Am. Chem. Soc.* **1962**, *84*, 3101.
[8] Greene, F.D.; Adam, W.; Cantrill, J.E. *J. Am. Chem. Soc.* **1961**, *83*, 3461.
[9] Williams, D.E. *Mol. Phys.* **1969**, *16*(2), 145.
[10] Novak, I.; Kovač, B. *Chem. Phys. Letts.* **2005**, *413*, 351.
[11] CSD November 2004 update, Version 1.7, filters used were 3D-coordinates determined, not disordered, R<0.1.
[12] Bartlett, P.D.; Funahashi, T. *J. Am. Chem. Soc.* **1962**, *84*, 2596.
[13] D'Alessandro, N.; Bianchi, G.; Fang, X.; Jin, F.; Schuchmann, H.-P.; von Sonntag, C. *J. Chem. Soc., Perkin Trans. 2,* **2000**, 1862.
[14] Watanabe, A.; Noguchi, N.; Fujisawa, A.; Kodama, T.; Tamura, K.; Cynshi, O.; Niki, E. *J. Am. Chem. Soc.***2000**, *122*, 5438.
[15] Fukuhara, K.; Nakanishi, I.; Kansui, H.; Sugiyama, E.; Kimura, M.; Shimada, T.; Urano, S.; Yamaguchi, K.; Miyata, N. *J. Am. Chem. Soc.* **2002**, *124*, 5952.
[16] Wayner, D.D.M.; Lusztyk, E.; Ingold, K.U.; Mulder, P. *J. Org. Chem.* **1996**, *61*, 6430.
[17] Lucarini, M.; Pedrielli, P.; Pedulli, G.F. *J. Org. Chem.* **1996**, *61*, 9259.
[18] Hall, S.R.; Raston, C.L.; White, A.H. *Aust. J. Chem.* **1980**, *33*, 295.
[19] Bock, H.; John, A.; Havlas, Z.; Bats, J.W. *Angew. Chem., Int. Ed.,***1993**, *32*,416.
[20] Allen , F.H.; Kennard, O.; Watson, D.G. *J. Chem. Soc. Perkin Trans.2.* **1987**, *12*, S1.

Part II

Group 4 Metal Alkoxides

Chapter 5

Introduction

5.1 Overview

The field of metal alkoxide chemistry has received a considerable amount of interest in recent decades as these species have found occupation in several areas under intense investigation.[1] One important area is in materials chemistry where metal and mixed-metal alkoxides have been widely used as precursors to technologically importantly high temperature superconducting oxides, primarily by sol-gel or chemical vapour deposition routes.[2,3,4,5] Secondly, and the motivation for the work in this thesis, is the importance of this important class of metal complexes as catalysts,[2,6,7] in which there has been an explosion of interest in the last 20 years.

The use of metal alkoxides in these disciplines and in various other roles has been extensively reviewed recently in a number of important papers and books.[8,9,10,11,12] Part II of this thesis is concerned with the application of structural analysis and crystallographic techniques, utilised initially in Part I, to the study of group 4 metal alkoxide complexes. This chapter presents an overview of the chemistry and exploitation of metal alkoxides, including a discussion of the structural and bonding features that are of particular relevance to the work herein. The study of electronic distribution by charge density analysis is also reviewed, along with a brief introduction to the use of high resolution X-ray and neutron diffraction data for such studies. This is followed by a discussion of the database techniques used in this study for searching and database creation. Additional detailed background information is given in the relevant discussion chapters.

5.2 Fundamental Characteristics of Group 4 Metal Alkoxides

5.2.1 General Features and Applications

Simple metal alkoxides have the general formula $[M(OR)_x]_n$, where M is a metal with a valency of x, R is an aryl or alkyl group and n is the degree of molecular association. Previous work in this area has widely explored simple homometallic transition metal oxides of this type and examples are known for most s- p- d- and f block elements. Group 4 derivatives are of particular interest in current chemical research, primarily as a result of their range of diverse properties and structures and due to their widespread importance in chemical and industrial applications. They are found, for example, in biological systems such as in siderophores and natural pigments,[13] in host-guest chemistry group 4 aryloxides are able to form interesting metallocalix[3,4]arenes structures,[14] and titanium catecholates are known to self-assemble into helicate coordination compounds.[15] In coordination chemistry, catechol ligands are able to stabilise unusual coordination polyhedra for these metals and this allows good tuning of electrochemical properties.[16] Group 4 complexes have also been applied widely as reagents in organic synthesis, for which there are examples of use in chelation-controlled stereoselective nucleophilic addition to ketones[17] and as alternatives to alkyllithium and Grignard reagents in chemoselective alkylation processes.[18] As mentioned previously, an important application of these complexes is in industry as they have been found to be extremely useful as precursors in the preparation of ceramic and glass materials as well as metal oxide films.[2,3,4,5,19]

While transition metal alkoxides have been extensively utilised as catalysts in a number of different processes[2,20] and the interest in metallocene-based catalysts has lead to the development of highly active catalytic species,[21,22,23,24] there has recently been a particular growth of interest into the use of non-cyclopentadienyl (cp) ligands, such as alkoxide and aryloxide ligands, at early d-block metal centres. The replacement of the 'soft'

cyclopentadiene ligands by 'hard' alkoxide and aryloxide donor ligands has generated both complementary and novel reactivity compared to the traditional metallocene catalysts.[25,26] Consequently, group 4 alkoxides have also been widely incorporated into catalyst design.[27,28,29] Of these titanium is of particular interest for use in the design of a catalyst as it is quite electropositive and comparatively small, making it highly Lewis acidic. The pioneering work by Meth-Cohn for example showed in 1970[30] that titanium tetraalkoxides also undergo insertion reactions with isocyanates, which demonstrates their potential catalytic activity. The reactivity of titanium tetra*iso*propoxide is also well documented and is known to be an excellent catalyst in esterification and ester interchange reactions.[31] Catalysts derived from group 4 alkoxides have also been used in [2+2] and [2+3] cylcoadditions[32], esterification and transesterification[33] processes and as asymmetric catalysts for enantioselective carbon-carbon bond forming reactions. Group 4 alkyoxides and aryloxides are also currently used as precursors for a variety of polymerisation reactions, which has been the case the 1950s when the first titanium based Ziegler-Natta type catalysts were developed[34] for use in the polymerisation of α-olefins.

This growing interest in the chemistry of the Group 4 metal alkoxides for these purposes has been promoted by the improvement in experimental techniques for synthesis and characterisation that has occurred over recent years. Whereas previously, structural determination was primarily taken from molecular weights and spectral data, the advancement of X-ray crystallography and reliable techniques for dealing with air- and moisture-sensitive compounds has lead to a greater understanding of the chemistry of metal alkoxides and allowed the rapid expansion of the field. These factors have provided impetus towards the design and synthesis of novel complexes and, consequently, there are now a considerable number of metal alkoxide structures published in the literature, a circumstance that prompts the systematic structural study of these complexes with regard to their potential use as catalysts. Furthermore, the current interest is not limited to the study of simple transition metal oxides but also includes mixed metal

alkoxides of group 4 complexes. Heterometallic alkoxides, which contain two or more different metals in the same complex, are known for group 4 alkoxides and examples with the alkali and alkaline earth metals as well as a for number of lanthanide complexes.

5.2.2 Physical and Chemical Properties

The structure and reactivity of metal complexes is strongly dependent on the steric and electronic properties of the ligands present, which offers opportunity for tuning the reactivity of the resulting metal complex towards a specific goal. The ligand system confers control over the reactivity of the metal centre in a number ways. The appropriate choice of ligand can hinder aggregation, leading to the formation of mononuclear species. The steric requirements of the ligand are also significant as substantial steric bulk around the metal, which may also hinder the approach of an incoming species, allowing the available space for approach of a reactant to be adjusted and hence guiding the reactivity. This factor is also particularly important in influencing the stereochemistry around the metal centre. The electronic properties of the complex are manipulated by the use of electron withdrawing or donating ligands.

The physical and chemical properties of Group 4 metal alkoxides have been extensively examined, starting with early systematic studies in the 1950s by Bradley *et al.*[35,36,37] These studies have shown that the physical properties of metal alkoxides are primarily determined by the size and shape of the R group on the alkoxide as well as by the valency, atomic radius, stereochemistry and coordination number of the metal. Due to the high electronegativity of oxygen the metal-oxygen bonds in alkoxides of metallic elements would be expected to be highly polarised ($M^{\delta+}$-$O^{\delta-}$-C) and so possess significant ionic character. The extent of this polarisation is determined by the identity of the metal involved and so varies between 65-80%.[2] As such, metal alkoxides would be expected to

exhibit properties characteristic of largely ionic bonding, however this is not found to be the case. Instead, these alkoxides are highly volatile and are often soluble in common organic solvents, properties more usually associated with covalent bond character. In order to explain this, a number of potential factors which may account for the attenuation in ionic character of the metal-ligand bonds have been put forward. Firstly, the inductive effect of the alkyl group in the alkoxide may play a role, as this allows stabilisation of the metal centre. A further factor may be the aggregation of these complexes into oligomeric clusters through the formation of alkoxide bridges between metals (Figure 5.1).

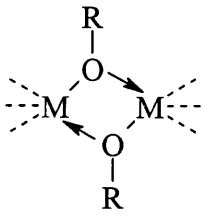

Figure 5.1: Self-association through alkoxo bridges.

Oligomerisation is a dominant feature of metal alkoxides unless inhibited by steric or electronic factors and the extent of aggregation (n) for the simple alkoxides $[M(OR)_x]_n$ has been found to increase the more electron deficient the metal atom is and also as the size of the metal atom increases. Steric considerations have been shown to be key factors in determining the degree of self-association in metal alkoxide complexes as increasing the steric demand of the peripheral alkyl groups inhibits aggregation.[2] Also, the possible donation of lone pair electrons in p-orbitals on oxygen into d-orbitals on the metal (Figure 5.2 below) can mitigate the ionicity of the bond.

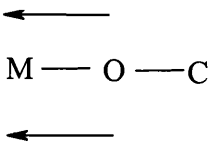

Figure 5.2: π donation from oxygen to metal center.

An alternate suggestion previously suggested in our group[38] proposes that the covalent-like properties of the compounds could be due to the lipophilic alkyl shell formed by the alkoxide ligands. (Figure 5.3).

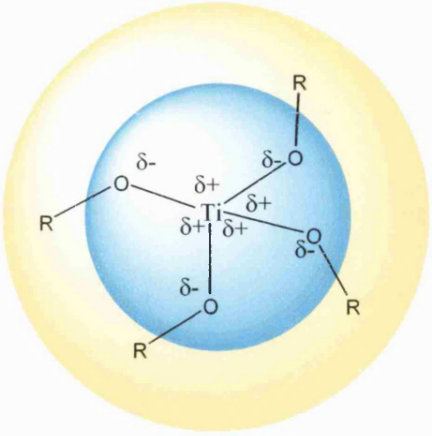

Figure 5.3: Ionic core and covalent periphery in titanium alkoxides.

While the metal–oxygen bond is polar and forms an ionic core the difference in electronegativities between the oxygen and R group is less and so forms a covalent periphery. This periphery surrounds the core and thus dominates the observed physical properties. The chemistry and reactivity of the metal alkoxides is dominated by the polar nature of the metal-oxygen bond. The polarisation of this bond, with a δ^+ charge on the metal and a δ^- charge on the oxygen, makes the metal susceptible to attack by nucleophiles and the oxygen to attack by electrophiles. As a result metal alkoxides are highly reactive towards hydroxylic reagents such as alcohols and phenols, and particularly water[4]. Although the detailed reaction chemistry of the metal alkoxide family of compounds will not be discussed here it is important to note their high reactivity with water, which leads to a need for stringent anhydrous conditions when carrying out reactions involving them if hydrolysis is to be avoided.

However, reactivity is not the only issue in catalysis. These species often show relatively poor selectivity, which must be improved on to develop a useful catalyst. In a successful catalyst the reactivity must be controlled, in order to impart selectivity to the catalysts activity. The ability to divide the metal coordination sphere into non-labile and reactive sites is a key feature of catalysts and this can be illustrated with regard to metal alkoxide species (Figure 5.4).

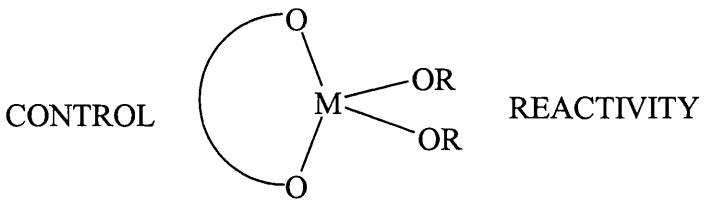

Fig 5.4: Division of metal coordination sphere.

The labile alkoxide ligands occupy mutually *cis* co-ordination sites in the metal complex; the incorporation of chelating ligands allows the formation of these complexes. This orientation is a key requirement in the mediation of reactions by metal complexes, indeed the success of metallocene catalysts of the group 4 metals is attributed to the fact that co-ligands necessarily take up *cis*-oid positions.[39] The interest in non-metallocene complexes of Group 4 metals as possible alternatives for polymerisation catalysts has in part stemmed from the principal that the coordination sphere of such catalysts might be more easily tuned by using non-cp based ligands.

The analysis of complexes under the Hard-soft acid-base (HSAB) system reveals an important difference for consideration between the alkyl- and aryl-oxide ligands in contrast to carbon-bonded ligand systems such as cp. Oxygen is considered a 'hard' ligand in this system. The principle that like prefers like means that Group 4 metals, due to the metals "hard" character, bind better to 'hard' ligands such as those that coordinate through nitrogen and oxygen rather than to ligands which coordinate via a 'softer' carbon

atom. As a result complexes where the M^{4+} ion is coordinating to N or O are considered to be much more common than complexes where the metal coordinates to carbon.

5.2.4 Metal-Ligand Bonding

As an important class of ligands for transition metals, the nature of the metal-ligand bonding in metal alkoxide complexes has incited intense interest for many years.[40,41,42,43,44,45,46] Alkoxide, and likewise aryloxide, ligands can adopt a variety of bonding modes within a metal complex. By far the most common bonding mode for aryloxide ligands is a terminal one in which the oxygen atom is bound to only one metal atom and a large number of compounds contain doubly bridging aryloxides. It is also possible to obtain triply and occasionally quadruply bridging aryloxides (Figure 5.5), though these are typically restricted to compounds containing extremely small ligands.

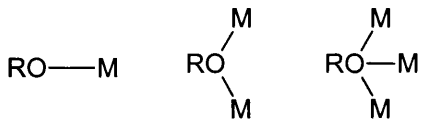

Figure 5.5: Possible bonding modes, terminal, μ^2 and μ^3 respectively, of alkoxide and aryloxide ligands (OR) to metal centres (M).

Previous studies have shown that the M-OR distance increases progressively on moving from terminal to double and triple bridging bonding modes, so that (μ_3) bridging > (μ_2) bridging > terminal. It is well established that terminal alkoxides usually bind in an approximately linear fashion[2] and that the M–O distances are generally found to be short and strong. In the past this effect has generally been attributed to the presence of multiple bond character the donation of lone pair π-electrons from the oxygen atoms to the vacant d-orbitals on titanium, with amounts of π donation ranging from two to four electrons.[47] Hence the expectation is that metal-oxygen bonding in these complexes is comprised of a

primary σ-type bond and also *via* two pπ-orbitals that are perpendicular to the M-O vector (Figure 5.6).

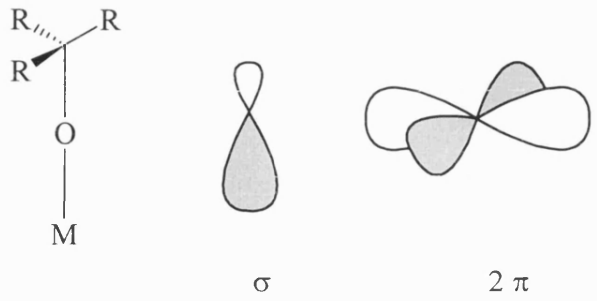

Figure 5.6: σ and 2π bonding orbitals on oxygen atom in alkoxide ligands.

This highlights the most widely discussed aspects of the bonding in alkoxide, aryloxide and related oxygen donor ligands to metal; that of the presence and extent of this type of oxygen-*p* to metal *d*- bonding (Figures 5.2 and 5.6) and also the relative contribution of an ionic bonding model. The presence of such π-donation of oxygen electron density from alkoxyl and aryloxyl substituents is routinely used to rationalise both structure and reactivity[37] and as such is has been the subject of intense examination. As the presence of such bonding should have some geometrical consequences for the oxygen atom, several groups have attempted to probe early transition metal alkoxides for structural evidence of these interactions. In general, larger M-O-C angles would be expected to be associated with greater amounts of π donation, and hence greater multiple bond character. While, on consideration of this a correlation between the bond length M-O and the bond angle MOR might be expected, previous work has suggested that the MOR angle cannot in general be used as a measure of metal *d* to oxygen π-bonding, and that the bonding in these compounds is in essence ionic.[48,49,50,51] Rothwell[52] and Parkin[53] have both investigated the M–O distance as a function of M–O–R angle for Nb, Ta, and Zr complexes, but found no correlation between the two parameters. More recently analogous data was plotted for complexes of the lanthanide element, Sm, and also failed to find any correlation.[54]

Instead, an electrostatic basis for the shortened M-O bonding has been proposed.[43] This has been rationalized by consideration of the difference in electronegativity between the two atoms. The M–O–R bond angle in this case was shown to be the result of strong steric control. These results substantially weaken the argument for structurally significant p interactions in metal alkoxide complexes.

The exception is a recent study where computational methods have been utilized to compare the M-O-C bond angles in a range of analogous titanium and germanium complexes of the general formula $MX_3(OMe)$, where M is the metal and X is a hydride or halide.[55] It was found that π donation is disfavoured in the germanium compounds due to the LUMO d-orbitals being too high in energy for interaction while the d-orbitals are at much lower energy in the titanium compounds. Analyses of the M-O-C angles in both series indicated that the titanium complexes were mainly linear, indicating multiple bonding character due to π donation, while the germanium complexes, which showed bond angles of approximately 120°, do not. The detailed analysis of the group 4 homo- and heterometallic alkoxides has not yet been carried out, but is essential in aiding the understanding of the catalytic reactivity of these species. So, while structural information is often used to support claims of multiple metal-ligand bonding, it is clear that this approach can be inconclusive and that in order to definitively quantify the number of electrons donated to the metal a thorough understanding of the charge distribution within complexes of this class must be achieved.

5.3 Experimental Studies on Bonding

5.3.1 Electronic Distribution

It has been noted that the nature of the metal-ligand bonding in transition metal complexes has important consequences for the structure and reactivity of that complex (Section 5.2.4). Consequently, considerable efforts have been made to understand the fundamental character of chemical bonds for this purpose. The electronic distribution of charge in metal complexes is crucial in determining the reactivity of that complex, in addition to imparting important information relevant to the bonding within the system. As a result there is a great deal of interest in the determination of the electronic charge distribution in many different fields. Chemical reactions in metal complexes are often studied to elucidate the affect of small changes in molecular composition on the electron distribution and the resulting modification of the observed physical and chemical properties. The analysis of the charge density is a method of directly studying the electronic properties of the compound under investigation. One method useful for this purpose is the study of the charge density of the relevant species obtained by the combination of accurate X-ray and neutron diffraction data. By providing an accurate description of the nuclear positions and electron distribution within a relevant species, X-n charge density analysis can be used to give insight into the nature of the bonding and elucidate electronic and structural features. Hence, making it possible to rationalise the observed reactivity, or potentially even influence future catalyst design.

5.3.2 Neutron Diffraction

As an alternative to using X-ray wavelength radiation in diffraction, it is also possible to use thermal neutrons. The principles of diffraction similar to those for X-ray diffraction discussed in Chapter 1, however there are some intrinsic differences in the nature of the scattering and in the treatment of the data which are fully detailed in several excellent

texts.[56,57,58] The extent of neutron scattering is measured by the area of the cross-section the different nuclei present to the beam. Neutrons, unlike X-rays, scatter from materials by interacting with the nucleus of an atom rather than the electron cloud. For neutron diffraction the scattering power of an atom is not strongly related to its atomic number and is of a similar order of magnitude for all atoms, approximately 0.5 x $10^{-12}cm^{-1}$, and the fluctuations in amplitude are only minor. As a result neighbouring elements, even isotopes of the same element, in the periodic table generally have substantially different scattering cross sections and can be distinguished in a neutron experiment. This is also advantageous as it is therefore much easier to sense light atoms, such as hydrogen, amongst heavier atoms. In addition, the position of hydrogen atoms is much more reliable when found by neutron methods. In X-ray methods covalent bonding, particularly for lighter elements such as hydrogen that have fewer core electrons in relation to valence electrons, causes the electron cloud to be displaced relative to the nucleus; upsetting the validity of the spherical atom assumption. Neutron diffraction is unaffected by this bias, and accurately finds the position of the hydrogen nucleus. The nature of this interaction also means that the neutron scattering power of atoms does not fall off with scattering angle, as is found for X-rays. Although the scattered intensity in a diffraction pattern will still decrease at higher angles due to the Debye-Waller temperature factor, this effect is considerably less severe for neutron experiments. This makes neutron scattering ideal for high-resolution studies. The consequent ability to access very high-resolution data makes neutron diffraction a highly precise method of studying structure.

Neutrons may be obtained from either spallation or reactor sources. Neutron diffraction experiments are often carried out under extreme conditions of sample environment such as high and low temperature, controlled atmospheres, high pressures and in chemical reaction cells. In terms of crystal size, neutron experiments, in general, require a large single crystal than for X-ray. This is one of the main drawbacks of single crystal neutron

diffraction compared with X-ray methods. With the relatively low flux of neutron sources and the rather weak scattering of most materials, usually crystals of several mm^3 are required to allow collection of a good data set in a reasonable data collection time. Generally, a crystal of approximately 1 mm^3 is required to consider a sample appropriate for neutron data collection.

As mentioned earlier, a major advantage to using neutrons is the ability to locate hydrogen atoms and refine both their positions and thermal parameters, which is not possible by other methods. Much of the structural work on hydrogen-bonded systems has made use of neutron diffraction. In addition, determination of the hydrogen anisotropic displacement parameters in short strong hydrogen bonds, such as O···O, allows for example the deduction of the shape of the potential well in which the atom sits. The combination of both X-rays and neutrons is a powerful tool in many studies, including the characterisation of host-guest interactions in, for example, zeolites, and in the determination of charge distributions in crystal structures. Of particular importance to the work in this thesis is the application of these techniques in charge density X-n studies, which will be discussed in further detail in the next section (5.3.3). Also, the study of magnetic moments is also an important application of neutron diffraction. As neutrons are spin ½ particles they therefore have a magnetic moment that can couple directly to spatial and temporal variations in the magnetisation of materials on an atomic scale, thus neutrons can also be used to study magnetic structure. Other uses include supramolecular chemistry and molecular engineering, in which neutron single crystal diffraction has an important role in defining the patterns of "weak" intermolecular interactions as these crucially involve hydrogen atoms, also thermal parameter studies, structural disorder, and phase transitions.

5.3.3 Charge Density Studies

During recent years charge density analysis has developed into a powerful tool in the study of a broad range of physical and chemical problems. Modern theories of reactivity and the design principles for new materials are based on the information gathered about the detailed structure of molecules, their properties and reactions, and the distribution of electronic charge in their atoms and chemical bonds. It is possible in principle, and now increasingly in practice, to obtain not just the positions of atoms in molecules but all other topological properties of the associated electron distribution.[59,60,61] It is the aim of charge density analysis to map the electron distribution in crystals and analyse all the detail that carries the information on chemical bonding. Topographical information on a number of complexes may allow trends and characteristics of the topology of various bonding types to be discovered. Intermolecular interactions, such as hydrogen bonds, are also well-suited to charge density analysis. The advances in the field are comprehensively summarized in a comprehensive review article covering publications up to 1998[62] and specific aspects of charge density analysis are reviewed in several other recent publications.[63,64,65]

In consideration of the facilities currently available, a charge-density experiment is often obtained by accurate X-ray diffraction measurements in combination with neutron diffraction measurements on the same compound (X-N method). Neutron diffraction gives complementary information to X-ray diffraction as it is scattered by the nucleus and not the electron cloud. This allows highly accurate nuclear positions along with an accurate electron density map to be obtained to lead to a complete description of the atom positions, electron distribution and bonding within the system.

The field of experimental charge density study[59,66] started in the late 1960s and 1970s through the use of deformation densities to show the accumulation of electron density in bonding and nonbonding (lone pair) regions of molecular crystals. The basis of the modern charge-density experiments is the use of the multipole model. This is a model of the electron density that allows a flexible parameterized description of the charge density, and the charge density of each molecule is described as a sum of the atomic densities. Each atom is described by a fixed, spherical core from a Hartree-Fock calculation, plus an aspherical Hartree-Fock valence density. Multipole modelling has become the *de facto* standard for charge-density refinement from single-crystal diffraction data. The advent of multipole models,[67,68,69] more accurate data collection, and faster computers has advanced the field by allowing the direct calculation of a variety of properties related to the charge density form the multipole parameters that model the static charge density distribution in the crystal. More recently the Atoms in Molecules (AIM) approach developed by Bader and co-workers of analysing the topology of the total charge density may be used in the analysis of both theoretical and experimental charge density data.[70,71] The AIM theory may be used to derive atomic charges, atomic volumes and molecular dipole moments from the charge density.

Furthermore, on the experimental front, recent advances in instrumentation through the coming widespread use of area detectors promises to revolutionise the charge density field by vastly reducing data collection times and by improving the redundancy.[72,73] The current interest in the field is generally attributable to the recent revolutionary improvements that have been made, such as in the development of new diffractometers, the automation of data collection, improved low-temperature techniques, development of area detectors, neutron diffraction and advances in computing power and software. X-ray data used may now come from tube, rotating-anode and synchrotron sources with three-circle, four-circle and Kappa geometry goniometers. Single-crystal neutron diffraction data from both reactor and spallation sources can be used in tandem with the X-ray data.

Standard data collection strategies are not sufficient in charge density analysis, as the data has to be of the highest quality. Due to the large number of parameters to be determined, and their relative sensitivity, extra care must be taken during data-collection. Many symmetry equivalent and replicate measurements, each with prolonged exposure times to enhance signal to noise ratios, are taken and carefully merged, this procedure is facilitated by the use of area detectors. Area detector data sets commonly have a large redundancy which means that after suitable averaging of multiply measured and symmetry equivalent reflections more reliable structure factor amplitudes are obtained. Additionally, at room temperature, crystals rarely scatter far enough in reciprocal space to provide enough high-angle data, therefore low temperature experiments are usually carried out. Cooling the crystal to low temperature is usually essential. An appreciable gain is achieved by cooling to liquid-helium temperature at which the thermal diffuse scattering and especially anharmonic thermal effects are much reduced. Cryostream low-temperature devices (100 K) are also commonly used, although much lower temperatures such as 30 K are attainable in the laboratory using liquid helium "HeliX" cryostats. The collection of data for a study of the charge density is an expensive and time-consuming process. As a result of these advances the time of experiment and computing power are becoming less and less of a limitation. This allows a charge density experiment to be performed in an increasingly routine fashion.

5.4 Structural Databases as a Research Tool

5.4.1 Crystal Structure Databases

The statistical analysis of structural data of related published complexes in an important technique which makes it possible to acquire a deeper insight into catalytic systems and the relationship between ligand properties and catalytic performance. The elucidation of structure-activity relationships involved in these systems may then allow the development of increasingly active and reactively controlled species. The importance of crystallography as a method for studying molecular structure has rapidly increased with the introduction of new diffractometers and new methods of structure solution and refinement over the years. These improvements have resulted in a rapidly increasing number of molecular structures being published and hence large quantities of data becoming available for analysis. The difficulty in collating and presenting such large amounts of data from numerous sources was recognised by the eminent physicist and crystallographer J.D. Bernal in 1948:

"...the growing abundance of primary structural publication and the confusion with which it sets out acts as a continuous brake, as an element of friction, to the progress of science."[74]

The advent of computer databases has made it possible to keep track of vast quantities of data on all manner of subjects, further allowing information from diverse sources to be gathered, categorised and stored in a meaningful order. They are particularly helpful in the management of crystal structure data, since this is easily stored in a standard digital format allowing the development of searchable databases for identifying statistical features and trends of solid state molecular structures based on large amounts of data from a very large number of compounds. There are four main databases available that

record crystal structure data along with associated bibliographical and chemical information:

Cambridge Structural Database (CSD)[75]: Small organic and organometallic structures

Brookhaven Protein Data Bank (PDB)[76]: Macromolecular structures

Inorganic Crystal Structure Database (ICSD)[77]: Inorganic and mineral structures

Metals Data File (MDF)[78]: Metals and alloys

These databases are fully retrospective and are updated regularly. All four of these databases came into being in the 60s and 70s when powerful computers became available for data processing and storage. Not just archives of crystal structure data, the true merit in these databases lies in the sophisticated searching, displaying and analytical programs associated with them, allowing valuable chemical and structural knowledge to be extracted from the vast amount of raw data. The work in this thesis falls solely in the remit of the CSD, and so the following section will introduce the background and working of this database, and related programmes, and outline the use of such systems as a genuine research tool.

5.4.2 The Cambridge Structural Database

The Cambridge Structural Database (CSD) is a fully retrospective database for the structural results obtained from X-ray and neutron diffraction studies of organic and organometallic molecules. It was developed and is run by the Cambridge Crystallgraphic Data Centre (CCDC) along with specialised programs developed to search, analyse and display data contained within the CSD. The CSD is updated binanually and can be run from Unix or Windows interfaces.

Each entry in the CSD represents an individual determination of a specific crystal structure, and is automatically assigned a unique reference code for identification purposes. This reference code has six alphabetic characters to identify the chemical compound, and a possible further two digits to differentiate between specific experimental determinations e.g. structure solutions by different authors or under different experimental conditions. The type of information that the CSD contains on each structure is categorised within the entry by its 'dimensionality' in order to facilitate rapid searching. 1D information consists of text and numerical data. This includes bibliographic data such as authors' names, literature citations and full journal references as well as chemical information such as compound name and formula. Further text on crystal properties and qualifying notes concerning experimental conditions may be included in this information field. 2D information describes the chemical connectivity of the structure, and consists of a 2D chemical diagram that is encoded as a connection table in terms of the atom and bond properties and the 2D coordinates. The atom properties include the element type, number of connected non-hydrogen atoms, number of terminal hydrogen atoms and the formal charge, while the bond properties are defined by chemical bond type and whether the bond is cyclic or acyclic. This information allows 2D and 3D substructure searching. 3D information contains geometric information on the crystal structure. The 3D atomic coordinates as well as crystallographic properties such as space group, crystal system and symmetry operators are stored in this information field. The 3D data also describes the extended crystal structure that is used in non-bonded structure searches.

The most recent CSD data retrieval program used to search the database is called ConQuest, this along with an older version called Quest have both been used in this thesis. In order to satisfy a particular query, the database is searched sequentially to find matches for the specified criteria. Searches in the data fields described above may be performed on the 1D, 2D or 3D information, for example constraints on bond lengths or

angles, may be used. The extended crystal structure may also be searched by defining inter- or intra- molecular non-bonded interactions. In addition, multiple criteria may also be applied to each search by using the logical operators AND, NOT and OR.

Entries which match all of the search criteria are called 'hits' and may be examined in 1D and 2D and manipulated in 3D on the output screen. Values for 3D constraints on bond lengths and angles may be transferred to other programs for 3D visualisation and manipulation (Mercury) or statistical analysis (VISTA or excel). VISTA is the CCDC statistical program for the analysis and display of geometric data obtained from searching the CSD and in the most recent release is available on both the Unix and windows platforms. When 3D parameters have been defined in a search ConQuest automatically generates files that can be read into the VISTA program where analysis of the search results related to that parameter can be performed. As one structure may contain more than one example of the particular parameter requested, and in these cases the data for each of the fragments is recorded. VISTA allows the data to be manipulated and displayed in a number of different ways, initially the molecular geometry and other parameters relating to a molecular or supramolecular substructure is displayed in a spreadsheet format. From this it is possible to produce histograms, scatter diagrams and polar histograms. Statistical analyses including linear regression and principle component analysis can also be performed. For each method, simple descriptive statistics are given about the data. In a graphical format the data can be further manipulated via the interactive window. Relevant areas or individual data points may be selected in order to display the compounds containing those fragments, and the 1D, 2D and 3D information obtained from ConQuest for the relevant reference codes may be examined. Outlying or incorrect data may be suppressed or removed from the data set altogether. VISTA can also generate postscript files of the plots.

PreQuest is the program that may be used to create and maintain an internal database of crystal structures before they are published. The entries then form a database that is private and may be updated and edited whenever necessary, and that is also fully searchable with the Quest/ConQuest program. Isostar is a knowledge base that contains information about particular intermolecular interactions in the form of scatterplots. IsoStar contains data derived from the CSD, the Protein Data Bank (PDB) and also theoretical interaction energies obtained using *ab initio* intermolecular perturbation theory (IMPT). The data relating to the distribution of a contact group around a specific central group is taken from many structures and displayed on the same 3D rotatable diagram generated by the RasMol visualisation program. In this visual manner the likely orientations of molecules towards each other can be quickly assessed and probability surfaces and distributions can be drawn. The contact geometries may be calculated, and contour scatterplots with user defined contour levels drawn. The program also hyperlinks scatterplots to original CSD or PDB entries. In addition to the scatterplots in Isostar, the ancillary program IsoGen makes it possible to generate scatterplots to user specifications.

5.4.3 Knowledge-Mining using the CSD

In addition to the isolation and characterisation of novel complexes, the systematic study of existing, related structures from one of the databases which store the particulars of published compounds can reveal important trends and lead to novel insights. Databases, such as the CSD, contain a large amount of detailed structural information on chemical bonding, molecular conformations and intermolecular interactions. Such a large quantity of data is difficult to analyse in a meaningful manner, and this function is facilitated by the software packages contained within the CSD. The statistical investigation of such data on chemical systems makes it possible to study a variety of chemical phenomena. It

allows the average values for geometrical parameters to be calculated and the easy identification of correlations between parameters within certain series of molecules.

The statistical analysis of such a large number of structures is valuable. For instance, unlike the study of features in individual structures, an anomalous feature that is consistently observed in a series of related structures is statistically significant and must be rationalised as it can not be ascribed to experimental errors or packing effects. So, a large number of crystal structures showing a consistent structural feature can be considered a systematic event. In addition to identifying intramolecular features, such analysis also provides a better understanding of the nature of hydrogen bonds and intermolecular interactions by facilitating the identification of frequently occurring interaction patterns and supramolecular synthons. Research into non-bonded and hydrogen bonded contacts and their effect on molecular environment increased dramatically with the release of Quest and its sophisticated non-bonded search module. An advantage with the database approach is that any distortion in individual interaction geometry is averaged out in the diverse sample of X-ray crystal structures.

The number of reported crystal structures is increasing rapidly and database analysis is fast becoming a recognised form of research in its own right as papers based solely on the analysis of previously published structures are becoming more common. The increasingly sophisticated analytical programmes available have allowed more complex analysis which has lead to the large number of studies that have been completed using the CSD. Mean molecular dimension studies are common, for example Allen *et al.* published "Tables of bond lengths from X-ray and neutron diffraction", their results all being generated from analysis of the CSD.[79] Database analysis has also been used in the fields of structure correlation,[80,81,82] determining conformational preferences[83,84,85] and studying intermolecular interactions. The utilisation of the CSD for has been thoroughly reviewed quite recently.[86]

The technique is, however, subject to some limitations. Perhaps most importantly, statistical studies assume the use of a random sample from the overall population. Studies on a database can never achieve this, since although structures covering an enormous chemical range have been published, this is not a truly random sample. The compounds most likely to be examined by crystallographic methods are often unusual so the database will inevitably be biased towards the unusual. There is no way of achieving a genuinely random sample, so it is necessary to treat the available data as only an approximation to a random sample. Furthermore, there is also much scepticism about the relevance of crystallographic results to molecular properties in solution as crystallography is a solid-state technique and features that exist in a crystal structure may not apply to the solution-state structure, this must be taken into consideration when using database analysis of solid–state compounds to justify aspects of solution-state reactivity. Despite these factors, the accessibility and coverage of the CSD provides an excellent opportunity for detailed analyses of structural features to uncover trends and elucidate structural features important in determining possible mechanisms of reactivity, which are worthwhile in many areas of study.

5.5 References

[1] Mehrotra, R.C.; Singh, A.; *Prog. Inorg. Chem.* **1997**, *46*, 239.
[2] Bradley, D.C.; Mehrotra,R.C.; Rothwell, I.P.; Singh, A. *Alkoxo and Aryloxo Derivatives of Metals*, Academic Press, London; **2001**.
[3] For example see: Bradley, D.C. *Chem. Rev.* **1989**, *89*,1317.
[4] Huger-Pfalzgraf, L.G. *New J. Chem.* **1987**, *11* 663.
[5] Flaschen, S.S. *J. Am. Chem. Soc.* **1955**, *77*, 6194.
[6] For example see: Schrock, R.R.; DePue, R.T.; Feldman, J.; Yap, K.B.; Yang, D.C.; Davis, W.M.; Park, L.; DiMare, M.; Schofield, M.; Anhaus, J.; Walborsky, E.; Evitt, E.; Kruger, C.; Betz, P. *Organometallics* **1990**, *9*, 2262.
[7] Schaverien, C.J.; Dewan, J.C.; Schrock, R.R. *J. Am. Chem. Soc.* **1986**, *108*, 2271.
[8] Hubert-Pfalzgraf, L.G. *Coord. Chem. Rev.*, **1998**, *180*, 967.
[9] Turova, N.Y.; Turevskaya, E.P.; Yanovskaya, M.I.; Kessler, V.G.; Tcheboukov, D.E. *Polyhedron*, **1998**, *17*, 899.
[10] Mehrotra, R.C.; Singh, A. *Prog. Inorg. Chem.*, **1997**, *46*, 239.
[11] Mehrotra, R.C.; Sogani, S.; Singh, A. *Chem. Rev.*, **1994**, *94*, 1643.
[12] Mehrotra, R.C.; Sogani, S.; Singh, A. *Chem. Soc. Rev.*, **1994**, *23*, 215.
[13] Raymond, K.N.; Carano, C.J. *Acc. Chem. Res.* **1979**, *12*, 183-190.
[14] Clegg, W.; Elsegood, M. R.J.; Teat, S.J.; Redshaw, C.; Gibson, V.C. *J. Chem.. Soc. Dalton Trans.* **1998**, 3037.
[15] Albrecht, M.; Kotila, S. *Angew. Chem. Int. Ed. Engl.* **1995**, *34*, 2134.
[16] Karpishin, T.B.; Stack, T.D.P.; Raymond, K.N. *J. Am. Chem. Soc.* **1993**, *115*, 182.
[17] Reetz, M.T.; Wenderoth, R.; Peter, R.; Steinbach, J.; Westermann, J. *J. Chem. Soc. Chem. Commun.*, **1980**, 1202.
[18] Tomioka, K. *Synthesis*, **1990**, 541.
[19] Bradley, D.C. *Chem. Rev.* **1989**, *89*, 1317.
[20] Masters, C. *Homogeneous Transition-Metal Catalysis – a gentle art*, Chapman and Hall; **1981**.
[21] Gibson, V.C.; Spitzmesser, S.K. *Chem. Rev.* **2003**, *103*, 283.
[22] Britovsek, G.J.P.; Gibson, V.C.; Wass, D.F. *Angew. Chem. Int. Ed.* **1999**, *38*, 428.
[23] Yang, X.; Stern, C.L.; Marks, T.J. *J. Am. Chem. Soc.* **1994**, *116*, 10015.
[24] Shapiro, P.J.; Cotter, W.D.; Schaefer, W.P.; Labinger, J.A.; Bercaw, J.E. *J. Am. Chem. Soc.***1994**, *116*, 4623.
[25] Visciglio, V.M.; Clark, J.R.; Nguyen, M.T.; Mulford, D.R.; Fanwick, P.E.; Rothwell, I.P.. *J. Chem. Soc.* **1997**, *119*, 3490.
[26] Vilardo, J.S.; Lockwood, M.A.; Hanson, L.G.; Clark, J.R.; Parkin, B.C.; Fanwick, P.E.; Rothwell, I.P. *J. Chem. Soc. Dalton Trans.* **1997**, 3353.
[27] Latesky, S.L.; Keddington, J.; McMullen, A.K.; Rothewell, I.P.; Huffman, J.C. *Inorg. Chem.* **1985**, *24*, 995.
[28] Chamberlaine, L.; Keddington, J.; Huffman, J.C.; Rothwell, I.P. *J. Chem. Soc. Chem. Commun.* **1982**, 805.
[29] Firth, A.V.; Stewart, J.C.; Hoskin, A.J.; Stephan, D.W. *J. Organomet. Chem.* **1999**, *591*, 185.
[30] Meth-Cohn, O.; Thorpe, D.; Twitchett, H.J. *J. Chem. Soc.* **1970**, 133.
[31] Boyle, T.; Barnes, D.L.; Heppert, J.A.; Morales, L.; Takusagawa, F. *Organometallics*, **1992**, *11*, 1112.
[32] Narasaka, K. *Synthesis*, **1990**, 1.
[33] Rehwinkle, H.; Steglich, W. *Synthesis*, **1982**, 826.
[34] Natta, G. *J. Polymer Sci*, **1955**, *16*, 143.
[35] Bradley, D.C; Mehrotra, R.C.; Wardlow, W. *J. Chem. Soc.* **1952**, 5020.
[36] Bradley, D.C; Mehrotra, R.C.; Wardlow, W. *J. Chem. Soc.* **1952**, 2027.
[37] Bradley, D.C; Mehrotra, R.C.; Swanick, J.D.; Wardlow, W. *J. Chem. Soc.* **1953**, 2025.
[38] Lunn, M. D., Ph.D. Thesis, University of Bath, Bath, UK, October, **2002**.
[39] Brintzinger, H.H.; Fischer, D.; Mulhaupt, R.; Rieger, B.; Waynouth, R.M. *Angew. Chem., Int. Ed. Engl.* **1995**, *34*, 1143.
[40] Bradley, D.C. *Chem. Rev.*, **1989**, *89*, 1317.
[41] Hubert-Pfalzgraf, L.G. *New J. Chem.*, **1995**, *19*, 727.
[42] Hubert-Pfalzgraf, L.G. *Coord. Chem. Rev.*, **1998**, *178–180*, 967.
[43] Shibasaki, M.; Yoshikawa, N. *Chem. Rev.*, **2002**, *102*, 2187.

[44] Aspinall, H.C. *Chem. Rev.*, **2002**, *102*, 1807.
[45] Coates, G.W. *J. Chem. Soc., Dalton Trans.*, **2002**, 467.
[46] Coates, G.W. *Chem. Rev.*, **2000**, *100*, 1223.
[47] See for example: Huheey, J.E.; Keiter E.A.; Keiter, R.L. *Inorganic Chemistry, Principles of Structure and Reactivity*, 4th edn., HarperCollins, New York; **1993**.
[48] Coffindaffer, T.W.; Steffy, B.D.; Rothwell, I.P.; Folting. K.; Huffman J.C.; Streib, W.E. *J. Am. Chem. Soc.*, **1989**, *111*, 4742.
[49] Steffey, B.D.; Fanwick, P.E.; Rothwell, I.P. *Polyhedron,* **1990**, *9*, 963.
[50] Smith, G.D.; Fanwick, P.E.; Rothwell, I.P. *Inorg. Chem.*, **1990**, *29*, 3221.
[51] Howard, W.A.; Trnka, T.M.; Parkin, G. *Inorg. Chem.*, **1995**, *34*, 5900.
[52] Steffey, B.C.; Fanwick, P.E. Rothwell, I.P. *Polyhedron*, **1990**, *9*, 963.
[53] Howard, W.A.; Trnka, T.M.; Parkin, G. *Inorg. Chem.*, **1995**, *34*, 5900.
[54] Hillier, A.C.;Liu, S.Y.; Sella, A.; Elsegood, M.R.J. *Inorg. Chem.*, **2000**, *39*, 2635.
[55] Dobado, J.A.; Molina, J.M. Uggla, R.; Sundberg, M.R. *Inorg. Chem.*, **2000**, *39*, 2831.
[56] Bacon, G.E. *The International Encyclopedia of Physical Chemistry and Chemical Physics*, Volume 1; **1963**.
[57] Wilson, C.C.; *Single Crystal Neuron Diffraction from Molecular Materials.* World Scientific; Singapore; **2000**.
[58] Hukins, D..L. *X-ray Diffraction By Disordered and Ordered Systems.* Pergamon Press; Oxford, **1981**.
[59] Coppens, P. *X-ray Charge Densities and Chemical Bonding.* OCP, Oxford; **1997**.
[60] Gillespie, R.J.; Popelier, P.L.A. *Chemical Bonding and Molecular Geometry.* Oxford Universtiy Press; Oxford; **2001**.
[61] Popelier, P. *Atoms in Molecules.* Prentice Hall, London; **2000**.
[62] Coppens, P. *Acta Cryst.* **1998**, A54, 779.
[63] Koritsanszky, T.S.; Coppens, P. *Chem. Rev.* **2001**, *101*, 1583.
[64] Coppens, P.; Iversen, B.; Larsen, F.K. *Coord. Chem. Rev.* **2005**, *249*, 179.
[65] Macchi, P.; Sirono, A. *Coord. Chem. Rev. 2003, 238-239*, 383.
[66] Tsirelson, V.G.; Ozerov, R.P. *Electron Density and Bonding in Crystals*; Institute of Physics Publishing, Bristol; **1996**.
[67] Hirshfield, F.L. *Acta Cryst.* **1971**, *B27*, 769.
[68] Steward, R.F. *Acta Cryst.* **1976**, *A32*, 566.
[69] Hansen, N.; Coppens, P. *Acta Cryst.* **1978**, *A34*, 909.
[70] Bader, R.F.W. *Atoms in Molecules: A Quantum Theory:* International Series of Monographs in Chemistry 22; Oxford University Press: Oxford, **1990**.
[71] Bader, R.F.W.; Essen, H. *J. Chem. Phys.* **1984**, *80*, 1943.
[72] Macchi, P.; Proserpio, D.M.; Sironi, A. *J. Am. Chem. Soc.* **1998**, *120*, 1447.
[73] Iverson, B.B.; Larsen, F.K.; Pinkerton, A.A.; Martin, A.; Darovsky, A.; Reynolds, P.A. *Acta Cryst.* **1999**, *B55*, 363.
[74] Bernal, J.D. *The Royal Society, Scientific Information Conference Report,* The Royal Society, London, **1948**, pp54.
[75] Cambridge Crystallographic Data Centre, Cambridge, UK.
[76] Brookhaven National Laboratory, Upton, New York, U.S.A.
[77] Gmelin Institute, Karlsruhe, Germany.
[78] National Research Council of Canada, Ottawa, Ontario, Canada.
[79] Allen , F.H.; Kennard, O.; Watson, D.G. *J. Chem. Soc. Perkin Trans.2.* **1987**, *12*, S1.
[80] Kirby, A.J. *Adv. Phys. Org. Chem.* **1994**, *29*, 87.
[81] Bürghi, H.-B.; Dunitz, J.D. *Acc. Chem. Res.* **1983**, *16*, 153.
[82] Bürghi, H.-B.; Dunitz, J.D. *Structure Correlation*, VCH; Weinheim, Germany; **1994**.
[83] Allen, F.H.; Harris, S.E.; Taylor, R. *J. Computer-Aided Mol. Des.* **1996**, *10*, 247.
[84] Böhm, H.-J.; Klebe, G. *Angew. Chem., Int. Ed. Engl.* **1996**, *35*, 1588.
[85] Rappoport, Z.; Biali, S.E.; Kaftory, M. *J. Am. Chem. Soc.* **1990**, *112*, 7742.
[86] Allan, F.H., Taylor, R. *Chem. Soc. Rev.* **2004**, *33*(8), 463.

Chapter 6

The Characterisation and Topological Analysis of a Metallo-organic Titanium (IV) Complex from Combined X-ray and Neutron Diffraction Data

6.1 Background

There is a great deal of interest in titanium alkoxide metal complexes as a result of their potential use as reagents and catalysts in a number of important fields, the function of such early transition metal alkoxides in such roles was discussed in Chapter 5. The molecular design of such catalysts, which possess specific reactivity and selectivity, has become increasingly important. The nature of the metal-ligand bonding in these complexes is fundamental to their reactivity and, within this context, has become widely discussed.[1,2,3,4] Hence, a thorough understanding of the bonding and electronic structure is desirable to provide invaluable insight into the reactivity of these metal complexes. It is the goal of this chapter to examine the electronic distribution within an example typical of the catalytically active early transition metal alkoxides. This chapter presents the results of a combined, low temperature (30 K) neutron and X-ray diffraction study and charge density analysis on the catalytically relevant titanium alkoxide $[(2\text{-py})CH_2O)]_2Ti(OCHMe_2)_2$, **12**, for this purpose. The use of charge density analysis on transition metal complexes will first be briefly reviewed, followed by the results of the X-ray and neutron diffraction experiments and a topological analysis, using the Atoms in Molecules (AIM) approach,[5] of the charge density derived from this combined data for **12**.

The analysis of charge density is used to extract detailed information on the electronic distribution, and thus on the nature of the bonding in crystals. Bader and co-workers have

shown that valuable chemical information can be retrieved from the total electron density distribution of a molecule, obtained by exploiting the AIM method of charge density analysis. This involves analysis of the topological features of the total electron density, such as critical points, density and the Laplacian of the density ($\nabla^2\rho$). The AIM approach has proven to be a powerful method, which can be equally well applied to theoretical and experimental charge densities and in the last few years has become increasingly common as the standard method for interpreting charge density data.[6,7,8,]

Although charge density analysis is now a well-established field in crystallography, to date the emphasis has primarily been focused on small molecules of biological interest and the exploitation of this technique has fully elucidated the link between bonding modes and topological properties for light atoms. The extension to organotransition metal complexes occurred quite early, but until recently the number of studies on these species remained comparatively small. This is chiefly due to the challenges faced in the analysis of metal systems. These problems include large absorption, extinction and anomalous dispersion effects, and also the possibilities of anharmonic thermal motion and anisotropic extinction. In addition, the low ratio of valence to core electrons in these compounds makes it difficult to study bonding features, as the contribution to structure factors from core electrons to a certain extent swamps the signal from valence electrons, except at low values of sin θ/λ.[9,10] Consequently, the electronic structure and bonding in these metal complexes is not as well understood as the properties of organic molecules and requires high accuracy in the measurement and correction of the data.

While, until recently, there have been few studies of the topology of the charge density of transition metal complexes based upon experimental work,[11,12,13] a number of theoretical studies have been published[14] and in the last decade many such papers reporting the electron

density distributions in transition metal complexes have begun to appear in the literature.[15] The combined experimental and theoretical charge density analysis has become increasingly used to investigate the bonding and electronic structure of metal based compounds.[16,17] While the analysis of experimentally determined charge densities is an area of growing in importance in the analysis of chemical bonding, such studies involving early transition metal compounds remain rare in the existing literature. Notable exceptions to this are the characterisation of agostic interactions in $EtTiCl_3$ (dmpe)[18] and the similar analysis of d^0 complexes[19] by combined theoretical and experimental analysis. The bonding in titanium complexes has received some attention in this field. Bader and Matta have recently published the theoretical analysis of the bonding of titanium to carbon ligands, within the framework of the atoms in molecules theory.[20] The study of metal-ligand bonding in titanium metallocenes, also by Bader, to provide insight into the nature of this interaction used a combined experimental and theoretical charge density study. Bader also performed an analysis of the bonding between Ti and cyclopentadienyl, diene and alkyl fragments.

It has been noted that our interest in metal alkoxides focuses on species with the general formula $M_xL_y(O^iPr)_z$ where M is a Group 4 metal and L is an anionic ligand other than a monodentate alkoxide. Titanium(IV) alkoxides are widely used as precatalysts for polymerisation reactions and in asymmetric organic transformations. We are interested in the development of titanium alkoxide systems as potential catalysts for the synthesis of polyurethanes and polyesters. In particular, we are studying single-site molecular precatalysts incorporating titanium alkoxide centres and chelating phenolic ligands. The use of these ligands, similar to the bidentate Schiff-bases ligands, in organometallic chemistry has been extensive because they are easy to prepare and they exert easily varied steric and or electronic effects on the resulting complexes.[21,22,23] These highly versatile ligands are ubiquitous in coordination chemistry due to the ease of variation of their steric and electronic

properties by variation of the substituents R, R' and R'' shown above. These compounds allow for formation of chelated aryloxide complexes, which are known for a huge range of metals with diverse uses including as catalysts for ethylene polymerisation and olefin metathesis. A feature of particular importance in these complexes is the nature of the metal-ligand bonding, an issue which was introduced in Chapter 5 (5.2.3). In such metal alkoxide complexes there has been noticeable interest and discussion in the literature over the presence and extent of multiple bonds between the metal centres and oxygen atoms on the ligands due to π-bonding from filled ligand orbitals to the empty metal d-orbitals. A detailed study of the electronic distribution in a representative model compound of this type will provide valuable insight into the bonding and reactivity, hence providing a route to the rational design of catalysts of improved activity and selectivity.

In summary, it is due the wide-ranging interest in this important class of metallo-organic compounds that a detailed analysis of the bonding between the metal centre and coordinated ligands is of significant interest. A thorough understanding of the nature of these interactions is crucial in elucidating the mechanisms by which these catalysts act. It is with this background in mind that we set about the present study, the combined X-ray and neutron charge density study of a titanium alkoxide compound. The remainder of this chapter will present the results of this study, and a discussion of the topological charge density analysis.

6.2 Synthesis and Isolation of $(pyCH_2O)_2Ti(O^iPr)_2$ (12)

Crystals of this sample were initially synthesised in our group by M. Lunn.[24] The preliminary studies indicated that the sample was appropriate for analysis by charge density techniques. Of primary importance is the fully ordered 150 K X-ray analysis, as disorder in the crystals greatly complicates any charge density analysis. This is also helped by the fact that the crystals do not contain any trapped solvent. The reaction was repeated for this experiment in order to grow crystals of a suitable size and quality for accurate X-ray and neutron data collections. The reaction of the ligand hydroxymethylpyridine ($pyCH_2OH$) with titanium tetraisopropoxide [$Ti(O^iPr)_4$] in a 2:1 stoichiometry proceeded in refluxing toluene which on cooling yielded an off-white crystalline solid. The product complex was isolated by removal of the solvent *in vacuo* to afford an analytically pure crystalline solid.

Crystals suitable for neutron diffraction measurements were obtained by slow recrystallisation from a saturated solution of toluene. After crystallisation the largest crystals were manually cleaned for misgrowth under a microscope and mounted, under inert conditions, on an aluminium pin and placed into a quartz capillary.

6.3 Molecular Structure of $(pyCH_2O)_2Ti(O^iPr)_2$ (12)

The accurate X-ray and neutron diffraction experiments on **12** were carried out at 30 K and the two crystal structures obtained are described in the following section. Numbering of these complexes is consistent between the two structures. Selected crystallographic data is given for each structure in this discussion and full crystallographic tables containing the atomic coordinates and the equivalent isotropic displacement parameters are listed in Appendix A. While in the analysis of the X-ray diffraction data the hydrogen atoms were all fixed by a riding model, in the neutron structure the hydrogen atoms were freely and anisotropically refined. All non-hydrogen atoms are anisotropically refined in both structures and no restraints have been used. A summary of the X-ray and neutron crystallographic data obtained for **12** is collected in Table 6.1. The molecular structure and numbering scheme of **12** for both the X-ray and neutron data set is shown in Figure 6.1.

	12 (X-ray)	**12 (Neutron)**
Empirical formula	$C_{18}H_{26}N_2O_4Ti$	$C_{18}H_{26}N_2O_4Ti$
M	382.31	382.3
Crystal system	Monoclinic	Monoclinic
Space group	$P2_1/n$	$P2_1/n$
a / Å	11.1340(2)	11.1409(4)
b / Å	14.5940(2)	14.5881(5)
c / Å	12.1090(2)	12.1066(4)
α / °	90	90
β / °	93.267(1)	93.245(2)
γ / °	90	90
U / Å^3	1964.39(5)	1964.46(12)
Z	4	4
μ (Mo-Kα) / mm^{-1}	1.293	1.204
Reflections collected	162475	10182
Independent reflections	25585	4024
R(int)	0.0985	0.0212
R1, wR2	0.0498, 0.1190 for 17665 data	0.0254, 0.0630 for 3859 data
R indices (all data)	0.0852, 0.1327	0.0285, 0.0641

Table 6.1: Crystal and refinement data for the 30 K X-ray and neutron experiments for complex **12**.

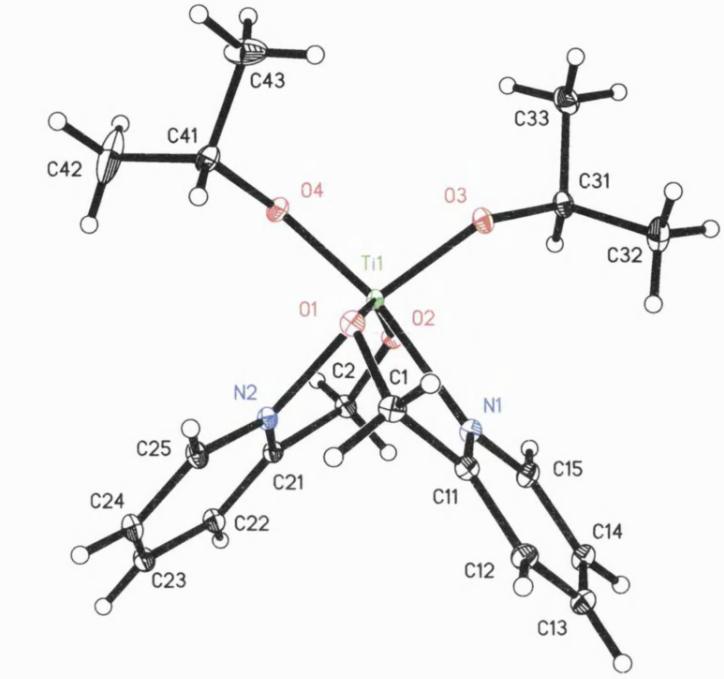

(a)

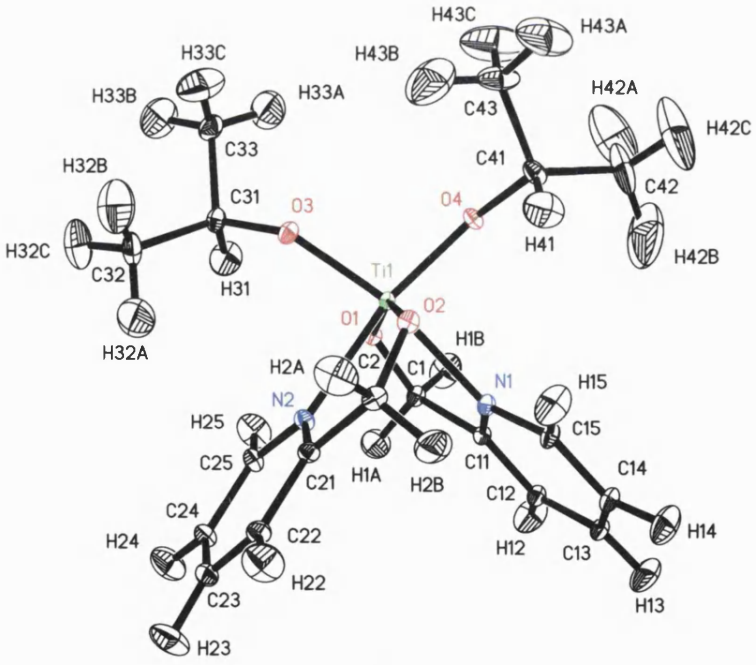

(b)

Figure 6.1: Molecular structure of **12** derived from (a) X-ray and (b) neutron data, hydrogen atoms omitted for clarity and ellipsoids shown at 50% probability.

The crystal structure for **12** contains one monomeric molecule of the complex only, in which two isopropoxide ligands and two chelating pyridyl ligands are coordinating to the titanium metal centre. The molecular geometry is found to be consistent with other reported titanium bis-pyridine-alkoxide complexes with monodentate ligands mutually cis and the N, O coordination occurring such that the pyridyl alkoxides are mutually trans. As mentioned earlier, in the refinement of the neutron data only, the hydrogen atoms were found and freely refined anisotropically, hence thermal ellipsoids for the neutron data set are shown, whereas for the X-ray structure the hydrogen atoms are shown as spheres of an arbitrary diameter.

The six donors around the metal centre adopts a distorted octahedral configuration such that, if a terminal isopropoxide and the trans pyridyl donor are considered as being in the axial positions, the remaining four equatorial ligands bend slightly away form the axial isopropoxide ligand toward the pyridyl nitrogen. Accordingly, the titanium atom is found to sit 0.25Å out of the plane formed by the four equatorial ligands [O(1), N(1), O(2), O(3)]. This distortion from a regular octahedral structure can be traced to the small bite angle (75°) of the chelating $pyCH_2O$ ligand. The aromatic rings in the ligands retain appreciable linearity, as the deviations of the ring atoms to a least squares plane (defined by all six atoms in the ring) are all less than 0.01Å.

Selected bond lengths and angles in complex **12** for both data collections are presented in Tables 6.2 and 6.3 respectively.

	X-ray	Neutron
Ti(1)-O(1)	1.9127(5)	1.910(2)
Ti(1)-O(2)	1.9100(4)	1.915(2)
Ti(1)-O(3)	1.8280(4)	1.836(2)
Ti(1)-O(4)	1.8351(5)	1.830(2)
O(1)-C(1)	1.3940(8)	1.387(1)
O(2)-C(2)	1.3910(7)	1.390(1)
O(3)-C(31)	1.4092(7)	1.404(1)
O(4)-C(41)	1.4081(7)	1.405(1)
Ti(1)-N(1)	2.2498(5)	2.246(2)
Ti(1)-N(2)	2.2463(5)	2.252(2)
C(11)-N(1)	1.3387(8)	1.336(1)
C(15)-N(1)	1.3470(7)	1.347(1)
C(21)-N(2)	1.3356(7)	1.337(1)
C(25)-N(2)	1.3492(7)	1.347(1)

Table 6.2: Selected bond lengths [Å] for complex **12**.

	X-ray	Neutron
O(1)-Ti(1)-O(2)	154.03(2)	153.98(9)
O(3)-Ti(1)-O(1)	93.15(2)	93.45(7)
O(4)-Ti(1)-O(1)	102.94(2)	103.23(7)
O(3)-Ti(1)-O(2)	103.15(2)	102.94(7)
O(4)-Ti(1)-O(2)	93.48(2)	93.13(7)
O(4)-Ti(1)-O(3)	101.78(2)	101.85(8)
C(1)-O(1)-Ti(1)	125.35(3)	125.78(7)
C(2)-O(2)-Ti(1)	125.79(4)	125.45(7)
C(31)-O(3)-Ti(1)	136.93(4)	140.63(8)
C(41)-O(4)-Ti(1)	140.60(4)	137.11(8)
O(1)-Ti(1)-N(1)	75.290(18)	75.03(5)
O(2)-Ti(1)-N(2)	75.011(18)	75.14(5)
N(2)-Ti(1)-N(1)	80.711(18)	80.66(5)

Table 6.3: Selected bond angles [°] for complex **12**.

The metal to ligand bond lengths in the complex are all of the expected order with the isopropoxide ligands having bond lengths of [1.8280(4)Å, Ti(1) –O(3); 1.8351(5)Å, Ti(1)-O(4)] and [1.836(2)Å, Ti(1) –O(3); 1.830(2)Å, Ti(1)-O(4)] in the X-ray and neutron structures respectively. These are consistent with the expected values for terminal isopropoxide bonds to titanium. The pyridyl nitrogen donors also have typical bond lengths

to the metal centre for interactions of this type [2.2498(5)Å, Ti(1) –N(1); 2.246(2)Å, Ti(1)-N(2)] and [2.2463(5)Å, Ti(1) –N(1); 2.252(2)Å, Ti(1)-N(2)]. These bonds from the central titanium atom to the nitrogen donors are, as expected, the longest metal-ligand distance observed in this species. The bonds to the pyridyl alkoxides are [1.9127(5)Å, Ti(1) –O(1); 1.9100(4)Å, Ti(1)-O(2)] and [1.910(2)Å, Ti(1) –O(1); 1.915(2)Å, Ti(1)-O(2)] which is also consistent with expected values. Each of the oxygen atoms in the ligands formally has two lone pairs and one pair of electrons involved in a σ-bond to the central metal atom. Consideration of the geometry around the oxygen atoms show slight deviations from pure sp^2 hybridisation; [125.35(3)°, C(1)-O(1)-Ti(1); 125.79(4)°, C(2)-O(2)-Ti(1); 136.93(4)°, C(31)-O(3)-Ti(1); 140.60(4)°, C(41)-O(4)-Ti(1)] for X-ray and [125.78(7)°, C(1)-O(1)-Ti(1); 125.45(7)°, C(2)-O(2)-Ti(1); 140.63(8)°, C(31)-O(3)-Ti(1); 137.11(8)°, C(41)-O(4)-Ti(1)] for neutron data which in partly due to the effect of chelation. The observed geometry also leaves potential for oxygen p-orbitals on the oxygen ligands to be involved in additional π-bonding with the empty d-orbitals on the metal centre, however this cannot be conclusively confirmed solely on geometric evidence.

Free rotation of the isopropoxide groups is manifested in the crystal structures as larger thermal ellipsoids for these atoms by comparison to the other ligands, as might be expected. This feature is particularly apparent in the neutron data set. **12** also exhibits two close intramolecular hydrogen bonds. These are illustrated in Figure 6.2 and the hydrogen bond parameters are presented in Table 6.4. These data are both derived from the neutron data due to the accurately found hydrogen atoms in this data set.

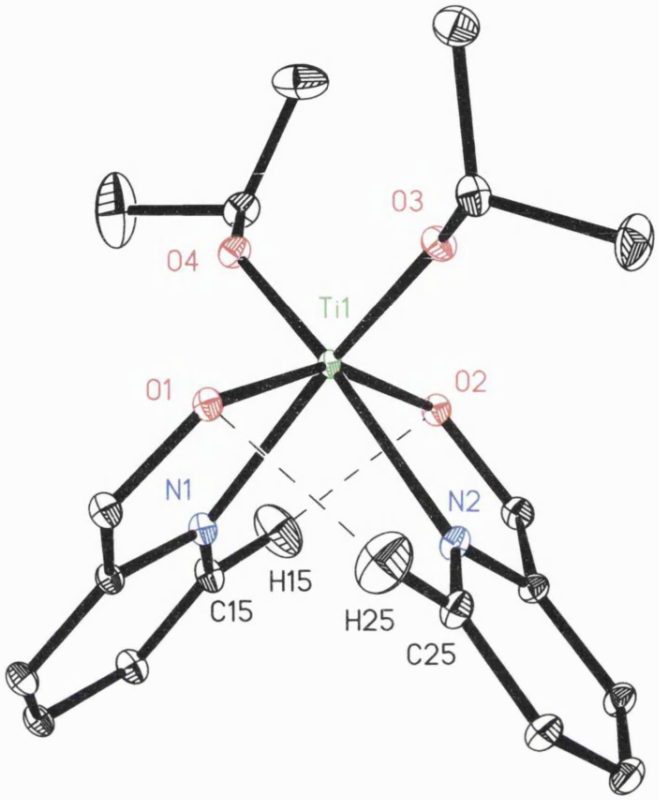

Figure 6.2: View of the two intramolecular C-H···O hydrogen bonds observed in **12** (shown as dashed lines), derived from neutron data and all atoms, including hydrogen atoms, shown by thermal ellipsoids at 50% probability. Hydrogen atoms not involved in the hydrogen bonding are omitted for clarity.

D-H...A	d(D-H)	d(H···A)	d(D···A)	<(DHA)
C(25)-H(25)···O(1)	1.087(2)	2.472(2)	3.040(2)	111.3(2)
C(15)-H(15)···O2()	1.088(2)	2.457(2)	3.036(2)	111.9(2)

Table 6.4: Hydrogen bond parameters in **12** [Å and °].

The technique of normalising bond lengths in X-ray structures uses a standard set of values, obtained from the neutron values.[25] This standard value for C-H···O is 1.083Å. The distance

exhibited in this structure for the intramolecular interactions is extremely similar to this standard value, indicating a typical interaction. As C···O distances of between 3.0 and 4.0Å are considered typical, these interactions may be considered to be rather short. However, as an intramolecular interaction this may be a result of the steric requirements of the metal-ligand coordination sphere and not necessarily due to the bond being particularly strong.

6.4 Experimental and Theoretical Charge Density Analysis of 12

To elucidate the charge density distribution in **12**, especially the bonding situation of the six distinct titanium-ligand bonds, we have performed a multipole refinement with the formalism from Hansen and Coppens[26,27] based on the combined X-ray and neutron data. The analysis of the bonding at the Ti centre has been carried by a combination of orbital-dependent and of orbital-independent techniques. The electronic structure of **12** is analysed in terms of Natural Bond Orbitals (NBO), whereas its electron density is analysed by Bader's Quantum Theory Atoms in Molecules (QTAIM). This section presents the results of these analyses. The work in this chapter was carried out in colloboration with Dr B. Tejerina at the Iowa State University and all of the theoretical and multipolar calculations presented in this section were carried out by Dr Tejerina.[28]

6.4.1 Geometry

The main geometrical parameters for the combined experimental data after multipole refinement and those of three separate theoretical analyses are collected in Table 6.5.

Bond	**Experimental**	**Theoretical**		
	Multipolar	HF	MP2	DFT
Ti(1)-O(1)	1.9149(9)	1.9079	1.946	1.9274
Ti(1)-O(2)	1.9121(10)	1.9079	1.9464	1.9274
Ti(1)-O(3)	1.8418(7)	1.8175	1.8315	1.8346
Ti(1)-O(4)	1.8353(5)	1.8175	1.8315	1.8346
Ti(1)-N(1)	2.2424(8)	2.3555	2.2790	2.3486
Ti(1)-N(2)	2.2442(7)	2.3555	2.2790	2.3486
O(1)-C(1)	1.3900(6)	1.3664	1.3995	1.3813
O(2)-C(2)	1.3931(7)	1.3664	1.3995	1.3813
O(3)-C(31)	1.4103(6)	1.3933	1.4255	1.4107
O(4)-C(41)	1.4108(5)	1.3933	1.4255	1.4107
N(1)-C(11)	1.3389(6)	1.3188	1.3449	1.3381
N(1)-C(15)	1.3512(6)	1.3273	1.3450	1.3413
N(2)-C(21)	1.3418(7)	1.3188	1.3449	1.3381
N(2)-C(25)	1.3490(5)	1.3273	1.3450	1.3413
C(1)-C(11)	1.5080(7)	1.5150	1.5137	1.5178
C(11)-C(12)	1.3985(7)	1.3907	1.3970	1.3992
C(12)-C(13)	1.3898(7)	1.3780	1.3943	1.3908
C(13)-C(14)	1.3987(7)	1.3904	1.3971	1.3989
C(14)-C(15)	1.3844(7)	1.3762	1.3927	1.3902
C(2)-C(21)	1.5088(7)	1.5150	1.5137	1.5178
C(21)-C(22)	1.3962(7)	1.3907	1.3970	1.3992
C(22)-C(23)	1.3881(7)	1.3780	1.3943	1.3908
C(23)-C(24)	1.4004(8)	1.3904	1.3971	1.3989
C(24)-C(25)	1.3856(8)	1.3762	1.3927	1.3902
C(31)-C(32)	1.5257(8)	1.5256	1.5214	1.5329
C(31)-C(33)	1.5256(8)	1.5251	1.5200	1.5327
C(41)-C(42)	1.5165(9)	1.5256	1.5214	1.5329
C(41)-C(43)	1.5229(8)	1.5251	1.5200	1.5327

Table 6.5: Molecular bond lengths (Å) for **12**.

As Table 1 suggests, the Ti-$O_{propoxide}$ bonds are clearly stronger than the Ti-O_{ligand} ones (shorter by almost 0.1 Å in average). As a test of the reliability of the theoretical results, Table 6.5 compares the experimental data with the results of DFT, MP2 and HF calculations. There is excellent agreement between the experimental and theoretical data, particularly in the homomeric C-C bonds. It is notable that the metal-chelating ligand bonds have better agreement with the DFT results, while the metal-isopropoxide bonds have better agreement with the MP2 theoretical treatment. With respect to the MP2 and DFT results in titanium complexes, in which the C-O bond lengths are longer and the Ti-O_{ligand} shorter at the MP2

level than the DFT, these results are consistent with published theoretical calculations on titanium alkoxide complexes.[29]

In addition, analysis of the geometric features of **12** indicates that a noticeable structural characteristic is the relative planarity of the two five-membered rings that define the interaction of Ti with the chelating pyridyl ligands (Table 6.6).

	Neutron	X-ray	Multipolar	HF	DFT	MP2
π	0.012/0.039	0.013/0.041	0.015/0.041	0.139	0.003	0.243

Table 6.6: 5-member ring puckering Ti-O-C-C-N.

There is a slight discrepancy between theory and experiments in the parameter π, a measure of the planarity of the Ti-O-C-C-N rings. [30] While *ab initio* HF and MP2 structures show a strong envelope-like conformation of such rings (π = 0.14 and 0.24 respectively), in the crystal and in the DFT structure these atoms are practically coplanar ($\pi \approx 0.0$).

6.4.2 Electronic Properties

In order to judge the main binding forces in the titanium-ligand interactions, we have performed an NBO analysis on **12**. The NBO analysis provides information on the nature of the bonding interactions within the complex. The NBO analysis takes into consideration all possible interactions between filled NBOs and empty NBOs and it is possible to estimate their energetic importance by the application of second-order perturbation theory. These interactions lead to a loss of occupancy in the donor NBOs and a gain in occupancy in the acceptor NBOs and are referred to as 'delocalisations'. NBO calculations have been performed on the HF wavefunction.

The results of the NBO analysis for the electronic structure of **12** are depicted in Figure 6.3. The HOMO and LUMO at the metal centre in addition to the relevant NBOs associated with the ligands are shown, with the populations of the valence orbitals included. In addition, the results of second order perturbation theory analysis, in order to judge donor-acceptor stabilisation energies, are presented in Table 6.7. This table presents the lone pair populations and relative stabilisations of the calculated NBOs between titanium and the donor ligands for **12**.

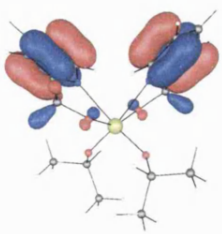

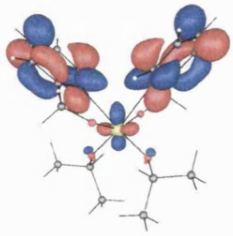

Canonical HOMO (left) and LOMO (right) of the RHF wave function.

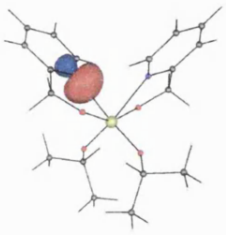

Lp N 1.828

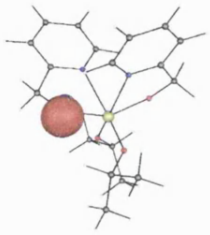

Lp(1) O(2) 1.922

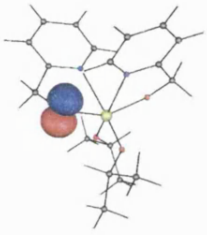

Lp(2) O(2) 1.872

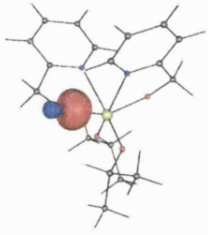

Lp(3) O(2) 1.789

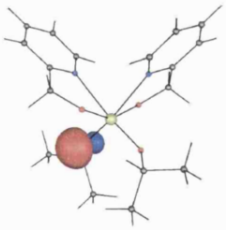

Lp(1) O(3): 1.890

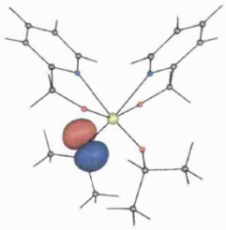

Lp(2) O3: 1.847

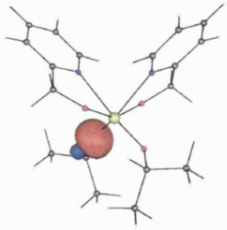

Lp(3) O(3) 1.764

Figure 6.3: Natural Bond Orbitals associated to the atoms of the ligands bound to the titanium atom, along with the occupancy of each the lone pairs on the ligand N and O atoms.

	Natural occupancy	$3d_{x^2-y^2}$ 0.423	$3d_{xz}$ 0.420	$3d_{z^2}$ 0.279	$3d_{yz}$ 0.275	$4s+3d_{xy}$ 0.222	$4s-3d_{xy}$ 0.214
$Lp(1)N1_{Lig}$	1.828	15.9	47.6			27.1	
$Lp(1)O2_{Lig}$	1.922	17.8					35.0
$Lp(2)O2_{Lig}$	1.872	13.3			18.9		
$Lp(3)O2_{Lig}$	1.789	108.6			26.1	28.3	35.5
$Lp(1)O3_{prop}$	1.890		17.6		17.6	27.7	
$Lp(2)O3_{prop}$	1.847			53.0			
$Lp(3)O3_{prop}$	1.764	45.2	115.1			46.6	10.8

Table 6.7: Energy stabilisation by donor (oxygen and niotrogen lone pairs) - acceptor (empty metal d orbitals) interactions (Kcal/mol) calculated by second order perturbation theory.

The Lewis structure for complex **12** in total has 14 lone pairs (7 unique by symmetry) on the ligand donor atoms, which are shown in both Figure 6.4 and Table 6.7. The NBO analysis of the HF-Wave-function reveals an electronic structure in which the bonding Ti–O is predominantly ionic. All four oxygen atoms have 3 lone pairs associated with an electronic occupancy of 1.92, 1.87, 1.79*e* on O(2) and 1.89, 1.85, 1.76*e* on O(3). The nitrogen atom in the ligand has one lone pair associated with it. From the longer distance N–Ti (2.356 Å) and from the direction, and population of this lone pair on the nitrogen (1.83*e*), this interaction may be best described as a highly polarised dative bond.

Second order perturbation theory analysis revealed no delocalisations from the titanium metal centre to any of the ligands. The most noteworthy delocalisations occur from the titanium atom to the six atom located in the coordination sphere. Due to this delocalisation from the filled ligand orbitals (lone pairs) to the empty metal d-orbtials, the least populated formal lone pairs on the ligand show the highest stabilisation energies. This stabilisation energy is useful as a measure of the bond strength. The strongest delocalisations occur from the third lone pair on the oxygen atom on the ligand, O(2) and O(3) by symmetry, to the titanium, showing that lone pairs which are least populated and associated with the highest stabilisation

are those part of the Ti-$O_{propoxide}$ bonds in this donor-acceptor view, in accord with the metric analysis. The lone pair on the nitrogen atoms holds 1.828 *e* having their most important stabilising interaction with the $3d_{xz}$ orbital of the titanium. Compared with the Lp(3) in the neighbouring oxygen atoms, the lower donating effect correlates and justifies the Ti-N distances which are substantially longer than that of the Ti-O interaction. The longer distance Ti-N also implies a less stable bond and therefore can readily leave the coordination position to other ligands by substitution.

A noteworthy feature of this analysis is the relative depletion of the lone pairs on the O_{ligand} atom. Lp(2) is depleted to a greater extent than lone pair 1, 1.872 and 1.922 respectively, even though the second order perturbation theory analysis revealed less interaction with the titanium metal centre from Lp(2). It is proposed that this observation is the result of the intramolecular hydrogen bonding interaction between the O_{ligand} and aryl hydrogen atom (Figure 6.3). Hence, this hydrogen bonding interaction from lone pair 2 on O(2) to the aryl hydrogen causes a depletion in occupancy of this NBO, relative to the other lone pair on this oxygen which is not subject to this interaction.

6.4.3 Topological Analysis of the Charge Density

The topological analysis of the charge density distribution, $\rho(r)$, and that of the Laplacian, $\nabla^2\rho(r)$, can give valuable insight into the chemical bonding. To characterise the bonding in **12** we have analysed both of these parameters in terms of Baders quantum theory of "Atoms in Molecules" (AIM).[31] Analysis of the charge density distribution by this method locates certain points where the gradient of $\rho(r)$ and $\nabla^2\rho(r)$ is zero. These are called critical points (CPs) and as a subset of these bond critical points (BCPs) are necessary to indicate the

presence of a bond. The interpretation of the charge density at the BCPs reveals important information relating to the nature of the bonding interactions. The following salient parameters at the bond critical points (BCPs) are listed in Table 6.8 and 6.9 for the experimental analysis and the two theoretical analyses respectively: charge density $\rho(r)$, Laplacian of the charge density $\nabla^2\rho(r)$ and bond ellipticity $\epsilon(r)$. The positional parameters of the BCP in the experimental data set are also given.

Bond Path	ρ_{BCP}[a]	$L(\rho)_{BCP}$[b]	R_{ij}[c]	d(X-BCP)[d]	d(BCP-Y)[e]	ε_{BCP}[f]
TI(1)-O(1)	0.700	5.891	1.9279	0.9005	1.0274	0.57
TI(1)-O(2)	0.706	10.100	1.9381	0.9284	1.0097	0.57
TI(1)-O(3)	1.011	13.986	1.8428	0.9035	0.9393	0.42
TI(1)-O(4)	0.891	8.840	1.8552	0.8710	0.9842	1.09
TI(1)-N(1)	0.470	4.227	2.2425	1.0385	1.2040	0.13
TI(1)-N(2)	0.467	4.166	2.2465	1.0393	1.2072	0.10
O(1)-C(1)	1.965	-6.453	1.3904	0.9707	0.4198	0.07
O(2)-C(2)	1.932	-5.402	1.3935	0.9745	0.4190	0.05
O(3)-C(31)	1.881	-12.271	1.4103	0.8278	0.5825	0.07
O(4)-C(41)	1.877	-12.240	1.4109	0.8279	0.5830	0.06
N(1)-C(11)	2.408	-19.612	1.3389	0.7144	0.6245	0.13
N(1)-C(15)	2.291	-24.012	1.3514	0.7828	0.5686	0.22
N(2)-C(21)	2.395	-19.193	1.3418	0.7144	0.6275	0.13
N(2)-C(25)	2.297	-24.406	1.3491	0.7839	0.5652	0.23
C(1)-C(11)	1.860	-18.173	1.5081	0.8101	0.6979	0.14
C(11)-C(12)	2.175	-23.079	1.3986	0.7695	0.6291	0.19
C(12)-C(13)	2.188	-23.565	1.3898	0.7462	0.6436	0.22
C(13)-C(14)	2.123	-22.357	1.3988	0.7160	0.6829	0.14
C(14)-C(15)	2.197	-24.271	1.3844	0.6220	0.7624	0.21
C(2)-C(21)	1.873	-18.144	1.5088	0.8188	0.6899	0.17
C(21)-C(22)	2.185	-23.333	1.3963	0.7689	0.6274	0.19
C(22)-C(23)	2.192	-23.696	1.3881	0.7462	0.6419	0.22
C(23)-C(24)	2.118	-22.257	1.4007	0.7167	0.6840	0.14
C(24)-C(25)	2.194	-24.199	1.3856	0.6228	0.7628	0.21
C(31)-C(32)	1.696	-14.612	1.5280	0.5105	1.0174	0.08
C(31)-C(33)	1.750	-16.785	1.5258	0.6265	0.8993	0.04
C(41)-C(42)	1.689	-14.394	1.5173	0.5092	1.0082	0.10
C(41)-C(43)	1.763	-16.886	1.5230	0.6248	0.8982	0.04

Table 6.8: Selected topological parameters at the BCP in the experimental data set refined by multipolar methods for **12**. Labels are consistent with those indicated in Figure 6.1. (a) The charge

density function ρ at the BCP (e Å^{-3}); (b) the Laplacian of ρ [$L(\rho) = -\nabla^2\rho$] at BCP (e Å^{-5}); (c) the BP length R_{ij}; (d) and (e) the BCP distance from the nuclear positions (Å) and (f) the ellipticity at the BCP.

Bond	DFT			MP2		
	ε^a	$\rho(r)^b$	$\nabla^2\rho(r)^c$	ε^a	$\rho(r)^b$	$\nabla^2\rho(r)^c$
O2-Ti1	0.133	0.716	13.066	0.148	0.706	12.148
O4-Ti1	0.103	0.900	16.624	0.130	0.918	16.559
N2-Ti1	0.065	0.286	4.288	0.035	0.341	5.186
C21-N2	0.078	2.305	-24.446	0.095	2.224	-21.501
C25-N2	0.089	2.279	-24.254	0.107	2.210	-20.966
C2-O2	0.020	1.917	-15.863	0.024	1.813	-14.849
H2A-C2	0.037	1.813	-21.326	0.033	1.825	-22.223
H2B-C2	0.034	1.822	-21.709	0.031	1.814	-22.110
C2-C21	0.091	1.742	-15.182	0.088	1.745	-15.492
C21-C22	0.200	2.105	-20.462	0.208	2.097	-20.408
C22-C23	0.206	2.122	-20.764	0.205	2.095	-20.421
C23-C24	0.189	2.094	-20.356	0.197	2.088	-20.383
C24-C25	0.228	2.140	-21.144	0.224	2.118	-20.929
H22-C22	0.016	1.866	-23.237	0.010	1.850	-23.491
H23-C23	0.007	1.878	-23.687	0.011	1.857	-23.639
H24-C24	0.016	1.872	-23.444	0.010	1.858	-23.726
H25-C25	0.023	1.912	-25.053	0.026	1.886	-25.218
C41-O4	0.029	1.730	-11.667	0.023	1.639	-10.045
C42-C41	0.041	1.678	-14.010	0.039	1.712	-14.803
C43-C41	0.039	1.678	-13.990	0.038	1.716	-14.873
H41-C41	0.027	1.865	-22.791	0.027	1.860	-23.223
H42A-C42	0.003	1.814	-21.277	0.003	1.808	-21.643
H42B-C42	0.005	1.804	-20.958	0.005	1.795	-21.202
H42C-C42	0.004	1.817	-21.318	0.005	1.810	-21.620
H43A-C43	0.004	1.828	-21.745	0.004	1.823	-22.169
H43B-C43	0.005	1.803	-20.915	0.006	1.795	-21.179
H43C-C43	0.004	1.814	-21.254	0.004	1.810	-21.683

Table 6.9: Selected topological parameters at the BCP calculated by theoretical methods DFT and MP2 for **12** (only those unique by symmetry included). Labels are consistent with those indicated in Figure 6.1. (a) The charge density function ρ at the BCP (e Å^{-3}); (b) the Laplacian of ρ [$L(\rho) = -\nabla^2\rho$] at BCP (e Å^{-5}); (c) the ellipticity at the BCP.

The most direct measure of bond order is the analysis of the value of the electron density function at the BCP. Also, the distances between BCP and nuclear positions (listed in Table 6.8) help visualize the BCP positions as bond "mass centres". The Laplacian (second

derivative of the charge density) parameter denotes the extent to which electron density is locally concentrated, [$\nabla^2\rho(r)<0$], or depleted [$\nabla^2\rho(r)>0$]. Overall, a relatively high charge density and a negative sign of the Laplacian at the BCP are considered to characterise a shared (covalent) interaction, while a low charge density and a positive value of the Laplacian indicates a closed-shell intereaction (i.e. ionic, hydrogen bond or van der Waals interaction). The parameter $\epsilon(r)$, the ellipticity, measures the asymmetry of the charge distribution between two bonded atoms and is commonly regarded to reveal the degree of π-character in a particular bond. High bond ellipticity in nonpolar bonds is considered to denote double bond character. However, a high bond ellipticity can also occur due to a high degree of bond strain or distortions in the molecule.

As found for simple aromatic hydrocarbons, the BCPs for the C-C bonds in the chelating ligands are located at a position close to the bond midpoints and in regions of negative Laplacian. These C-C aromatic bonds show charge density parameters that are consistent with covalent bonding, specifically a high $\rho(r)$ and large negative values for the Laplacian. The experimental values of these parameters in the C-C aromatic bonds are in the expected range with the observed values for $\rho(r)$ = 2.123-2.197 e Å^{-3}, and for $\nabla^2\rho(r)$ = -22.257-24.271 e Å^{-5}. The large, positive values of $\epsilon(r)$ are also comparable with published values for similar bonding environments and range from 0.14-0.22 (published e.g. for benzene $\rho(r)$ = 2.15, $\nabla^2\rho(r)$ = -16.9 and $\epsilon(r)$ = 0.22[16] and for a 5-membered nitrogen containing heterocycle $\rho(r)$ = 2.16, $\nabla^2\rho(r)$ = -19.5 and $\epsilon(r)$ = 0.27).[32] The Laplacian parameter in the homonuclear C-C bonds is somewhat underestimated in the theoretical calculations, however the charge density and particularly the ellipticity parameters show good agreement. This discrepancy with theory has been noted previously.[16]

In the isopropoxide ligands the ellipticity values for the C-C bonds are lower, $\epsilon(r) = 0.04$-0.10, which is consistent with single bonding expected in these fragments. The BCPs also occur slightly further from the midpoint, it seems reasonable to suggest that this is a result of polarity induced by the proximity of the electronegative C-O group as in polar bonds the midpoint is known to move closer to the electronegative atom.[16] The charge density and value of the Laplacian are correspondingly slightly smaller in these bonds. There is good agreement between the experimental and theoretical values calculated for the bonds in this fragment.

In the heteronuclear C-O bonds, which are formally single bonded, a low ellipticity is again found; $\epsilon(r) = 0.05$-0.06. The BCPs also lie significantly closer to the O atom, in accordance with a greater accumulation of density concentration on the more electronegative oxygen atoms. In these C-O bonds the experimental data indicate reasonably high electron density, $\rho(r) = 1.881$-1.965 e Å^{-3}, and negative Laplacians, $\nabla^2\rho(r) = -5.402$ - -12.271 e Å^{-5}. It is worth noting that the ligand C-O have slightly raised charge density and lowered values for the Laplacian relative to the isopropoxide C-O bonds.

As found for the C-O bonds, the polar C-N bonds in the heterocylic ligand exhibit BCP at a position removed slightly from the midpoint, approaching the more electronegative atom. In general the values of the charge density and the Laplacian in these interactions reflect the trends described for the C-O bonds. Experimentally, the C-N bonds show a high charge density, $\rho(r) = 2.291$-2.408 e Å^{-3}, and large negative values for the Laplacian, $\nabla^2\rho(r) = -19.163$ - -24.406 e Å^{-5}, confirming these interactions are shared (covalent). There is a high degree of ellipticity in these heteronuclear bonds, $\epsilon(r) = 0.13$-0.23, which is expected due to

delocalisation around the ring. Together the C-C and C-N bonds have the largest values of negative Laplacians at the BCPs and reasonably large ellipticities, denoting their π-character.

The non-ring C-C bonds experimentally give high charge densities and large negative values for the Laplacian as expected for covalent interactions, $\rho(r) = 1.860, 1.873$ e Å^{-3} and $\nabla^2\rho(r) = -18.173, -18.144$ e Å^{-5}. These bonds are formally single, however both show relatively large ellipticities; $\epsilon(r) = 0.14$ and 0.17. This may be indicative of some double bond character induced by delocalisation across the whole ligand. This is corroborated by the earlier remark stating the planarity of this 5-membered ring in the experimental crystal structure, as planarity allows the correct orientation of orbitals for delocalisation.

The only available comparison for the Ti-O metal-ligand interactions is the theoretical analysis on H_3TiOMe by Molina *et al.*[4] These interactions have not previously been examined by experimental charge density methods. There are no previously published experimental or theoretical charge density analyses for Ti-N bonds to our knowledge. For convenience, the structure of the titanium core for **12** is shown in Figure 6.4 with the most relevant topological parameters from Tables 6.8 and 6.9 included for the (a) experimental, (b) DFT, and (c) MP2 level calculations respectively.

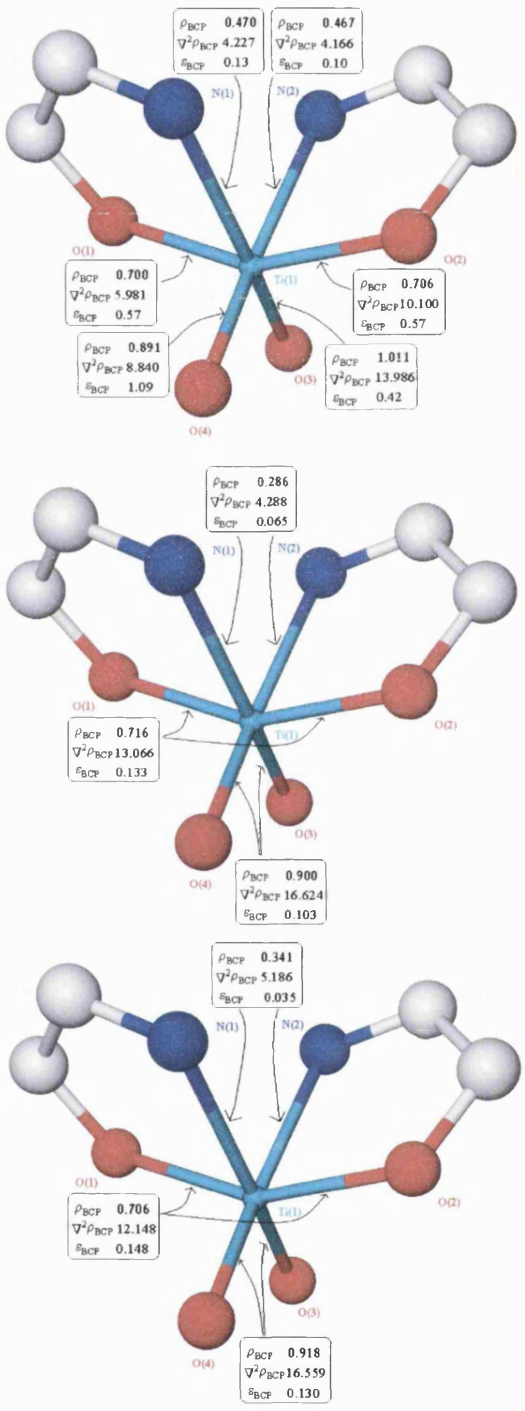

Figure 6.4: Core structure of **12** wherein the nuclei are denoted by spheres and the bond paths by lines. The values of the properties $\rho(r)$, $\nabla^2\rho(r)$ and $\varepsilon(r)$ are displayed for the experimental (a), DFT (b) and MP2 (c) calculations respectively.

There are essentially three types of metal-ligand bond in **12**, Ti-O_{ligand}, Ti-$O_{isopropoxide}$ and Ti-N. The analysis of both experimental and calculated parameters implies that the Ti-$O_{propoxide}$ bonds, which occupy equatorial positions in the octahedral geometry, appear again to be the strongest and the Ti-N the weakest. The experimental data show an interesting feature in the position of the BCPs along the bond vector. It is observed in **12** that in all of the bonds between Ti and the atoms of the coordination sphere, the BCP positions are located very near to bond midpoint. However, while in Ti-N bonds they are slightly closer to N (*ca.* 7%), in both types of Ti-O they surprisingly stand slightly displaced (av. *ca.* 5%) towards Ti.

All of the titanium-ligand bonds display positive values for the Laplacian (local depletion of electrons) and quite low, but still significant, values of the charge density at the BCPs. These properties, a relatively low value of the electron density and a positive value for the Laplacian at the BCP, are characteristic for closed shell interactions, which suggest that the metal-ligand bonding in **12** is predominantly ionic. This is because positive values for the Laplacian indicate the local depletion of electron density at the BCP. The largest charge density occurs on O(3), $\rho(r) = 1.011$ e Å^{-3}, the Ti(1)-O(3) bond also exhibits the largest positive value for the Laplacian, $\nabla^2\rho(r) = 13.986$ e Å^{-5}, and the smallest ellipticity for Ti-O in this study, $\epsilon(r) = 0.42$. The other Ti-$O_{isopropoxide}$ bond exhibits slightly lower, but still positive, values of both charge density, $\rho(r) = 0.891$ e Å^{-3}, and Laplacian, $\nabla^2\rho(r) = 8.840$ e Å^{-5}, at the BCP. The bond ellipticity for this interaction is the largest observed in this molecule at $\epsilon(r) = 1.09$. The Ti-O_{ligand} interactions both display similar values of charge density and bond ellipticity; $\rho(r) = 0.700$ e Å^{-3}, $\epsilon(r) = 0.57$ [Ti(1)-O(1)] and $\rho(r) = 0.706$ e Å^{-3}, $\epsilon(r) = 0.57$ [Ti(1)-O(2)]. These ellipticity values are quite large, suggesting that there may be some π-contribution to the metal ligand bonding in all the Ti-O, and most particularly Ti(1)-O(4),

bonds. It is notable that there are clear differences between the ellipticities of these different Ti-O interactions.

The titanium-nitrogen bonds in **12** have smaller, but still positive, values for the Laplacian than the analogous interactions of the metal with oxygen. For Ti(1)-N(1) $\nabla^2\rho(r) = 4.227$ e Å^{-5} and for Ti(1)-N(2) $\nabla^2\rho(r) = 4.166$ e Å^{-5}. This indicates that the Ti-N bonds have a greater degree of covalent character than do the Ti-O interactions. Both Ti-N bonds also have very low values of charge density at the BCPs; $\rho(r) = 0.470$ e Å^{-3} and $\rho(r) = 0.467$ e Å^{-3} for Ti(1)-N(1) and Ti(1)-N(2) respectively. The low values for ellipticity obtained for the Ti-N interactions are quite low, $\epsilon(r) = 0.13$ [Ti(1)-N(1)] and $\epsilon(r) = 0.10$ [Ti(1)- N(1)], which supports a primarily σ-bonding interaction.

There are a number of slight discrepancies between the experimental and theoretical values of the topological parameters discussed above for the metal-ligand interactions. The experimental value of the ε_{BCP} shows a clear higher value for the Ti-O_{ligand} compared to the Ti-$O_{propoxide}$ bonds, whereas the theoretical values are very comparable. This is inconsistent with the observation of the bond lengths and BCP positions (Table 6.8). While a higher ellipticity generally indicates a greater π character, typically due to a larger double bond character, it has been shown that a higher ε_{BCP} can also be the result of bond strain, or can arise as an effect of distortions or through-space interactions[31,33]. It is proposed that the elevated ellipticity values observed in the experimental study on **12** is, at least partially, due to these factors and not solely the result of π–bonding character in the metal-ligand interactions. Another subtle, but nonetheless interesting, discrepancy between experimental and theoretical data appears in the values of the Laplacian of ρ. While the values of $L(\rho)_{BCP}$

for the two types of Ti-O bond paths are comparable in the theoretical data, the experimental values show a clear higher positive Laplacian for $Ti\text{-}O_{propoxide}$ compared to $Ti\text{-}O_{ligand}$.

In general, high positive values of the Laplacian indicate ionicity over covalency. However, we need to consider the bonding of the whole ligand to the Ti centre, by looking at the topology of the Ti-O-C-C-N ring. For this reason it is useful to consider the 2-dimensional surface of the Laplacian function. Figure 6.6 shows the Laplacian of the charge density, $\nabla^2\rho(r)$, plotted on the L.S. plane determined by the 5-membered ring (Ti-O-C-C-N).

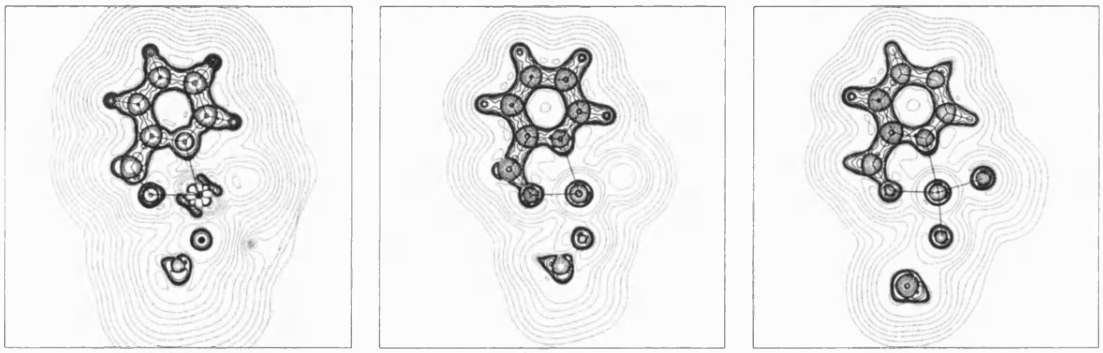

Figure 6.5: 2-D plot of the Laplacian of the charge density, $\nabla^2\rho(r)$, for the experimental (a), DFT (b) and MP2 (c) calculations respectively. Plot taken in the plane of the 5-membered ring (Ti-O-C-C-N). Positive values of $\nabla^2\rho(r)$ are marked by dashed lines and negative values by solid lines.

The Laplacian distribution for atoms in molecules is observed as alternating zones of charge concentration and charge depletions, corresponding to quantum shells within the molecule.[31] Maxima occurring in the outermost region of charge concentration, termed the valence shell charge concentration (VSCC), correspond to the electron pairs in the Lewis model and hence indicate the presence of bonds or lone pairs.[31,34,35] In accordance with the local maxima in the experimental and the theoretical models are clearly seen in Figure 6.5 for the atoms in the

ligands. For the oxygen and nitrogen atoms there are maxima in the bond directions towards the metal centre. In the case of transition metals there are no VSCC but instead ligand induced charge concentrations (LICC), which occur on the opposite side of the metal centre. The Laplacian in the experimental model exhibits unusual features around the titanium atom so it not possible to analyse this feature. This is a result of inadequate modelling of the transition metal by the hexadecapole expansion used in these calculations. Hence, improvements to the model of the titanium atom are necessary in order to allow further investigation of the M-L bonding features in the Laplacian.

6.5 Concluding Remarks

This study reports the analysis of the topology of the total charge density and its Laplacian, obtained by combined experimental and theoretical studies, of the monomeric titanium alkoxide species $[(2\text{-py})CH_2O)]_2Ti(OCHMe_2)_2$ using the AIM method. A key motivation behind this work was the expectation that quantitative information regarding the bonding between the metal and ligands would provide insight into their reactivity, and hence provide direction for future catalyst design.

This investigation highlights several important features relating to the metal-ligand bonding. NBO analysis has shown that there are no significant delocalisations from the titanium metal centre to the ligands, but that delocalisations from lone pairs on the ligand donor atoms to the empty metal d-orbitals are present. The most significant of these occurs from lone pairs on the oxygen donors on both the pyridyl ligands and the isopropoxide groups. It is also worth noting that the occupancy of the oxygen on the pyridyl ligand is depleted relative to that of the isopropoxide oxygen atom, providing evidence for the intramolecular hydrogen bonding interaction indicated in the analysis of the molecular structure [C(15)-H(15)···O(2) and C(25)-H(25)···O(1)]. Reduced delocalisation to the metal from the nitrogen donor atom relative to the oxygen was also observed, which is consistent with the longer M-L bond lengths observed for these.

The topological analysis of the charge density revealed shared (covalent) bonding interactions within the ligands, as expected. The topological parameters obtained for these bonds are consistent or published values obtained by experimental and theoretical means. The M-L interactions all exhibit positive values for the Laplacian at the BCP, a feature which is commonly regarded as evidence of open-shell (ionic) bonding. These bonds also exhibit

relatively high ellipticities, suggesting the presence of π-bonding. As high values for the ellipticity can also be caused by strain within the molecule this attribute is not conclusively proven on this evidence. However, alongside consideration of the NBO evidence of delocalisation from ligand to metal, it is proposed that some degree of π-bonding is indeed present.

In conclusion, the charge density analysis reported in this chapter supports a predominantly ionic model for the M-L bonding in titanium alkoxide complexes such as **12**. Electronic analysis also indicates that the oxygen ligands participate in π-bonding to the empty metal d-orbitals *via* lone pairs. While there is generally good agreement between the theoretical and experimental data in this analysis, the hexadecapole expansion used to model the titanium atom in the experimental data set is clearly inadequate, as illustrated in Figure 6.5. Further work in this area will include the improved modelling of titanium in the experimental data in order to allow an accurate analysis of the Laplacian, and hence the reactive sites, around this metal atom. This is necessary in order to fully explain the reactivity of **12** and hence to influence the design of more effective catalysts.

6.6 Experimental

General Considerations

All manipulations were performed under a dry argon atmosphere using standard Schlenk-line and glovebox techniques. Glassware was dried for several hours prior to use in an oven maintained at 130 °C. All solvents were distilled from the appropriate drying-agents under a nitrogen atmosphere, degassed and then stored under argon. 2-hydroxymethylpyridine and titanium tetraisopropoxide were obtained from Aldrich. Deuterated NMR solvents were purchased from Goss Scientific Ltd. and, where appropriate, dried before use.[

Characterisation Details

Elemental analyses were performed by the University of Bath Microanalysis Service on an Exeter Analytical Inc. CE-440 Elemental Analyser. NMR spectra were recorded on a Bruker Avance 300 spectrometer at 293 K in sealed tubes at ambient temperature. Chemical shifts are reported in units of ppm referenced to the chemical shifts of residual protio solvent resonances ($CHCl_3$ δ 7.27). Mass spectra for samples were submitted for analysis at EPSRC National Mass Spectroscopy Service Centre by GC-EI-MS at a very low cone voltage, but the molecular ions were not detected and will not be reported here.

X-ray diffraction study of $(pyCH_2O)_2Ti(O^iPr)_2$ 12:

A colourless block of **12** ($C_{18}H_{26}O_4N_2Ti_1$) of dimensions 0.28 x 0.38 x 0.40 mm^3 was analysed by X-ray diffraction. See Chapter 2.4 for full details of X-ray equipment and software packages utilised. T = 30(2) K, θ_{max} = 55.98 °, 162475 reflections measured, of which 25585 independent (R_{int} = 0.0985), μ = 0.459 mm^{-1} (no absorption correction).

Structure solved by direct methods (SHELXS-97) and refined on F^2 by full-matrix least-squares (SHELXL-97), 231 parameters, $R_1 = 0.0498$, $wR_2 = 0.1190$ (data $I > 2\theta(I)$). Hydrogen atoms were placed in calculated positions with a riding refinement.

Neutron diffraction study of $(pyCH_2O)_2Ti(O^iPr)_2$ 12: A colourless single crystal of **12** ($C_{18}H_{26}O_4N_2Ti_1$) of dimensions 2.6 x 2 x 4.1mm, was packed in quartz wool inside a thin walled (0.5mm) quartz capillary which was then glued to the base of the aluminium pin. This mounting procedure was carried out under inert conditions in a glove box. The sample ensemble was mounted on a Displex cryorefrigerator on the thermal beam instrument D19 at the ILL equipped with two position sensitive detectors one curved 4^0 x 64^0 and one flat 20^0 x 20^0. The wavelength was 1.3158(1)Å from a focusing Ge (115) monochromator in reflection. The crystal was cooled at 2.0 degrees per minute to 30K while monitoring several strong reflections, there was no significant change in intensity or mosaic spread. The unique reflections to a 2-theta value of 36^0 were then measured in equatorial geometry with omega scans. All unique higher angle data to a 2-theta value of 100^o were then recorded with normal-beam geometry or equatorial geometry (ILL programs Hklgen and Mad). The omega range was scanned to a constant monitor count of 24000 corresponding to 5.1 seconds per step for all values of 2-theta. Several standard reflections were measured at intervals throughout the experiment and showed no significant variation. The Bragg intensities were integrated in 3-D using the ILL program Retreat. The refined unit cell dimensions at 30K were 11.1409 14.5881 12.1066 90.000 93.2481 90.0000 v= 1964.4758. The space group was confirmed as monoclinic $P2_1$. All hydrogen and non-hydrogen atoms were refined anisotropically.

The intensities were corrected for attenuation by the cylindrical Vanadium and Aluminium heat shields (minimum and maximum transmission coefficients 0.7075 and 0.5352) and by the crystal itself ($Ti(C_6H_6ON)_2(O^iPr)_2$, μ (neutron) = 2.50 cm^{-1}) at 1.3158Å with the program D19abs. The coherent scattering amplitudes used in the refinement were those tabulated by Sears. In all 10182 reflections were measured resulting in 4024 unique hkl's: R(int)=0.0212. Structure refinement using SHELXL-97 gives R1= 3.05% and wR2= 0.1267 (for I>2σI) with 461 parameters.

Computational Details:

The electronic structure is analysed in terms of Natural Bond Orbitals, NBO,[36,37] version 5.0,[38] and the theoretical electron density by AIM Theory. The 6-31+[39]G(2d[40]) basis set was used for the titanium atom[41] and the nitrogen and oxygen atoms attached to the metal centre. For carbon and hydrogen the 6-31G(d[42]) basis set was used.

Analysis of the data required the use of multipolar refinement. According to the independent atom model, the static molecular charge density is defined as the superposition (sum) of the isolated, rigid, spherical densities of the N atoms at the nuclear position $\boldsymbol{R}_i$ in the molecule.[43]

$$\rho(\boldsymbol{r}) = \sum_{i=1}^{N} \rho_i(\boldsymbol{r} - \boldsymbol{R}_i)$$

Multipolar expansion: The aspherical atom model [44]

$$\rho_i(\boldsymbol{r}) = \rho_c(\boldsymbol{r}) + \kappa^3 P_v \rho_v(\kappa \boldsymbol{r}) + \sum_{l=0}^{l_{max}} \kappa'^3 R_l(\kappa' \boldsymbol{r}) \sum_{m=-l}^{+l} P_{lm} d_{lm}(\theta, \phi)$$

where P_v, P_{lm}, κ, and κ' are refineable parameters. The atomic scattering factors were taken from ref [45]. and the multipolar expansion for all atoms except hydrogen, was considered up to

hexadecapoles (l_{max}=4). The atomic positions of the hydrogen atoms and their anisotropic displacement parameters were not refined but fixed at the values observed in the neutron diffraction experiment at 30 K. Two sets of hydrogen atoms were considered (aromatic and aliphatic) for which the κ parameter was refined while the κ' were fixed at 1.20. The refinement was accomplished by the program XDLSM[46] in the package XD.[27]

Synthesis of $(pyCH_2O)_2Ti(O^iPr)_2$ (12):

A solution of 2-hydroxymethylpyridine 0.96 mL, 10 mmol), was prepared in dry toluene (10 mL) under an inert atmosphere. The resulting solution was added via cannula to a solution of titanium tetraisopropoxide (1.5 mL, 5 mmol) in dry toluene (10 mL) at –78°C. The resulting colourless solution was vigorously stirred for one hour, allowed to warm to room temperature and then heated to reflux. The solvent was removed *in vacuo* to give a white solid product. This product was suspended in hexane (10 mL) and toluene added until dissolution occurred on warming. Standing at room temperature yielded a crop of large colourless blocks of **1** (1.72 g, 90%). M.p. 116-117 °C; ^{1}H NMR (300 MHz, $CDCl_3$, 25 °C, TMS): δ = 0.9 (d, ^3J(H,H) = 6 Hz, 12H; CH_3); 4.6 (sept, ^3J(H,H) = 6 Hz, 2H; CH); 5.5 (s, 4H; CH_2); 7.1 (m, 4H; ArH); 7.6 (m, 2H ArH); 8.5 (m, 2H, ArH); $^{13}C\{^1H\}$ NMR (75 MHz, $CDCl_3$, 25 °C, TMS): δ = 24.6, 73.3, 74.2, 117.9, 120.8, 136.5, 146.1, 165; elemental analysis calcd (%) for $C_{18}H_{26}N_2O_4Ti$ (382.3): C 56.6, H 6.86, N 7.33; found: C 56.0, H 6.71, N 7.33.

6.7 References

[1] Bradley, D.C.; Mehrotra,R.C.; Rothwell, I.P.; Singh, A. *Alkoxo and Aryloxo Derivatives of Metals*, Academic Press, London; **2001**.
[2] Bradley, D.C. *Chem. Rev.*, **1989**, *89*, 1317.
[3] Coffindaffer, T.W.; Rothwell, I.P.; Huffman, J.C. *Inorg. Chem.* **1983**, *22*, 2906.
[4] Dobado, J.A.; Molina, J.M. Uggla, R.; Sundberg, M.R. *Inorg. Chem.*, **2000**, *39*, 2831.
[5] Bader, R. F. W. *Atoms in Molecules: A Quantum Theory*; Oxford University Press: Oxford, **1990**.
[6] Bader, R.F.W. *J. Phys. Chem, A* **1998**, *102*, 7314.
[7] Coppens, P. *Acta Cryst.* **1998**, A54, 779.
[8] Koritsanszky, T.S.; Coppens, P. *Chem. Rev.* **2001**, *101*, 1583.
[9] Coppens, P. *Isr. J. Chem.* **1977**, *16*, 144.
[10] Feil, D. *Isr. J. Chem.* **1977**, *16*, 149.
[11] Pillet, S.; Wu, G.; Kulsomphob, V.; Harvey, B.G.; Ernst, R.D.; Coppens, P. *J. Am. Chem. Soc.*, **2003**, *129*, 1937.
[12] Kožíšek, J.; Hansen, N.K.; Fuess, H. *Acta Cryst.* **2002**, *B58*, 463.
[13] Whitten, A.E.; Dittrich, B.; Spackman, M.A.; Turner, P.; Brown, T.C. *J. Chem. Soc. Dalton Trans.* **2004**, 23.
[14] Abramov, Y.A.; Brammer, L.; Klooster, W.T.; Bullock, R.M. *Inorg. Chem.* **1998**, 37, 6317.
[15] Silvi, B.; Gatti, C. *J. Phys. Chem. A* **2000**, *104*, 947 and references therein.
[16] Koritsanszky, T.S.; Coppens, P. *Chem. Rev.* **2001**, *101*, 1583.
[17] Coppens, P.; Iversen, B.; Larsen, F.K. *Coord. Chem. Rev.* **2005**, *249*, 179.
[18] Scherer, W.; Hieringer, W.; Spiegler, M.; Sirsch, P.; McGrady, G.S.; Downs, A.J.; Haaland, A.; Pederson, B. *Chem. Commun.* **1998**, 2471.
[19] Scherer, W.; Sirsch, P.; Shorokhov, D.; Tafipolsky, M.; McGrady, G.S.; Gullo, E. *Chem. Eur. J.* **2003**, *9*, 6057.
[20] Bader, R.F.W.; Matta, C.F. *Inorg. Chem*, **2001**, *40*, 5603.
[21] Blaser, H.-U. *Chem Rev.* **1992**, *92*, 935-952.
[22] Nitta, H.; Uu, D.; Kudo, M.; Mori, A.; Inoue, S. *J. Am. Chem. Soc.* **1992**, *114*, 7969.
[23] El-Hendawy, A.M.; AlkubaisiAbd El-Ghany El-Kourashy, A.H.; Shanab, M.M. *Polyhedron* **1993**, *12*, 2343.
[24] Lunn, M. D., Ph.D. Thesis, University of Bath, Bath, UK, October, **2002**.
[25] Desiraju, G.R.; Steiner, T. *The Weak Hydrogen Bond In Structural Chemistry and Biology*, IUCr Monographs on Crystallography; Oxford Science Publications, Oxford University Press, New York, **1999**; pp8-9.
[26] Hansen, N.; Coppens, P. *Acta Cryst.* **1978**, *A34*, 909.
[27] Koritsanszky, T.; Howard, S. T.; Su, Z.; Mallinson, P. R.; Richter, T.; Hansen, N. K.; *XD, Computer program package for multipole refinement and analysis of electron densities from diffraction data*; Free University of Berlin; Berlin, Germany, **1997**.
[28] Tejerina, B. Departement of Chemistry, Iowa State University, Ames, Iowa, 50011.
[29] Dobado, J.A.; Molina, J.M.; Uggla, R.; Sundberg, M.R. *Inorg. Chem.* **2000**, *39*(13), 2831.
[30] The parameter π is define as $\sqrt{\sum_{i=1}^{N}\frac{\delta_i^2}{N-3}}$, where δ is de deviation of the atom *i*, with respect the Least-square plane defined by the N atoms of the ring.
[31] Bader, R.F.W. *Atoms in Molecules: A Quantum Theory:* International Series of Monographs in Chemistry 22; Oxford University Press: Oxford, **1990**.
[32] Tafipolsky, M.; Scherer, W.; Öfele, K.; Artus, G.; Pedersen, B.; Herrmann, W.A.; McGrady, G.S. *J. Am. Chem. Soc.* **2002**, *124*, 5865.
[33] Popelier P. L. A., *Coord. Chem. Rev.*, **2000**, *197*, 169;
[34] Bader, R.F.W.; MacDougall, P.J. Lau, C.D.H. *J. Am. Chem. Soc.* **1984**, *106*, 1594.
[35] Rincön, L.; Almeida, R. *J. Phys Chem. A.* **1998**, *102*, 9244.
[36] Reed, A. E., Curtiss, L. A.; Weinhold, F. *Chem. Rev.* **1988**, *88*, 899.

[37] Foster, J. P.; Weinhold, F. *J. Am. Chem. Soc.* **1980**, *102*, 7211.
[38] *NBO 5.0*, Glendening, E. D.; Badenhoop, J. K.; Reed, A. E.; Carpenter, J. E.; Bohmann, J. A.; Morales, C. M.; Weinhold, F. *Theoretical Chemistry Institute*, University of Wisconsin, 2001.
[39] Clark, T.; Chandrasekhar, J.; Schleyer, P. v. R. *J. Comp. Chem.* **1983**, *4*, 294.
[40] Frisch, M. J.; Pople, J. A.; Binkley, J. S. *J. Chem. Phys.* **1984**, *80*, 3265.
[41] Ahlrichs *et al.*; unpublished results. The basis sets were obtained from the *Extensible Computational Chemistry Environment Basis Set Database*, Version 7/30/02, as developed and distributed by the Molecular Science Computing Facility, Environmental and Molecular Sciences Laboratory which is part of the Pacific Northwest Laboratory, P.O. Box 999, Richland, Washington 99352, USA, and funded by the U.S. Department of Energy.
[42] Hariharan, P. C.; Pople, J. A. *Theoret. Chimica Acta* **1973**, *28*, 213.
[43] Stewart, R. F. Acta Cryst. **1976**, A32, 565.
[44] Hansen, N. K.; Coppens, P. *Acta Cryst.* **1978**, *A34*, 909.
[45] Clementi, E.; Roetti, C. *Atomic Data and Nuclear Data Tables* **1974**, *14*, 177.
[46] Mallinson, P. R.; Wozniak, K.; Smith, G. T.; McCormack, K. L. *J. Am. Chem. Soc.* **1997**, *119*, 11502.

Chapter 7

Structural Studies on Group 4 Metal Alkoxide Complexes as Represented in the Cambridge Structural Database

7.1 Background

Group 4 metal complexes are widely used in a number of catalytic roles making them excellent candidates for further development as catalysts.[1] The development of such metal alkoxides in this role has, in the last 20 year in particular, provoked a great deal of interest in this field, as discussed more fully earlier in Chapter 5.2. The elucidation of structure-activity relationships involved is a particularly important goal in the field, which would provide direction for the rational design of increasingly active and reactively controlled species. While Chapter 6 was concerned with the examination of a combined X-ray and neutron charge density analysis as a means of achieving this, the present chapter encompasses surveys of the CSD and an in-house database, containing structures synthesised within the group, for the same purpose. This chapter will begin with a brief summary of the utilisation of statistical analysis so far in the literature for these species.

Knowledge acquired from crystallographic databases is now beginning to play a major role in inorganic structural chemistry.[2,3,4] As over 50% of the entries in the CSD contain a transition metal, the systematic study of metal-organic species now represents an important family of database analyses and a number of excellent reviews have been recently published with regard to this.[5,6,7] However, in order to maximise the usefulness of the vast amount of chemical information currently available it is necessary to elucidate specific patterns and trends from the data. Within the systematic study of metal-organic species the study of bonding and geometry is becoming increasingly examined as a means to elucidate trends and patterns with a view to providing insight into the reactivity

species.[8,9] The primary aim of the research in this chapter is to explore the huge wealth of information on the Group 4 metal alkoxide complexes in the CSD, from a statistical viewpoint, concentrating in particular on titanium. Although the individual structures of published works have been previously discussed, and in some cases small scale structure correlations have been studied, there has so far been relatively little full database work on these compounds. One exception to this is the determination of tables of average bond lengths in organometallic compounds and coordination complexes of the d- and f- block elements *via* the statistical analysis of the X-ray and neutron distances in the CSD by Orpen *et al.*[10] Another, more focused analysis is that of group 4 and 5 aryloxides in which the variation of metal-ligand bonds (M-O) with bond angle (M-O-Ar).[11] No distinct correlation between the two parameters was found. Other reports investigating this structural feature were discussed in Chapter 5.2.4. Furthermore, despite the large number of group 4 alkoxide complexes known, a clear relation between ligand parameters and catalyst performance is still lacking. Consequently the systematic analysis of the crystal structures for published, and unpublished, group 4 metal alkoxides offers a route to extract geometric information which can be used to gain knowledge regarding the structure/activity relationships within these complexes.

In this chapter bond lengths, coordination geometries and the subject of correlation between the two parameters are analysed in both the CSD and an in-house database consisting on unpublished structures from within the group. It was decided to investigate parameters from homometallic Group 4 complexes, as this class has known potential for catalytic activity and for this reason such complexes also make up the in-house database, hence providing a useful comparison. A summary of the contents of the in-house database, including a 2-D chemical diagram and basic author and crystal information is included in the appendices. The remainder of this chapter presents the findings of this investigation.

7.2 Structural Aspects of Group 4 Metal Complexes

7.2.1 Metal Centre Geometry

The effect on geometry of a metal centre by the identity of the ligand groups surrounding it is one feature which can be examined from accurate crystal structure data. A worthwhile aspect of this is the analysis of the deviation of the metal complexes for the ideal geometry for a given number of ligands in the coordination sphere. As discussed in Chapter 5.2.2, the study of metal complexes containing both labile isopropoxide ligands and chelating oxygen donor ligands, to provide a measure of control, is of particular interest in the field. Group 4 metal complexes with the general formula $[M(L)_2(OR)_x]_n$, fulfil these requirements and are intensely examined in the field (see Chapter 5). As these complexes have six donor atoms they should, therefore, ideally adopt an octahedral arrangement. An increased deviation from this arrangement leads to 'strain' within the complex as bonds are drawn away from the optimal values. The identity of the ligands can influence this deviation. One cause of a significant deviation in the arrangement of ligands is where chelating ligands are present, as is the case in many potential alkoxide catalysts. Where such ligands are present the geometry around the metal is influenced by the steric and geometric requirements of the chelate. Sites of reactivity, which are of particular interest, may be indicated by strain in the geometry of the ligand sphere. Consequently, geometrical data extracted from the CSD can be used to look at the relative ideality of the bonding around a metal centre, and so denote areas of interest.

A method using the RMS as an indicator of distortion of the metal geometry has been used for similar studies of other metal complexes in a variety of geometries.[12,13] The method uses the RMS deviation of all the interbond angles around the metal atom to provide a measure of the deviation from ideal geometry. For each ML_6 fragment the 15 interbond angles were extracted from the database, and the RMS deviations of these angles from their ideal was evaluated using the formula:[9]

$$\delta_{oct} = [\ \Sigma\ \{(a_i - a_{ideal})^2\}/15]^{1/2}$$

Figure 7.1: Formula used to calculate deviation from ideal octahedral symmetry.

The result is a value of δ_{oct} which describes the overall deviation of the complex from an ideal octahedral geometry. The CSD has been examined and these interbond angles extracted using the CCDC program ConQuest. In addition to this, the creation of an in-house database of presently unpublished results from our group allows the facile extraction of geometric data which is relevant to this deviation from an ideal ligand arrangement for complexes with known catalytic activity. The results of these investigations are presented in Tables 7.1 and 7.2 for the CSD and in-house searches respectively.

It should be noted that the number of observations, N_{obs}, represents the number of crystallographically independent observations not simply the number of hits. In addition, δ_{oct} represents the deviation from ideal geometry as described in Figure 7.1 above, and σ represents the sample standard deviation of the mean values of δ_{oct}. Histograms for the chelated titanium structures in the database and the in-house results are also shown in Figures 7.2 and 7.3. These are additionally presented on the same axes scale for ease of comparison. Further histograms for each of the metals investigated here and presented in Table 7.1 can be found in the Appendices.

	Total		Non-chelated		Chelated	
	N_{obs}	δ(σ)	N_{obs}	δ(σ)	N_{obs}	δ(σ)
Titanium	1324	10.0 (4.1)	135	4.4 (3.0)	1189	10.7 (3.7)
Zirconium	519	11.6 (5.3)	75	4.6 (2.9)	444	12.8 (4.6)
Hafnium	83	11.7 (5.3)	15	3.8 (2.6)	69	13.5 (4.0)

Table 7.1: ML_6 complexes from the CSD, numbers (N_{obs}) and mean values of δ_{oct}, in degrees, from the ideal geometry and their sample standard deviation σ.

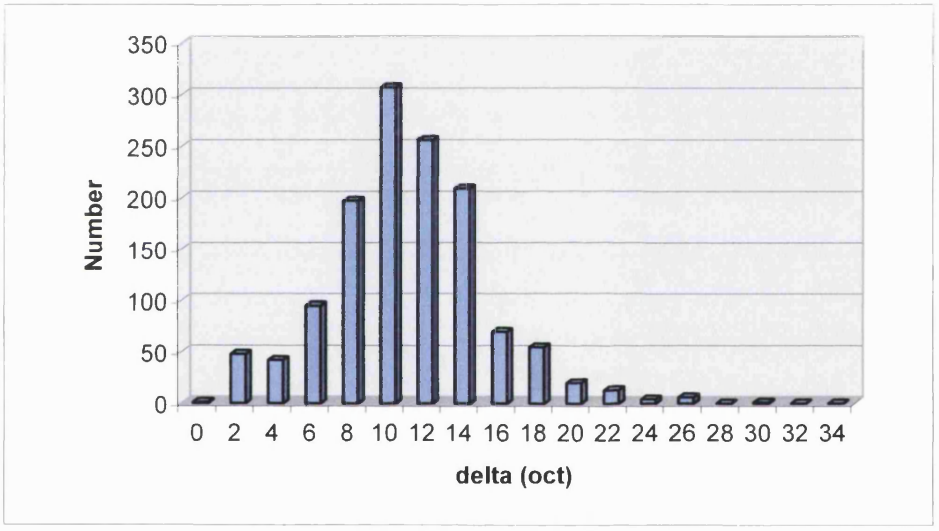

Figure 7.2: Histogram showing the distribution of δ_{oct} for titanium six-coordinate complexes in the CSD (in degrees).

	N_{obs}	δ(σ)
Titanium	36	9.8 (2.2)

Table 7.1: ML_6 complexes from the in-house database, numbers (N_{obs}) and mean values of δ_{oct}, in degrees, from the ideal geometry and their sample standard deviation σ.

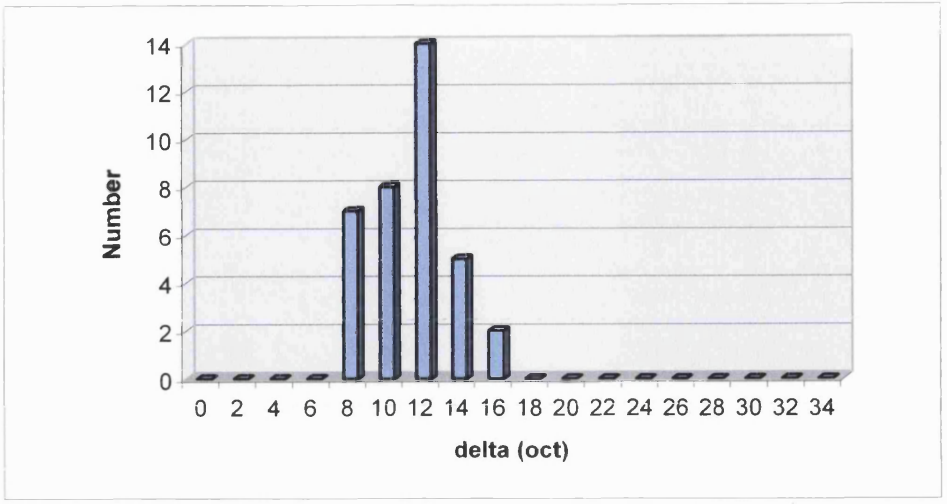

Figure 7.3: Histogram showing the distribution of δ_{oct} for titanium six-coordinate complexes in the in-house database (in degrees).

These results highlight several noteworthy structural features in these complexes. Firstly, the number of observations in each category indicates the importance of the geometry for the different metals. This is manifested in the data by there being many more observations for the first and second row metals, and relatively few for the third row metal. This is both a result of the relative abundance of crystal structure data and a reflection of the importance of the octahedral geometry for each individual metal. For example, as the larger metals are able to reach higher coordination numbers, the ML_6 geometry as a result becomes less common for that metal and hence relatively fewer octahedral complexes are obtained. The distortions seen in these ML_6 complexes are also relatively small by comparison to those published for ML_4 and ML_5 complexes. These much larger distortions are often due to weakly complexing additional ligands[11] and while these complexes are rare for Group 4 complexes, one such zirconium complex was noted in this investigation.[14] Although formally designated six-coordinate, the zirconium was also weakly coordinated to a seventh ligand, thus greatly distorting the geometry. This example was removed from the data analysis to avoid falsely skewing the results.

Analysis of individual outliers also indicated that extremely 'ideal' geometries are generally the result of extremely rigid ligand structures, such as porphyrins.

Furthermore, as might be expected on consideration of the metal coordination sphere, the larger metals exhibit larger distortions in δ_{oct}. The chelated metal centres show significantly larger deviations than found for non-chelated complexes, which is consistent with those previously published for later transition metals.[12] The small values of up to *ca.* 5° for non-chelated complexes are slightly larger than those predicted by Martin and Orpen,[8] 1-3°, which are attributable to experimental uncertainty and crystal packing effects, but compare reasonably well to the values noted in other transition metal structures, also *ca.* 5%.[12] The chelate complexes show much larger values of δ_{oct} for each of the metals studied, in fact over double the distortion found for the analogous non-chelates. This shows that the favourable energy change of chelate formation is able to outweigh the unfavourable energy of distorting the L-M-L bonds away from their optimal values. The larger metals appear to be able to support a larger distortion; this is presumably due to the steric interactions between the ligands being less important than for the smaller metals where even small deviations bring the ligands into relatively close contact. The results from the in-house database for titanium are comparable with the chelated structures of the results obtained on examination of the CSD for similar group 4 complexes, showing no evidence of unusual stress or strain.

7.3 Effect of Ancillary Ligands on the Labile Groups

The influence of the ancillary ligands on the reactivity of the metal complex was discussed in Chapter 5.2. It is generally held that the identity of the ancillary ligands may be used to tune the reactivity and selectivity of such metal complexes. As the reactivity of the complex is strongly dependent on that of the labile ligands, one important effect in

this respect is the effect the ancillary ligands have on the bond length between the metal and the labile ligands. It might be expected that ligand influence which weakens, and hence lengthens, the bond between the metal and the labile ligands would improve reactivity. One way in which this feature is measurable in complexes with the general formula $[M(L)_2(O\textit{i}Pr)_x]_n$ is by examining the influence of the X-Ti-X angle at a chelating ligand on the length of the Ti-O*i*Pr bond. The parameter describing the angle between the approach of the two ligand atoms involved in the chelation, in this case X-Ti-X, is commonly termed the 'bite' angle. The size of the 'bite' angle may be expected to affect the reactivity of the product by influencing the strength of the Ti-O*i*Pr bond. One possible mechanism for influence is that strain in the chelate at the metal centre may induce weaker, and hence longer bonds to the labile isopropoxide ligands. The following study uses both the CSD and our in-house database to investigate this proposition.

Initially, it is important to analyse the Ti-O*i*Pr bond distances found in the CSD, with no other constraints for a point of reference. For this purpose, the CSD was searched for Ti-O*i*Pr bond lengths. The results of this investigation are presented in the form of a histogram in Figure 7.4.

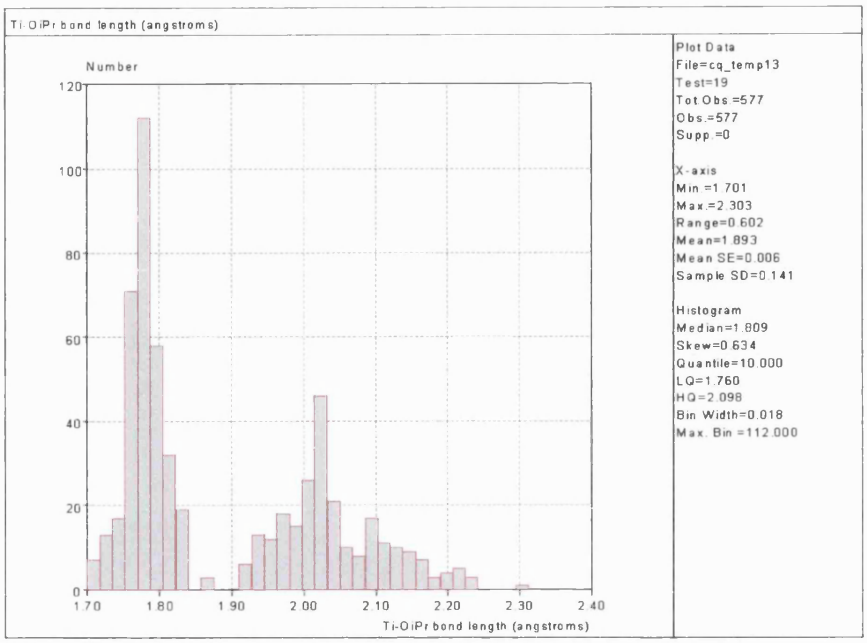

Figure 7.4: Histogram showing the distribution of Ti-O*i*Pr bond lengths for titanium complexes in the CSD.

One important conclusion found is that the resulting distribution obtained for Ti-O*i*Pr bond lengths is clearly bimodal in nature. The overall range in bond length is 0.6Å, with the mean at 1.90Å. On closer examination the two clusters proved to represent the terminal and bridging modes of bonding for titanium alkoxides, with the bridging alkoxides making up the broader distribution at a longer bond length. Consequently, the terminal alkoxide bonds cluster around a mean value of 1.78Å (σ 0.03) and the bridging alkoxides a mean of 2.04Å (σ 0.08). In addition to the full results in Figure 7.4, the histograms for these two individual classes, with statistical results, can be found in the Appendices.

The complexes in the database containing Ti-O*i*Pr were further analysed to judge the effect of the five- and six-membered chelates on the Ti-O*i*Pr bond length. Geometric parameters were extracted for the complexes containing either a five- or six-membered chelating ligand to the metal and an isopropoxide ligand. These further detailed analyses

are presented in scatterplots obtained from VISTA in Figures 7.5 and 7.6 for five- and six-membered chelates respectively.

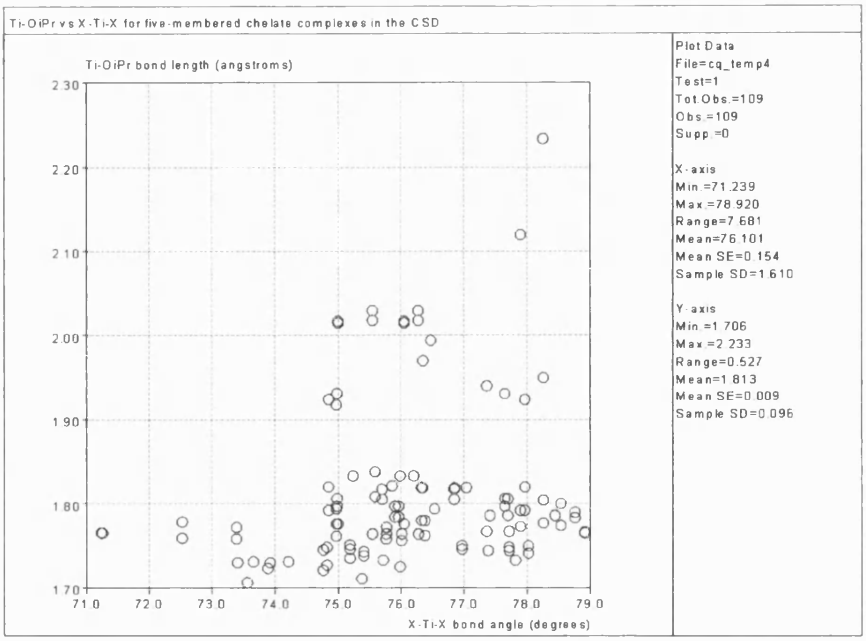

Figure 7.5: Scatterplot showing the distribution of X-Ti-X versus Ti-O*i*Pr bond lengths for titanium complexes with five-membered chelates in the CSD.

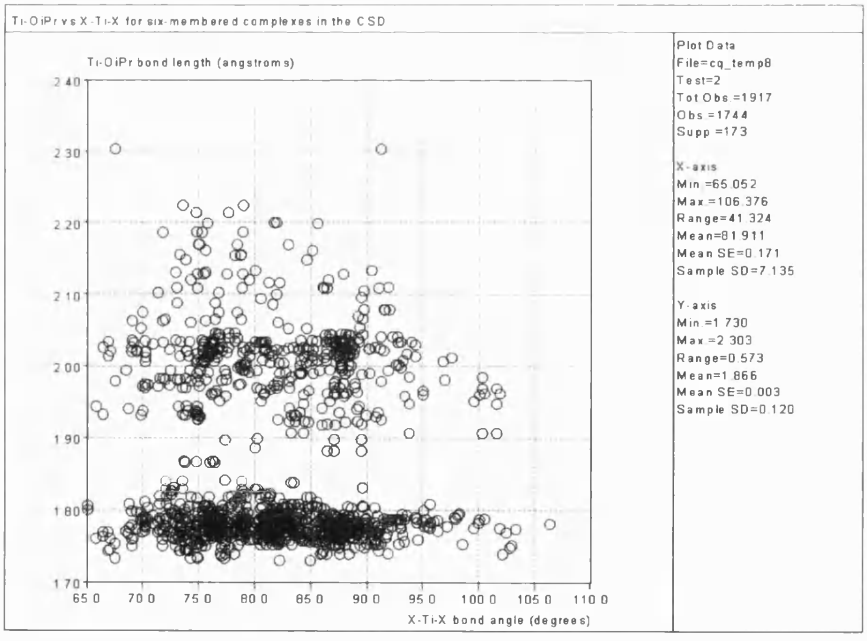

Figure 7.5: Scatterplot showing the distribution of X-Ti-X versus Ti-O*i*Pr bond lengths for titanium complexes with six-membered chelates in the CSD.

It should be noted that here are far fewer examples of five-membered chelates (N_{obs} 109) than there are for six-membered chelates (N_{obs} 1744). The bimodal distribution due to the difference in bond length between terminal and bridging isopropoxide ligands is clearly present, as found in the unconstrained Ti-O*i*Pr bond lengths. There is also a distinct difference between the five- and six-membered chelates. The five-membered chelates fall into a narrower distribution of X-Ti-X bond angles, with the distribution of angles in the five-membered chelates around 8°, while in the six membered chelates it is over 40°. This result is not unexpected due to the reduced flexibility in the smaller ring size. However, there is otherwise no clear correlation relating shorter Ti-O*i*Pr bond lengths to less acute bond angles at the chelate.

An analogous search was performed on the in-house database to provide a comparison, as these unpublished structures have known potential for catalytic activity.[15] This was carried out using the same search fragment as used in the CSD search.

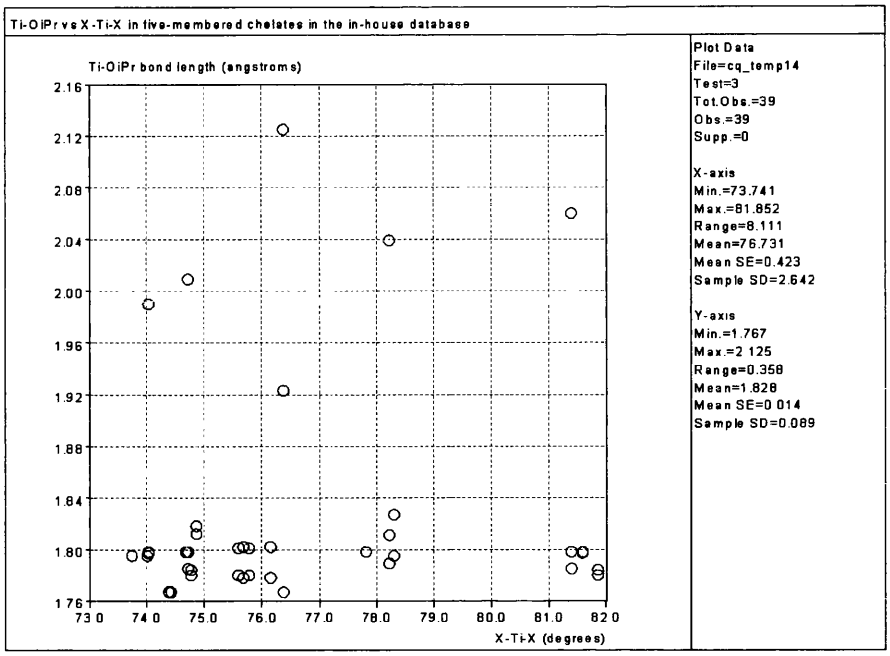

Figure 7.7: Scatterplot showing the distribution of X-Ti-X versus Ti-O*i*Pr bond lengths for titanium complexes with five-membered chelates in the in-house database.

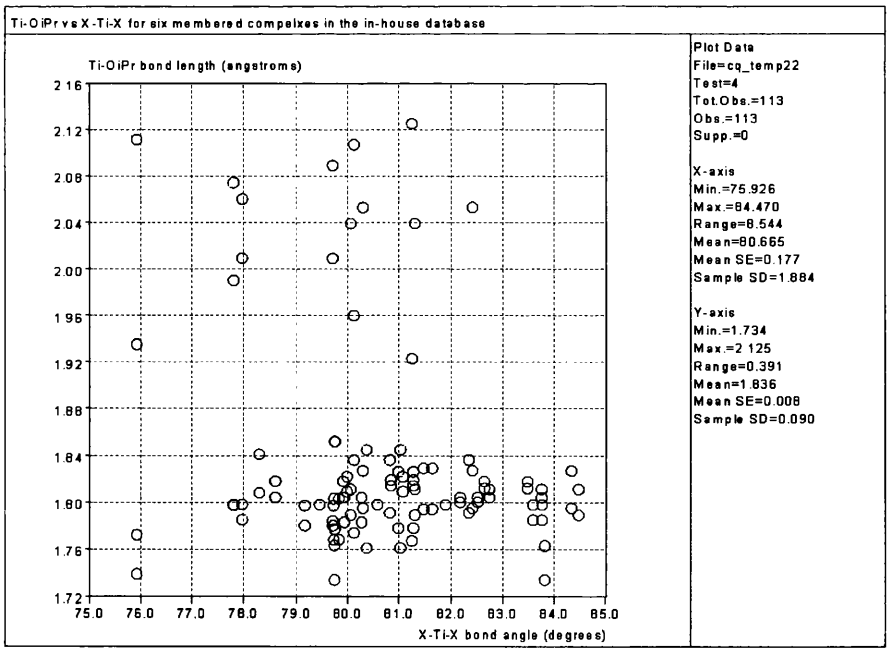

Figure 7.8: Scatterplot showing the distribution of X-Ti-X versus Ti-O*i*Pr bond lengths for titanium complexes with six-membered chelates in the in-house database.

Again, the bimodal distribution due to the terminal and bridging alkoxides is evident in these results. This search of our in-house database is also consistent with the CSD results in that it indicates some differences between the five- and six-membered chelates. However, the mean X-Ti-X angles in these two classes are more similar in range in these analyses due to the structurally closely related complexes that make up the database. The range for the five-membered chelates is 8° with a mean of 76°, while for the six-membered chelates the range is 9° with a mean of 81°. There is otherwise no significant correlation between the bite angle in the bis-donor chelate and the Ti-O*i*Pr bond length, hence it must be concluded that this proposed mechanism by which these potential catalysts promote catalytic activity is not observable in the solid state geometric parameters.

7.5 Concluding Remarks

The coordination chemistry of the group 4 transition metal alkoxides has been extensively explored by both academic and industrial groups in recent decades. However, the systematic analyses of crystallographic data in this area remain relatively rare. This chapter has assessed both the geometry at the metal centre and the effect of chelating ancillary ligands on the lability of the isopropoxide groups.

Values for the distortion from 'ideal' octahedral geometry for group 4 complexes with the general formula ML_6 have been evaluated. It has been demonstrated that for the group 4 metals without chelating ligands at the metal centre, distortions of up to *ca.* 5° are found. These are generally considered to be a consequence of experimental uncertainty in crystal structure determination and packing effects within the crystals. The complexes with chelating ligands proved to make up a large proportion of the complexes in the database and exhibited greater distortions of up to *ca.* 14°. These larger distortions indicate that the energy taken to distort the L-M-L bonds away from their optimal values is adequately compensated by the energy gain in chelate formation.

Furthermore, the effect of ancillary ligands in titanium isopropoxides on the Ti-O*i*Pr bond length has been examined in both the CSD and an in-house database. The parameters studied were the influence of the 'bite' angle at the metal centre in a chelating ligand with the Ti-O*i*Pr bond length. A bimodal distribution due to a difference in bonding modes is found throughout, although no correlation between the angle and bond length was found.

7.6 Experimental

Cambridge Structural Database Analysis

Crystal structures containing the molecular fragments studied were located in the CSD using the ConQuest program (version 1.26).[16] Data for these analyses were retrieved for all structures with a match to the search fragment from the November 2004 version of the database, containing 325,709 entries. Only entries where R<0.10, not polymeric with no errors and where atomic coordinates are given were considered in the analyses. Data analyses were performed using either VISTA[2] or EXCEL programs. Many individual structures were examined as chemical and stereochemical diagrams in ConQuest, VISTA or the visualisation program Mercury[13] during the analysis. Further information about the individual searches are included in the appropriate discussion sections.

7.7 References

[1] Bradley, D.C.; Mehrotra,R.C.; Rothwell, I.P.; Singh, A. *Alkoxo and Aryloxo Derivatives of Metals*, Academic Press, London; **2001**.
[2] Allen, F.H.; Kennard, O. *Chem. Des. Autom. News* **1993**, *8*(1), 31.
[3] Allen, F.H. *Acta Cryst.* **2002**, *B58*, 380.
[4] Bruno, I.J.; Cole, J.C.; Edgington, P.R.; Kessler, M.; Macrae, C.F.; McCabe, P.; Pearson, J.; Taylor, R. *Acta Cryst.* **2002**, *B58*, 389.
[5] Auf der Heyde, T.P.E. *Structure Correlation*, edited by Bürgi, H.-B.; C Dunitz, J.D., Verlag Chemie, Weinheim; **1994**, pp337-386.
[6] Bürgi, H.-B. *Acta Cryst.* **1998**, *A54*, 873.
[7] Orpen, A.G. *Acta Cryst.* **2002**, *B58*, 398.
[8] Martin, A.; Orpen, A.G. *J. Am. Chem. Soc.* **1996**, *118*, 1464.
[9] Orpen, A.G. *Act Cryst.* **1998**, *D54*, 1194.
[10] Orpen, A.G.; Brammer, L.; Allen, F.H.; Kennard, O.; Watson, D.G.; Taylor, R. *J. Chem. Soc., Dalton Trans.* **1989**, *12*, S1.
[11] Bradley, D.C.; Mehrotra,R.C.; Rothwell, I.P.; Singh, A. *Alkoxo and Aryloxo Derivatives of Metals*, Academic Press, London; **2001**, pp. 473-478
[12] Harding, M.M. *Acta Cryst.* **2000**, *D56*, 857.
[13] Howard, J.A.K.; Copley, R.C.B.; Yao, J.W.; Allen, F.H. *Chem. Commun*, **1998**, 2175.
[14] Refcode JAMWOJ for pseudo-seven coordinate zirconium complex removed from hit list.
[15] Lunn, M. D., Ph.D. Thesis, University of Bath, Bath, UK, October, **2002**.
[16] Bruno, I.J.; Cole, J.C.; Edgington, P.R.; Kessler, M.; Macrae, C.F.; McCabe, P.; Pearson, J.; Taylor, R. *Acta Cryst.* **2002**, *B58*, 389.